Sloshing

Topside Storage Tank Application on Floating Offshore Structures

N. van Dijk

TU Delft Delft University of Technology

Sloshing

Topside Storage Tank Application on Floating Offshore Structures

by

N. van Dijk

In partial fulfillment of the requirements for the degree of

Master of Science
in Offshore & Dredging Engineering

at the Delft University of Technology
Faculty Mechanical, Maritime and Materials Engineering,
to be defended publicly on Tuesday August 23, 2016 at 12:00 AM.

Student number:	4250028	
Project duration:	December 7, 2015 – August 23, 2016	
Thesis committee:	Prof. Dr. Ir. R.H.M. Huijsmans,	TU Delft, chair
	Dr. Ir. S.A. Miedema,	TU Delft
	Dr. Ir. I. Akkerman,	TU Delft
	Ir. S.M. Hosseini Zahraei,	TU Delft
	Ing. M.J. de Vor,	CB&I

An electronic version of this thesis is available at http://repository.tudelft.nl/.

TU Delft

Abstract

Offshore structures with partially filled storage tanks may experience sloshing of the cargo when exposed to waves. Inventive use on the topside result in storage tanks which are built as an integrated part of the deck structure. Weight control and available space is often a critical issue for offshore projects and can be improved by this application. CB&I have decided to carry out a research related to the occurrence of sloshing and impact pressures for these, so called, in-deck tanks. The sloshing assessment procedure is an important part of the structural strength checks. Sloshing occurs when the natural period of the fluid coincides to the motions of the storage tank. Four factors mainly contribute to the sloshing phenomenon. Namely, tank dimensions, fill, fluid properties and motion characteristics. However, the complex, chaotic and non-linear behaviour of sloshing makes it hard to predict or estimate impact pressures.

In-deck tanks are applied at the topside of the Aasta Hansteen SPAR project, carried out by CB&I. The application of these tanks faced difficulties concerning the sloshing assessment procedure. There is no method applicable related to this situation. Therefore, a conservative method has been defined as a temporary solution. For future implementation of these tanks, better understanding and knowledge of fluid behaviour is essential. In order to tackle this problem, a CFD analysis is carried out in two phases and concludes with a statistical analysis in order to estimate sloshing impact pressures. The first phase relates to a general 2D CFD simulation for various cases. The second phase includes 2D long time simulations of sloshing cases extracted from the first phase.

The results of the first phase show that no sloshing occurs for the Aasta Hansteen SPAR related cases. Where the motion period of 60 seconds is too far away from the period of the 1^{st} wave mode, which is around 8 seconds. FPSO related cases contain a period around 10 seconds and show sloshing impact behaviour. The impacts occur specifically for longer tank lengths and higher filling levels as these cases coincide better with the motion behaviour of the tank. Noted that the combination of input parameters for which sloshing occurs is highly dependent on the forced excitation on the tank, where sloshing behaviour is sensitive to changes of these parameters. Furthermore, a motion case analysis is added and different sea states are assessed from mild to harsh tank motion excitations. Resulting in sloshing for harsher sea states and higher accelerations. Overall, sloshing impacts conclude in the order of 100 kPa - 300 kPa. The impact area includes the vertical wall and 2.4 meters on the top of the tank. In the event of non-impulsive oscillating behaviour (no sloshing), one can apply the linear theory for an accurate prediction of the pressures. However, when the fluid motion becomes chaotic and non-linear, there is no method able to accurately predict the impact pressures.

The results of the second phase contain the sloshing impact order of magnitude for eight individual sloshing cases. With difference in fluid, tank length, fill and motion type. Six of these cases can be compared to one another and resulted in a fill/length ratio of 0.063 for the highest impact pressures. A lower viscosity of the fluid seems to increase the sensitivity to sloshing behaviour. Filling levels of 50% - 70% show high sloshing impacts, where 80% fill does not result in sloshing anymore. The increase of tank lengths results in higher sloshing impacts. Briefly summed up: 7m no sloshing, 12m semi sloshing, 15m sloshing impact order 150 kPa - 200 kPa and 20m sloshing impact order 300 kPa - 500 kPa. Two fitting curves are used in order to establish the Exceedance Probability Function. Namely, the Generalized Pareto and Kernel Smoothing. Both show a good fitting, but present different behaviour in the so called 'tail' of the Probability Density Function. A good distribution of this 'tail' result in a better Exceedance Probability Function. A decision on the best fitting curve is not made due to the lack of sufficient simulated statistical data. The sensitivity analysis proved the Kernel Smoothing fitting more robust compared to the Generalized Pareto. Also, the reduction of statistical data resulted in the highest sensitivities within the sensitivity analysis. Which underlines the need of more simulation and statistical data for improvement of the results.

Keywords: Sloshing CFD ComFLOW In-deck Tank Impact Pressures

Preface & Acknowledgements

The publication of this report is the final part in obtaining the Master of Science degree in Offshore Engineering. Roughly three years back I proposed a goal for myself. To combine my technical interest, motivation and capabilities in order to achieve a Masters degree. As a result I proudly present this final product. During the Master my interest was mainly focused towards hydrodynamics, which resulted in the decision for the specialization of Floating Structures. Concluding with this thesis on the complex fluid phenomenon called sloshing.

First, i would like to thank René Huijsmans for being chairman and his continuous feedback during my graduation. I would also like to thank Matin Hosseini Zahraei for all the assistance, discussions, support and time. You where always available to answer my critical questions throughout these last 6 months. Thank you Sape Miedema and Ido Akkerman for reading this thesis and being part of the committee. At CB&I many thanks to Menno de Vor for his support, time and feedback during the whole graduation. Also thanks to Mohammad Shariat Ahmadi and Payman Veisi Zadeh for their time and critical insights during the project. At the TU Delft i would also like to thank Reza Karimi and Peter Wellens for their time and providing me with valuable feedback on complex topics that I've encountered. Concluding i would like to thank my fellow students and friends at the TU Delft. Alex Lotgering for keeping me motivated and Oliver Feng for the inspiring talks.

A closing thank you is reserved for my family and friends that always supported me during this Master. In addition, special thanks to my girlfriend Nicky for her continuous motivation and support.

I wish you an interesting and pleasant read.

Niels van Dijk
Delft, August 2016

Summary

Introduction
Floating offshore structures that contain storage tanks may experience sloshing of the cargo when exposed to environmental conditions, such as wind, waves and current. These structures move in six degrees of freedom, defined as surge, sway, heave, roll, pitch and yaw. For the design of the Aasta Hansteen SPAR Topside EPC project, carried out by CB&I, an inventive use of the topside structure has been applied. For optimal use of the available space, storage tanks are built as an integrated part of the deck structure, so called 'in-deck tanks'. Weight control and available space is often a critical issue for offshore projects and can be improved by this application. However, difficulties arise concerning the sloshing assessment procedure, which is an important part of the structural strength checks. There is no method applicable related to this situation. Therefore, a conservative method has been defined as a temporary solution. For future implementation of these tanks, better understanding and knowledge of fluid behaviour is essential. Sloshing occurs when the natural period of the fluid coincides to the motions of the storage tank. Four factors mainly contribute to the sloshing phenomenon. Namely, tank dimensions, fill, fluid properties and motion characteristics. However, the complex, chaotic and non-linear behaviour of sloshing makes it hard to predict or estimate impact pressures.

Research Methodology
In order to tackle this problem, CFD simulations by ComFLOW are carried out. The simulations are divided into two phases. The first phase relates to a general 2D CFD simulation for various cases. The main aim for this phase is the definition of cases and gather know-how of the CFD software. With the help of a research scenario study, a list of cases is defined for simulation. The broad approach of this phase illustrates the urgency of a general sloshing understanding of in-deck tanks. The second phase includes 2D long time simulations of sloshing cases extracted from the first phase. Statistical post processing is used to interpret the data and achieve the main goal, the order of magnitude for different sloshing cases. The most influential topics of the framework and assumptions are briefly discussed. (1) This research primarily focuses to the sloshing impact pressures in FPSO applications. (2) Both verification and validation of the ComFLOW executable are carried out. (3) The in-deck tanks are considered smooth, rectangular and closed.

CFD - Phase 1
After a research scenario study, the first phase conclude in a list of 66 cases which are divided into seven distinct groups. The first group is related to the Aasta Hansteen SPAR project and fully focused on the occurrence of sloshing. The second till sixth group correlates to an FPSO where difference in tank size, material, fill levels and motions is widely assessed. The seventh and last group relates to the verification of the CFD simulations by conducting a grid independence study. The result of each case is labeled as no sloshing, semi-sloshing or sloshing. No sloshing relates to non-impulsive oscillating pressures. Semi-sloshing is the transition zone between oscillating and sloshing fluid behaviour. Concluding with sloshing, which holds impulsive sloshing impact behaviour. The results of each group is briefly summed up below.

Group 1 The first set of cases include an assessment of the applied in-deck tanks for the Aasta Hansteen SPAR. The results show that no sloshing occurs for all SPAR related cases. The 60 seconds motion period of the SPAR is too far from the sloshing natural period, which is around 8 seconds.

Group 2 The second set of cases start with the sloshing assessment of the FPSO pitch motion (9.7 s), where four different tank lengths are included. The results show no sloshing for a 7 m long tank. Tank lengths 12 m and 15 m resulted in semi-sloshing, and the 20 m cases presented sloshing behaviour. Therefore, 7 m tank lengths are excluded for further simulation cases.

Group 3 The third set of cases include different fill levels, tank lengths and fluid types, with the same FPSO pitch motion. The results of group 3, in combination with group 2, are presented in the table and figures on the next page.

Fluid Type	Fill	Tank length			
		7 m	12 m	15 m	20 m
Water	30%	-	*30*	*40*	*45*
	50%	18	*40*	*50*	**90**
	60%	-	*40*	*45*	*50*
	70%	-	*35*	**100**	**80**
MEG	45%	-	*40*	**70**	*60*
	50%	20	*40*	*50*	**95**
	70%	-	*40*	*50*	**100**
	80%	-	*55*	*55*	*70*

Phase 1 - Overall results - FPSO MC2-Pitch
Pressure values in kPa, for no sloshing, *semi sloshing*, **sloshing**

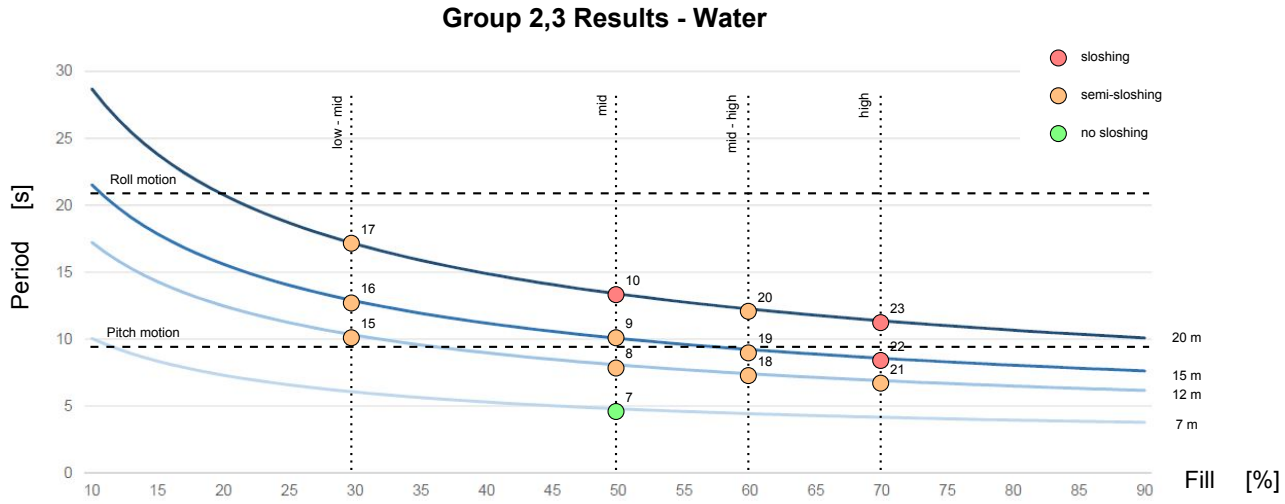

Phase 1 - Overall results Water - Compared to 1^{st} natural sloshing mode

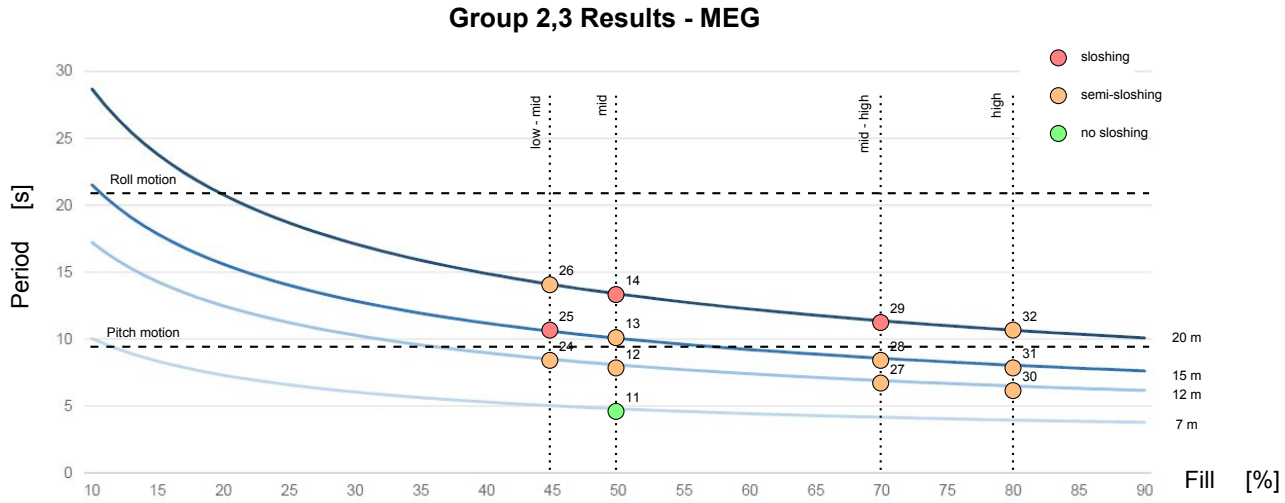

Phase 1 - Overall results MEG - Compared to 1^{st} natural sloshing mode

Group 4 The fourth set of cases studies varying heeling angles of the FPSO pitch motion that relates to different areas in the world. Whereby a standard 50% water fill is chosen. Again, the results are presented in the table below.

			Motion Cases						
			3 - Pitch	5 - Pitch	4 - Pitch	7 - Pitch	2 - Pitch	2- Roll	6 - Pitch
		Area \ Units	West Coast Africa	North Cape	North West Australia	Gulf of Mexico	West Coast Norway	West Coast Norway	East Canada
H_s		m	4.8	12.7	13.8	15.7	16.3	16.3	18.5
Natural Period		s	9.7	9.7	9.7	9.7	9.7	20.8	9.7
Heeling angle		deg	2.63	6.23	6.77	7.71	8.00	16.00	9.08
Max. x acc.		m/s²	0.24	0.63	0.68	0.78	0.81	0.34	0.92
Max. z acc.		m/s²	0.01	0.03	0.04	0.05	0.06	0.05	0.07
Max. ϕ acc.		deg/s²	0.99	2.61	2.84	3.23	3.36	1.46	3.81
Tank length	7	m	-	-	-	-	-	20	-
	12	m	18	*35*	*38*	*35*	*40*	*35*	*40*
	15	m	*25*	*35*	*48*	*40*	*55*	*40*	**60**
	20	m	*30*	*35*	*42*	**100**	**90**	*60*	**65**

Phase 1 - Motion results - FPSO 50% water fill
Pressure values in kPa, for no sloshing, *semi sloshing*, **sloshing**

Group 5 The fifth set of cases relates to the FPSO roll motion, which includes a period of 20.8 seconds. The period of the natural first wave mode is around 10 seconds. Resulting in semi-sloshing behaviour. Due to the longer period and bigger heeling angle, the occurring pressures are in the same order as semi sloshing of the pitch motion. The results are implemented in the table above.

Group 6 The sixth set of cases includes an extended time duration of four sloshing cases. Instead of thee periods, six periods are simulated. Resulting in the occurrence of more severe sloshing impacts. The order of sloshing impact increased from 100 kPa to 300 kPa, which underlines the need of long time simulations.

Group 7 The last and seventh case of the first phase relates to the verification of the ComFLOW executable. The results and elaboration for these cases are described in the second phase.

The result of phase 1 includes nine sloshing cases. From these cases the sloshing impact area can be extracted. Both sides of the tank show an identical hot spot zone where high impact pressures occur. The impact area contains the vertical wall and 2.0 - 2.4 m on the top of the tank.

Furthermore, a method comparison has been carried out. There are different methods and theories on the calculation of pressure in storage tanks. Four of them are selected to possibly be applicable for the in-deck tanks. Namely, conservative method of CB&I, empirical method of DNV, analytical hydrostatic pressures and the analytical linear theory. After processing the results of phase 1, a comparison can be made between ComFLOW and the proposed methods. Resulting that for the case of no sloshing, the linear theory accurately describes the pressures inside the in-deck tank. Whereas for the semi-sloshing and sloshing cases, none of the methods or theories are able to calculate the sloshing pressures. This is due to the non-linear and chaotic behaviour of the fluid when hitting resonance conditions. In order to resolve this issue, the second phase is dedicated into the prediction of the sloshing impact pressures.

CFD - Phase 2
The second phase conclude in a list of 12 cases which are divided into 3 distinct groups. When continuing counting, the eighth group includes 8 selected (sloshing) cases of phase 1. Where group nine and ten relates to the verification and validation of the ComFLOW executable. After conducting long time simulations of group 8, statistical post-processing analysis is done in order to generate the Exceedance Probability Function (EPF). The statistical analysis is carried out by application of classification notes related to LNG membrane tanks, which are applicable for in-deck tanks as well. The statistical procedure holds five steps and is elaborated briefly.

1. Application of Peak-over-Threshold method. This method identifies impact peaks and filters out noise in the pressure signal. A sloshing event is defined as an impact pressure when it exceeds the specified pressure threshold. The threshold is set well above the noise level to exclude any semi-sloshing behaviour from the analysis.

2. After the Peak-over-Threshold method is applied, the identified sloshing impacts need to be counted and binned. This is done by a histogram from the Threshold value up to the maximum impact value. The resulting histogram is of great importance for the fitting curves linked to the Probability Density Function.

3. In order to create the Probability Density Function (PDF), the histogram needs to be normalized. After normalization, mathematical fitting is conducted in order to extrapolate beyond measured data. It should be noted that mathematical fits have no relation to the fundamental physics dominating the randomness of sloshing impacts. By conducting a fitting analysis, two type of fittings resulted to be applicable. Namely, the Generalized Pareto (GP) and Kernel Smoothing (KS) fitting curves.

4. After partial integration of the PDF, the Cumulative Density Function (CDF) can be defined. In order to test the goodness of the fitting curves, a Two-Sampled Kolmogorov-Smirnov test is conducted. This test evaluates the maximum difference between the data and fitting curve and test if this is within a certain boundary value. The boundary value is defined by the number of samples that the data contains. Therefore, this test forces a better fit when more data is available.

5. The final step involves inverting the CDF into the Exceeding Probability Function (EPF). The EPF is presented with a vertical logarithmic scale and gives insight into the probability and order of magnitude for sloshing impact pressures. The different nature of the two fitting curves, GP and KS, is shown clearly in the EPF graph. After the data stops and mathematical extrapolation starts, each fitting proceed differently in the 'tail' of the PDF. Where the Generalized Pareto converges to a horizontal asymptote, the Kernel Smoothing converges to an vertical asymptote. The most reliable fitting curve that illustrates the 'tail' best is up for debate. The vertical asymptote of the Kernel Smoothing fitting represents a logical physical property. With a fixed motion, fill, fluid and tank length, there has to be a maximum impact pressure possible. There is not more energy and impact potential then a certain value. Which coincides perfectly with the vertical asymptote of the Kernel Smoothing fitting. However, one may discuss that fitting curves have no physical meaning whatsoever. More statistical data and analysis would improve the decision for the best fitting curve.

Group 8 After the application of the statistical analysis, one can conclude the results related to the 8 long time simulation cases. In order to extract sloshing impact values of the EPF, the probability return period is set to 100 years (10^{-2}) and coincides with the return period of the extreme sea state ship motions defined in the research scenario study. The overall results of the second phase are presented in the table below

Case	Length [m]	Fill	Fluid	Motion		Pressure [kPa]	
				Case	Type	GP	KS
67	20	50%	water	2	Pitch	295	310
68	20	50%	MEG	2	Pitch	220	230
69	15	70%	water	2	Pitch	215	235
70	20	70%	water	2	Pitch	495	325
71	15	45%	MEG	2	Pitch	165	150
72	20	70%	MEG	2	Pitch	310	310
73	20	50%	water	7	Pitch	1380	670
74	20	50%	water	6	Roll	290	275

Phase 2 - Overall Results

After analyzing the results of the second phase, six cases (67 - 72) can be compared to one another and resulted in a fill/length ratio of 0.063 for the highest impact pressures. Noted that more data and simulations are necessary in order to distract a more reliable and robust ratio. Comparisons of the fluid, fill, length and motion resulted in the following brief conclusions. A lower viscosity of the fluid seems to increase the sensitivity to sloshing behaviour. Filling levels of 50% - 70% show high sloshing impacts, where 80% fill does not result in sloshing anymore. The increase of tank lengths results in higher sloshing impacts. Briefly summed up: 7m no sloshing, 12m semi sloshing, 15m sloshing impact order 150 kPa - 200 kPa and 20m sloshing impact order 300 kPa - 500 kPa. As mentioned, two fitting curves are used in order to establish the Exceedance Probability Function. Both show a good fitting, but present different behaviour in the so called 'tail' of the Probability Density Function. A good distribution of this 'tail' result in a better Exceedance Probability Function. A decision on the best fitting curve is not made due to the lack of sufficient simulated statistical data.

Furthermore, a sensitivity analysis is carried out for both fitting curves. The sensitivity of the threshold, binning and data extraction has been tested. The random data filter sensitivity is arguable but is added due to the grid independence issue. Resolving all local sloshing pressures at the right location and at the right time is not certain. Therefore, one can omit random data in order to mimic the influence on the statistical results. The sensitivities are dependent on each case, therefore it is not possible to formulate a general safety number. The data-cut and data-random filters shows the highest sensitivity of 30% - 50%, which underlines the need of more simulation and statistical data for improvement of the results. The results can be presented as a mean sensitivity deviation for every case related to each of the two fitting curves and concludes in a so called sensitivity tornado, presented in the figure on the next page. The tornado shows clearly that the Generalized Pareto fitting is more sensitive and concludes the Kernel Smoothing to be slightly more robust.

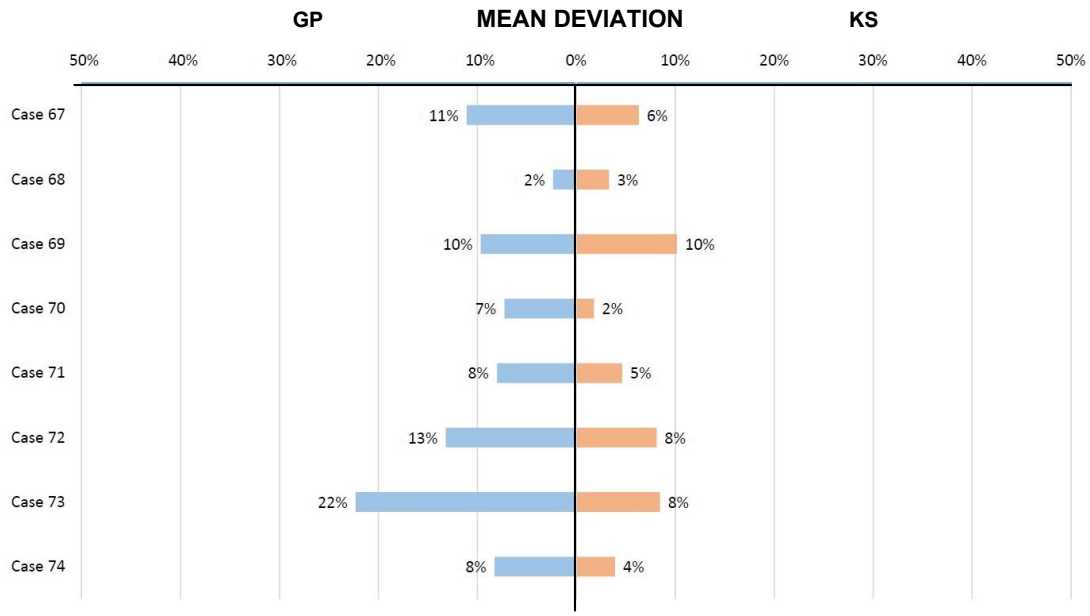

Sensitivity Tornado - Mean Deviation

Group 9 The ninth set of cases relates to the verification of the ComFLOW executable. Verification includes the main question of: do we solve the equations right?

In order to verify ComFLOW a grid independence study is carried out. This includes the assessment that variation in mesh size should not influence the results. Or in other words, it checks if all the local sloshing pressures at a certain location and time are resolved to the same value. Two zones can be defined for grid independence, a scatter zone and the convergence zone. Logically, the convergence zone contains the mesh size and fineness for which the result converges to a fixed value. However, when the mesh is not fine enough for the fluid behaviour that occurs, the mesh is labeled to be in the scatter zone. The start of the convergence zone depends heavily on the non-linearity and chaotic behaviour of the fluid.

Both phases contained mesh refinements from 10 cm - 1 cm (Phase 1) up to 1 cm - 0.25 cm (Phase 2). This resulted in clear convergence for the no sloshing cases, as these cases are non-chaotic and almost linear. Unfortunately, problems occurred for the verification of sloshing cases. While pushing the computational limitations, no clear convergence could be presented. In addition, a mean pressure distribution has been created and shows a clear trend and phase of the sloshing impact. Overall one can conclude that the results look trustworthy and reasonable.

Group 10 The tenth and last set of cases relates to the validation of the ComFLOW executable. This is done by comparison of numerical results to a benchmark test. Validation includes the main question of: do we solve the right equations?

Due to the lack of experimental or numerical results related to in-deck tank scenarios, general validation of global fluid motion is conducted. Benchmark test of a parallelepiped-shape tank, where one dimension is much smaller than the two others and mimics 2D, are carried out. These tests included a surge and a roll motion case that result in different fluid impact types. Footage of these experiments are compared to the simulation result of ComFLOW.

For both assessed cases of surge and roll motion, ComFLOW presents good fluid behaviour in comparison to the experimental results. The fluid impact of both cases is well simulated by ComFLOW and underline the capability of ComFLOW to simulate sloshing behaviour. However, it should be noted that due to discrepancies between the ComFLOW results and benchmark test videos, local pressures simulated by ComFLOW should be treated with caution.

Concluding Recommendations

At the start of this research little was known about the fluid behaviour in in-deck tanks. The situation for which sloshing could occur was totally unknown. After conducting this research, the fluid behaviour and contribution of the influence parameters are better understood. However, during the research new questions arise as well. Recommendations for future work by expanding the knowledge of sloshing for in-deck tanks is briefly listed below.

- **Development of ComFLOW results in better performance and capabilities.**
  ComFLOW is continuously in development and has a big update scheduled for the end of 2016. The addition of automatic local grid refinement and parallel processing will contribute to a more accurate and faster simulation. These updates increase the potential of conducting longer time simulations, which results in the improvement of accuracy for the sloshing impact order of magnitude.
- **Investigate three-dimensional simulations by coupling pitch and roll motion.**
  Given the computational limitations, a combination of pitch and roll motion proved to be to expensive to implement. However, the update of ComFLOW could be promising to combine motions and carry out three-dimensional analysis.
- **Investigate the use of baffles for sloshing reduction.**
  The application of sloshing reduction possibilities is not in the scope of this research. However, it could be interesting to gather more insight on the sloshing reduction with the use of baffles. The relevance of this recommendations depends on whether the sloshing is considered a problem.
- **Investigate coupling effects of the in-deck tank and floating structure.**
  Coupling effects between the in-deck tank and floating structure are not analysed in this research. The coupling should be analyzed when more specific cases can be defined, which are related to future projects. The general origin and lack of detailed motion information of the offshore structure makes it hard to carry out a reliable coupling analysis in this stage.
- **Investigate the fatigue analysis of sloshing behaviour in in-deck tanks.**
  There has been no analysis done related to fatigue. Besides high sloshing impact pressures, fatigue is another possible issue for storage tanks. An indication of the lifetime for in-deck tanks could be important to gather more knowledge of.
- **Investigate grid independence for verification.**
  Grid independence was not achieved for sloshing cases. Again, the update of ComFLOW can help to apply finer meshes. Which should conclude in convergence of pressure deviations and therefore grid independence.
- **Carry out experiments for improved validation.**
  The validation of ComFLOW related to the simulated cases of this research is not ideal. In order to achieve better validation, experiments related to the defined cases could be carried out. This shall improve the reliability and interpretation of the sloshing impact order of magnitude.

Contents

Abstract iii

Summary vii

List of Figures xvii

List of Tables xix

Nomenclature xxi

1 Introduction 1
- 1.1 General Background . . . 1
- 1.2 Problem Definition . . . 2
- 1.3 Scope . . . 2
- 1.4 Relevance of Scope . . . 2
- 1.5 Objectives . . . 3
- 1.6 Thesis Outline . . . 3

2 Research Methodology 5
- 2.1 Strategy Evaluation . . . 5
- 2.2 Sloshing Assessment Procedure . . . 6
- 2.3 Framework . . . 7
- 2.4 Assumptions . . . 7
- 2.5 Alternatives . . . 8

3 Physical Model 9
- 3.1 Fluid characteristics . . . 9
- 3.2 Coordinate System . . . 10
- 3.3 Fluid flow . . . 12

4 Empirical & Conservative Methods 15
- 4.1 Conservative Method CB&I . . . 15
- 4.2 Rules and Regulations . . . 17

5 Analytical Model 19
- 5.1 Hydrostatic Pressure Model . . . 19
- 5.2 Linear Model . . . 20

6 ComFLOW 23
- 6.1 Mathematical Model One-Phase Flow . . . 23
- 6.2 Numerical Model . . . 24

7 CFD - Phase 1 27
- 7.1 Case Definition . . . 28
- 7.2 Results . . . 31
- 7.3 Method Comparison . . . 34

8 CFD - Phase 2 37
- 8.1 Case Definition . . . 37
- 8.2 Statistical Analysis . . . 39
- 8.3 Results . . . 44
- 8.4 Sensitivity Analysis . . . 50
- 8.5 Verification & Validation . . . 52

9 Conclusions & Recommendations **57**
9.1 Conclusions . . . 57
9.2 Recommendations . . . 60

Bibliography **61**

A Sloshing Impact Type - Illustrations **63**

B ComFLOW **67**
B.1 Mathematical Model One-Phase Flow . . . 68
B.2 Numerical Model . . . 70
B.3 Main Input File . . . 76
B.4 Motion Input Files . . . 81

C CB&I Case Study **85**
C.1 Fluid Type . . . 86
C.2 Fill . . . 86
C.3 Tank Geometry . . . 87
C.4 Motions . . . 90

D Phase 1 - CFD **97**
D.1 Pre-Processing . . . 98
D.2 Post-Processing . . . 98
D.3 Results - Pressure Tables . . . 99

E Phase 2 - CFD **103**
E.1 Pre-Processing . . . 104
E.2 Post-Processing . . . 104
E.3 Results - Statistical Analysis . . . 105
E.4 Results - Sensitivity Tornado's . . . 138

F Verification ComFLOW **141**
F.1 Phase 1 . . . 143
F.2 Phase 2 . . . 149

G Validation ComFLOW **155**
G.1 Phase 2 . . . 156

List of Figures

2.1 Sloshing Assessment Procedure - Red tiles are excluded from this research. 6

3.1 SPAR Structure - Coordinate System 10
3.2 FPSO Vessel & In-deck Tank - Coordinate System 11
3.3 Illustration - Non-impulsive sloshing oscillation pressure 12
3.4 Illustration - Impulsive sloshing impact pressure 13
3.5 Flow chart - Sloshing impact types 13

4.1 Sketch - 2D Load case of Aasta Hansteen SPAR 15
4.2 Sketch - 2D Load case redefined as CB&I conservative method 16
4.3 Sketch - 2D pressure distribution of DNV empirical method 17

5.1 Sketch - 2D Hydrostatic pressure 19

6.1 Cartesian grid and grid refinement 24

7.1 Results Water - Group 3 compared to 1^{st} natural sloshing mode 32
7.2 Results MEG - Group 3 compared to 1^{st} natural sloshing mode 32
7.3 Sketch - Sloshing impact area of 2D In-deck tank 33
7.4 Method Comparison - No Sloshing - Case 7 34
7.5 Method Comparison - Semi Sloshing - Case 13 35
7.6 Method Comparison - Sloshing - Case 14 35

8.1 Impression of mesh refinement 38
8.2 Statistical Analysis - Peak Over Threshold method 39
8.3 Sketch - Force box post-processing set-up of 2D In-deck tank 40
8.4 Statistical Analysis - Binned histogram of sloshing impacts 40
8.5 Statistical Analysis - Probability Density Function 41
8.6 Statistical Analysis - Cumulative Density Function 42
8.7 Statistical Analysis - Exceedance Probability Function 43
8.8 Phase 2 Result - Overall comparison 44
8.9 Phase 2 Result - Fluid type comparison 46
8.10 Phase 2 Result - Fill comparison 47
8.11 Phase 2 Result - Tank length comparison 48
8.12 Phase 2 Result - Motion comparison 49
8.13 Sensitivity Tornado - Mean Deviation 50
8.14 Verification - Grid independence zones 52
8.15 Verification - Mean pressure distribution 53
8.16 Validation - Case 77 - Surge (C16) 55
8.17 Validation - Case 78 - Roll (C18) 56

List of Tables

3.1 Definition - Six degrees of freedom 10

4.1 Definition - Load cases of CB&I conservative method 16

7.1 Phase 1 - Grid size and Calculation times for 30 s simulation time. l = 20 m and H = 1.8 m 27
7.2 Phase 1 - Overview Case Definition - Part I 29
7.3 Phase 1 - Overview Case Definition - Part II 30
7.4 Phase 1 - Fluid & Fill results - FPSO MC2-Pitch Pressure values in kPa, for no sloshing, *semi sloshing*, **sloshing** 31
7.5 Phase 1 - Motion results - FPSO 50% water fill Pressure values in kPa, for no sloshing, *semi sloshing*, **sloshing** 33

8.1 Phase 2 - Grid size and Calculation times for 30 s simulation time. l = 20 m and H = 1.8 m 37
8.2 Phase 2 - Overview Case Definition 38
8.3 Phase 2 - Overall Results 44
8.4 Sensitivity Study - Results 50

Nomenclature

Latin

Symbol	Description	Units
a_t	Combined acceleration of x- and z- axis	$\mathrm{m\,s^{-2}}$
b	Width of the tank	m
C	Convective coefficient operator	–
f	External body forces	N
$f_{m,n}$	Surface profile eigen mode for m,n = 1,2,3…	m
g	Gravitational acceleration	$\mathrm{m\,s^{-2}}$
G	Gradient operator	–
h	Fluid height, fill	m
H	Height of storage tank	m
$k_{m,n}$	Wave number for m,n = 1,2,3…	–
$k_{f,lower}$	Empirical constant, lower impact pressure	–
$k_{f,s}$	Empirical constant, oscillation pressure	–
$k_{f,upper}$	Empirical constant, upper impact pressure	–
l	Length of storage tank	m
L	Length FPSO	m
n	Normal vector	–
p	Pressure	Pa
Q_0	Volume storage tank	$\mathrm{m^3}$
R	Sum convective, diffusive and body forces	N
S_0	Area bottom storage tank	$\mathrm{m^2}$
t	Time	s
T	Period	s
u	Velocity vector fluid flow	$\mathrm{m\,s^{-2}}$
V	Viscous diffusive coefficient operator	–

Greek

Symbol	Description	Units
α	Angle of rotation	deg
α_k	Max. allowable safety margin, Kernel Smoothing	–
α_p	Max. allowable safety margin, Generalized Pareto	–
γ	Angle between bottom and wall of the tank	deg
Γ	Boundary of domain	m
δ	Angle between mean surface and wall of the tank	deg
$\kappa_{m,n}$	Eigen coefficient for m,n = 1,2,3…	m
μ	Dynamic viscosity	$\mathrm{m^2\,s^{-1}}$
ν	Kinematic viscosity	Pa s
$\varphi_{m,n}$	Natural sloshing modes for m,n = 1,2,3…	m
ρ	Density	$\mathrm{kg\,m^{-3}}$
Σ	Mean free surface	m
$\omega_{m,n}$	Natural eigen frequency for m,n = 1,2,3…	1/s
Ω	Control volume of domain	$\mathrm{m^3}$
Ω_{01}	Stokes-Joukowski potential	km
∇	Gradient operator	–

Acronyms

2D	Two dimensional
3D	Three dimensional
ABS	American Bureau of Shipping
ALS	Accidental Loading Conditions
API	American Petroleum Institute
BV	Bureau Veritas
CB&I	Chicago Bridging & Iron company
CDF	Cumulative Density Function
CFD	Computational Fluid Dynamics
COG	Centre Of Gravity
DNV	Det Norske Veritas
DOF	Degree Of Freedom
EPC	Engineering Procurement Construction
EPF	Exceeding Probability Function
FLNG	Floating Liquid Nitrogen Gas
FPSO	Floating Production Storage Offloading
GP	Generalized Pareto
ISO	International Standardization Organization
KS	Kernel Smoothing
LNG	Liquid Nitrogen Gas
LR	Lloyd's Register
MC	Motion Case
MEG	Mono Ethylene Glycol (Antifreeze)
PDF	Probability Density Function
RMS	Root-Mean-Squared
SMT	Sloshing Model Test
SPAR	Single Point Anchor Reservoir
TUD	Technical University Delft
ULS	Ultimate Limit State
VOF	Volume Of Fluid

1 Introduction

1.1. General Background

For the development and production of an oil or gas field a production facility is needed. In the offshore industry, the production facility is often part of the so called 'topside'. There are many different offshore structures designed and built over the years for example; a FPSO, a FLNG or a SPAR structure. These structures float and move in six degrees of freedom, defined as surge, sway, heave, roll, pitch and yaw. A visualization can be found in Figure 3.1 and 3.2, section 3.2 at page 10. Environmental forces like wind, waves and current, influence the motion and behaviour of the floating structure. These motions are forcing fluids inside the structure to move as well.

With the production of oil and gas, various processes have to be conducted at the topside. One can think of the treatment of the produced substance, or well management. For the design of the Aasta Hansteen SPAR Topside EPC Project, carried out by CB&I, an inventive use of the topside structure has been applied. For optimal use of the available space, storage tanks are built as an integrated part of the deck structure, so called 'in-deck tanks'. The cellar plate forms the top part of the tank. The bottom of the tank is made from a stiffened plate welded to the bottom flanges of the primary beams, having the web of the beam as the tank side wall. The dimensions of the in-deck tank may vary according to the storage requirements or space availability. The application of in-deck tanks is possible for all type of offshore structures. Weight control and available space is often labeled as a critical issue for offshore projects. Therefore, one prefers the use of available steel instead of adding extra steel for tank equipment.

The in-deck tank is exposed to different pressures. Namely, self-weight, hydrostatic pressure, inertial load, vent head, sloshing pressure and external loads. Various limit states and pressure combinations are applied for the different parts of the in-deck tank; top, bottom and side walls. The sloshing assessment procedure is an important part of the strength checks necessary. For example, unity checks of the stress and possible deflection.

Sloshing or slosh occurs to a fluid when there is motion of the liquid inside an object. A distinction of sloshing pressures can be made. Namely, impulsive and non-impulsive pressures. Impulsive pressures are rapid pressure pulses between the liquid and the solid boundaries. This is referred to as sloshing behaviour of a fluid. Non-impulsive pressures are ordinary dynamics pressures for an oscillating fluid, they are slowly varying pressures that result from standing waves. These pressures are often referred to as oscillation pressures. More elaboration on the different fluid pressures is described in chapter 3.3.1. The impulsive sloshing of the fluid arises when the natural period of the fluid in the tank and the motion of the tank are close to each other. When both natural periods coincide, so called resonance occurs. During resonance conditions, the fluid behaves in a chaotic manner and sloshing impact pressures may increase drastically. The motion of sloshing is a highly non-linear and irregular process. It represents a dynamic extension of internal pressure effects beyond the static pressure. Various factors can influence its behaviour, like; motion characteristics, tank dimensions, filling levels and fluid properties. The complexity and chaotic behaviour of sloshing makes it hard to predict or estimate resulting pressures.

1.2. Problem Definition

The application of in-deck tanks in the Aasta Hansteen SPAR project faced difficulties concerning the sloshing pressures. No clear method or approach to estimate the sloshing pressures was present. Literature nor Rules and regulations describe an approach applicable for these type of tanks. To cope with this problem, a conservative method has been defined by CB&I. However, this approach is considered a temporary solution.

For possible future application of the in-deck tanks, more insight on fluid behaviour is essential. With a specific focus on the sloshing pressures. The basic problem of sloshing involves the estimation of the pressure distribution, impact area, forces, moments and natural frequencies of the free liquid surface. Due to the chaotic and highly non-linear behaviour of sloshing, no mathematical solution can be defined analytically. Therefore, a different approach in determining the sloshing pressures is necessary.

1.3. Scope

The scope of this research contains the assessment of sloshing behaviour in the so called in-deck tanks. Sloshing behaviour consist of different topics, for instance; fluid behaviour and pattern, occurrence of sloshing, sloshing impact areas and pressure order of magnitude. These topics are mainly focused on the resulting part of the sloshing research. On the contrary, the input parameters for sloshing have been studied as well. Which are, as motioned in the general introduction; motion characteristics, tank dimensions, filling levels and fluid properties.

The aim of this research is to get a better understanding of the sloshing behaviour for specific cases. The different variables and tank applications make it impossible to answer such a general research topic in detail. A methodology strategy is chosen in order to tailor this research specifically for possible future application of in-deck tanks. Where the framework and assumptions indicate the boundaries of the research. A study is carried out to define the scenarios which are best suited to be assessed.

Normally, in order to get an understanding of fluid behaviour, experiments are carried out. With the help of model scale test, fluid behaviour can be observed and measurements taken. This is especially effective for well-defined cases. However, when the list of cases increase, scale model test for every case becomes financially unattractive. Therefore, the use of a numerical model may help out to gain a broad insight on the sloshing phenomenon. Nowadays, a balanced combination of numerical models and experiments are widely used in the industry. The numerical models are often referred to as CFD simulations. CFD stands for Computational Fluid Dynamics and include numerical methods in order to simulate non-linear and dynamic problems. The use of CFD is increasing rapidly in the last decade due to major improvements of software capabilities, computational power and a decrease of hardware costs.

1.4. Relevance of Scope

One may question, why would more insight on the sloshing behaviour be relevant? Most offshore structures are considered huge, with massive steel frames and plates. How can sloshing in storage tanks cause problems when they are relatively small compared to the structure?

Especially in the offshore, where weight control is a big issue and considered important, one prefer to design accurately and without over dimensioning. Furthermore, the relation between the strength and the fatigue life of the construction have to be highlighted. Structural engineers are anxious to know all the forces that act upon and inside the structure they are designing. Hence the interest for fluid behaviour in storage tanks. While it may seem innocent, sloshing can result in high pressures and decrease of fatigue life.

The assessment of sloshing behaviour will give more understanding on this phenomenon. With a specific relation to in-deck tanks, it may result in a tool that can be used in future designs of offshore structures. Furthermore, as mentioned in the scope, the research is tailored for the specific application of in-deck tanks. The range of different cases assessed can be converted into a sensitivity study. Where a CFD approach is the perfect way to carry out such a broad study.

This research also contributes to the planning of the leading engineer. General knowledge of the sloshing pressure is important related to the structural assessment of the in-deck tank boundaries. For an accurate design of preliminary structural set-up and properties, it is favourable to have well founded input of the possible sloshing pressures. Whereby, in an early stage of designing, the stress levels and deflections of the tank walls can already be checked. Solid initial input of the sloshing phenomenon is important, because an in-depth and specially trimmed assessment of the sloshing is normally conducted in a later stage of the structural design in a project. Initial assessment of the sloshing exclude surprises and may reduce possible delay of the project.

1.5. Objectives

The goal of this research is to develop an approach on the analysis of possible sloshing behaviour inside in-deck tanks. Related to the specific fluid behaviour, occurrence of sloshing, sloshing pressures and impact areas. In order to reach this goal a number of objectives are defined.

Establish boundaries of the case definition for the input parameters; tanks size, fill level, fluid type and tank motions:

- Research scenario study
- Case Definition

Objectives for the CFD simulation carried out by ComFLOW:

- Phase 1 - Simulation of general cases
- Phase 2 - Simulation of selected sloshing cases
- Verification and validation of CFD model

After the completion of the objectives above, the following objectives can be met:

- Comparison of CFD results (Phase 1)
- Statistical application to CFD results (Phase 2)
- Analysis and interpretation of simulated data.
- Establish conclusions, recommendations and final report

1.6. Thesis Outline

This thesis report is organized in chronological order with respect to the research. Chapter 1 introduces the subject supported by a problem definition, scope, relevance of scope and the objectives. Chapter 2 includes the methodology which includes the strategy, framework, assumptions and alternatives.

Chapter 3 describes the physics included in the research. Followed by chapters 4 and 5 which elaborate on Empirical methods and Analytical models related to sloshing. Where Chapter 6 describes the CFD ComFLOW executable.

Chapter 7 and 8 include the case definition, results and result analyses for both Phase 1 and Phase 2. Concluding with Chapter 9, which contains the Conclusions & Recommendations.

2

Research Methodology

The research methodology generally describes the process that is used to collect information and data for the purpose of making decisions. Quantitative techniques have been used with the employment of mathematical models and the process of measurements. The research methodology applied includes the definition of research scenarios, a two-phased CFD analysis, concluding with a statistical evaluation in order to interpret the results.

2.1. Strategy Evaluation

There are different ways to study or evaluate a phenomenon like sloshing, as described in 2.5 Alternatives. However, the core of this research includes the use of CFD software to simulate the fluid behaviour inside in-deck tanks. Two important checks have to be made in order to give more insight on how the simulated values can be interpreted. Namely, validation and verification. Often the application of CFD is directly related to the issue of computational limitations. Due to limited computational power and time, a balance between the time simulation and grid size accuracy is sought. The maximum computational capabilities are used in the available time frame of the research.

Several classification societies describe a sloshing assessment procedure for LNG membrane tanks, namely, Bureau Veritas [3] (BV), Det Norske Veritas [7] (DNV) and Lloyd's Register [18] (LR). This procedure can be applied for in-deck tanks as well and perfectly illustrates which part is included or excluded for this research, presented in Figure 2.1 on the next page.

No experiment related to the in-deck tank cases is carried out and is excluded from the research. This decision has a significant impact on the validation of the CFD results. However, a different option for validation is carried out with the comparison to benchmark tests.

The main part of the research focuses towards numerical simulations and the analysis of sloshing cases. However, no sloshing cases will also be assessed. In the event that no sloshing occurs and the fluid inside is oscillating, occurring pressures are limited and linear fluid behaviour can be expected. There is no clarity on a method or approach that is best suited to calculate the pressures in this event. A shortlist of possibilities include a static approach, a method applied by CB&I, an empirical method and an analytical model. This concludes in a comparison of the different methods, presented in chapter 7.3 at page 34, where the best method is illustrated.

As mentioned, the research is split into two phases. Phase 1 is related to the execution of a general 2D CFD simulation. Part of this phase is the definition of the cases and gather know-how of the CFD software. A well-balanced list of cases is defined in Chapter 7.1 with the help of a research scenario study, described in Appendix C. The broad approach of this phase illustrates the urgency of a general sloshing understanding related to in-deck tanks. The analysis of the results from phase 1 should conclude the cases where sloshing does occur. Phase 2 includes long time simulations of the sloshing cases in order to generate statistical data. Statistical post processing is used to interpret the data and achieve the main goal, the order of magnitude for different sloshing cases.

2.2. Sloshing Assessment Procedure

A sloshing assessment procedure for LNG membrane tanks is described by Lloyd's Register [18] and can be applied in this research as well, presented in Figure 2.1 below.

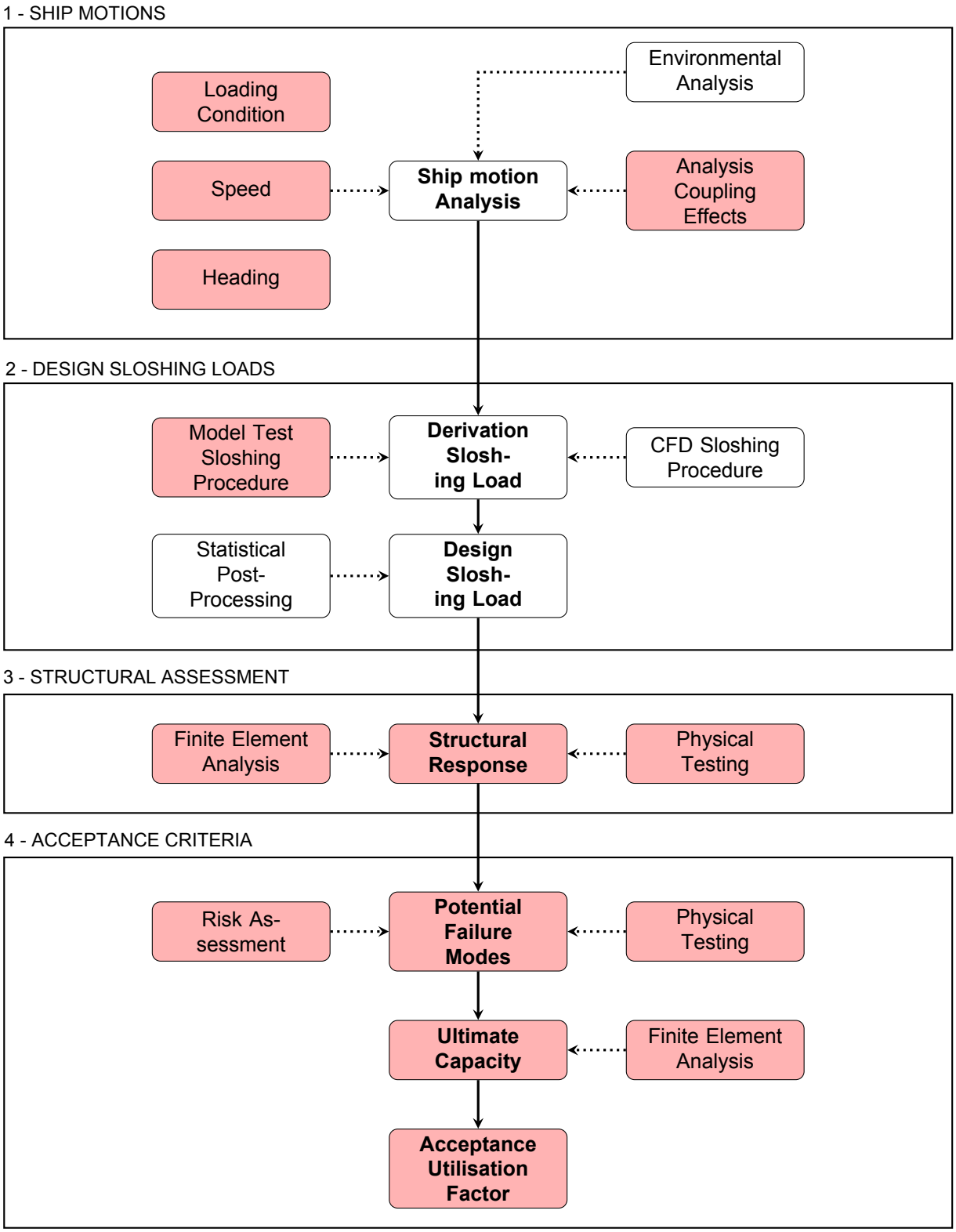

Figure 2.1: Sloshing Assessment Procedure - Red tiles are excluded from this research.

2.3. Framework

The framework indicates the boundary of the research. Critical decisions of what is included and excluded in this research is listed.

- After a preliminary study and discussion within CB&I, it is chosen to fully dedicate this research to the possible in-deck tank application on FPSO's. Complementing with a basic analysis of the in-deck tank application for the Aasta Hansteen SPAR.
- Two types of analysis can be made in relation to sloshing, namely, the fatigue lifetime and strength of the structure. This research will only focus on the strength analysis. Which relate to the sloshing impact pressures and general fluid behaviour. Consequently, any research into the fatigue lifetime is excluded.
- In collaboration with the Delft University of Technology, the CFD software package of ComFLOW is provided. This CFD software will be used for the simulations of the defined research scenarios. More elaboration on the CFD executable is defined in Chapter 6 at page 23.
- The research contains CFD simulations for specific parameters of the in-deck tank, so called 'cases'. Due to restrictions of time and limitations of resources not all possible situations or in-deck tank dimensions can be analysed. Think about limited computational power to carry out a CFD analysis. Therefore, a selection of scenarios has been made. This resulted in a two-phased CFD approach. First, a list of 66 scenarios are simulated in 2D, concluding with a thorough analysis of the results. With the help of this analysis, sloshing cases are selected for a more in-depth 2D CFD analysis with a longer time duration. Complementing with a total of 78 simulation cases. More details on the cases that have been defined for phase 1 can be found in Chapter 7.1 at page 28.
- With the use of CFD software packages, one have to be cautious for the results that are simulated. In what way does the simulation meet reality and what kind of conditions and assumptions are applied. In order to evaluate the core of this issue, two important check-ups of validation and verification are done. In short, verification holds, do we solve the equations right? Where validation includes, do we solve the right equations? Verification of the ComFLOW executable is done with a so called 'grid independence study'. More detail on this topic can be found in appendix F at page 141. Validation of CFD software is preferred to be done with experiments. However, this is not feasible within this research. Other options are a comparison to analytical methods or other numerical data available. The ComFLOW executable has been validated extensively with experiments for specified fluid behaviour. However, sloshing behaviour in in-deck tanks is not included in this validation. This calls for a different approach of validation. Therefore, a comparison with experimental benchmark tests is carried out. Which can be considered the best validation possibility that can be implemented in this research. More detail on this topic can be found in appendix G at page 155.
- The most important challenge is the interpretation of the simulated results, as conclusions of the results have to be defined with caution. A well founded understanding of what the results mean is key. Therefore, a statistical post-processing analysis is carried out. This analysis is described in chapter 8.2 at page 39.

2.4. Assumptions

In extension of the framework, assumptions have been made in order to bound the research to a manageable project.

- The in-deck tank is considered smooth and rectangular within the established effective length and breadth. In reality the tank contains small notches, holes, beams and occasionally equipment and pipelines through or in the tank. These disturbances create extra friction and has a positive effect on reducing the sloshing pressure. When neglected, the absolute maximum pressures that may occur in the tank are simulated. Therefore, the assumption of a rectangular and smooth tank, can be interpreted as a possible extra safety margin for the highest sloshing pressures. Concluding in the worst case of sloshing behaviour, which coincides perfectly with the ULS and ALS conditions applied for the strength calculations of the structure.

- A specific note has to be made relating to the disturbances mentioned above. They are fully excluded from this research. No assessment have been done on possible impact pressures on them. As the disturbances are too case specific, no decent generalization is possible. In the event of future application of in-deck tank, a specific assessment for these disturbances have to be made.
- The rectangular tanks is assumed to be closed at all times. The material of the tank is considered to be impermeable. Therefore any vents or holes in the tank are excluded.
- The deformation effect of the tank boundaries will not be taken into account. The fluid behaviour itself, or any external force does not effect the tank boundaries. The tank is assumed to be rigid. The only considered external force is gravity, $\mathbf{f} = \mathbf{g} = (g_x, g_y, g_z)^T$.
- In order to establish the numerical model which is used in ComFLOW, fundamental assumptions are made. The fluid in the domain is assumed to be homogeneous and incompressible. Thus ρ = *constant* everywhere at all time. This consequently implies that $\partial\rho/\partial t = 0$ and $\nabla\rho = 0$. More elaboration on the fluid properties can be found in section 3.1 at page 9.
- The tank is filled with only two components, air and the fluid defined to be inside the tank. It is assumed that there are no other solids, liquids or gasses present. Concluding in only one fluid for the simulation domain. Temperature variation or any subsequent result of temperature variation is ignored.
- When the in-deck tanks are operational, the fluid inside may be used for a wide variety of processes. Some of the processes include pressures or possibilities for back pressures. As the in-deck tank is assumed to be closed, any external pressure fluctuations are excluded.
- The coupled motion analysis between the sloshing inside the in-deck tank and offshore structure behaviour is excluded. It is recognized that coupled motions are always present. However, the influence of sloshing related to the offshore structure behaviour is not the focus of this research.

2.5. Alternatives

It is chosen to use CFD in order to simulate the fluid behaviour and estimate sloshing pressures. However, there are also other alternatives to get an understanding of the sloshing behaviour for in-deck tanks.

The best alternative compared to CFD would be experiments. Experiments could even give a better insight compared to CFD simulations. However, the financial aspect of conducting experiments is the main showstopper. To carry out a significant amount of cases would be to expensive. Therefore, normally a combination of CFD analysis and experiments is carried out. Whereby the use of CFD simulations covers the quantitative aspect in number of cases. While experiments validate the CFD approach and cover the qualitative aspect of checking the numerical method.

Another alternative could be an analytical approach. One of these Analytical models is described in chapter 5. However, the application of analytical models for non-linear fluid behaviour is severely restricted. When the fluid inside the tank hit resonance conditions and starts sloshing, the fluid behaviour becomes highly non-linear. From the moment non-linearity is present, analytical models are limited in accurately predicting fluid behaviour.

Furthermore, rules, regulations and guidelines can give more clarity on the issue of sloshing. There are a few guidelines that describe something on the sloshing topic. Mostly these formulations are described from a empirical point of view and are related to LNG tanks. However, again firm restrictions on the application of the formulas are stated. Chapter 4 describes an empirical approach stated by rules and regulations.

3

Physical Model

The physical model is defined first and describes the assumptions and rules that are applied during the research. It helps to make clear what is implemented or neglected in the calculations and simulations.

3.1. Fluid characteristics

The Fluid characteristics implemented in the physical modal are related to the Navier-Stokes equations used in the numerical model. In order to solve the Navier-Stokes equations, certain assumptions have to be made. Which is stated in section 2.4 Assumptions in Section 2 Research Methodology. The list of fluid characteristics assumed is stated below.

- **Homogeneous - Inhomogeneous;** a fluid is considered homogeneous when there is a smooth distribution, without discontinuities or jumps, and hold the same properties everywhere. The opposite concludes for an inhomogeneous fluid. The fluids considered in all the models are homogeneous.
- **Compressible - Incompressible;** an incompressible fluid implies that the volume of the fluid will not reduce by an increase of pressure. Therefore, the fundamental requirement of an incompressible fluid is a constant density within an infinite small volume. Compressibility matters especially for gasses under high pressures. Again the opposite holds for a compressible fluid. The fluids present inside the in-deck tanks are considered incompressible. Thus ρ = *constant* everywhere at all time. This consequently implies that $\partial\rho/\partial t = 0$ and $\nabla\rho = 0$.
- **Viscous - Inviscid / Rotational - Irrotational;** viscosity and rotation of a fluid are closely related to one another. When a fluid is viscous and shear effects are present, the fluid is considered to be rotational. The opposite holds for an inviscid fluid. Where the shear effects are zero and the fluid is irrotational. However, a more detailed subdivision can be made of local and global rotation. The in-deck tank is considered to be rectangular and smooth, which conclude in locally irrotational behaviour of the fluid. However, during the occurrence of sloshing, wave breaking and overturning occurs (illustrated in chapter 3.3 fluid flow). This concludes in a global rotational behaviour of the fluid.

3.2. Coordinate System

In order to give a clear visualisation of the coordinate systems used, Figures 3.1 (SPAR) and 3.2 (FPSO) are presented below. Furthermore, Table 3.1 illustrates the units for the six degrees of freedom. This should avoid misconceptions of the dimensions and axes presented in this report. An SPAR and FPSO are the only offshore structures considered in this research.

	Surge	Sway	Heave	Roll	Pitch	Yaw
DOF	η_1	η_2	η_3	η_4	η_5	η_6
Position	x	y	z	ϕ	θ	ψ
Unit	[m]	[m]	[m]	[rad]	[rad]	[rad]
Velocity	u	v	w	p	q	r
Unit	[m/s]	[m/s]	[m/s]	[rad/s]	[rad/s]	[rad/s]
Acceleration	a_x	a_y	a_z	a_ϕ	a_θ	a_ψ
Unit	[m/s²]	[m/s²]	[m/s²]	[rad/s²]	[rad/s²]	[rad/s²]
Forces & Moments	F_x	F_y	F_z	M_x	M_y	M_z
Unit	[kN]	[kN]	[kN]	[kN m]	[kN m]	[kN m]

Table 3.1: Definition - Six degrees of freedom

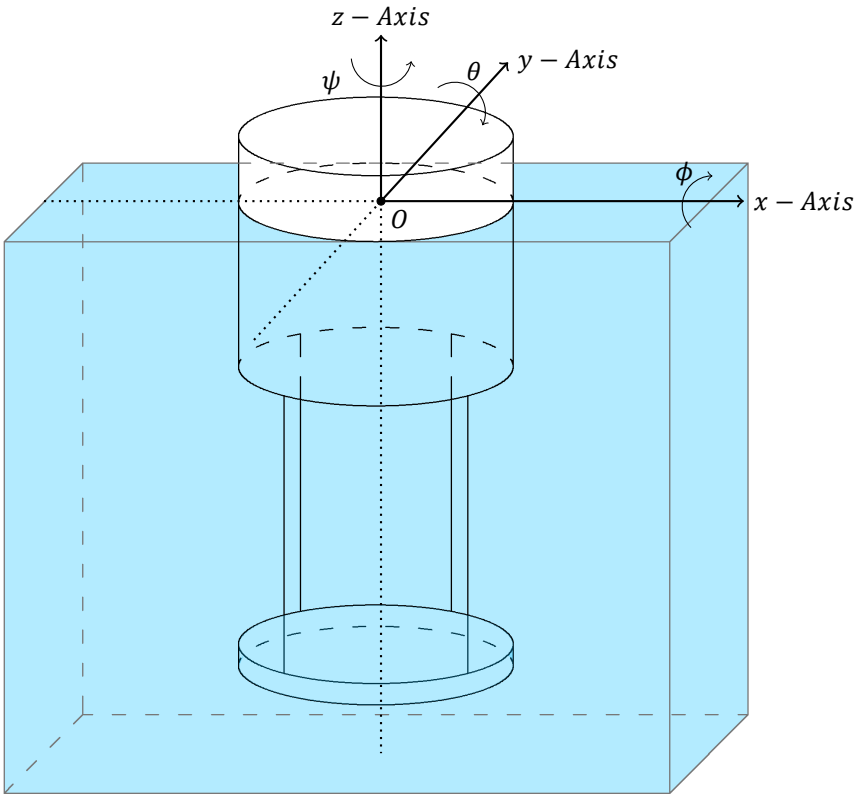

Figure 3.1: SPAR Structure - Coordinate System

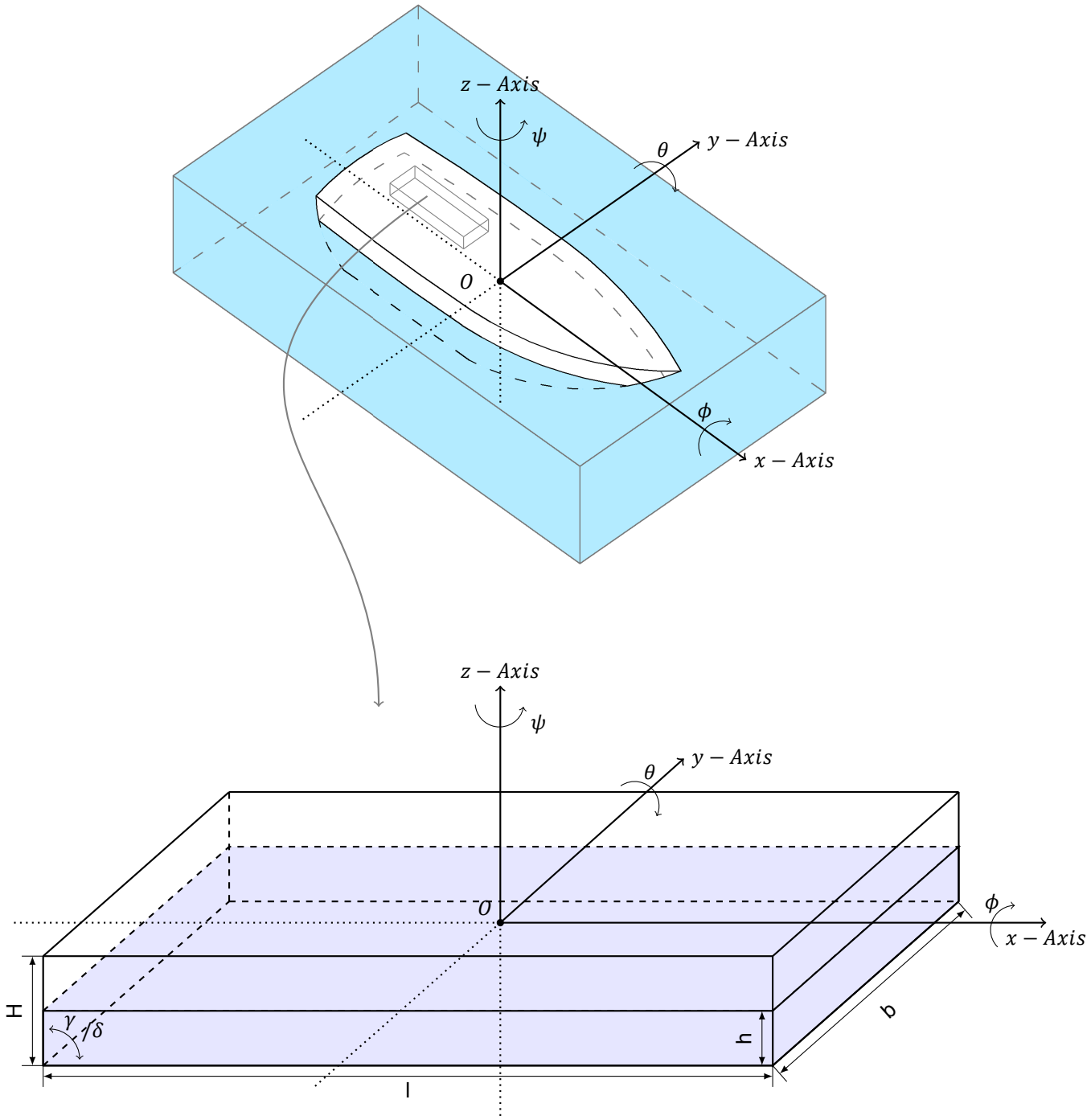

Figure 3.2: FPSO Vessel & In-deck Tank - Coordinate System

3.3. Fluid flow

Sloshing behaviour is expected when the natural frequency of the tank motion is close to the natural frequency of the fluid in the tank. The amplitude and behaviour of the slosh, in general, depends on various parameters. Namely, the DOF, amplitude and frequency of the tank motion, but also the fill level, liquid properties and tank geometry. The sloshing of fluids in tank compartments is a highly non-linear phenomenon. Where the loads and pressures produced may result in structural damage of the tank. Sloshing occurs in various fluid behaviour and fluid impact types. The interpretation and definition of sloshing varies in different literature. Therefore, the following sub-chapters describe and illustrate the definition of sloshing considered and helps to get an idea of different fluid flow types.

3.3.1. Sloshing Pressures

The sloshing of a liquid is interpreted as dynamic behaviour and can be divided into two types of dynamic pressures. Some literature refers to impact and oscillating pressures, others to impulsive and non-impulsive pressures. Therefore, a sloshing impact pressure is defined as impulsive, while oscillating pressures are defined as non-impulsive. Impulsive pressure are rapid pressure pulses between the liquid and solid boundaries. These pressures occur when the resonance conditions are met and sloshing is active. Non-impulsive pressures are ordinary dynamic pressures for an oscillating fluid, described is slowly varying pressures that result from standing waves. In this state of low dynamic pressures, the natural periods vary sufficiently and no sloshing is present.

Figures 3.3 and 3.4 below, show snapshots of three time instances for two different fluid behaviour cases. One is related to non-impulsive oscillating behaviour and the second relates to impulsive sloshing impact behaviour. A clear difference is present after the impact of the fluid. In the oscillating case, the fluid slowly returns to starting conditions. Where for the impulsive case a jet is formed due to the sloshing impact. For clarity purposes the impulsive sloshing behaviour is defined by impact pressures, sloshing. Where non-impulsive sloshing behaviour is defined by oscillating pressures, no sloshing. In the event of a transition period between impact and oscillating pressures, one may call it semi-sloshing.

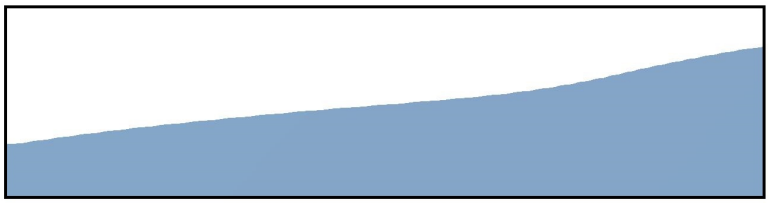

(a) t_1 Before impact

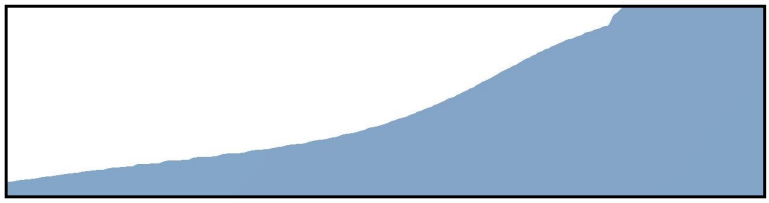

(b) t_2 During impact

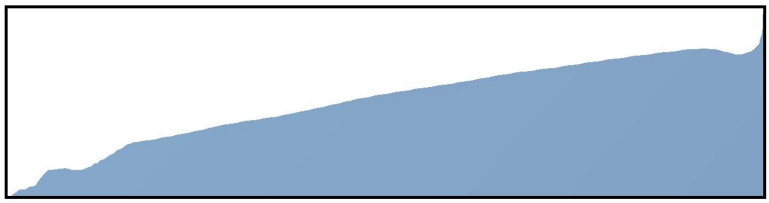

(c) t_3 After impact

Figure 3.3: Illustration - Non-impulsive sloshing oscillation pressure

(a) t_1 Before impact

(b) t_2 During impact

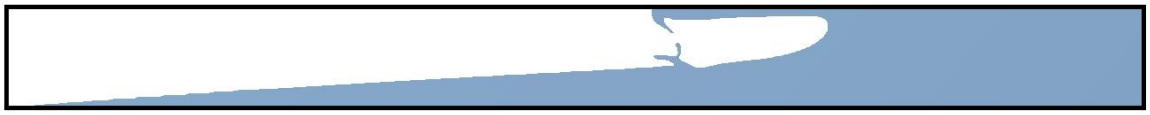

(c) t_3 After impact

Figure 3.4: Illustration - Impulsive sloshing impact pressure

3.3.2. Fluid impact types

After the separation of sloshing type. One can go in more detail and describe different sloshing impact behaviour as well. Based on numerous model test and numerical computations, Bureau Veritas [3] and Faltinsen [15] illustrate and define two groups for sloshing impacts. Namely, side wall impact (low fillings) and roof impact (high fillings). Related to these fillings, various impact types for the side wall and roof are described, listed in Figure 3.5 below. An illustration of these various impact types can be found in Appendix A

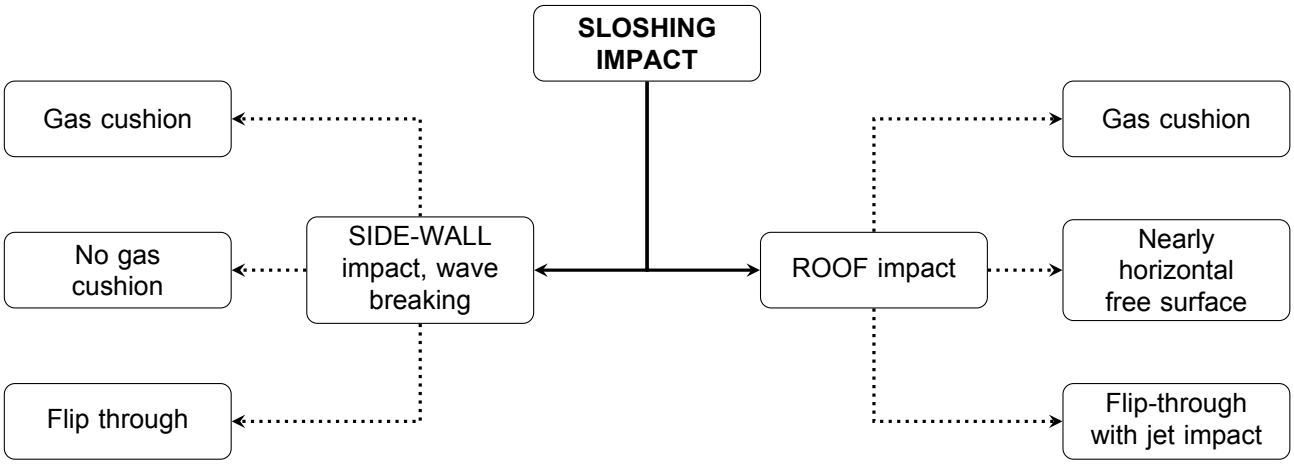

Figure 3.5: Flow chart - Sloshing impact types

3.3.3. 3D Flow phenomena

As described in 2.3 Framework, only 2D scenarios are considered in this research. This concludes the exclusion of 3D flow phenomena. Where any 3D sloshing or flow phenomenon is not included in the simulations. Even though the CFD simulations shall only consist of a 2D approach, it is important to take notion of 3D flow phenomena.

2D simulations do not take the vertical displacement of the fluid COG into account. Which is related to large amplitudes of free surface motion. A 2D approach also fails to predict the complex surface phenomenon of rotary sloshing. This phenomenon include non planar unstable motion of the free surface associated with rotation of the nodal diameter.

Swirling rotary wave motions may occur during horizontal harmonic excitations and may cause diagonal waves. Ibrahim [17] describes two rotary sloshing experiments in shallow liquid tanks. One experiment include a circular container, where the other used a centaur G tank with conical walls. The forced motions are usually set under lateral sinusoidal excitations. The different tank shapes relate to critical fill levels of the fluid where the rotary sloshing occurs. The rotary wave motion lagged the excitation by approximately 180 degrees and appeared to be spatially out of phase. As the excitation frequency was slowly increased to the resonance frequency. Both normal and rotary slosh combined and formed a complex result whose phase shifted with frequency. Eventually, the rotary slosh component became the dominant factor with a phase shift of 270 degrees. Further slow increase of the frequency to the natural frequency resulted in pure normal slosh with the disappearance of the rotary wave.

4

Empirical & Conservative Methods

4.1. Conservative Method CB&I

In-deck tanks are applied for the first time in the Aasta Hansteen SPAR project of CB&I. Insufficient understanding of the fluid behaviour and occurring pressures caused problems. A conservative approach had been established that should predict the sloshing pressures in the tank. This approach consist of the following design basis and assumptions:

- Acceleration values includes the heel effect for global analysis. The additional hydrostatic load due to maximum heeling is hereby assumed to be considered. Therefore, only the lateral accelerations of the x and z axis are taken into account. And exclude the rotational accelerations.
- The in-deck tank is assumed to be full of liquid at all times except during transport conditions, when its empty.
- The minimum sloshing pressure on web frames and girder panels in cargo and ballast tanks shall be taken as 20 kN/m². As prescribed by rules and regulations, DNV [8].
- Presence of vent head is included. Where its assumed that the vent head is also fully filled with liquid at all times.

Six load cases are defined and included in the unity check of the construction members. A sketch of the in-deck tank situation for maximum pressures is presented in Figure 4.1, followed by the load cases listed in Table 4.1. Normally, a unity check for different combinations of load cases and load factors is performed. Resulting in a list of limit states, for example; ULS, ALS and SLS conditions.

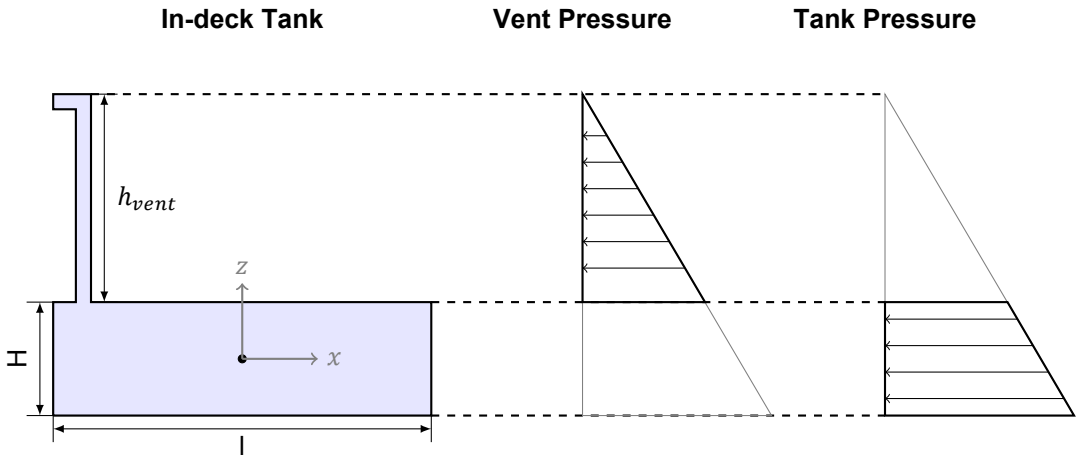

Figure 4.1: Sketch - 2D Load case of Aasta Hansteen SPAR

Load case	Description
L1	Self weight of tank plates
L2	Hydrostatic load
L3	Hydrostatic load due to inertia
L4	Vent head
L5	Sloshing load
L6	Slamming load (external force on tank)

Table 4.1: Definition - Load cases of CB&I conservative method

In order to implement this method for comparison purposes, some refinement is done. The theoretical assumptions stated in section 2.4 are applied and result in the exclusion of load cases; (1) self weight, (4) vent load and (6) external slamming load. Which leaves the hydrostatic, inertial and sloshing load. As the tank is assumed to be closed and excluded from any external forces. Concluding in the sketch and equations presented in Figure 4.2 and Eq. (4.1) -(4.3).

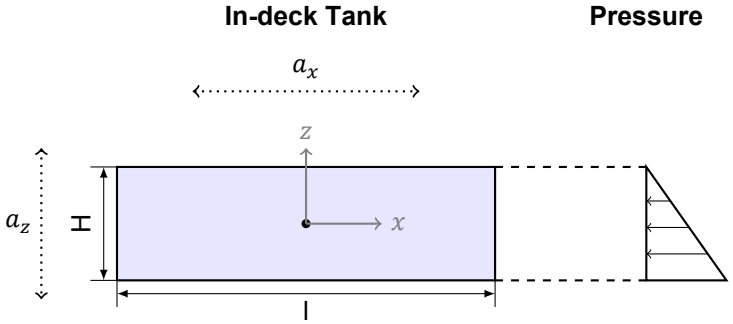

Figure 4.2: Sketch - 2D Load case redefined as CB&I conservative method

L2 - Hydrostatic Load

$$p_h = H \cdot \rho \cdot g \qquad p_h(z) = \left| z - \frac{1}{2}H \right| \cdot \rho \cdot g \tag{4.1}$$

L3 - Inertial Load

$$p_i = (H \cdot \rho) \cdot a_t \qquad p_i(z) = \left(\left| z - \frac{1}{2}H \right| \cdot \rho \right) \cdot a_t \tag{4.2}$$

Where $a_t = a_x + a_z$ is defined as the combined acceleration and motion acting on the in-deck tank.

L5 - Sloshing Load

$$p_s = 20 \quad kPa \tag{4.3}$$

The load case combination varies for the tank bottom, wall and top. Concluding in Eq. 4.4, 4.5 and 4.6 below.

$$p_{\,top}(z) = H \cdot \rho \cdot |a_x| + 20 \cdot 10^3 \tag{4.4}$$

$$p_{\,wall}(z) = \left| z - \frac{1}{2}H \right| \cdot \rho \cdot g + \left(\left| z - \frac{1}{2}H \right| \cdot \rho \right) \cdot a_t + 20 \cdot 10^3 \tag{4.5}$$

$$p_{\,bot} = H \cdot \rho \cdot g + H \cdot \rho \cdot a_t \tag{4.6}$$

4.2. Rules and Regulations

The leading agencies developing up-to-date rules and regulations related to offshore structures are analyzed. This includes; International Organization of Standardization (ISO) , Det Norske Veritas (DNV), American Bureau of Shipping (ABS), Lloyd's Register (LR), Bureau Veritas (BV) and American Petroleum Institute (API). For each classification institute, the applicable regulations that may contribute to an empirical formulation are filtered and stated.

The ISO [16] contains a small description on sloshing in cargo tanks of ships. Sloshing is the dynamic magnification of internal pressure acting on the boundaries of partially filled tanks due to internal fluid motion. Sloshing occurs if the natural periods of the fluid and the motions of the structure are similar. In some cases, the fitting of swash bulkheads or other baffle devices can be necessary to minimize sloshing effects. Sloshing-induced actions shall be considered in the structural design. Sloshing analysis shall be performed for affected tanks of floating structures as necessary.

Multiple DNV codes include a statement on sloshing, [6], [21], [5]. Where [8] describes several formulae for the minimum sloshing pressure on web frames and girder panels in cargo and ballast tanks. The general minimum sloshing pressure in tanks without double sides and bottoms shall be taken as 20 kN/m². However, for the strength members located less than 0.25 l away from transverse wash and end bulkheads, the pressures shall not be takes less than presented in Figure 4.3 below. In other words, the sloshing pressures at the tank boundaries. One can conclude that the area of the impact are hot-spots of high sloshing pressures. The sketch presented defines the impact area for both the oscillating pressures and impact pressures. In the case of tanks oscillations, the sloshing pressures is described in Eq. (4.7).

In case of sloshing under resonant conditions, the impact pressures for both the upper and lower part of the tank are defined by Eq. (4.8) and (4.9). Hereby an important design condition to apply this regulation cannot be met. The rules describe that the $l > 0.13L$ should be met. In-deck tanks in this order of magnitude, around 40 meters, will never exist. This design condition shall therefore be neglected.

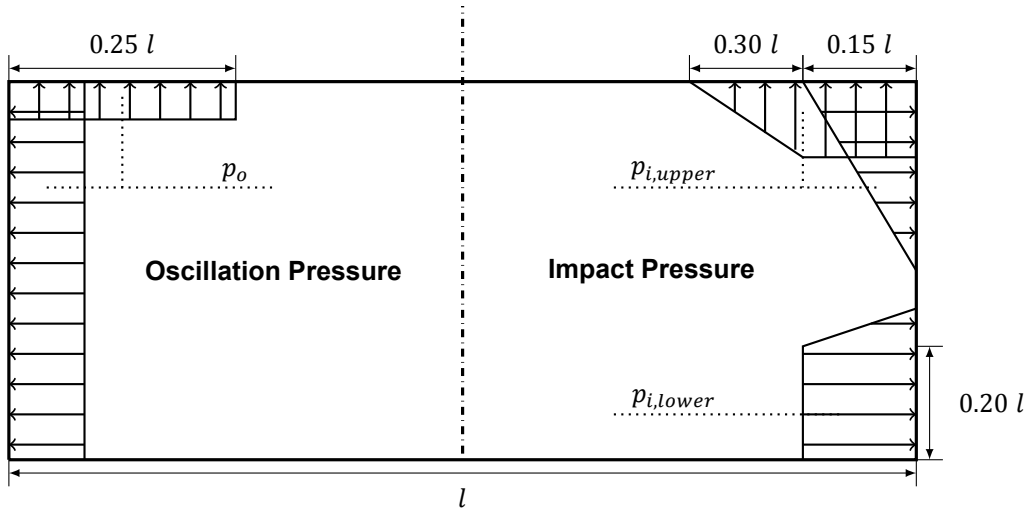

Figure 4.3: Sketch - 2D pressure distribution of DNV empirical method

$$p_o = \rho \cdot g \cdot l \cdot k_{f,s} \cdot \left[0.4 - \left(0.39 - \frac{1.7 \cdot l}{L}\right) \cdot \frac{L}{350}\right] \tag{4.7}$$

$$p_{i,upper} = \rho \cdot g \cdot k_{f,upper} \cdot \left(\frac{220 \cdot l}{L} - 7.5\right) \cdot \sin^2 \gamma \qquad \text{for,} \quad \frac{l}{L} < \frac{350 + L}{3550} \tag{4.8}$$

$$p_{i,lower} = 1.42 \cdot \rho \cdot g \cdot k_{f,i,lower} \cdot l \cdot \sin^2 \delta \tag{4.9}$$

ABS [22] regulation contains standards related to liquefied gas carriers with independent tanks. Even though the fluid substance is different to the fluids of the in-deck tank, the approach on sloshing behaviour could give some indication. The regulations prescribe that the dynamic load of sloshing should be considered in the structural evaluation. Furthermore, a description of the free surface natural period is defined. The liquid motion natural period have to be examined for all cargo tanks which are partially filled between 10% and 90%. Critical filling levels have to be avoided so that the natural periods of the free surface and tank motion does not coincide. The natural periods of the fluid motions in the tank are to be at least 20% greater or smaller than that of the relevant ship's motion.

If critical filling levels cannot be avoided, use of so-called bulk heads are recommended to use. As they eliminate the possibility of resonance. This option may be waived if it can be demonstrated through the application of model experiments or numerical simulation that sloshing impacts can be withstand by the tank boundary structure. A description on the calculation of the natural periods is described by Eq. (4.10). If one rewrites this equation, it can directly be related to Eq. (5.7) and Eq. (5.8) described in section 5.2.1 Natural modes. Repetitions of this formula can be found in DNV [7] and Faltinsen [15] as well.

$$T_x = \frac{l^{\frac{1}{2}}}{k_a} \qquad \text{With,} \quad k_a = \sqrt{\frac{\tanh(Z)}{\frac{4\pi}{g}}} \qquad \text{and} \quad Z = \frac{\pi \cdot h}{l} \tag{4.10}$$

LR [19] describes a small paragraph on sloshing in cargo tanks of ships, specifically related to LNG. The sloshing loads on a cargo containment system and internal component, induced by any specific motions, shall be evaluated based on allowable filling levels. When significant sloshing induced loads are expected to be present, special tests and calculations are required which covers the full range of intended filling levels. LR refers to experimental tests and CFD simulations that would give more insight on sloshing behaviour. More elaboration on the issue of experiments, CFD simulations and post-processing for LNG membrane tanks is described by Lloyd's Register [18].

BV and API have no significant rules or regulations related to sloshing inside tanks which includes empirical methods. However, BV published a guidance note on the design of sloshing loads for LNG membrane tanks, [3].

The implementation of three guidance notes BV [3], DNV [7] and LR [18]) on the design of sloshing loads for LNG membrane tanks is described in chapter 8.2 Statistical Analysis.

5

Analytical Model

5.1. Hydrostatic Pressure Model

Lets consider the most basic analysis of fluid pressure first, which is the hydrostatic pressure. All the dynamic factors of the tank behaviour, like velocity and acceleration, are excluded. The assumption of excluding dynamic forces is accepted for cases of high motion periods and low accelerations. Figure 5.1 describes the moment of maximum heeling in order to calculate the maximum hydrostatic pressures that could occur.

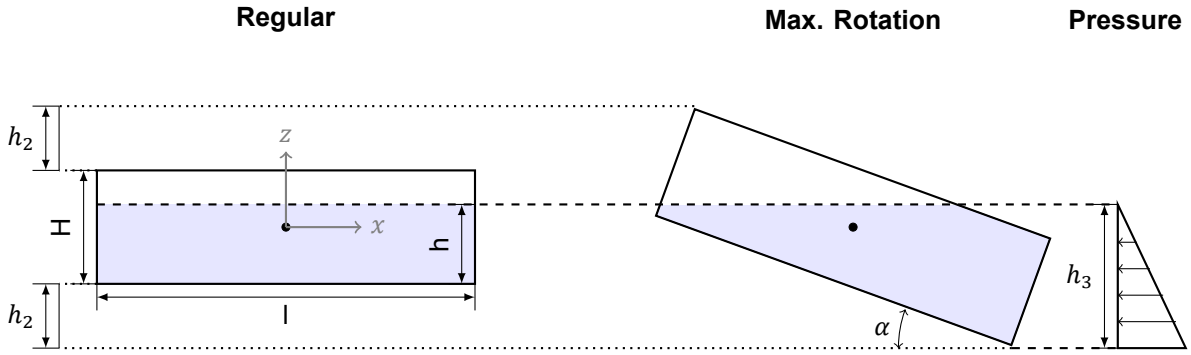

Figure 5.1: Sketch - 2D Hydrostatic pressure

The pressure calculation for specific points in the tank is represented by Eq. (5.1) - (5.4) below.

$$h_2 = \frac{l \cdot \sin(\alpha)}{2} \tag{5.1}$$

$$h_3 = \frac{h}{H} \cdot (H + 2h_2) \tag{5.2}$$

$$p_{max} = \rho \cdot g \cdot h_3 \tag{5.3}$$

$$p_{max}(x,z) = \left\langle \underbrace{\left[h_3 - \left(\frac{H}{2} + h_2\right)\right]}_{h_4} - \underbrace{\left[\left(\frac{|x|}{\frac{1}{2}l} \cdot h_2\right) + (z - h_2)\right]}_{h_{x,z}} \right\rangle \cdot \rho \cdot g \tag{5.4}$$

where Eq. (5.4) Is only valid if $h_4 > h_{x,z}$, otherwise max. point pressure result in ($h_4 < h_{x,z}$) $p_{max} = \rho \cdot g \cdot h$. In the event of $p_{max} < 0$ no hydrostatic pressure is present and $p_{max} = 0$.

5.2. Linear Model

Faltinsen [15] describes different sorts of linear models related to the topic of sloshing. Unfortunately, most models are not applicable to the in-deck tank sloshing situation. However, two analytical methods prove themselves useful. Namely, the natural modes and a linear theory. The natural mode approach gives insight on the order of magnitude for the resonant period, which is an important parameter in the sloshing assessment. Furthermore, the linear theory can be considered as the best way to describe sloshing pressures in a linear sense.

5.2.1. Natural modes

To start of a sloshing assessment, one needs to know the natural modes. The natural frequencies and corresponding natural eigen modes are nontrivial solutions for a tank with no excitations, where liquid mass conservation is a constraint. Figure 3.2 defines the inertial coordinate system referred to, with $\sum_0$ as the mean free surface, Q_0 as the tank volume and S_0 as the bottom surface of the tank, respectively.

First, the derivation for the natural frequency related to the mode of the free surface is described. Starting with a spectral boundary value problem using the linear sloshing problem approach in combination with kinematic and dynamic boundary conditions. Which result in

$$\begin{aligned} &\nabla^2\varphi = 0 \quad in \quad Q_0\,; \frac{\partial\varphi}{\partial n} = 0 \quad on \quad S_0 \\ &\frac{\partial\varphi}{\partial z} = \kappa\varphi \quad on \quad \sum_0\left(\kappa = \frac{\omega^2}{g}\right)\,; \int_{\sum_0}\varphi\, dxdy = 0 \end{aligned} \tag{5.5}$$

Where κ defines the spectral parameter in the boundary condition on $\sum_0$.

The goal is to find non-trivial solutions of the homogeneous spectral boundary problem, Eq. (5.5). This is done by separating the spatial variables, which leads to the following analytical solution for a three dimensional rectangular tank

$$\begin{aligned} &f_m^{(1)}(x) = \cos\left[\frac{n\pi\left(x+\frac{1}{2}l\right)}{l}\right] \qquad f_n^{(2)}(y) = \cos\left[\frac{m\pi\left(y+\frac{1}{2}b\right)}{b}\right] \\ &\varphi_{m,n}(x,y,z) = f_m^{(1)}(x) f_n^{(2)}(y)\frac{\cosh\left[k_{m,n}(z+h)\right]}{\cosh(k_{m,n}h)} \end{aligned} \tag{5.6}$$

with,

$$\begin{aligned} &\frac{\omega_{m,n}^2}{g} = k_{m,n}\cdot\tanh(k_{m,n}\cdot h) \\ &k_{m,n} = \pi\sqrt{\left(\frac{m}{l}\right)^2+\left(\frac{n}{b}\right)^2} \qquad , m+n\neq 0 \end{aligned} \tag{5.7}$$

Where m (related to the x-axis) and n (related to the y-axis) are defined to be the wave modes, $k_{m,n}$ are the wave numbers of the natural sloshing modes $\varphi_{m,n}$ for $m,n \geq 1$. When $n = 0$, $k_{m,0}$; the wave number coincides for two-dimensional sloshing along the x-axis. Furthermore, g represents the gravitational acceleration, h the fill level, and $f_m^{(1)}(x)$ and $f_n^{(2)}(y)$ the natural surface profiles.

The analytical solution provides the natural frequency related to the specific wave mode. In order to determine the natural period of the specific wave mode, the following relation is used

$$\omega_{m,n}\cdot T_{m,n} = 2\pi \tag{5.8}$$

The natural period of the 1st mode is an important indicator for the occurrence of sloshing. Therefore, ($\omega_{1,0}$) can be used for a two-dimensional analysis of the natural sloshing periods. While the natural sloshing mode is derived for a tank with no excitation, it can give a basic insight in the order of magnitude for the sloshing period. A substitution of the natural frequency (5.7) into (5.8) results in

$$T_{1,0} = \frac{2\pi}{\sqrt{\frac{g\pi}{l} \cdot \tanh\left(\frac{\pi h}{l}\right)}} \tag{5.9}$$

Where $T_{1,0}$ can be described as the natural sloshing frequency for the 1st natural sloshing mode of the 2D longitudinal tank slice.

5.2.2. Linear Modal Theory

Faltinsen [15] describes a linear model method that transforms the sloshing problem to a system of ordinary differential equations. A case of a rectangular tank under 3DOF forced excitations is described and derived. The model concludes in Eq. 5.10 and can be subdivided into a hydrostatic, hydrodynamic, potential and modal part

$$p_{max} = \underbrace{\rho \cdot g \cdot (h + 0.5 \cdot l \cdot \phi)}_{\text{static}} + \underbrace{\rho \cdot (0.5 \cdot l \cdot a_x + h \cdot a_z)}_{\text{dynamic}} - \underbrace{\Omega_{01}(x,z) \cdot a_\phi}_{\text{potential}} + \underbrace{\rho \sum_{i=1}^{\infty} \beta_m \cdot \bar{\kappa_m} 1 \cdot \omega_i(x,z)}_{\text{modal}} \tag{5.10}$$

The linear modal method focuses on the potential and modal part of the pressure equation. Where Ω_{01} represents the Joukowski Potential and β_i the wave elevations of the natural sloshing modes. In order to calculate β_i one makes use of the tank motions and hydrodynamic coefficients. A step-by-step approach for the calculation of the potential and modal part is described below.

Step 1 Find the natural sloshing modes, which are derived in section 5.2.1 previously.

Step 2 The Stokes-Joukowski potential.

$$\Omega_{01}(x,z) = -xz + 4 \sum_{m=1}^{\infty} \frac{l^2 \left[(-1)^m - 1\right]}{(j\pi)^3} \times f_m(x) \cdot \frac{sinh\left(\pi m \frac{z+0.5h}{h}\right)}{cosh\left(\pi m \frac{h}{2l}\right)} \tag{5.11}$$

Step 3 Hydrodynamic coefficients.

$$\mu_m = \frac{\rho l}{2\kappa_m} \qquad \text{where,} \qquad \omega_m^2 = g\kappa_m \tag{5.12}$$

$$\lambda_{2m} = \rho \left(\frac{l}{m\pi}\right)^2 \cdot \left[(-1)^m - 1\right] \qquad \lambda_{01m} = 2\rho l^3 \frac{(-1)^m - 1}{(m\pi)^3} \cdot tanh\left(\frac{\pi m h}{2l}\right)$$

Step 4 Right hand side function $K_m(t)$.

$$K_m(t) = -P_m \left[\ddot{\eta_2}(t) + S_m \ddot{\eta_4} + g\eta_4(t)\right] \qquad where, \qquad P_m = \frac{\lambda_{2m}}{\mu_m} \qquad S_m = \frac{\lambda_{01m}}{\lambda_{2m}} \tag{5.13}$$

Step 5 Solve for β_m

$$\ddot{\beta_m}(t) + \omega_m^2 \beta_m(t) = K_m(t) \tag{5.14}$$

6

ComFLOW

In order to simulate sloshing behaviour, various CFD software packages are applicable. There is a wide variety of CFD software, both commercial and open source, that are able to simulate sloshing. In this research the software package ComFLOW is used. ComFLOW is a program for the numerical simulation of fluid flow based on Navier-Stokes equations. The main objective for the ComFLOW project is the development of a user-friendly and validated numerical tool for marine and offshore industries to study complex free surface problems. The flexibility of it's application makes ComFLOW a suitable package to use.

Two dimensional CFD simulations are carried out with the application of two phases. Elaboration on the case definition for each phase is described in Chapter 7, Phase 1, and Chapter 8, Phase 2. This chapter will describe the mathematical and numerical models of the ComFLOW executable that are used. Namely, conservation laws, computational domain and grid, temporal discretization, solution technique and CFL-number. Elaboration and detail on the fundamentals are clarified by van der Plas et al. [24], Düz [4] and Kleefsman [10].

6.1. Mathematical Model One-Phase Flow

When the fluid is treated as a homogeneous continuum, as described in section 2.4 at page 7, the conservation laws of physics can be used to describe the fluid flow in a given domain. The laws subjected are the conservation of mass and conservation of momentum. Where the conservation law of energy is effectively replaced by the incompressibility condition of the fluid.

Conservation Laws

Derivations of the conservation laws are well documented and for the sake of brevity, only the final forms of these laws are stated below.

Conservation of mass

In an arbitrary and fixed control volume Ω with boundary Γ, conservation of mass can be stated in integral form as follows

$$\int_{\Gamma} \mathbf{u} \cdot \mathbf{n} \, d\Gamma = 0 \tag{6.1}$$

where $\mathbf{u} = (u, v, w)^T$ is the flow velocity and $\mathbf{n}$ is the normal vector pointing outward along the boundary of the control volume. The term on the left hand side of (6.1) denotes the net inflow of mass through the boundary of the control volume, which is equal to zero.

Conservation of momentum
Based on another fundamental physical principle, Newton's second law, the conservation of momentum for fluid flow can be stated. Taken the assumptions into account, the equation can be written as

$$\int_{\Omega} \frac{\partial \mathbf{u}}{\partial t}\, d\Omega + \int_{\Gamma} \mathbf{u}\,\mathbf{u}\cdot\mathbf{n}\, d\Gamma = -\frac{1}{\rho}\int_{\Gamma} p\mathbf{n}\, d\Gamma + \nu \int_{\Gamma} \nabla\mathbf{u}\cdot\mathbf{n}\, d\Gamma + \int_{\Omega} \mathbf{f}\, d\Omega \tag{6.2}$$

Where ν is the kinematic viscosity, $\nu = \mu/\rho$. $\nabla = (\partial/\partial x, \partial/\partial y, \partial/\partial z)^T$ is the gradient operator and **f** represents the external body forces acting on the fluid such as gravity, centrifugal and Coriolis forces. In equation (6.2), the term on the left indicates the time rate of increase of momentum in Ω. The increase is related to the three parts on the right hand side, respectively: The net inflow of momentum through the boundary Γ, contribution from the surface forces acting on the surface of the control volume, and contribution from the body forces which act directly on the fluid in Ω.

As the incompressibility condition effectively replaces the conservation law of energy, two conservation laws are left in order to model the numerical method. Now, an exact study is required to discretize each term of the Eqs. (6.1) and (6.2).

Boundary and free surface conditions
Two boundary conditions are used in the numerics of the ComFLOW executable. Namely, the solid boundary and free surface condition. The employment of a proper set of boundary conditions for a specific fluid flow makes all the difference for the solution to be unique, stable and accurate. The derivation and equations of the boundary and free surface conditions can be found in Appendix B. Furthermore, the evolution of the free surface in time with respect to the underlying velocity field must be modelled as well. This is established using the volume-of-fluid (VOF) method, which will be explained in the numerical model.

6.2. Numerical Model

Before starting the numerical treatment of the terms in the governing equations, the computational framework of the spatial discretization in the numerical method is described. This includes the computational domain and grid. Prolonged by an elaboration on the object and fluid configuration, cell labeling and spatial discetization of the governing equations, which are stated in Appendix B.

Computational Domain and Grid
The computational domain Ω is rectangular and a Cartesian grid or grid refinement has been applied. The spatial step of the grid is defined as a 'cell size' number in order to identify the fine or coarseness of the grid. In the ideal situation one likes to indicate the cell size by number of cells per fluid flow feature. However, in the case of different sloshing scenarios, this is not a clear solution. Figure 6.1 below provides a visualization of the two different grid types applied.

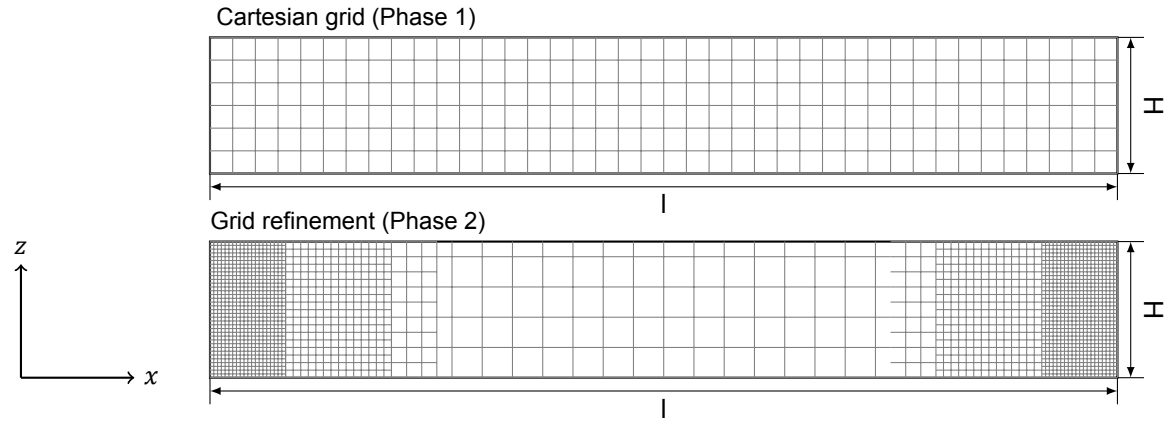

Figure 6.1: Cartesian grid and grid refinement

Spatial discretization of the governing equations
In order to spatially discretize the governing equations inside the computational domain, the finite volume formulation is applied. Each term of the governing equations will be treated separately based on the numerical framework explained in the previous sections. The discretization will be carried out for the 2D application. For the sake of simplicity. The extension to 3D is considered to be straightforward.

When the matrix-vector notation is used, the equations of motion (Eq. (6.1) and (6.2)) can be rewritten as

$$\mathbf{D}\mathbf{u}_h = 0 \tag{6.3}$$

$$\Omega \frac{d\mathbf{u}_h}{dt} + \mathbf{C}(\mathbf{u}_h)\mathbf{u}_h + \mathbf{V}\mathbf{u}_h + \mathbf{G}p_h = 0 \tag{6.4}$$

where $\mathbf{D}$ and $\mathbf{G}$ denote the discrete divergence and gradient operators. Ω is a diagonal matrix containing the sizes of the control volumes, where, $\mathbf{u}_h$ contains the discrete velocities, p_h contains the discrete pressures, and $\mathbf{C}(\mathbf{u}_h)$ and $\mathbf{V}$ include the convective and viscous diffusive coefficient operators, respectively.

At this moment the specific discretization technique, symmetry preserving discretization, comes into play. After the analysis related to the discrete energy of the discrete governing equations, Verstappen and Veldman [25] state that it decreases in time when the symmetry preserving discretization is employed. Resulting, consequently, in a stable system. This allows that a solution to the system motioned above can be determined on any arbitrary grid. More information can be found in Dröge and Verstappen [9].

The detailed discretization of the continuity and momentum equations can be found in Appendix B.

Temporal discretization and solution technique
The discetization of the equations of motion (6.1) and (6.2) in time will be explained briefly. This process is realized with the use of the first-order Euler forward method. For a simple time derivative term $d\varphi/dt = f(\varphi)$, the forward Euler takes the following form

$$\varphi^{n+1} = \varphi^n + \Delta t f(\varphi^n) \tag{6.5}$$

Now, for a better explanation of the solution technique that is used in the ComFLOW program, the equations of motion shall be rewritten in a more schematic formulation. The conservation of Mass and conservation of Momentum, respectively

$$\text{div}\ \mathbf{u}^{n+1} = 0 \tag{6.6}$$

$$\frac{\mathbf{u}^{n+1} - \mathbf{u}^n}{\Delta t} + \frac{1}{\rho}\ \text{grad}\ p^{n+1} = \mathbf{R}^n \tag{6.7}$$

where n and $n+1$ represent the old and new time level, Δt is the time step, and $\mathbf{R}$ contain all the convective, diffusive and body forces

$$\mathbf{R}^n = -(\mathbf{u}^n \cdot \text{grad})\mathbf{u}^n + \nu\ \text{div grad}\ \mathbf{u}^n + \mathbf{F}^n \tag{6.8}$$

where ν is the kinematic viscosity.

When discretizing the continuity equation (6.6) at the new time level, a divergence-free velocity field is ensured. If the terms of Eq. (6.7) are rearranged, it can be rewritten to

$$\mathbf{u}^{n+1} = \bar{\mathbf{u}}^n - \frac{\Delta t}{\rho}\ \text{grad}\ p^{n+1} \tag{6.9}$$

where

$$\bar{\mathbf{u}}^n = \mathbf{u}^n + \Delta t \mathbf{R}^n \tag{6.10}$$

Whereby the term $\bar{\mathbf{u}}^n$ is referred to as an auxiliary velocity and calculated first in the solution process.

After the substitution of Eq. (6.9) into (6.6), the so called Poisson equation can be defined

$$\text{div grad } p^{n+1} = \frac{\rho}{\Delta t} \text{ div } \vec{\mathbf{u}}^{n} \tag{6.11}$$

The Poisson equation is solved by application of the SOR (Successive Over Relaxation) and BiCGSTAB pressure solvers. The interested reader can find more elaboration on the solvers at Veldman [1] and Sonneveld [23]. Once the new (p^{n+1}) pressure field is obtained, the velocity field for the new time level can be calculated with Eq. (6.9).

CFL-number

When the pressure solution is found, the new velocity field can be computed. As described in the solution technique above. Subsequently, the free surface displacement is determined using the VOF-method combined with a local height function. Described by Kleefsman [10] and Veldman [14]. Finally, the time step is adjusted using the CLF-condition approach. Adjustment of the time step takes place in relation to a certain CLF-number, which is calculated by

$$CFL = max_{i,j,k}\left(\frac{\mid u_{ijk} \mid \delta t}{h_{x,i}} + \frac{\mid v_{ijk} \mid \delta t}{h_{y,j}} + \frac{\mid w_{ijk} \mid \delta t}{h_{z,k}}\right) \tag{6.12}$$

In this equation u, v, w are velocity components and h_x, h_y, h_z denote the mesh sizes in the corresponding directions. If the computed CLF-number is greater than the `clfmax`, which is defined by the user in the input file, the time step will be decreased. If the computed CLF-number is smaller than the `clfmin` during 10 consecutive steps, the time step will be doubled. The set-up of the CLF-number is to focus the calculation time on the important moments of fluid velocity changes. Which concludes in an improvement of the calculation time without losing precision. In the application of ComFLOW a constant CFL-number is used for the `clfmin` and `clfmax`. The recommendation for sloshing cases concluded in `clfmin = 0.2` and `clfmax = 0.5`. Which is also described in the input file in Appendix B.

7

CFD - Phase 1

As described in chapter 2 Research Methodology, the first phase of 2D CFD simulations consist of a general approach. There are four parameters that influence the behaviour of the fluid inside the in-deck tank. These are; fluid type and properties, fill level, tank geometry and floating structure motions. It can be interpreted that the parameters have direct influence on possible sloshing behaviour. Combinations of these four parameters will result in a long list of cases. With the help of reference projects and reports from CB&I, a research scenario study has been carried out. Resulting in fixed boundaries for the variable parameters. The content of the CB&I reports are classified and not publicly accessible. Therefore, no reference to any of these reports can be made. More information and results from the research scenario study is described in Appendix C.

The number of scenarios that can be assessed is highly dependent on the calculation time of the numerical simulation. After test runs and availability of computing power, the following Table 7.1 can be defined.

Cell [cm]	Grid [-]	Number of cells [-]	Real Time [s]	Time Factor [s_{sim}/s_{real}]
10	200 * 1 * 18	3600	368	1/12
5	400 * 1 * 36	14,400	2,939	1/98
3	667 * 1 * 60	40,020	19,710	1/657
2	1000 * 1 * 90	90,000	38,294	1/1276
1	2000 * 1 * 180	360,000	411,368	1/13712

Table 7.1: Phase 1 - Grid size and Calculation times for 30 s simulation time.
l = 20 m and H = 1.8 m

A balance of the cell size and simulation time has been established. The long list of cases in combination with limited computational power concludes in the ideal cell size of 3 cm. The other cell sizes of this table shall be implemented for the verification of the CFD executable.

Phase 1 includes a list of 66 cases, which have been defined in collaboration with colleagues of CB&I. This chapter includes a detailed case definition list, followed by the simulated results. More elaboration on the results and the pre- and post processing of ComFLOW can be found at Appendix D.

The chapter concludes with a method comparison. This comparison should determine the best approach to calculate fluid pressures for oscillation cases. In the next Phase, the focus will shift completely towards impact pressure cases.

7.1. Case Definition

In the process of the research case set-up, groups are formed. A total of 66 cases are divided into 7 distinct groups. The first group is related to the Aasta Hansteen SPAR project and fully focused on the occurrence of sloshing. The second till sixth group correlates to the Skarv FPSO where difference in tank size, material, fill levels and motions is widely assessed. The seventh and last group relates to the verification of the CFD simulations by conducting a grid independence study. A short elaboration of each group is described and followed by Table 7.2 and 7.3, where the cases are listed.

Group 1 - SPAR

Cases 1 - 6, 60

The first set of cases include an assessment of the applied in-deck tanks for the Aasta Hansteen SPAR. The purpose of this simulation is to prove that no sloshing will occur considering the worst motions of the SPAR, Motion Case 1 - Pitch (C.4.3 at page 92). The period of the SPAR, around 60 seconds, is far off the natural period of the fluid in the tank which is around 10 seconds. Calculated by using Eq. 5.9 at page 5.9.

To fully exclude any sloshing behaviour for the Aasta Hansteen SPAR, a worst possible case is described. Noted that the tank length of 20 meter is not present in the in-deck tank lay-out for the current Aasta Hansteen SPAR project.

Group 2 - FPSO Tank size

Cases 7 - 14

The second set of cases start with the sloshing assessment of an FPSO type of vessel. This includes an initial study to the different type of geometry for in-deck tanks. Four different type of tanks are established and assessed for a fixed fill level, fluid material and motion case. More elaboration on the motion case is described in C.4.4 at page 93. Initial calculations by the natural free surface period, indicated that sloshing may occur during these type of motions. The cases showed that for the 7 meter tank type no sloshing occurs. Therefore, this type of tank is excluded for further sloshing analysis. Furthermore, no distinct conclusion could be drawn for the different fluid types. A more detailed analysis for both fluid types is necessary.

Group 3 - FPSO Material & Fill

Cases 15 -32

After the initial analysis of Cases 7 - 14, more thorough analysis has been done for the different fill levels and tank types which are related to the invariable fluid and motion case. The defined Low-Mid, Mid-High and High scenarios of the fluid fill are assessed, in combination with the high potential sloshing in-deck tank types. The first part of this group, cases 15 - 23, are specifically related to Water.

For the Cases 24 - 32 the same approach has been used that is described in the previous paragraph. However, now the relation to MEG is conducted.

Group 4 - FPSO Nautical Zones

Cases 33 - 47

After the assessment for different fill levels and fluid types, the focus will shift to different sea states and areas in the world. This is studied with varying Motion cases. More information for the different motion cases can be found in appendix C.4 at page 90. For this assessment a ’base case’ of 50% Water fill has been used. Again the different tank geometry is included.

Group 5 - FPSO Roll motion

Cases 48 - 51

Cases 7 - 47 have shown a widespread analysis of the pitch motion of an FPSO, which can be related to a period of 9.7 seconds. For this period severe sloshing may occur in some specific cases. In order to broaden the perspective, the roll motion of 20.8 seconds is taken into account as well. Again the ’base case’ of 50% water for all four tank types have been conducted. The worst motion case has been picked, which is MC 6.

Group 6 - FPSO Extended time duration

Cases 52 - 55

As described in the research scenario appendix, C, the normal duration of the simulation has been set at two (SPAR) and three (FPSO) cycles. However, some cases have shown a occurrence of sloshing peaks in the last cycle. In order to improve the knowledge of these cases a more extensive time simulation is conducted. Instead of 3 cycles, the doubled amount of 6 cycles is assessed. The cases that are simulated with a longer duration are: 14, 22, 43 and 47.

Group 7 - Grid independence (Verification)

Cases 56 - 59, 61 - 66

The last group of cases is linked to the verification of the CFD model. This is done for the so called 'grid independence study'. For this study a subdivision is made for the no sloshing, semi sloshing and sloshing cases. First the assessment for the sloshing case has been carried out. The results showed no grid Independence. Therefore the choice of a subdivision is made to also include a study related to a no sloshing and semi sloshing case.

The first four cases (56 - 59) of this group are related to a case where sloshing occurs, chosen to be case 14. The cell size that has been simulated already is 3 cm. The other cell sizes that are assessed are: 10 cm, 5 cm, 2 cm and 1 cm. More elaboration on the verification is described in Appendix F at page 141.

Next are three cases (61 - 63) related to the 'no sloshing' case 7. For the 1 cm cell size, the computational time necessary turned out to be disproportional. Therefore, the cell sizes 10 cm, 5 cm and 2 cm are simulated. On top of the 3 cm simulation of case 7.

The last three cases (64 -66) are related to the 'semi sloshing' case 45. Semi-sloshing is the transition zone between actual sloshing and no sloshing (oscillating behaviour). Again the cell sizes 10 cm, 5 cm and 2 cm are simulated.

Phase 1 - Case Definition

Case	Offshore Structure	Tank		Fill	Fluid	Motion		Numerical Accuracy [cm]	Cycles
		length [m]	height [m]			case	type		
1	SPAR	12	1.8	50%	water	1	Pitch	3	2
2	SPAR	12	1.8	60%	water	1	Pitch	3	2
3	SPAR	12	1.8	70%	water	1	Pitch	3	2
4	SPAR	12	1.8	61%	MEG	1	Pitch	3	2
5	SPAR	12	1.8	70%	MEG	1	Pitch	3	2
6	SPAR	12	1.8	80%	MEG	1	Pitch	3	2
7	FPSO	7	1.8	50%	water	2	Pitch	3	3
8	FPSO	12	1.8	50%	water	2	Pitch	3	3
9	FPSO	15	1.8	50%	water	2	Pitch	3	3
10	FPSO	20	1.8	50%	water	2	Pitch	3	3
11	FPSO	7	1.8	50%	MEG	2	Pitch	3	3
12	FPSO	12	1.8	50%	MEG	2	Pitch	3	3
13	FPSO	15	1.8	50%	MEG	2	Pitch	3	3
14	FPSO	20	1.8	50%	MEG	2	Pitch	3	3
15	FPSO	12	1.8	30%	water	2	Pitch	3	3
16	FPSO	15	1.8	30%	water	2	Pitch	3	3
17	FPSO	20	1.8	30%	water	2	Pitch	3	3
18	FPSO	12	1.8	60%	water	2	Pitch	3	3
19	FPSO	15	1.8	60%	water	2	Pitch	3	3
20	FPSO	20	1.8	60%	water	2	Pitch	3	3

Table 7.2: Phase 1 - Overview Case Definition - Part I

Case	Offshore Structure	Tank		Fill	Fluid	Motion		Numerical Accuracy [cm]	Cycles
		length [m]	height [m]			case	type		
21	FPSO	12	1.8	70%	water	2	Pitch	3	3
22	FPSO	15	1.8	70%	water	2	Pitch	3	3
23	FPSO	20	1.8	70%	water	2	Pitch	3	3
24	FPSO	12	1.8	45%	MEG	2	Pitch	3	3
25	FPSO	15	1.8	45%	MEG	2	Pitch	3	3
26	FPSO	20	1.8	45%	MEG	2	Pitch	3	3
27	FPSO	12	1.8	70%	MEG	2	Pitch	3	3
28	FPSO	15	1.8	70%	MEG	2	Pitch	3	3
29	FPSO	20	1.8	70%	MEG	2	Pitch	3	3
30	FPSO	12	1.8	80%	MEG	2	Pitch	3	3
31	FPSO	15	1.8	80%	MEG	2	Pitch	3	3
32	FPSO	20	1.8	80%	MEG	2	Pitch	3	3
33	FPSO	12	1.8	50%	water	3	Pitch	3	3
34	FPSO	15	1.8	50%	water	3	Pitch	3	3
35	FPSO	20	1.8	50%	water	3	Pitch	3	3
36	FPSO	12	1.8	50%	water	4	Pitch	3	3
37	FPSO	15	1.8	50%	water	4	Pitch	3	3
38	FPSO	20	1.8	50%	water	4	Pitch	3	3
39	FPSO	12	1.8	50%	water	5	Pitch	3	3
40	FPSO	15	1.8	50%	water	5	Pitch	3	3
41	FPSO	20	1.8	50%	water	5	Pitch	3	3
42	FPSO	12	1.8	50%	water	6	Pitch	3	3
43	FPSO	15	1.8	50%	water	6	Pitch	3	3
44	FPSO	20	1.8	50%	water	6	Pitch	3	3
45	FPSO	12	1.8	50%	water	7	Pitch	3	3
46	FPSO	15	1.8	50%	water	7	Pitch	3	3
47	FPSO	20	1.8	50%	water	7	Pitch	3	3
48	FPSO	7	1.8	50%	water	2	Roll	3	3
49	FPSO	12	1.8	50%	water	2	Roll	3	3
50	FPSO	15	1.8	50%	water	2	Roll	3	3
51	FPSO	20	1.8	50%	water	2	Roll	3	3
52	FPSO	20	1.8	50%	MEG	2	Pitch	3	3
53	FPSO	15	1.8	50%	water	6	Pitch	3	3
54	FPSO	15	1.8	70%	water	2	Pitch	3	3
55	FPSO	20	1.8	50%	water	7	Pitch	3	3
56	FPSO	20	1.8	50%	MEG	2	Pitch	10	3
57	FPSO	20	1.8	50%	MEG	2	Pitch	5	3
58	FPSO	20	1.8	50%	MEG	2	Pitch	2	3
59	FPSO	20	1.8	50%	MEG	2	Pitch	1	3
60	SPAR	20	1.8	70%	water	1	Pitch	3	3
61	FPSO	7	1.8	50%	water	2	Pitch	10	3
62	FPSO	7	1.8	50%	water	2	Pitch	5	3
63	FPSO	7	1.8	50%	water	2	Pitch	2	3
64	FPSO	12	1.8	50%	water	7	Pitch	10	3
65	FPSO	12	1.8	50%	water	7	Pitch	5	3
66	FPSO	12	1.8	50%	water	7	Pitch	2	3

Table 7.3: Phase 1 - Overview Case Definition - Part II

7.2. Results

The results are described for each group, as defined in the case definition. As mentioned, Appendix D presents more elaboration on the results for every single case.

Group 1 - SPAR

No sloshing occurs for the Aasta Hansteen SPAR related cases. The pitch motion period of 57.5 s is too far away from the natural period of the 1^{st} wave mode, which is between the 6.5 - 8.1 s. Therefore, sloshing was not expected. Variation of fill levels, for both water and MEG, do not give notable behaviour differences. The pressure increase between water and MEG is directly related to density difference and hydrostatic pressures. Even the artificially created worst case for the SPAR (case 60), do not show any indication towards sloshing. The oscillation pressures are calculated with the use of the linear modal theory, described at section 5.2. The magnitude of occurring pressures resulted in 20-25 kPa for water and 25-30 kPa for MEG.

Group 2 - FPSO Tank size

The natural period of the 1^{st} wave mode for different tank lengths varies from 4.8 - 13.5 s. The natural pitch motion of the FPSO is 9,7 s. CFD results show the transition period from oscillations (7 m tank) to semi sloshing (12 m, 15 m tank) and sloshing (20 m). The 7 m tank is to small for sloshing to occur, where just oscillations are present. Therefore, this type of tank is excluded in further sloshing case analysis. The magnitude of the occurring pressures is included in Table 7.4.

Group 3 - FPSO Material & Fill

Again a wide range of 1^{st} mode natural periods is present, 6.5 - 17.2 s. Sloshing is expected to occur in these cases, as the FPSO natural period of 9,7 s lies within the range. The periods closely coincides and all the cases in this group show at least semi sloshing behaviour. For water, sloshing occurs in the 70% fill of the 15 m and 20 m lengths, on top of the 50% fill case for the 20 m tank mentioned in group 2. For MEG, sloshing occurs in the 45% fill for the 15 m length and 70% fill for the 20 m length. The 50% fill case for the 20 m length is already mentioned in group 2. The magnitude of the occurring pressures are all included in Table 7.4 on the next page.

A more general conclusion that can be drawn is the unrelated occurrence of sloshing. The results show that only a specific set of input parameters create sloshing. A range definition for sloshing, related to input parameters is impossible to determine. Sloshing behaviour seems to be to sensitive for input parameter changes. Also, high fill levels (80% or higher) seems to leave no space in the tank for the wave mode to create its shape and sloshing to occur. Furthermore, if the tank is too long compared to a low fill level, no sloshing impact behaviour is present. Lastly, the increase of fill level influences the semi-sloshing pressures. Which seem to be directly related to the hydrostatic pressure.

Fluid Type	Fill	Tank length			
		7 m	12 m	15 m	20 m
Water	30%	-	*30*	*40*	*45*
	50%	18	*40*	*50*	**90**
	60%	-	*40*	*45*	*50*
	70%	-	*35*	**100**	**80**
MEG	45%	-	*40*	**70**	*60*
	50%	20	*40*	*50*	**95**
	70%	-	*40*	*50*	**100**
	80%	-	*55*	*55*	*70*

Table 7.4: Phase 1 - Fluid & Fill results - FPSO MC2-Pitch
Pressure values in kPa, for no sloshing, *semi sloshing*, **sloshing**

Comparison to 1^{st} natural sloshing mode

Beside the pressures presented in Table 7.4 and 7.5, a comparison to the 1^{st} natural sloshing mode is made. Case 7 to 32 is therefore integrated into Figures 7.1 and 7.2 below.

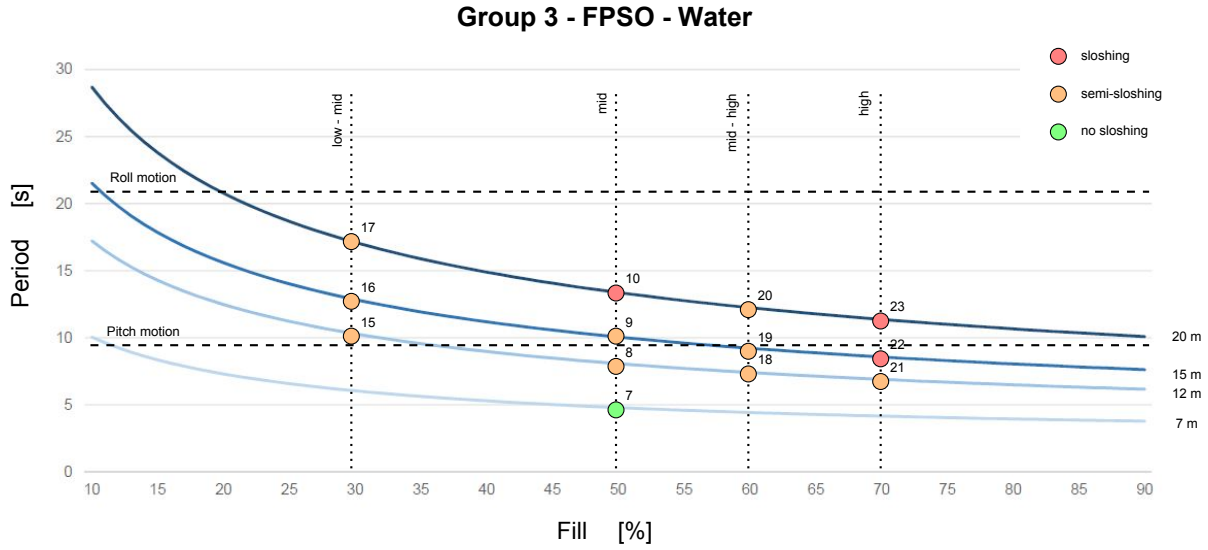

Figure 7.1: Results Water - Group 3 compared to 1^{st} natural sloshing mode

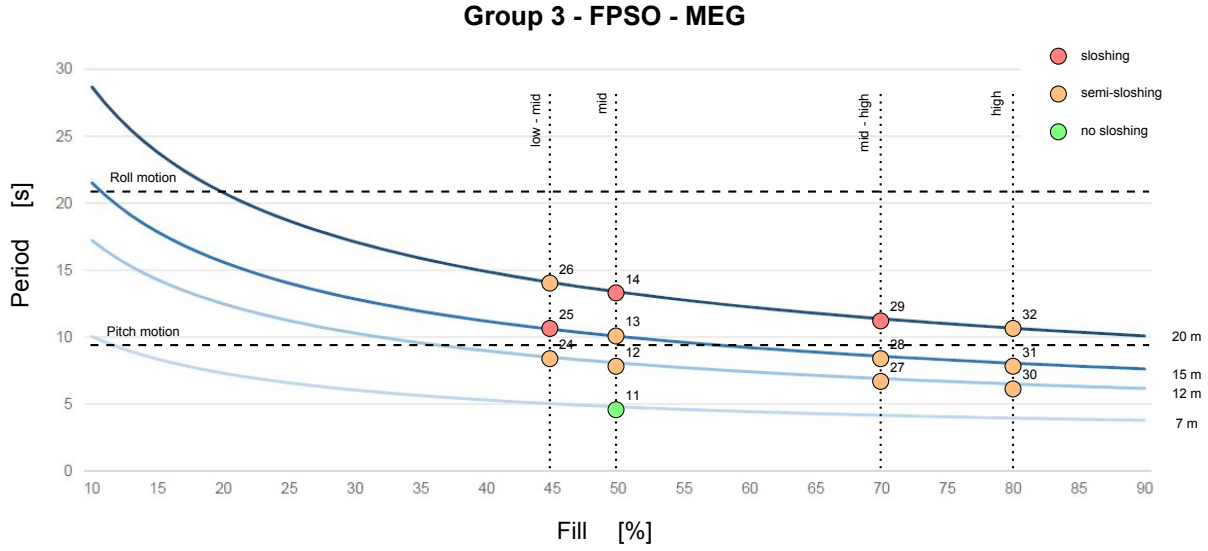

Figure 7.2: Results MEG - Group 3 compared to 1^{st} natural sloshing mode

Group 4 - FPSO Nautical Zones

The Nautical Zones can be found in Figure C.5 of Appendix C. The 1^{st} mode natural period for the 50% water filled tanks of 12, 15 and 20 m lies in the range of 8.1 - 13.5 s. Not only the natural period of the FPSO (9,7 s) is important to focus on. Also the difference in tank accelerations gives an indication of sloshing occurrence. Sloshing occurs for more severe sea states and tank accelerations, especially with tank length of 20 m . An overview of the occurring pressures for each motion case is listed in Table 7.5 below.

			Motion Cases						
			3 - Pitch	5 - Pitch	4 - Pitch	7 - Pitch	2 - Pitch	2- Roll	6 - Pitch
		Area \ Units	West Coast Africa	North Cape	North West Australia	Gulf of Mexico	West Coast Norway	West Coast Norway	East Canada
H_s		m	4.8	12.7	13.8	15.7	16.3	16.3	18.5
Natural Period		s	9.7	9.7	9.7	9.7	9.7	20.8	9.7
Heeling angle		deg	2.63	6.23	6.77	7.71	8.00	16.00	9.08
Max. x acc.		m/s²	0.24	0.63	0.68	0.78	0.81	0.34	0.92
Max. z acc.		m/s²	0.01	0.03	0.04	0.05	0.06	0.05	0.07
Max. ϕ acc.		deg/s²	0.99	2.61	2.84	3.23	3.36	1.46	3.81
Tank length	7	m	-	-	-	-	-	20	-
	12	m	18	*35*	*38*	*35*	*40*	*35*	*40*
	15	m	*25*	*35*	*48*	*40*	*55*	*40*	**60**
	20	m	*30*	*35*	*42*	**100**	**90**	*60*	**65**

Table 7.5: Phase 1 - Motion results - FPSO 50% water fill
Pressure values in kPa, for no sloshing, *semi sloshing*, **sloshing**

Group 5 - FPSO Roll motion
The roll behaviour of the FPSO has a natural period of 20.8 s, where the natural period of the 1^{st} mode related to the fluid in the tank lies in the order of 4.8 - 13.5 s. The result is the occurrence of semi sloshing behaviour. Due to the longer period and bigger heeling angle, pressures that occur are in the same order as the semi sloshing of FPSO pitch motion. The occurring sloshing pressures are implemented in Table 7.5.

Group 6 - FPSO Extended time duration
Four sloshing cases were selected and doubled in time duration. Especially case 55 (related to case 47), which include a MC 7-Pitch with 20 meter length and 50% water fill, showed interesting results. A huge pressure spike of three times the 'normal' sloshing pressures occurred in the sixth and last period. Where the sloshing impact pressures so far was up to 100 kPa, this pressure peak reached an height of 300 kPa. The second phase of longer time durations will give more insight and knowledge on the real high sloshing spikes.

Group 7 - Grid independence (Verification)
This last group is fully dedicated to the grid independence study of all three types of fluid behaviour. Namely, no sloshing, semi sloshing and sloshing. A detailed analysis can be found in Appendix F.

Sloshing Impact Area
Phase 1 concludes nine sloshing cases; 10, 14, 22, 23, 25, 29, 43, 44 and 47. Both sides of the tank show a hot-spot zone where high pressures occur. These sloshing cases present an impact area of the vertical wall and 2.0 - 2.4 meter on the top of the tank. Figure 7.3 below presents the impact area.

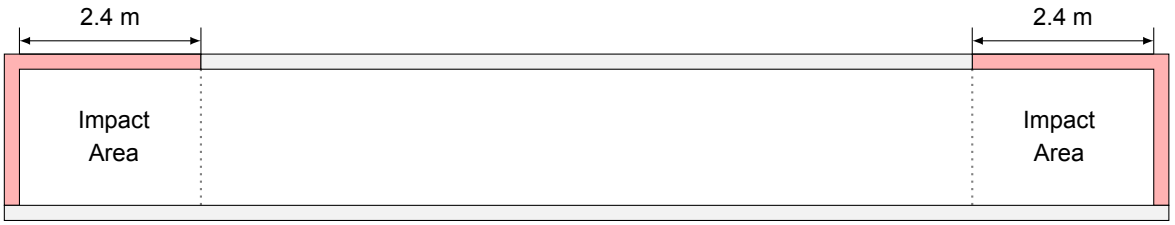

Figure 7.3: Sketch - Sloshing impact area of 2D In-deck tank

7.3. Method Comparison

After processing the simulated results of Phase 1, a comparison of the suggested methods can be made. Summarised; the conservative method of CB&I, empirical method described by the classification society, hydrostatic pressure model, linear model and the numerical ComFLOW model. A comparison is made with the first 14 simulated cases, where a sloshing, semi-sloshing and no-sloshing case are selected. The simulated data of ComFLOW is hatched in blue.

No Sloshing

Cases 1 - 7 and 11

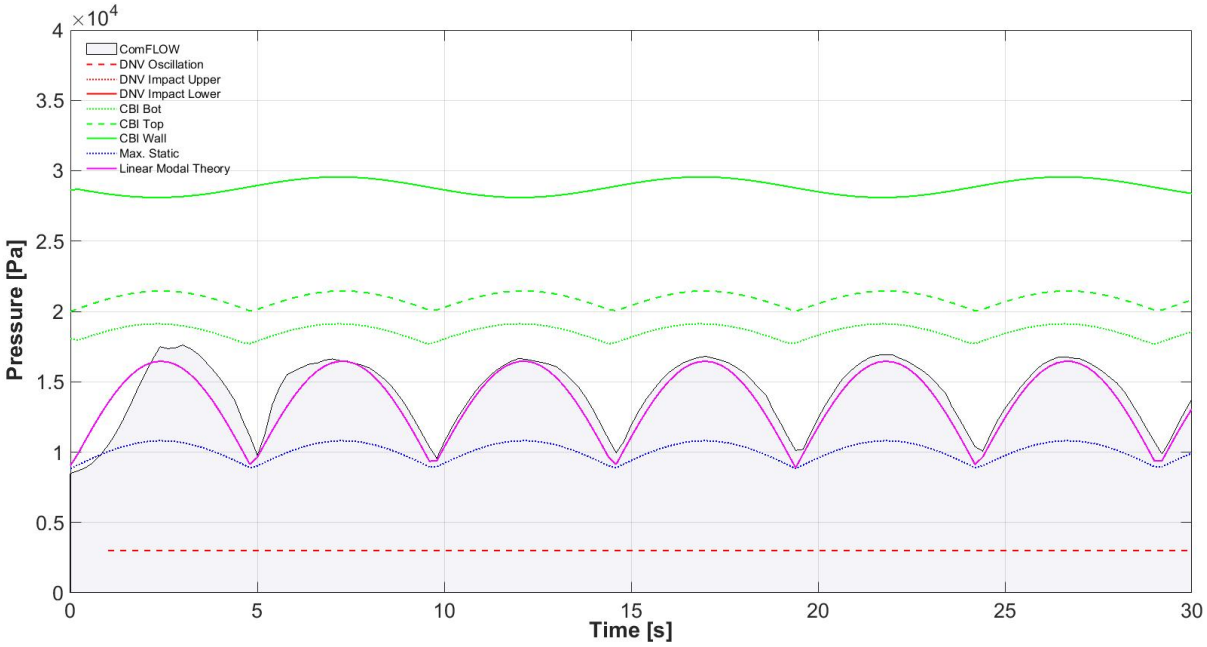

Figure 7.4: Method Comparison - No Sloshing - Case 7

No sloshing is present for cases 1 - 7 and case 11, which show oscillating pressures. Case 7 is selected to illustrate the method comparison. However, the same pressure distributions apply for the other fluid oscillating cases as well. Figure 7.4 presents the application of the different models compared to the simulated results of ComFLOW. One can clearly conclude that the linear model is best applicable for the cases without sloshing. The pressure distribution follows the simulated results perfectly. The method applied by CB&I is conservative and unnecessarily overestimates the pressures. The empirical formulas of the DNV are totally off. This is mainly due to the reason that the classification notes are related to LNG tanks. Where tank lengths of 30 - 40 are more realistic.

The linear model accurately predicts the pressure distribution for the cases of no sloshing. However, the results show a possible simplification of this model. When one recalls the linear modal theory, the pressure is build up of static, dynamic, potential and modal pressures. The potential and modal pressures do not contribute to much in relation to the static and dynamic pressures. Therefore, for simplification purposes, one can neglect the potential and modal pressures. Which leaves the following equation for calculating oscillating cases

$$p_{max} = \rho \cdot g \cdot \left(h + \frac{1}{2} l \cdot \phi\right) + \rho \cdot \left(\frac{1}{2} l \cdot a_x + h \cdot a_z\right) \tag{7.1}$$

Semi Sloshing *Cases 8, 9, 12 and 13*

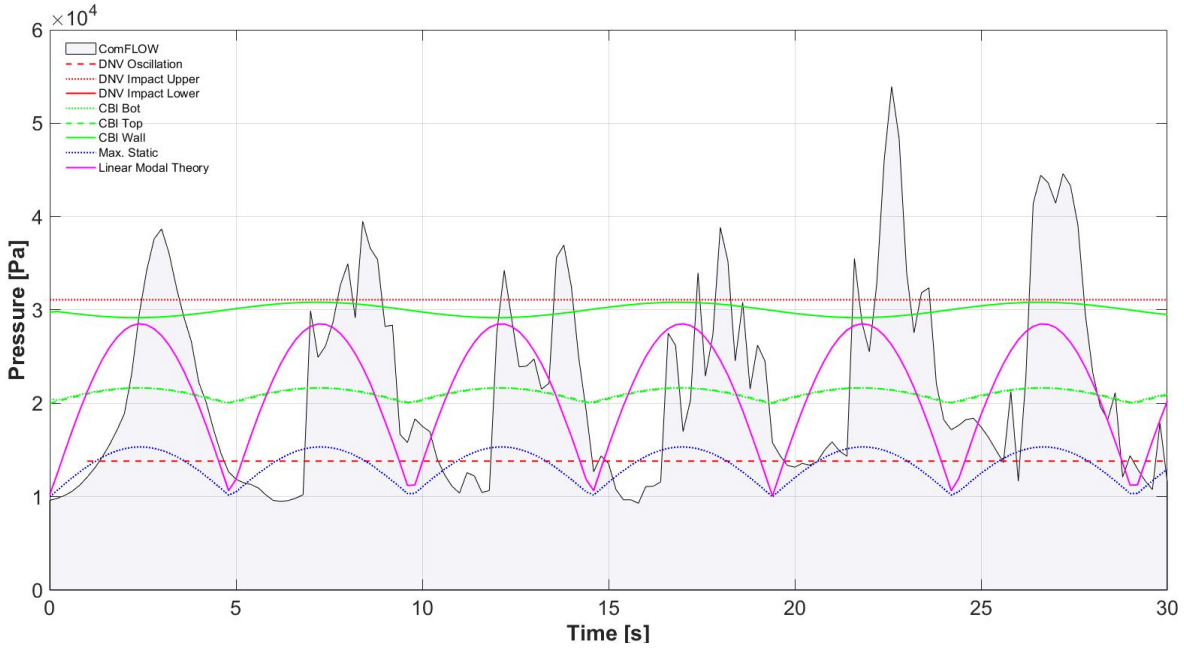

Figure 7.5: Method Comparison - Semi Sloshing - Case 13

Sloshing *Cases 10 and 14*

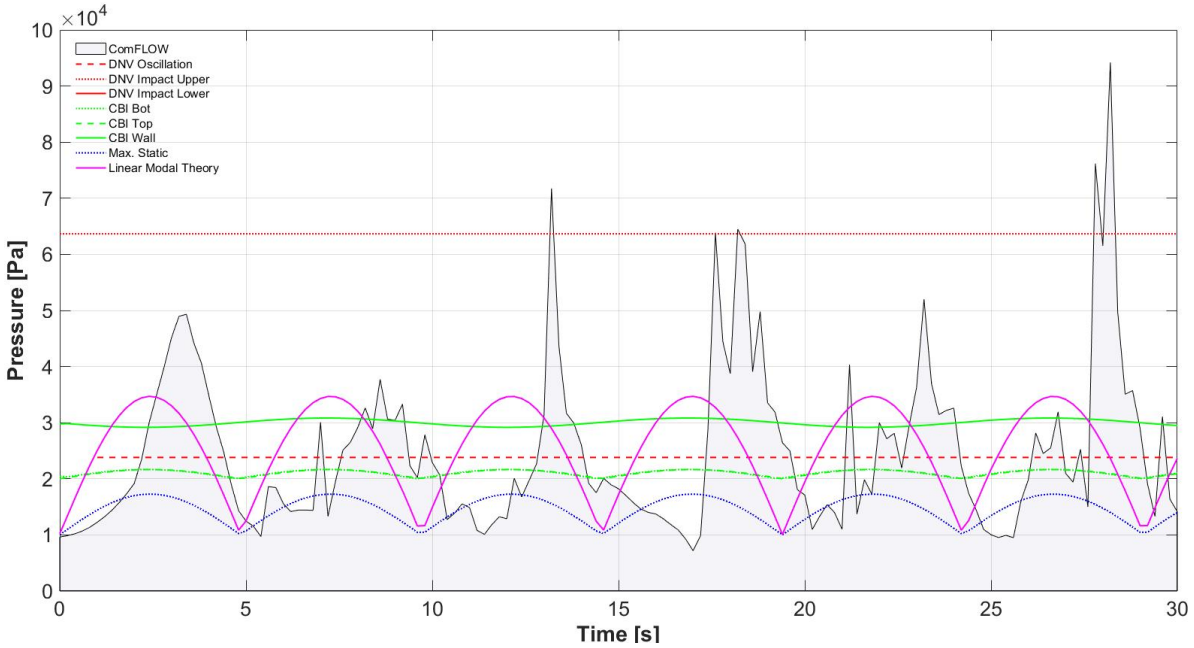

Figure 7.6: Method Comparison - Sloshing - Case 14

One can conclude that all the models are not able to predict semi sloshing or sloshing behaviour. Where the increase of non-linear sloshing behaviour result in growing errors compared to the linear models. A solution to predict sloshing pressures is integrated in Phase 2 of the research.

8

CFD - Phase 2

As described in chapter 2 Research Methodology, the second phase of 2D CFD simulations consist of a more detailed approach. The result of phase 1 concluded with several sloshing cases. In this second phase the sloshing cases are subjected to long time simulations in order to generate statistical data. With the help of a statistical analysis, post-processing is done and conclude in the order of magnitude for sloshing impact pressures. Furthermore, the verification and validation of the ComFLOW executable is assessed.

The number of cycles and cell number is dependent on the calculation power and project time available. A balance of the cell size and simulation time is established after test runs and availability of computing power, concluding in Table 8.1.

Cell [cm]	Number of cells [-]	Real Time [s]	Real Time [h]	Time Factor $[s_{sim}/h_{real}]$
8 - 1	352,913	30,115	8	1/0.3
4 - 0.5	1,411,650	312,335	87	1/3
2 - 0.25	5,646,600	4,502,885	1,251	1/42
1 - 0.125	22,586,400	23,157,685	6,433	1/215

Table 8.1: Phase 2 - Grid size and Calculation times for 30 s simulation time.
l = 20 m and H = 1.8 m

In order to balance the maximum simulation progress in combination with an accurate cell size, 8 - 1 cm is chosen for the long time simulations. The other finer cell sizes shall be implemented for the verification of the CFD executable.

Phase 2 includes a list of 12 cases, which have been defined in collaboration with colleagues of CB&I. This chapter includes a detailed case definition list, followed by the statistical analysis, results, sensitivity analysis, verification and validation. More elaboration on the results and the pre- and post processing of ComFLOW can be found at Appendix E.

8.1. Case Definition

For the detailed simulations of Phase 2 three distinct groups can be defined. The eighth group consist of Phase 1 sloshing cases for a long time duration. The ninth group is related to an extensive grid sensitivity study, verification. Where the tenth and last group describes two cases related to the validation of the ComFLOW model.

For both the sloshing cases (group 8) and grid sensitivity study (group 9), local grid refinement is applied. As illustrated in Figure 6.1 in section 6.2, the mesh becomes finer at the outer ends on the in-deck tank. The mesh refinement is related to the sloshing behaviour and impact area resulting from the 1st Phase simulations, Figure 7.3. On the next page, Figure 8.1 illustrates the mesh refinement in detail.

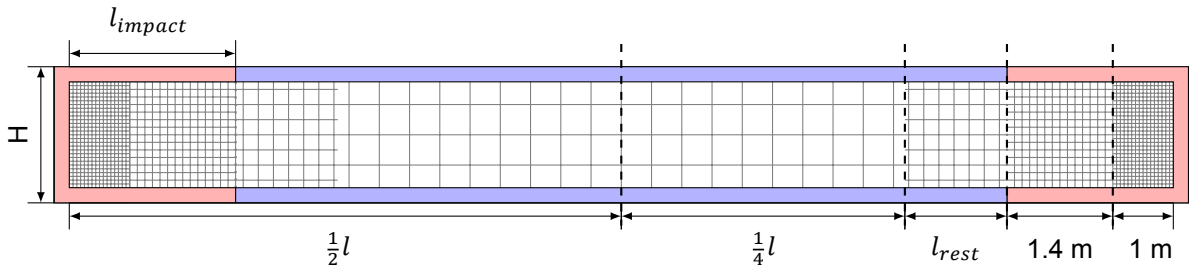

Figure 8.1: Impression of mesh refinement

Group 8 - Sloshing Cases Phase 1

Cases 67 - 74

Group 8 can be interpreted as the core group of the second phase, which mainly contain the sloshing cases of Phase 1. Seven sloshing cases of pitch motion and one semi-sloshing case of roll motion are included. Therefore, excluding 2 sloshing cases of the 1^{st} phase. This decision is made due to the computational limitations of the calculation server of the TU Delft. The initial aim of 250 cycles proved to be challenging. Even after a prolonged simulation period, an average of 125 cycles has been reached.

Group 9 - Extensive Grid independence (Verification)

Cases 75 - 76

Cases 75 - 76 include extensive grid Independence study. The grid refinements of Phase 1 where not sufficient enough for the sloshing cases to show any sign of grid independence. Due to an increase in computational power for the second case a more extensive grid independence study is carried out. Initially, four cases where established. However, due to insufficient simulated data, two of them are excluded from the verification analysis. More elaboration on the grid independence can be found in Appendix F.

Group 10 - HexaPOD (Validation)

Cases 77 - 78

The last two cases are related to the validation of the ComFLOW CFD model. A benchmark test is used for validation of liquid impacts. This test includes experiments of single fluid impacts inside a 2D rectangular tank. More elaboration can be found in Appendix G Validation.

Phase 2 - Case Definition

Case	Offshore Structure	Tank		Fill	Fluid	Motion		Numerical Accuracy [cm]	Cycles
		length [m]	height [m]			case	type		
67	FPSO	20	1.8	50%	water	2	Pitch	8 - 1	115
68	FPSO	20	1.8	50%	MEG	2	Pitch	8 - 1	110
69	FPSO	15	1.8	70%	water	2	Pitch	8 - 1	125
70	FPSO	20	1.8	70%	water	2	Pitch	8 - 1	125
71	FPSO	15	1.8	45%	MEG	2	Pitch	8 - 1	80
72	FPSO	20	1.8	70%	MEG	2	Pitch	8 - 1	165
73	FPSO	20	1.8	50%	water	7	Pitch	8 - 1	130
74	FPSO	20	1.8	50%	water	6	Roll	8 - 1	70
75	FPSO	20	1.8	50%	MEG	2	Pitch	4 - 0.5	3
76	FPSO	20	1.8	50%	MEG	2	Pitch	2 - 0.25	3
77	HexaPOD	0.95	0.67	85%	water	8	Surge	0.2	1
78	HexaPOD	0.95	0.67	85%	water	9	Pitch	0.2	1

Table 8.2: Phase 2 - Overview Case Definition

8.2. Statistical Analysis

The statistical analysis of sloshing impact pressures is carried out by application of classification notes related to LNG membrane tanks. Det Norske Veritas [7], Lloyd's Register [18] and Bureau Veritas [3] all describe an elaborate statistical analysis for determining failing probabilities of fluid tanks. The analysis is divided into two parts. The so called 'long term' and 'short term' distribution of sloshing impact loads. Short term distributions are related to a specific sea state, heading and tank filling i.e. case definition, and based on 3 hour storm conditions of the sea state. Resulting in a failure probability of the storage tank for a specific case. The long term distribution is derived by the combination of short term distributions. In the ideal case, the long term distribution contains the sum of all expected seas states, wave headings and tank filling encounters. Concluding in a total probability of failure of the storage tank.

Due to the general roots of this research, only the short term distribution is applied on the eight long term simulation cases (case 67 - 74). Computational limitations does not allow a simulation of 3 hours (1,115 cycles) and resulted in an average around 125 cycles (0.33 hours) instead. In order to analyze extreme values, such as impact pressures, much statistical data is needed to generate a reliable 'tail' of the Probability Density Function. Where a longer duration of the simulation should give more reliable statistical distributions. However, within the limits of the research no more statistical data could be simulated and produced.

The statistical procedure applied is described in five steps. These steps are described one by one with an example of case 67.

1. First a Peak-over-Threshold method is applied. This method identifies impact peaks and filters out the noise in the pressure signal. A sloshing event is defined as an impact pressure when it exceeds the specified pressure threshold. The threshold should be set well above the noise level to exclude any semi-sloshing behaviour from the analysis. For each case the threshold may differ, where the fill level and length of the tank have a great influence on this value. An example of the Peak-over-Threshold method is presented in Figure 8.2 below.

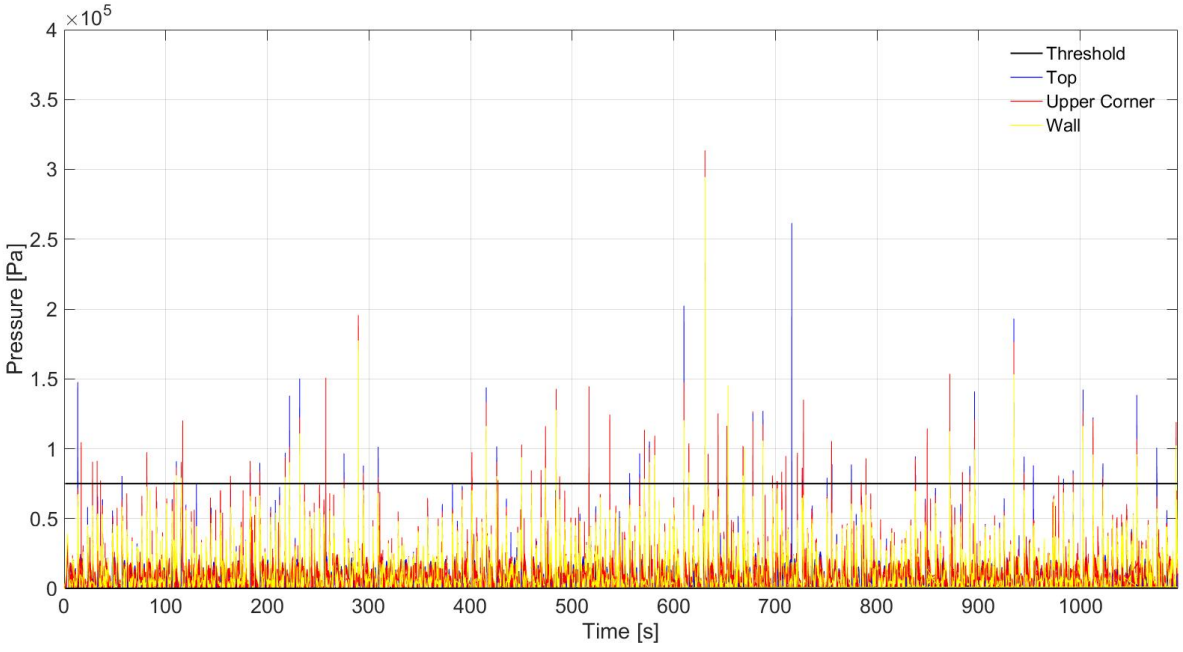

Figure 8.2: Statistical Analysis - Peak Over Threshold method

Figure E.2 presents the monitor points and force boxes defined for post-processing. One can conclude from simulation results that the Impact pressures of sloshing are present on the wall, upper corner and top of the tank. Therefore, the bottom force boxes are excluded from the statistical analysis of the sloshing impact. Figure 8.3 below describes the force boxes used in the statistical analysis. Where again the impact zone is grouped by colour. Logically, the force boxes on both sides of the tank are integrated as one. The three different colours establish a better insight on the binned impact pressures of the histogram, described in step 2.

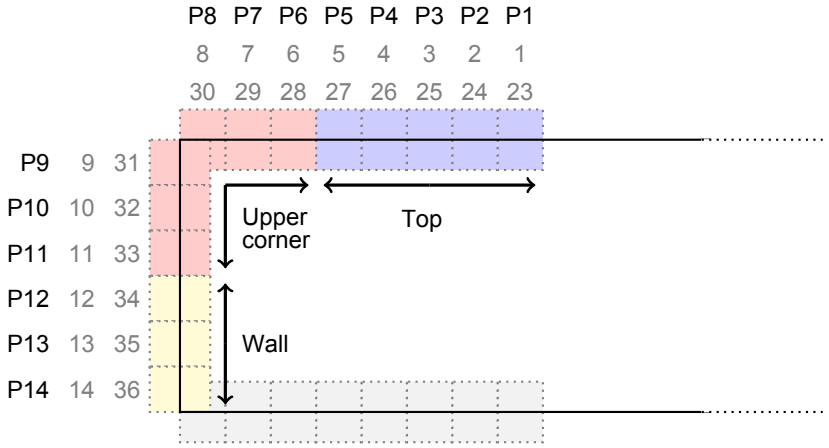

Figure 8.3: Sketch - Force box post-processing set-up of 2D In-deck tank

2. After the Peak-over-Threshold is applied, the identified sloshing impacts need to be binned. This is done by a histogram from the Threshold value up to the maximum impact value, presented in Figure 8.4 below. Note, the binning of the three impact zones overlap and are not summed in the histogram. This prevents the double counting of impact pressures.

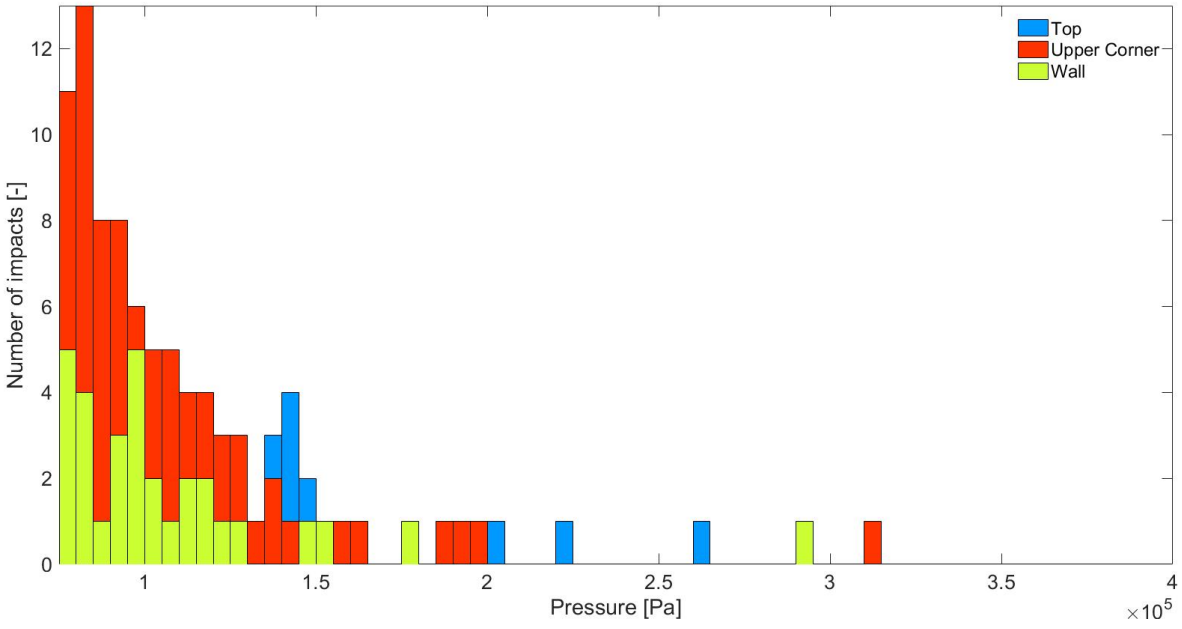

Figure 8.4: Statistical Analysis - Binned histogram of sloshing impacts

3. The next step is the normalization of the histogram, which generates the Probability Density Function (PDF). For extrapolation beyond measured data, a mathematical fit is applied. It should be noted that the mathematical fits have no relation to the fundamental physics dominating the randomness of the impacts. All three societies (DNV, BV and LR) recommend different fitting curves for sloshing in LNG tanks. This non-uniform recommendation of fitting curves precisely underline the randomness of these fittings. Even statisticians argue on the best fitting curve and the sensitivity in different applications. After several fitting tests of the simulated data, only the Generalized Pareto (GP), recommended by BV, presented a good fit to the simulated results. The other proposed fittings, weibull (DNV) and log-normal (LR), did not fit and are excluded from the statistical analysis.

   However, also other fitting possibilities are tested. Whereby the Kernel Smoothing (KS) showed promising fitting results. A kernel smoother is a statistical technique for predicting a real valued function by using the noisy observations, when no parametric model for this function is known. The estimated function is smooth and highly dependable of the input values and observations. In-depth elaboration and application of the kernel smoother is described by Bowman and Azzalini [2]. The resulting smooth function shall be compared with the Generalized Pareto fitting curve.

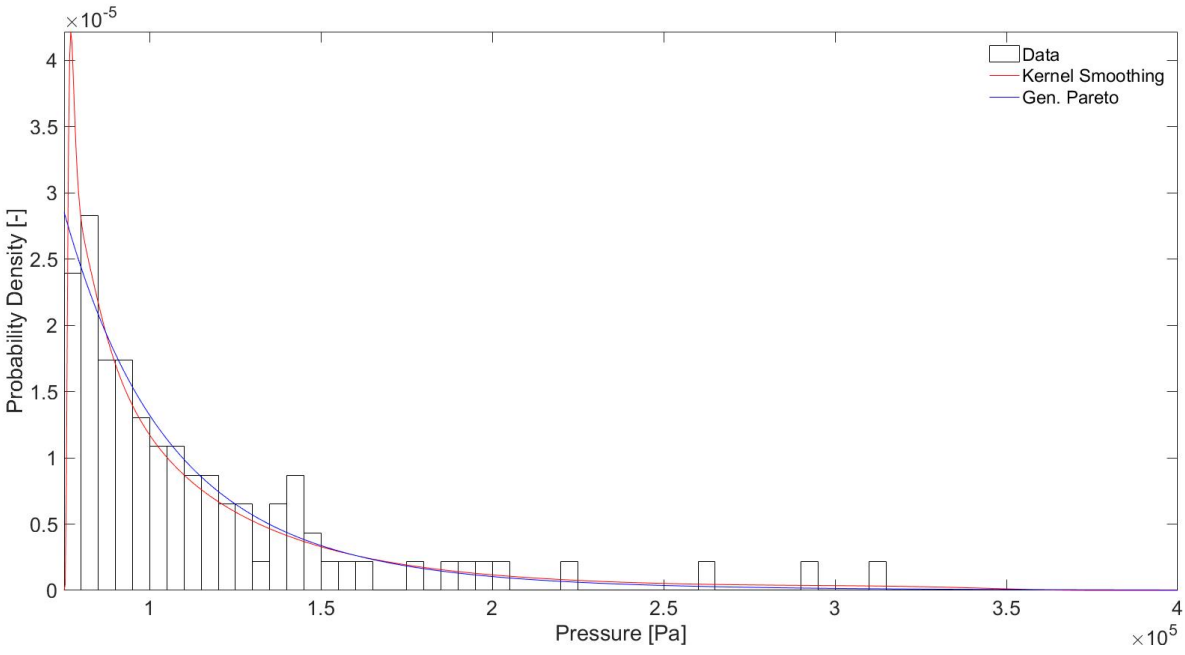

Figure 8.5: Statistical Analysis - Probability Density Function

Figure 8.5 above illustrates the fitting curve relation to the binned histogram data. One clear issue arises immediately, the simulated statistical data contains peaks and dips in binning areas where this is not expected. The issue is primarily related to the limited statistical data. Logically, with more data, these histograms should behave smoother. However, a clear trend is still noticeable. The number of sloshing impacts gradually decrease with an increase of impact pressure. At a certain point gaps arise, which illustrate extreme sloshing impacts. A reliable and good fitting in this part of the histogram is challenging. Recalling the statement that much statistical is needed to generate a reliable tail.

4. Partial integration of the PDF concludes into the Cumulative Density Function (CDF). Presented in Figure 8.6 below.

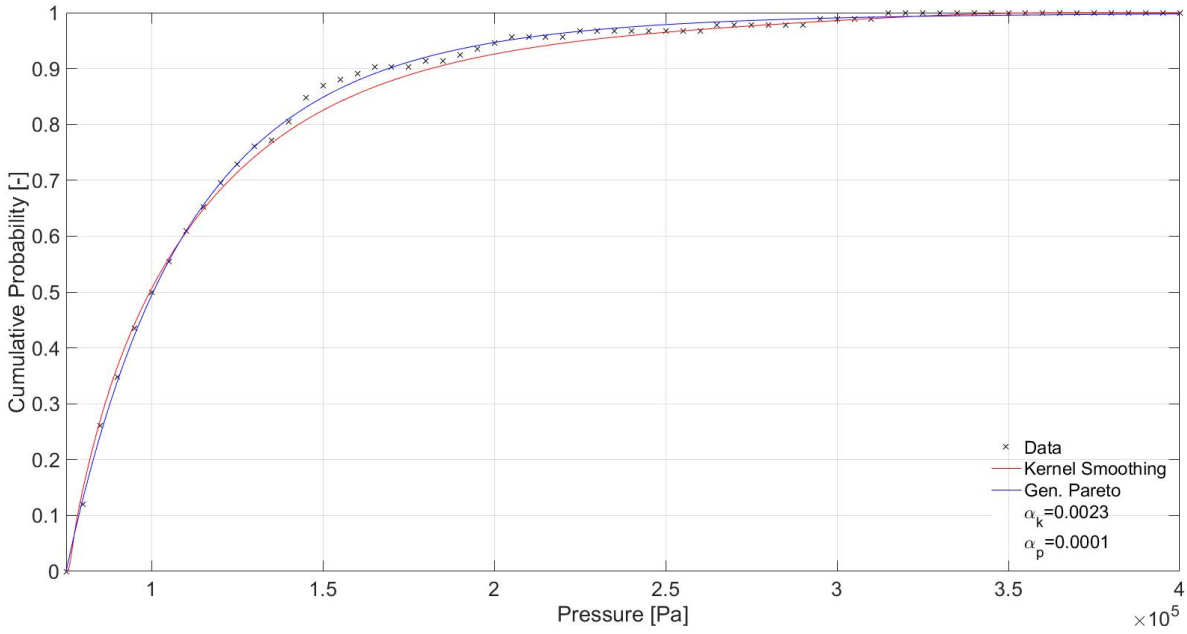

Figure 8.6: Statistical Analysis - Cumulative Density Function

In order to test the goodness of the fit, a Kolmogorov-Smirnov test is applied, Massey [20]. With the help of a Two-Sampled Kolmogorov-Smirnov test one can evaluate the difference between the Cumulative Density Functions of two sampled data. This test is a distribution-free (nonparametric) method for comparing empirical and mathematical distributions, based on the largest vertical distance between the two cumulative distribution functions. The test statistic concludes in

$$D_{m,n} = max\left(\left|\hat{F}_1(x) - \hat{F}_2(x)\right|\right) \tag{8.1}$$

where $\hat{F}_1(x)$ is the first CDF sample of size m and $\hat{F}_2(x)$ is the second CDF sample of size n. The null hypothesis H_0 defines that both samples are distributed from the binned sloshing impact histograms. Rejection of the null hypothesis at α is present when

$$D_{m,n} > D_{m,n,a} \tag{8.2}$$

where $D_{m,n,a}$ is the critical value related to the Kolmogorov distribution. The critical value depends on the number of samples (m,n) and α. Value α can be interpreted as a safety margin for the critical value. For example, $\alpha = 0.05$ result in 95% of the critical value, reducing the maximum allowable CDF difference for acceptance or rejection. The resulting α for the Generalized Pareto (α_p) and Kernel Smoothing (α_k) are included in the legend of the CDF plot. Any non-zero value indicates an acceptance of the test. Where a zero value indicates a rejection. Rejection of the fitting curve is mainly due to the fluctuating statistical data.

5. The final step includes inverting the CDF into the Exceeding Probability Function (EPF). Presented with a logarithmic scale on the vertical axis in Figure 8.7 below.

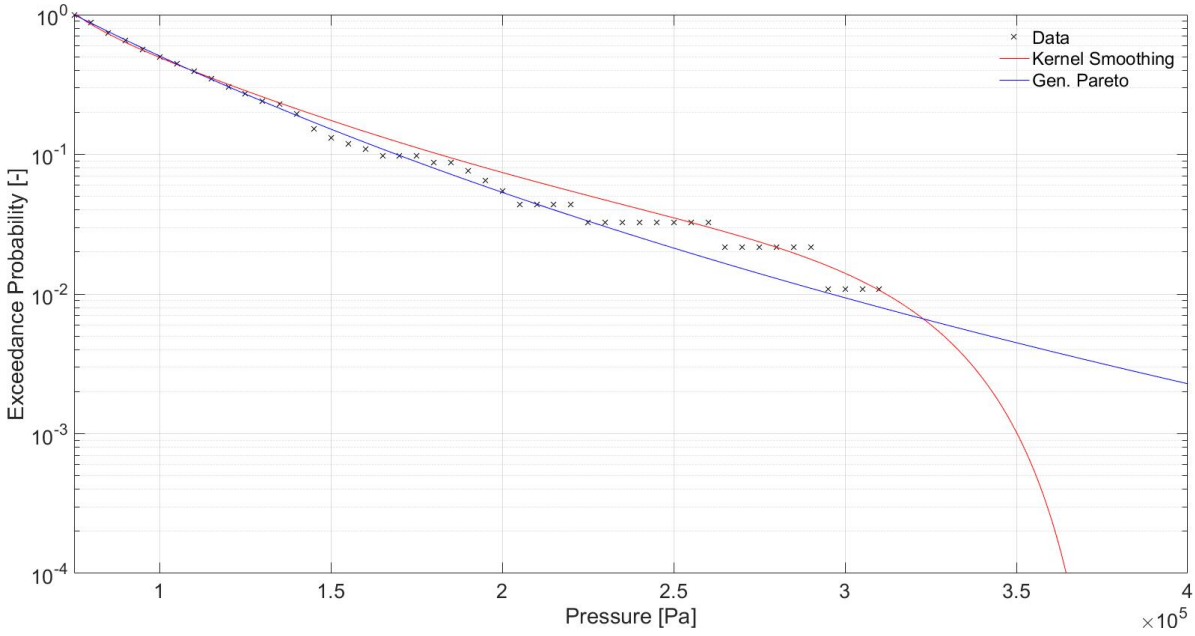

Figure 8.7: Statistical Analysis - Exceedance Probability Function

The EPF gives insight into the order of magnitude of the sloshing impact pressures. When a sloshing impact pressure occurs, the EPF represents the probability and magnitude of the impact.

The EPF presents a clear difference of the Generalized Pareto and Kernel Smoothing fitting curves. Especially after the data stops, each fitting proceed differently. Where the Generalized Pareto converges to an horizontal asymptote, the Kernel Smoothing converges to an vertical asymptote. The reliability of each of these fittings is up for debate and can be redirected to the 'tail' of the fitting curve.

8.3. Results

After the application of the statistical analysis, one can conclude the results. Appendix E contains an elaborate presentation of the statistical analysis for each case. Table 8.3 below holds the resulting pressures for the eight sloshing cases. The pressures of the fitting curves is interpreted by a 100 year return period, which coincides with the return period of the extreme sea state and ship motions, elaborated in Appendix C.

Case	Length [m]	Fill	Fluid	Motion		Pressure [kPa]	
				Case	Type	GP	KS
67	20	50%	water	2	Pitch	295	310
68	20	50%	MEG	2	Pitch	220	230
69	15	70%	water	2	Pitch	215	235
70	20	70%	water	2	Pitch	495	325
71	15	45%	MEG	2	Pitch	165	150
72	20	70%	MEG	2	Pitch	310	310
73	20	50%	water	7	Pitch	1380	670
74	20	50%	water	6	Roll	290	275

Table 8.3: Phase 2 - Overall Results

Six cases, 67 - 72, can be compared by a $\frac{\text{Fill}}{\text{Length}}$ ratio with the resulting pressures, which are presented in Figure 8.8 below. One can conclude that the ratio of 0.063 result in the highest pressures for both water and MEG cases. Furthermore, the difference in pressure of the GP, water and MEG, behaves in a scatter sense. However, more data and simulations seem to be needed in order to generate a consistent and reliable ratio graph for in-deck tank conditions.

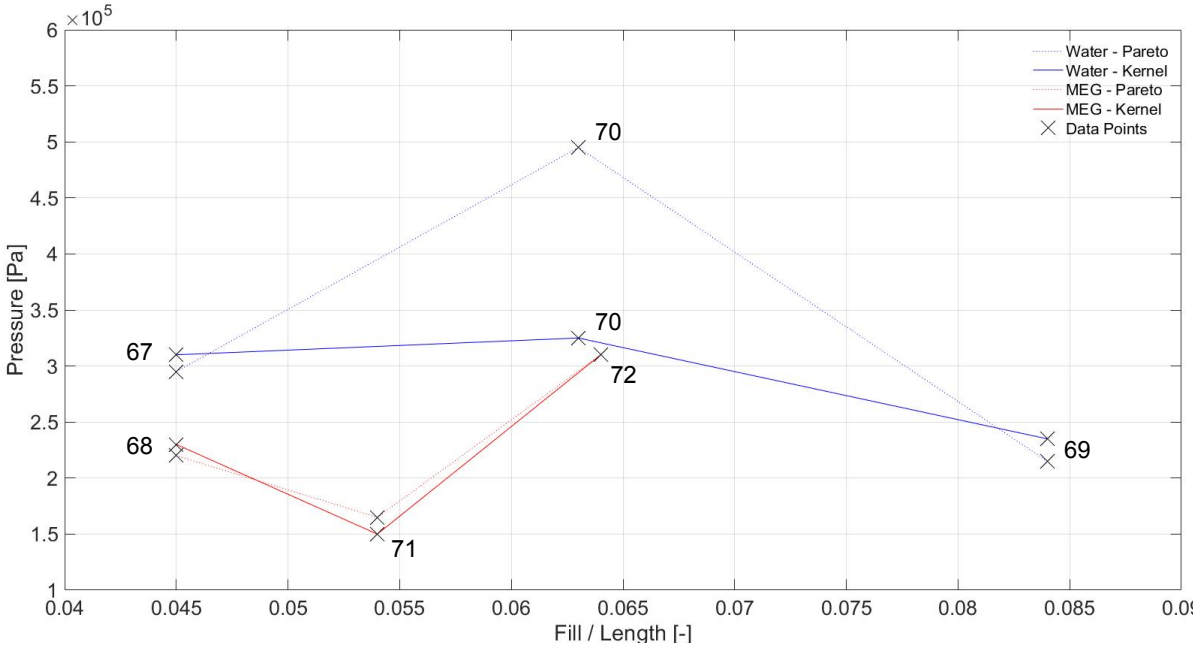

Figure 8.8: Phase 2 Result - Overall comparison

The results from case 67 - 74 can be coupled to the four sloshing influence parameters. Namely, fluid, fill, tank length and motions. A comparison is made related to these parameters and the resulting graphs of the comparisons can be found in Figures 8.9 - 8.12 at pages 46 - 49.

FLUID COMPARISON
A comparison of fluid type can be made for case 67 and 68 related to a 50% fill and 20 meter tank length. But also for case 70 and 72 related to a 70% fill and 20 meter tank length. The generalised Pareto fitting show in both cases that water results in a higher pressure impact magnitude. The KS fitting presents the same behaviour for 50% fill. However, in the case of 70% both type of fluids are in the same order of magnitude. Water has a lower density and viscosity but a higher surface tension compared to MEG. One may interpret that a lower viscosity of the fluid could contribute to more chaotic and extreme behaviour under the same circumstances. Concluding that a lower viscosity is more sensible to sloshing behaviour. The bandwidth of possible sloshing seem to be larger.

FILL COMPARISON
The 50% and 70% filling level results present a clear order of magnitude difference. 50% fill cases 67, 68 and 71 conclude an impact pressure in between 150 - 310 kPa, where 70% fill cases 69, 70 and 72 conclude 215 - 495 kPa. These results coincide with the logical assumption that more fluid has a higher impact pressure potential. It also underlines that 70% is not the maximum fill for sloshing to occur. Phase 1 concluded that a fill of 80% will not result in sloshing anymore.

TANK LENGTH COMPARISON
The results prove the claim that the tank length is one of the sensitive input parameters for sloshing and the order of magnitude for the pressure impacts. The 20 m tank length provides a much larger impact pressure compared to the 15 m tank length cases. The 15 m cases have an order of magnitude 150 - 235 kPa, where the 20 m tanks presents impact pressures from 225 up to 1380 kPa. One can conclude that a longer tank length contains more fluid, therefore increases in sloshing impact potential. Furthermore, a longer tank length has a higher natural sloshing period which coincide better with the motion periods.

MOTION COMPARISON
Together with the tank length, the motion of the tank has a big influence on the sloshing behaviour and impact pressures. The most extreme motion case 6 (East Coast Canada) show a far higher impact pressure order of magnitude compared to the MC2 (West Coast Norway) case. The higher heeling angle and accelerations have a big impact on the sloshing pressures. The order of magnitude for case 67 (MC2) results in 300 kPa, where case 73 (MC6) show a magnitude of 670 kPa (KS) and 1380 kPa (GP).

The second phase did not focus on the roll motion of the tank. But even though the roll motion (case 74) is 20.7 s and the pitch motion (case 67) 9.7 s, it still results in high impact pressures that are in the same order of magnitude as pitch. This result show the relevance of three dimensional simulations and the combination of both roll and pitch motion.

Case 73
A special note should be made related to case 73. The elaborate results, at page E.30, show a histogram with numerous high impact pressures. The interpretation of the fitted results should be done with caution, as the binning of the histogram does not allow for a good fit of the tail. The other cases does not face this problem, as their impact pressures are not as high as case 73.

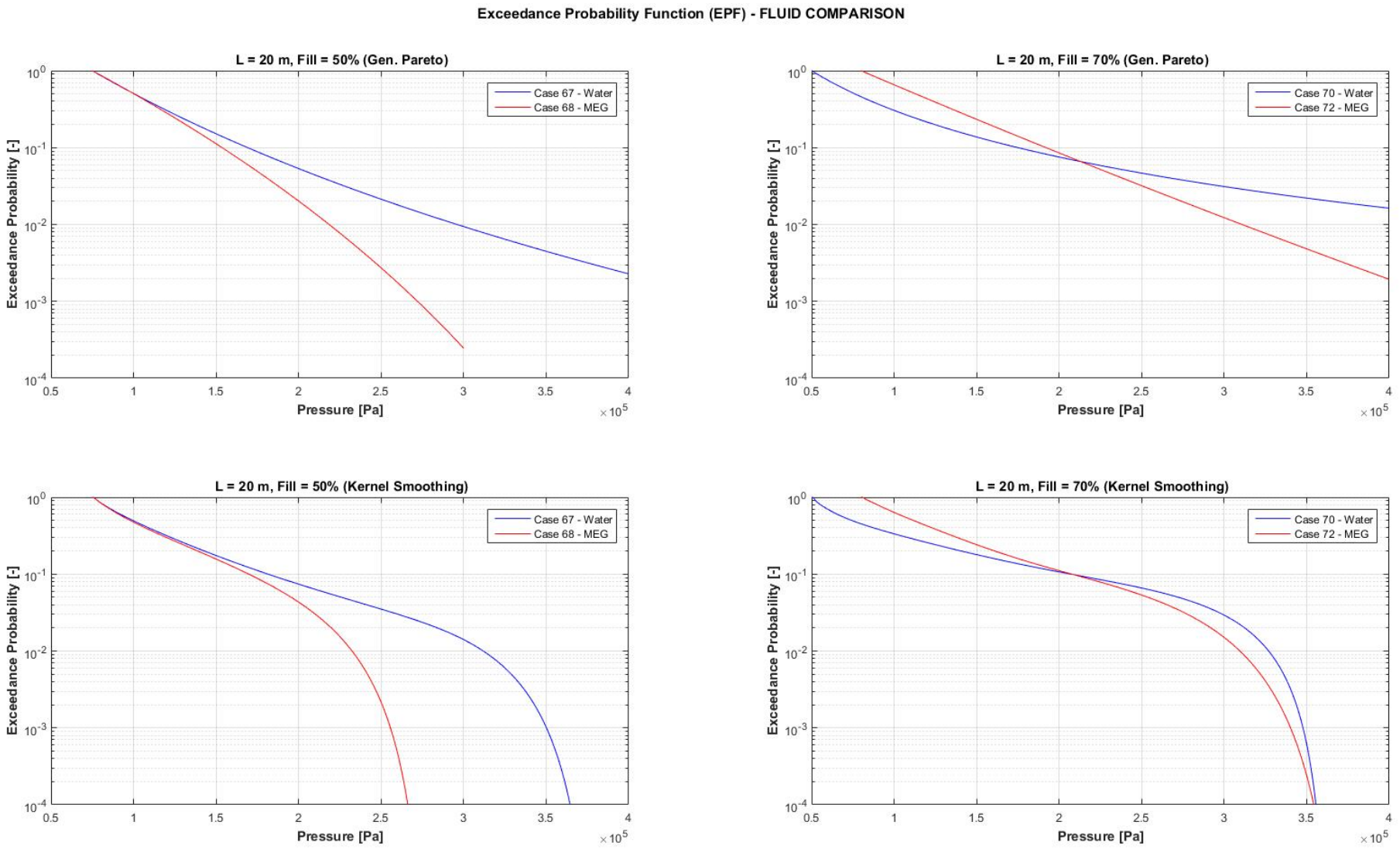

Figure 8.9: Phase 2 Result - Fluid type comparison

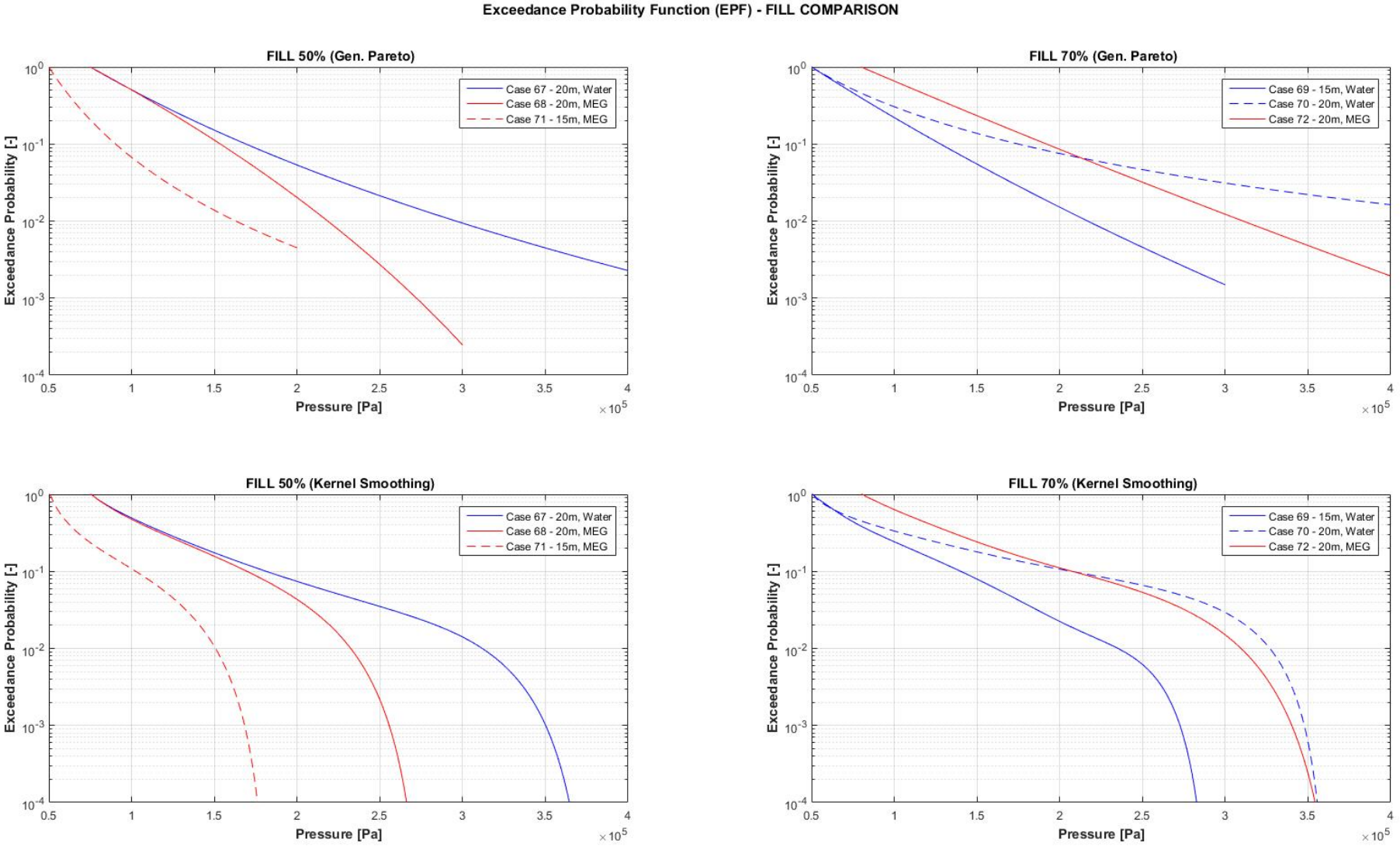

Figure 8.10: Phase 2 Result - Fill comparison

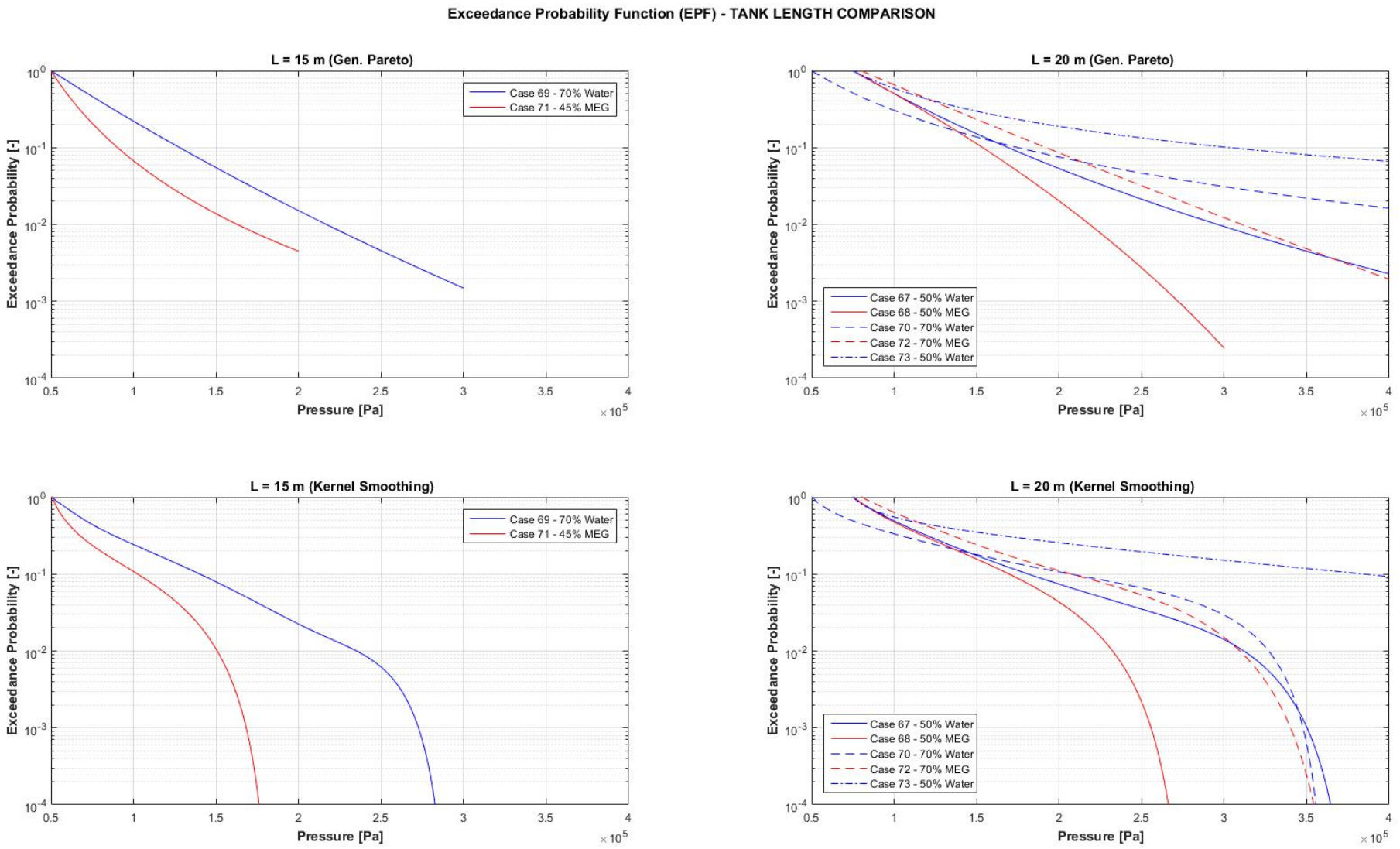

Figure 8.11: Phase 2 Result - Tank length comparison

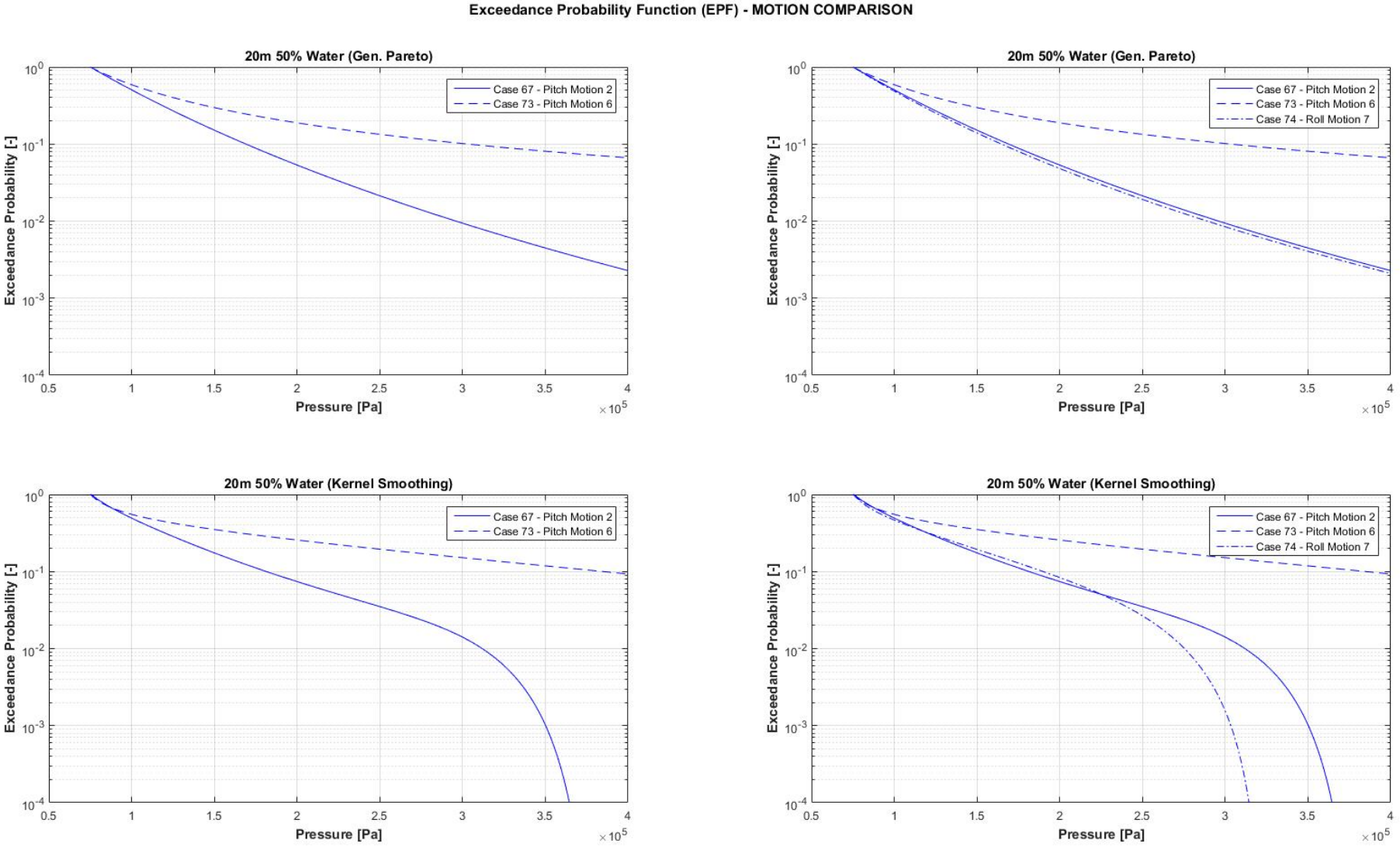

Figure 8.12: Phase 2 Result - Motion comparison

8.4. Sensitivity Analysis

The sensitivity analysis of the statistical results includes four groups. Sensitivity of the threshold, binning, data (cut) and data (random). For the threshold a sensitivity is chosen of -20% and +20%. Followed by a binning sensitivity of -50% and +50%. For the data sensitivity, two approaches are used. One consist of a data cut and the other of a completely random filter. Lets take a 1000 s simulation for example. The data cut will exclude the last 250 s (-25%) or 500 s (-50%) of the simulated data. Where the random filter excludes 250 s totally random of the 1000 s simulated data.

The results of this sensitivity study is listed in Table 8.4 below, for which the values are extracted at the 100 year return period (10^{-2}) of the EPF. Furthermore, a sensitivity tornado of the mean deviation is illustrated in Figure 8.13.

Case	Fitting	Normal	Threshold		Bin		Data (cut)		Data (rdm)	
			-20% [kPa]	+20% [kPa]	-50% [kPa]	+50% [kPa]	-25% [kPa]	-50% [kPa]	-25% [kPa]	-50% [kPa]
67	GP	295	260	320	275	305	320	205	320	325
	KS	310	290	325	305	315	320	230	320	320
68	GP	220	220	220	210	215	220	230	220	205
	KS	230	210	235	235	240	230	245	230	235
69	GP	215	210	240	220	230	225	230	195	145
	KS	235	215	245	230	240	240	250	185	155
70	GP	495	445	460	420	510	530	475	475	460
	KS	325	315	340	320	325	335	330	325	325
71	GP	165	125	150	165	145	175	150	175	160
	KS	150	135	165	145	145	155	150	155	145
72	GP	310	280	325	310	315	250	250	220	375
	KS	310	290	320	305	310	265	270	240	320
73	GP	1380	1170	910	1280	1370	890	1000	1495	700
	KS	670	630	685	660	675	655	495	675	485
74	GP	290	295	265	260	340	305	290	290	355
	KS	275	245	280	265	285	280	285	280	285

Table 8.4: Sensitivity Study - Results

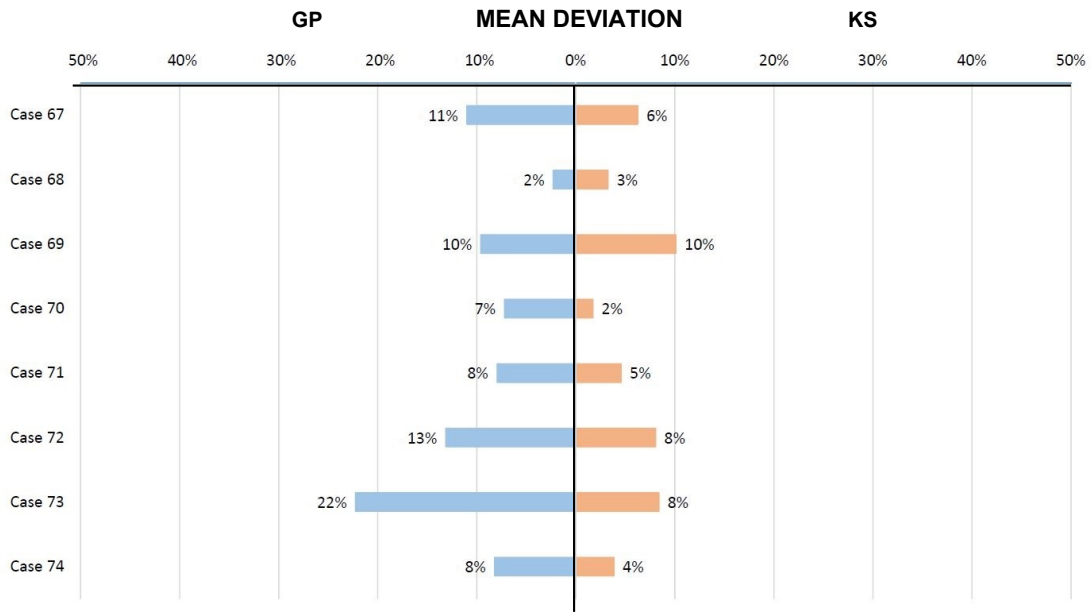

Figure 8.13: Sensitivity Tornado - Mean Deviation

The sensitivity analysis of the threshold, binning and data cut-off is considered to be quite straightforward. However, one can argue on the analysis of a randomized data filter. This sensitivity is assessed because of the grid independence issue. Resolving all local sloshing pressures at the right location and at the right time is not certain. Considering this limitation, one can omit random data in order to mimic its influence on our statistical results.

Sensitivity tornado's are made for each sensitivity group and can be found in Appendix E at page 138. Where Figures E.35 - E.38 at pages 138 - 139 illustrate the results for each sensitivity group. In order to study the sensitivity of each fitting curve, an average deviation for each case is made, illustrated in Figure 8.13. In that way, one can assess the sensitivity of each case related to one of the two fitting curves, Gen. Pareto and Kernel.

It can be concluded that the GP fitting show a more sensitive deviation for each of the assessed cases. Where the highest deviations are noticed for case 73. Considering the mean deviation, one can conclude that the KS fitting is more robust to sensitivities.

THRESHOLD SENSITIVITY
The Threshold sensitivity consist of two peaks, with 34% and 24% pressure deviation. Followed by resulting deviation sensitivities within 15%. The Generalized Pareto fitting can be considered more sensitive. The top four cases of sensitivity all relates to this fitting curve. Furthermore, the -20% threshold show a higher deviation of most cases compared to the +20%.

BIN SENSITIVITY
The binning sensitivity can be considered small with a maximum deviation of 17%. Again, the Generalized Pareto function is more sensitive to binning deviation. The Kernel fitting even stays within 4% deviation. Both the +50% and -50% of the binning value show the same amount of deviation.

DATA (CUT) SENSITIVITY
The data cut off sensitivity results in a deviation up to 36%. The simulated data can already be interpreted as minimal. Logically, a data cut-off shall result in high deviations. Both fitting curves show a high sensitivity to the data cut off. However, the difference between -25% and -50% data cut off is big. The -25% cut off result in a high peak of 36% related to case 73. Where the 50% data cut off result in an overall high deviation of approximately 30%. The cases of low deviations for the data cut off appear to have a consistent pressure impact distribution.

DATA (RANDOM) SENSITIVITY The random data sensitivity is related to the grid dependency of ComFLOW. Overall, a random data filter results in the same order of sensitivity compared to the data cut-off. Again, the peak of the sensitivity is for case 73, 49%. Also, the -50% random data filter appears to have a much higher sensitivity compared to the -25% filter, as expected. Both data filter methods show a high sensitivity of the same order of magnitude.

8.5. Verification & Validation

In order to give more insight on how the simulated results can be interpret, verification and validation have to be conducted. The sections below describes the results and conclusions. More detail and elaboration can be found in Appendix F Verification and Appendix G Validation.

8.5.1. Verification Results

Verification of the ComFLOW executable is done by a so called 'grid independence study'. Verification includes the main question of: **do we solve the equations right?**

A grid independence study checks if all the local sloshing pressures at a certain location and time are resolved to the same value, independent of grid size. Figure 8.14 illustrates two zones, scatter and convergence, where the horizontal axis states the cell size and the vertical axis defines the deviation of the value at a specific location and time. In order to achieve grid independence, the deviation of values should converge. The start of the convergence zone for the fineness of the mesh, depends heavily on the non-linearity of the fluid.

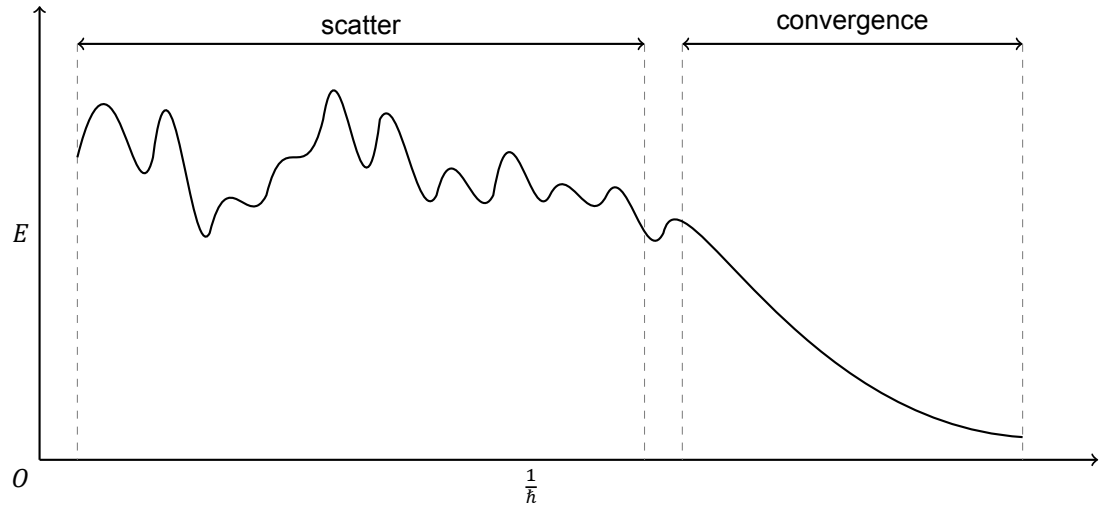

Figure 8.14: Verification - Grid independence zones

Phase 1

The verification of phase 1 consist of an analysis for different fluid behaviour. Namely, no sloshing, semi sloshing and sloshing. A mesh refinement is conducted for 10 cm, 5 cm, 3 cm, 2 cm, and in the sloshing case also 1 cm, call size. The no sloshing cases show a strong convergence of the results and can be interpreted as grid independent. However, both semi sloshing and sloshing cases does not show any sign of convergence. Concluding that the cell size is not sufficient enough and grid dependent.

Phase 2

The verification of phase 2 focused on the sloshing case with more refinement of the grid. Local mesh refinement is conducted and resulted in cell sizes 1 cm, 0.5 cm and 0.25 cm on the edge of the tank. Unfortunately, the refinement does not show convergence and can be concluded to still be in the scatter regime. The next step includes averaging the pressure distribution to its period and generate a mean distribution. The mean distribution is obtained by averaging the three periods into one, resulting in Figure 8.15 on the next page. No clear convergence can be concluded from the results, but a trend is present. Also, further analysis by the application of a RMS level and Peak-to-RMS ratio did not show a clear convergence sign.

Even though no clear grid independence can be shown, the results look trustworthy and reasonable. The mean pressure distribution shows a clear trend and phase of the sloshing impact. Both the RMS level and ratio show scatter behaviour up to a cell size of 1 cm. Finer mesh cases present a stable convergence that could imply entering the convergence zone of the grid

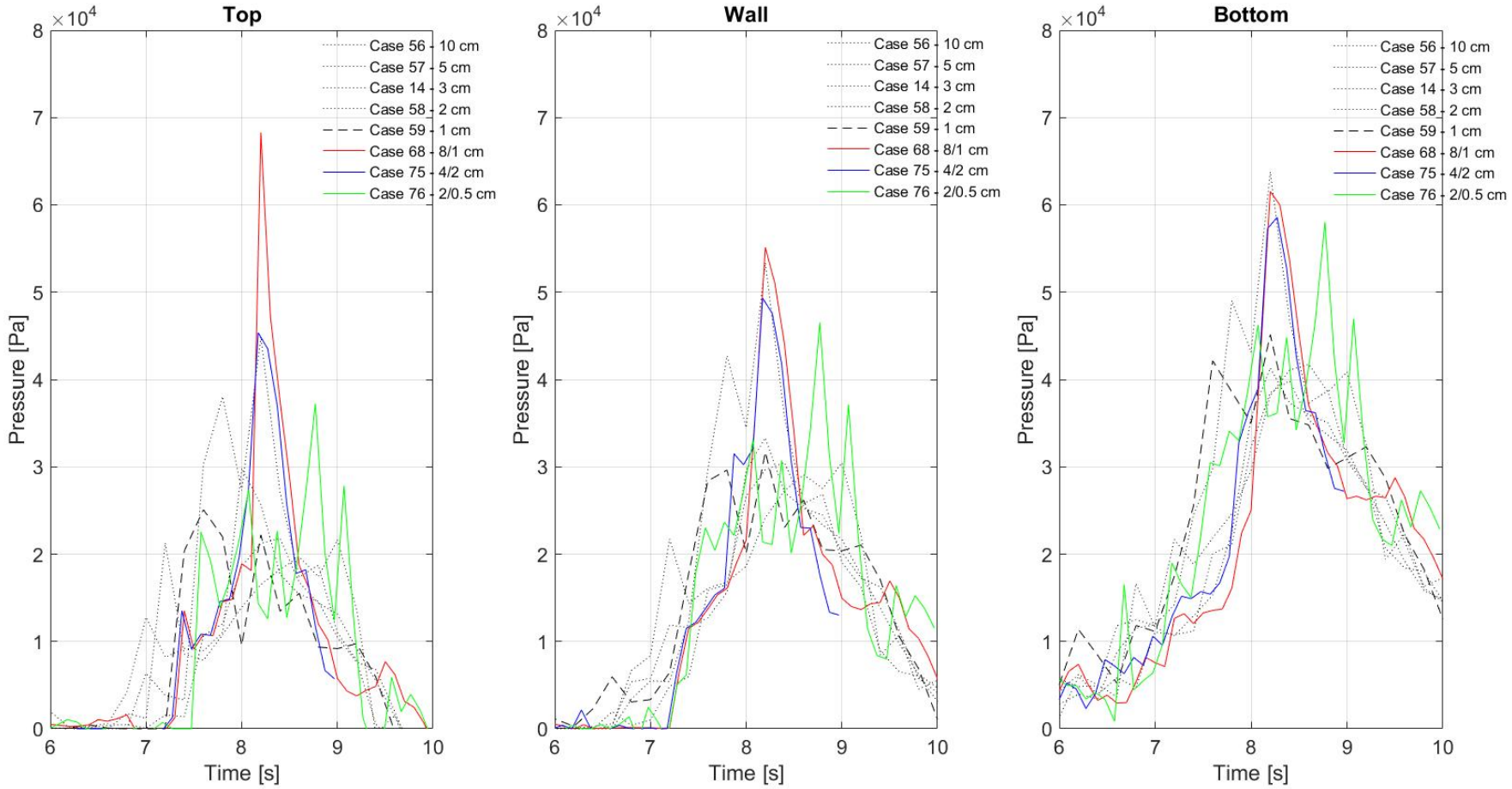

Figure 8.15: Verification - Mean pressure distribution

8.5.2. Validation Results

Validation of the ComFLOW executable is done by comparison of numerical results to a benchmark test. Validation includes the main question of: **do we solve the right equations?**

The validation will only include a comparison for global liquid impacts and behaviour. Local and detailed liquid behaviour does not lie in the scope of this research and is excluded. ComFLOW has already been validated in a broad sense, as described in the ComFLOW manual van der Plas, P. et al [24]. However, there is no validation done related to sloshing in storage tanks. Therefore, the best possibility within the scope is a comparison to results of a benchmark test related to fluid impacts.

Two benchmark tests on Sloshing Model Test (SMT) installations have been conducted and involved nine participants. The context of these benchmark tests is the comparison of fluid behaviour, especially impact pressures, from sloshing model test performed by different laboratories involving the same input conditions. The benchmark include a 2D rectangular tank filled with water and air. Two cases are selected for partly validating ComFLOW. Loysel et al. [11] describes the results of the 1^{st} benchmark test, where Loysel et al. [12] and Neugebauer et al. [13] present the results of a 2^{nd} benchmark test. Note, the comparison to these cases is not sufficient to fully validate ComFLOW for liquid impacts, but it's considered a basis.

The test tank can be defined as a parallelepiped-shape where one dimension is much smaller than the two others, therefore considered to be 2D. Furthermore, the tank consists of a nominal 85% water fill for both motion cases. The simulation is conducted with a two-phased flow of water and compressible air. A critical note has to be made in relation to the tank geometry. ComFLOW has a hard time mimicking the experimental fluid behaviour with the geometry used in the experiments. This is caused by a specific moment where the free surface nearly touches the top of the tank, $t = 1.1s$ and $t = 1.2s$ respectively. In order to simulate the exact same fluid behaviour with the given tank dimensions, the grid has to be extremely fine. Therefore, it is chosen to increase the height of the tank slightly with 5 mm. Concluding in an increase of the tank height from 0.670 m to 0.675 m (0.75%).

Case 78

This case holds a translation along the x-axis (surge) with an amplitude of 33 mm and a period of 0.975 s. It has been designed to create a large air pocket, where this kind of impact generates oscillating low frequency loads with a uniform moderate pressure inside the pocket. It is expected that the behaviour is easily captured and can be repeated accurately.

Figure 8.16 on page 55 present the results of the simulation compared to the experiment of the benchmark test. One can conclude good coinciding behaviour of the simulation during and after impact, t = 1.6 s and t = 1.8 s. However, the free surface show discrepancies in relation to the experimental results.

Case 79

This case holds a rotation along the y-axis (pitch) with an amplitude of 4.5 ºand a period of 1.207 s. It has been designed to generate a travelling pulse. The free surface hits the ceiling with a certain angle large enough for the gas to escape easy, so no air pockets are created.

Figure 8.17 on page 56 present the results of the simulation compared to the experiment of the benchmark test. Again, one can conclude good behaviour of ComFLOW in comparison to the experiment. Where the impact and after impact snapshots, t = 1.8 s and t = 2.0 s, show good resemblance.

Conclusion

It should be noted that due to discrepancies between the ComFLOW results and benchmark test videos, local pressures simulated by ComFLOW should be treated with caution. Furthermore, global fluid behaviour show a good and reliable resemblance.

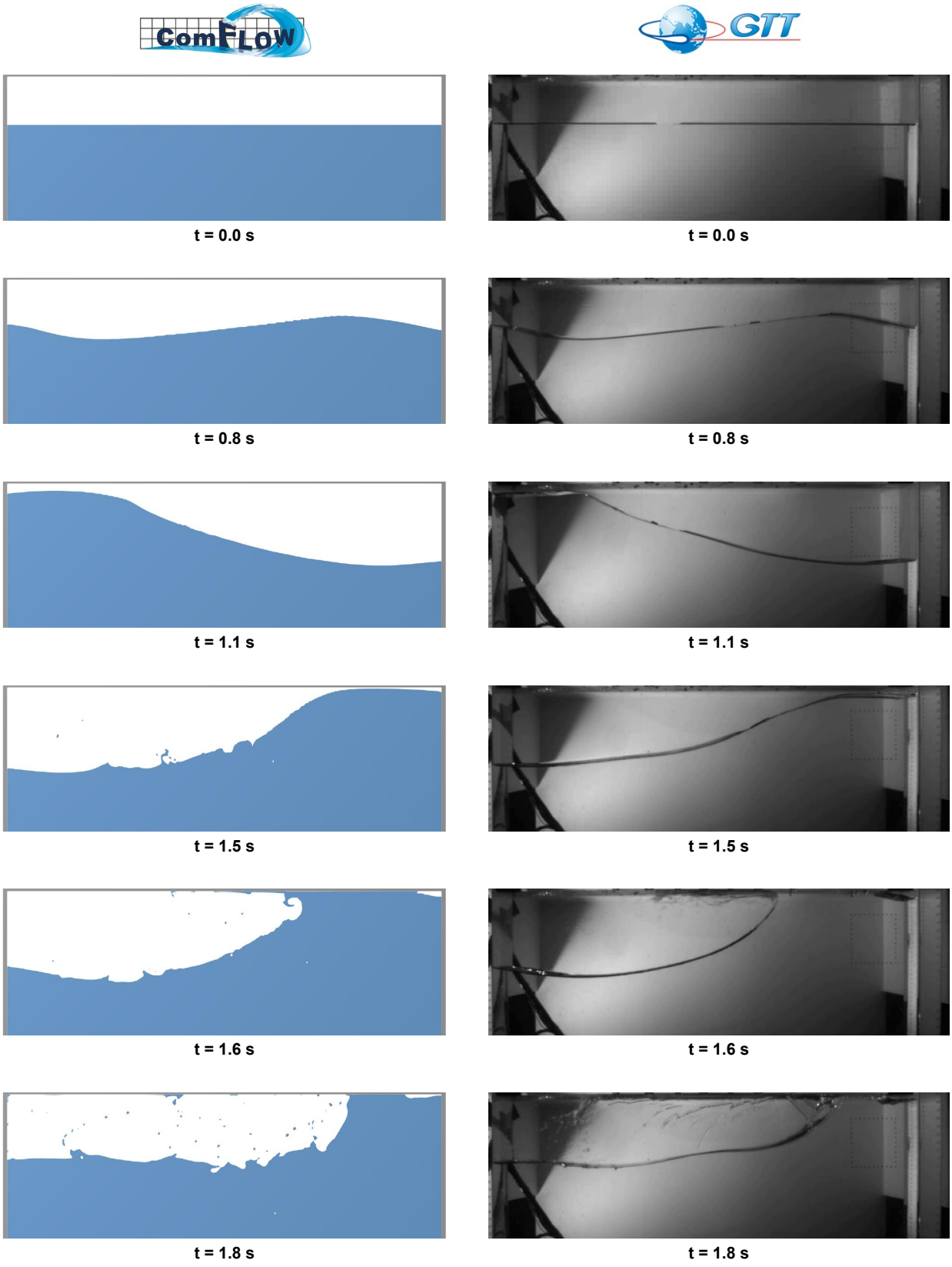

Figure 8.16: Validation - Case 77 - Surge (C16)

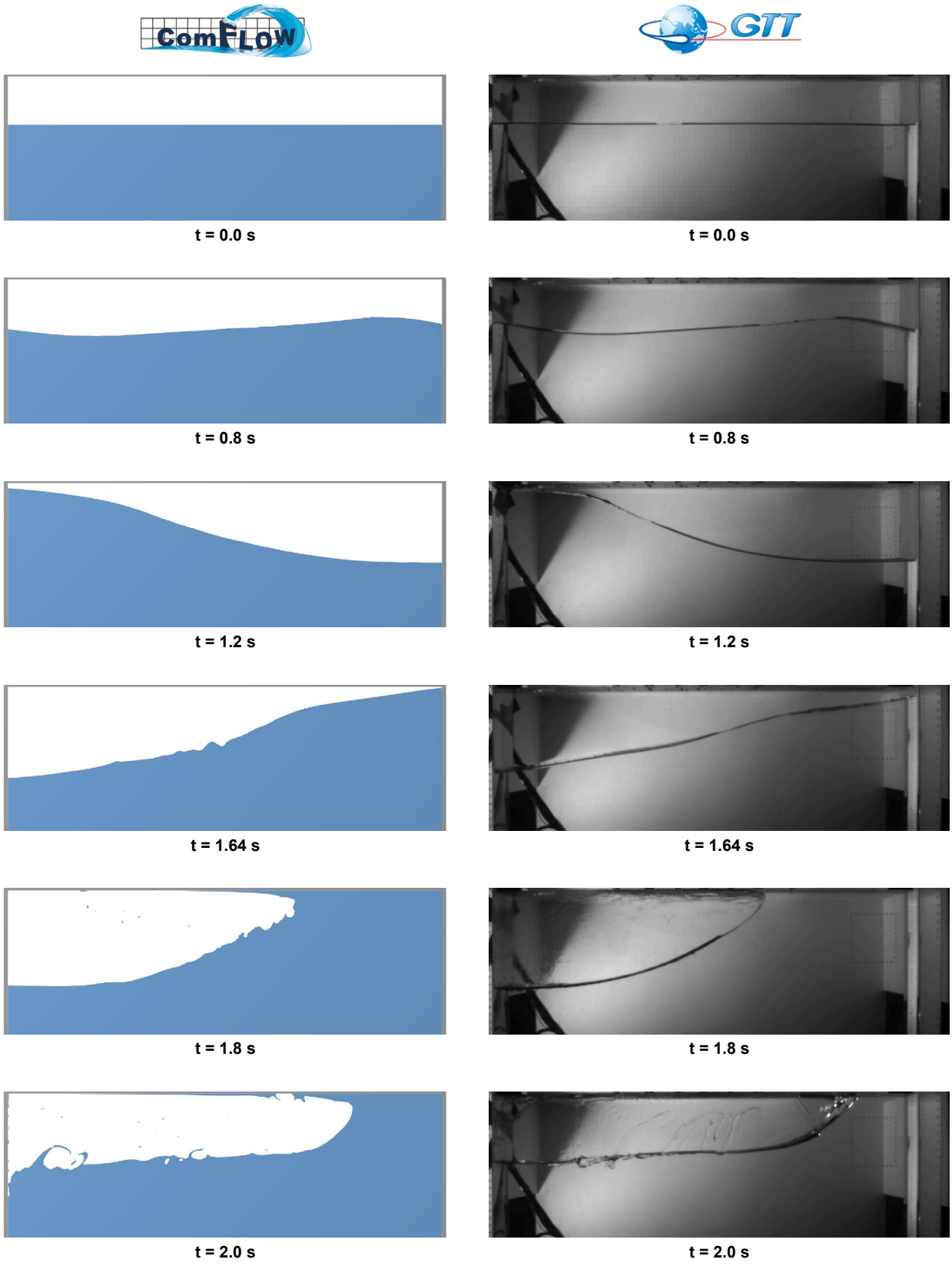

Figure 8.17: Validation - Case 78 - Roll (C18)

9

Conclusions & Recommendations

At the start of this research the following scope was set:

- *The scope of this research contains the assessment of sloshing behaviour in so called in-deck tanks, for a better understanding of the sloshing natural frequencies, impact area and impact pressure magnitude.*

In order to achieve this goal, ComFLOW simulations have been carried out in two phases. The first phase included a general understanding of the fluid behaviour, where the second phase contained a statistical analysis of long time simulations for selected sloshing cases. This chapter will reflect upon the scope by providing conclusions and recommendations.

9.1. Conclusions

Sloshing behaviour is expected when the natural frequency of the tank motion is close to the natural frequency of the fluid in the tank. Four parameters can be defined which influence the sloshing. Namely, fluid type, fill, effective sloshing length and the tank motion. Fluid behaviour in tanks can be divided in two types, non-impulsive oscillating behaviour and impulsive sloshing impact behaviour. For sloshing impacts a subdivision can be made into side wall impacts (low fillings) and roof impacts (high fillings). In order to indicate sloshing behaviour, one makes use of the so called natural modes. The natural period of the 1st mode is an important indicator for the occurrence of sloshing. The natural sloshing mode is derived purely based on effective sloshing length and fill, and gives insight in the order of magnitude for the sloshing period.

Phase 1

Reference projects and reports from CB&I resulted in a case study, which determined the input boundaries for the CFD simulations. The first phase of simulations contained a general approach in order to generate a global understanding of the fluid behaviour for various cases. A list of 66 cases have been established, which are subdivided into seven groups. These groups contain a variety of tank lengths, material, fill and motion combinations.

- The first group relates to the Aasta Hansteen SPAR. The gap in motion period of 57.5 s compared to the natural sloshing period (8 s) is too large and therefore no sloshing occurs. Concluding in non-impulsive oscillating fluid behaviour.
- The second group contained a tank length sloshing assessment for 7 m, 12 m, 15 m and 20 m lengths with 50% fill of water and MEG. Resulting in non-impulsive oscillations for 7 m lengths, semi-sloshing for 12 m and 15 m lengths, and impulsive sloshing impacts for 20 m tank lengths. One can conclude a high influence of the tank length parameter for sloshing. Also, the 7 m tank lengths are excluded in further analysis.

- The third group included the assessment of the residual tank lengths compared to different fill levels of water and MEG. All cases presented semi-sloshing behaviour, where specific cases for 15 m and 20 m tank lengths showed clear sloshing impacts. Sloshing behaviour seems to be sensitive for input parameter changes and occurs when a certain mixture of parameters is present. High fillings of 80% leave no space in the tank for the wave to create its shape and sloshing to occur.
- The fourth group analyzed the different nautical zones e.i. motions of the tank. Where for the same pitch period (9.7 s), the heeling angle, velocity and acceleration varied. The results show the occurrence of sloshing impacts for tank lengths of 15 m and 20 m in combination with heeling angles of 7.7 degrees or higher. Again, the other cases show mainly semi sloshing.
- The fifth group focused on the roll motion of the FPSO (20.8 s). Even though the period does not coincide with the natural period of the first mode, 5 - 13.5 s, it resulted in semi-sloshing behaviour in the same order of magnitude as pitch motion.
- The sixth group assessed an extended time simulation for four selected sloshing cases. It resulted in the occurrence of a huge pressure peak 3 times as high compared to other sloshing cases. These results inspired to carry out a statistical analysis for the second phase of the research, where long time simulations are able to capture the extreme sloshing impact cases.
- The last and seventh group of the first phase is linked to the verification, grid independence, of ComFLOW. This topic is elaborated in the paragraph of verification.

The order of magnitude for sloshing impact cases concluded at 100 kPa - 300 kPa, with an impact area of 2.4 m for the tank top and the whole vertical wall. There are not enough cases simulated to extract a bandwidth for the periods of the motion and the tank to coincide. However, Figures 7.1 and 7.2 present the overall consensus.

Lastly, a method comparison has been carried out to indicate if any empirical, conservative or analytical method can be used to calculate impulsive or non-impulsive fluid behaviour. The conservative method of CB&I is considered inaccurate in all cases of fluid behaviour. The empirical method described by the DNV is normally applied to LNG storage tanks of around 40 meters in length. Therefore not applicable at all for in-deck tanks of 12 m - 20 m. The resulting pressures are totally off and do not make any sense in all cases of fluid behaviour. The linear theory show good and accurate results for describing non-impulsive oscillating pressures (no sloshing). However, when non-linear behaviour starts to occur (semi-sloshing, sloshing), this theory can not predict the pressures accurately anymore. Concluding that for non-impulsive oscillating pressures, Eq. 7.1 can be used to indicate the maximum occurring pressure in the tank.

Phase 2

Seven sloshing cases and one roll case are picked from the first phase to be subjected to long time simulations. The produced statistical data is used to undergo a post-processing analysis in order to end up with Exceedance Probability Function. The EPF graphs of each case illustrate the possible magnitude of the sloshing impact related to the probability.

The statistical post processing analysis contains a 'short term' approach of the sloshing assessment procedure. Much statistical data is needed in order to generate a reliable 'tail' of the Probability Density Function. The reliability of this tail is directly related to the extreme sloshing impact values of the EPF. The statistical analysis is applied by five steps. Namely, Peak-over-Threshold method, Binning of sloshing impact pressures, PDF, CDF and concluding with the EPF. Two fitting curves are used in order to generate the PDF, the Generalized Pareto and Kernel Smoothing. In order to test the goodness of the fitting curves, a two sampled Kolmogorov-Smirnov test is applied. This test evaluate the maximum difference between the CDF of two sampled data distributions. The two fitting curves show totally different behaviour for the tail of the EPF. Where the GP converges to a horizontal asymptote, the KS converges to a vertical asymptote. However, the vertical asymptote of the Kernel Smoothing fitting represents a logical physical property. With a fixed motion, fill, fluid and tank length, there has to be a maximum impact pressure possible. There is not more energy and impact potential then a certain value. Which coincides perfectly with the vertical asymptote of the Kernel Smoothing fitting. However, one may discuss that fitting curves have no physical meaning whatsoever. More statistical data and analysis would improve the decision for the best fitting curve.

The resulting pressures for the eight motion cases are concluded by interpreting a 100 year return period. Due to their significance and main scope of the research, the table below present these results again.

Case	Length [m]	Fill	Fluid	Motion		Pressure [kPa]	
				Case	Type	Gen. Pareto	Kernel
67	20	50%	water	2	Pitch	295	310
68	20	50%	MEG	2	Pitch	220	230
69	15	70%	water	2	Pitch	215	235
70	20	70%	water	2	Pitch	495	325
71	15	45%	MEG	2	Pitch	165	150
72	20	70%	MEG	2	Pitch	310	310
73	20	50%	water	7	Pitch	1380	670
74	20	50%	water	6	Roll	290	275

Phase 2 - Overall Results

After analyzing the results of the second phase, six cases (67 - 72) can be compared to one another and resulted in a $\frac{\text{Fill}}{\text{Length}}$ ratio of 0.063 for the highest impact pressures. Furthermore, a comparison of the four influential parameters is made and briefly discussed at each bullet point below.

- Water has a lower density and viscosity but a higher surface tension compared to MEG. In the comparison cases of water and MEG, water shows a clear sign of higher sloshing impact pressures. Therefore, one may interpret that a lower viscosity of the fluid could contribute to more chaotic and extreme fluid behaviour under the same circumstances.
- One can firmly underline that sloshing occurs within the range of 50% - 70% fill. Phase 1 concluded that sloshing does not occur anymore with an 80% fill or higher.
- The tank length proves to be a sensitive input parameter. The 20 m tank lengths show more extreme sloshing impact pressures compared to the 15 m tank under the same circumstances. The impact order of magnitude increases drastically. Note, apparently the pitch motion period of 9.7 s coincides best with the 20 m tank compared to the other tank lengths.
- The motion input has, together with the tank length, a great influence on the sloshing impact pressures. Where higher accelerations result in a rapid increase of the impact pressure. The second phase did not focus to much on the roll motion case. However, the impact pressure order of magnitude is in the same range. This result shows the relevance of three dimensional simulations.

The sensitivity analysis includes the assessment of the threshold, binning, data-cut and data-random. The random data filter sensitivity is arguable but is added due to the grid independence issue. Resolving all local sloshing pressures at the right location and at the right time is not certain. Therefore, one can omit random data in order to mimic the influence on the statistical results. The sensitivities are dependent on each case, therefore it is not possible to formulate a general safety number. The data-cut and data-random filters shows the highest sensitivity of 30% - 50%. Furthermore, an average deviation for each case show that the Generalized Pareto fitting is more sensitive and concludes the Kernel Smoothing to be slightly more robust.

The verification of the ComFLOW executable contained a grid independence study. The non-impulsive oscillating case presented a strong convergence of the results and is interpreted as grid independent. Unfortunately, no clear convergence can be concluded for the semi-sloshing and sloshing cases. However, a mean pressure distribution is made and shows a clear trend and phase of the sloshing impact. Even though no grid dependence can be concluded, the results look trustworthy and reasonable.

The validation of the ComFLOW executable included a visual comparison of fluid behaviour. For both assessed cases of surge and roll motion, ComFLOW presents good fluid behaviour in comparison to the experimental results. The fluid impact of both cases is well simulated by ComFLOW and underline the capability of ComFLOW to simulate sloshing behaviour. However, it should be noted that due to discrepancies between the ComFLOW results and benchmark test videos, local pressures simulated by ComFLOW should be treated with caution.

9.2. Recommendations

At the start of this research little was known about the fluid behaviour in in-deck tanks. The situation for which sloshing could occur was totally unknown. After conducting this research, the fluid behaviour and contribution of the influence parameters are better understood. The scope and problem for this research is covered and more clarity to the possible impact pressure order of magnitude is presented. However, during the research new questions arise as well.

The recommendations listed below describe future work that could answer those questions and would expand the knowledge of sloshing in in-deck tanks for offshore applications.

- **Development of ComFLOW results in better performance and capabilities.**
  ComFLOW is continuously in development and has a big update scheduled for the end of 2016. The addition of automatic local grid refinement and parallel processing will contribute to a more accurate and faster simulation. These updates increase the potential of conducting longer time simulations, which results in the improvement of accuracy for the sloshing impact order of magnitude.
- **Investigate three-dimensional simulations by coupling pitch and roll motion.**
  Given the computational limitations, a combination of pitch and roll motion proved to be to expensive to implement. However, the update of ComFLOW could be promising to combine motions and carry out three-dimensional analysis.
- **Investigate the use of baffles for sloshing reduction.**
  The application of sloshing reduction possibilities is not in the scope of this research. However, it could be interesting to gather more insight on the sloshing reduction with the use of baffles. The relevance of this recommendations depends on whether the sloshing is considered a problem.
- **Investigate coupling effects of the in-deck tank and floating structure.**
  Coupling effects between the in-deck tank and floating structure are not analysed in this research. The coupling should be analyzed when more specific cases can be defined, which are related to future projects. The general origin and lack of detailed motion information of the offshore structure makes it hard to carry out a reliable coupling analysis in this stage.
- **Investigate the fatigue analysis of sloshing behaviour in in-deck tanks.**
  There has been no analysis done related to fatigue. Besides high sloshing impact pressures, fatigue is another possible issue for storage tanks. An indication of the lifetime for in-deck tanks could be important to gather more knowledge of.
- **Investigate grid independence for verification.**
  Grid independence was not achieved for sloshing cases. Again, the update of ComFLOW can help to apply finer meshes. Which should conclude in convergence of pressure deviations and therefore grid independence.
- **Carry out experiments for improved validation.**
  The validation of ComFLOW related to the simulated cases of this research is not ideal. In order to achieve better validation, experiments related to the defined cases could be carried out. This shall improve the reliability and interpretation of the sloshing impact order of magnitude.

Bibliography

[1] E.E.F. Botta and A.E.P. Veldman. On local relaxation methods and their application to convection-diffusion equations. *Journal of Computational Physics*, 48:127–149, 1981.

[2] A. W. Bowman and A. Azzalini. *Applied Smoothing Techniques for Data Analysis*. Oxford University Press Inc., 1st ed. edition, 1997.

[3] Bureau Veritas (BV). Ni 554 dt r00 e - design sloshing loads for lng membrane tanks. Electronic PDF version, May 2011.

[4] B. Düz. *Wave Generation, Propagation and Absorption in CFD Simulations of Free Surface Flows*. Delft University of Technology, 1st ed. edition, 2015. ISBN-13 978-94-6169-748-6.

[5] Det Norske Veritas AS (DNV). Dnv-rp-c205 environmental conditions and environmental loads. Electronic PDF version, April 2007. Sec.4 C-500.

[6] Det Norske Veritas AS (DNV). Dnv-os-c102 structural design of offshore ships. Electronic PDF version, October 2012. Sec.7.

[7] Det Norske Veritas AS (DNV). No. 30.9 - sloshing analysis of lng membrane tanks. Electronic PDF version, August 2014.

[8] Det Norske Veritas AS (DNV). Rules for classification of ships pt.3. Electronic PDF version, January 2015. Ch.1 Sec.4 304.

[9] M. Dröge and R. Verstappen. A new symmetry-preserving cartesian-grid method for computing flow past arbitrary shaped objects. *Int. Journal for Numerical Methods in Fluids*, 47:979, 2005.

[10] Kleefsman et al. A volume-of-fluid based simulation method for wave impact problems. *Journal of Computational Physics*, 206:363–393, 2005.

[11] Loysel et al. Results of first sloshing model test benchmark. ISOPE, June 2012.

[12] Loysel et al. Results of 2012-2013 sloshing model test benchmark. ISOPE, June 2013.

[13] Neugebauer et al. Experimental and numerical investigation of single impacts in a 2d tank. ISOPE, June 2014.

[14] Veldman et al. The numerical simulation of liquid sloshing on board spacecraft. *Journal of Computational Physics*, 224:82–99, 2007.

[15] O.M. Faltinsen and A.N. Timokha. *Sloshing*. Cambridge University Press, 1st ed. edition, 2009. ISBN-13 978-0-521-88111-1.

[16] European Committee for Standardization (ISO). Iso 19904-1:2006 floating offshore structures - pt. 1. Electronic PDF version, November 2006. Ch.7 Sec.6.

[17] R.A. Ibrahim. *Liquid sloshing dynamics, theory and applications*. Cambridge University Press, 1st ed. edition, 2005. ISBN-13 978-0-521-83885-6.

[18] Lloyd's Register (LR). Sloshing assessment guidance document for membrane lng operations. Electronic PDF version, May 2009.

[19] Lloyd's Register (LR). Classification of offshore units pt. 11. Electronic PDF version, July 2014. Ch.4.

[20] F.J. Massey. The kolmogorov-smirnov test for goodness of fit. *Journal of the American Statistical Association*, 46(253):68–78, 1951.

[21] Norsok. N-003 actions and action effects. Electronic PDF version, September 2007. Sec.4 C-500.

[22] American Bureau of Shipping (ABS). Liquefied gas carriers with independent tanks. Electronic PDF version, January 2010. Sec.3.

[23] P. Sonneveld. Cgs, a fast lanczos-type solver for nonsymmetric linear systems. *SIAM Journal on Scientific and Statistical Computing*, 10(1):36–52, 1989.

[24] P. et al. van der Plas. Manual comflow version 3.9.x / 4.0. ComFLOW Project,University of Groningen, 2015.

[25] R. Verstappen and A.E.P. Veldman. Symmetry-preserving discretization of turbulent flow. *Journal of Computational Physics*, 187:343, 2003.

A

Sloshing Impact Type - Illustrations

SIDE WALL IMPACT - Gas cushion

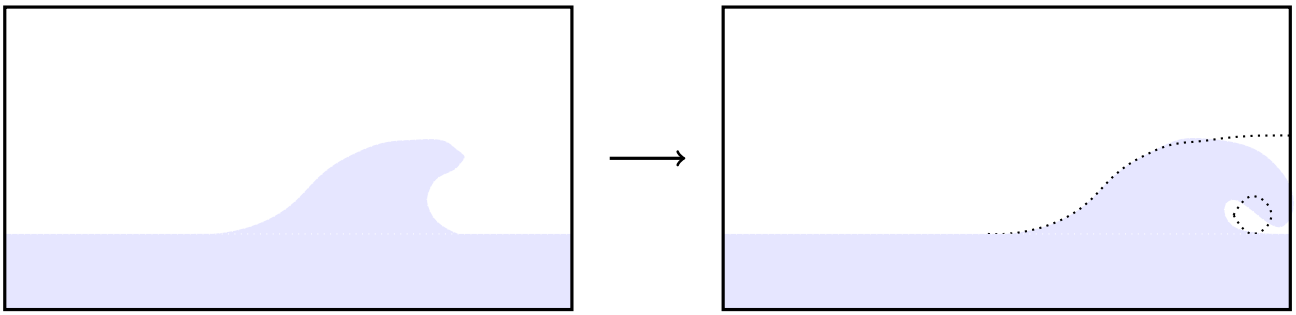

Figure A.1: Low Filling - SIDE WALL IMPACT - Gas cushion
A gas cushion occurs when the wave breaks before the wall.

SIDE WALL IMPACT - No gas cushion

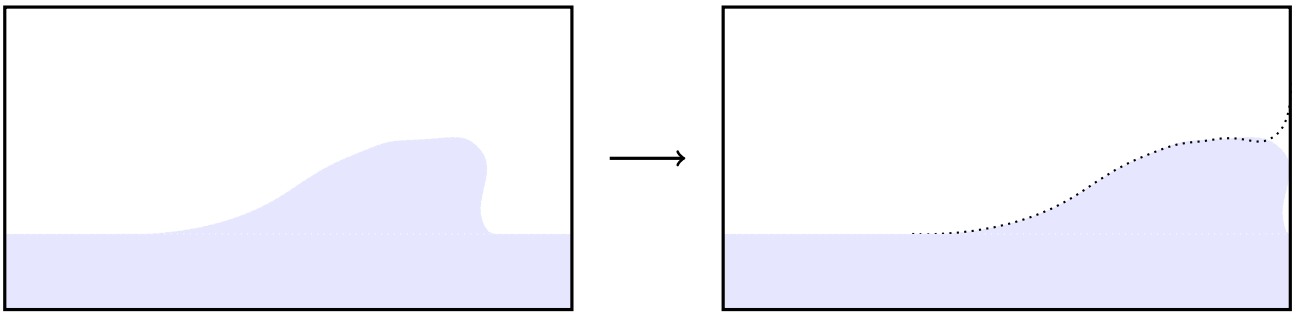

Figure A.2: Low Filling - SIDE WALL IMPACT - No gas cushion
In the event of a progressive wave, frontal impact occurs.

SIDE WALL IMPACT - Flip through

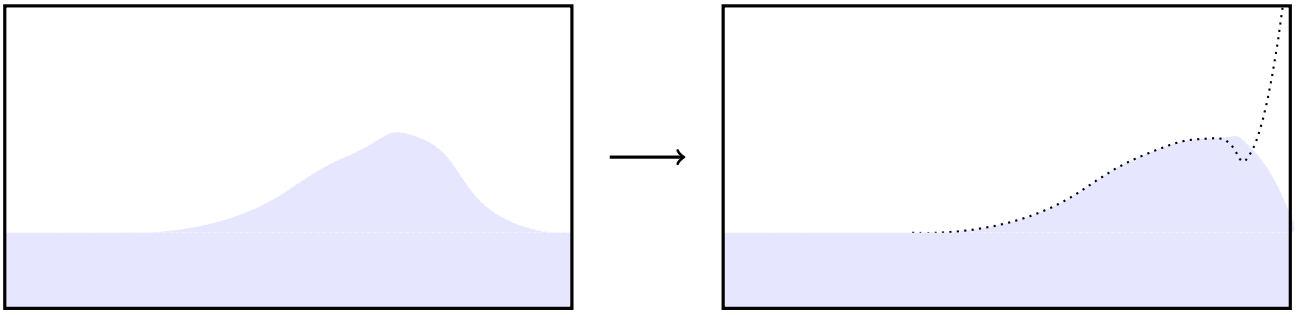

Figure A.3: Low Filling - SIDE WALL IMPACT - Flip through
Steep wave approaches wall without impacting, jet flow is generated at the wall.

ROOF IMPACT - Gas cushion

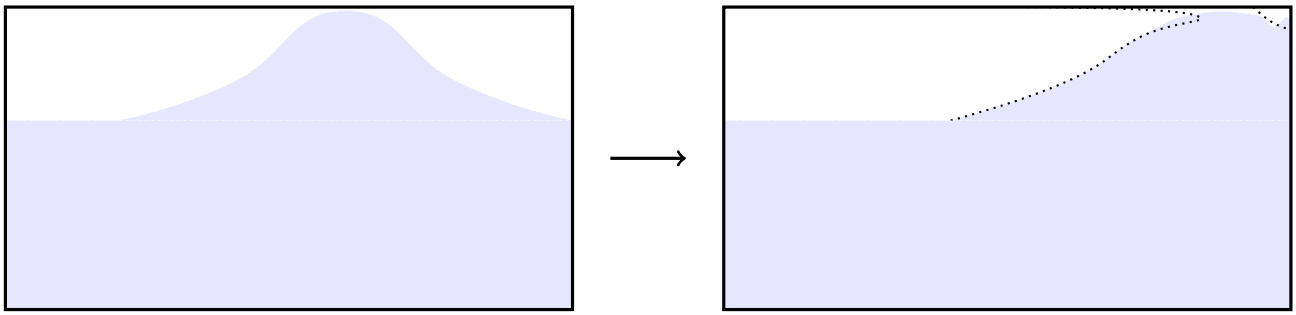

Figure A.4: High Filling - ROOF IMPACT - Gas cushion
Impact with gas cavity.

ROOF IMPACT - Nearly horizontal free surface

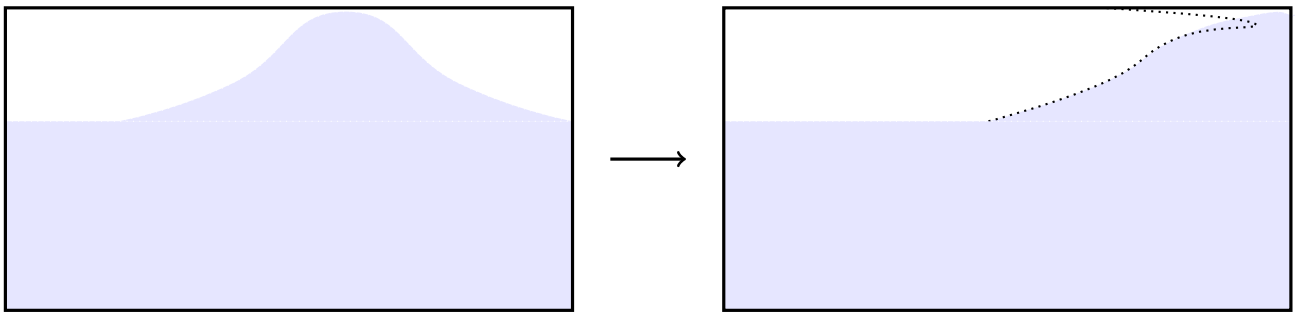

Figure A.5: High Filling - ROOF IMPACT - Nearly horizontal free surface
Flat impact of nearly horizontal free surface.

ROOF IMPACT - Flip through with jet impact

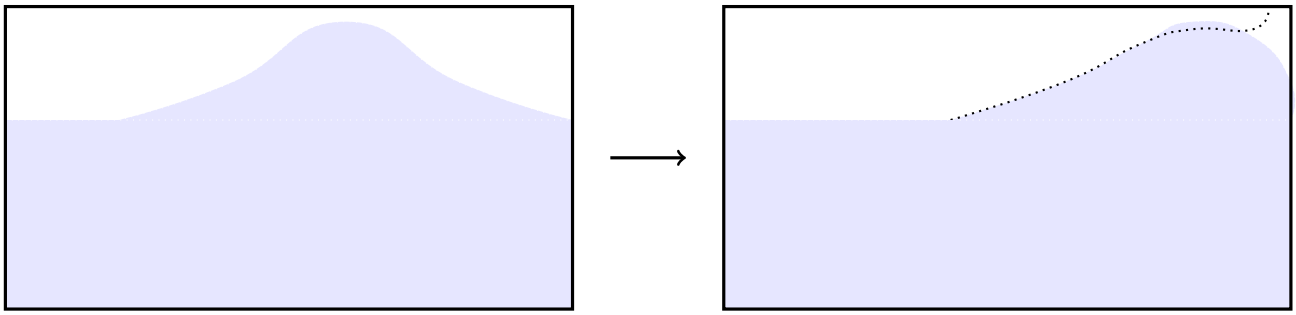

Figure A.6: High Filling - ROOF IMPACT - Flip through with jet impact
High-curvature free-surface impact with a high velocity jet.

B

ComFLOW

This Appendix will include more elaboration of the ComFLOW executable. First, the mathematical and numerical model of ComFLOW is described. Followed by an example of the input file used for the numerical simulations.

The elaboration of the executable include the conservation laws, boundary and free surface conditions, computational domain and grid, cell labeling, discretization and the solution technique. In order to keep the elaboration complete and thorough, a repetition of some parts is possible.

The elaboration of the input file includes an example where each step is published and followed by a short elaboration. The Pre-Processing files, Appendix D (Phase 1) and Appendix E (Phase 2), present the calling sequence and input files.

B.1. Mathematical Model One-Phase Flow

When the fluid is treated as a homogeneous continuum, as described in section 2.4 at page 7, the conservation laws of physics can be used to describe the fluid flow in a given domain. The laws subjected are the conservation of mass and conservation of momentum. Where the conservation law of energy is effectively replaced by the incompressibility condition of the fluid.

B.1.1. Conservation Laws

Derivations of the conservation laws are well documented and for the sake of brevity, only the final forms of these laws are stated below.

Conservation of mass

In an arbitrary and fixed control volume Ω with boundary Γ, conservation of mass can be stated in integral form as follows

$$\int_{\Gamma} \mathbf{u} \cdot \mathbf{n} \, d\Gamma = 0 \tag{B.1}$$

where $\mathbf{u} = (u, v, w)^T$ is the flow velocity and $\mathbf{n}$ is the normal vector pointing outward along the boundary of the control volume. The term on the left hand side of (B.1) denotes the net inflow of mass through the boundary of the control volume, which is equal to zero.

Conservation of momentum

Based on another fundamental physical principle, Newton's second law, the conservation of momentum for fluid flow can be stated. Taken the assumptions into account, the equation can be written as

$$\int_{\Omega} \frac{\partial \mathbf{u}}{\partial t} \, d\Omega + \int_{\Gamma} \mathbf{u} \, \mathbf{u} \cdot \mathbf{n} \, d\Gamma = -\frac{1}{\rho} \int_{\Gamma} p\mathbf{n} \, d\Gamma + \nu \int_{\Gamma} \nabla \mathbf{u} \cdot \mathbf{n} \, d\Gamma + \int_{\Omega} \mathbf{f} \, d\Omega \tag{B.2}$$

Where ν is the kinematic viscosity, $\nu = \mu/\rho$. $\nabla = (\partial/\partial x, \partial/\partial y, \partial/\partial z)^T$ is the gradient operator and **f** represents the external body forces acting on the fluid such as gravity, centrifugal and Coriolis forces. In equation (B.2), the term on the left indicates the time rate of increase of momentum in Ω. The increase is related to the three parts on the right hand side, respectively: The net inflow of momentum through the boundary Γ, contribution from the surface forces acting on the surface of the control volume, and contribution from the body forces which act directly on the fluid in Ω.

As the incompressibility condition effectively replaces the conservation law of energy, two conservation laws are left in order to model the numerical method. Now, an exact study is required to discretize each term of the Eqs. (B.1) and (B.2). This will be the main subject of section B.2.

B.1.2. Boundary and free surface conditions

This section includes the explanation of the boundary conditions imposed on various boundaries that may be encountered in the domain. A critical part of the numerical method is the application of physical and initial boundary conditions in order to solve the governing equations in a computational domain. The specification of the boundary conditions allows us to obtain particular solutions from the governing equations. The employment of a proper set of boundary conditions for a specific fluid flow makes all the difference for the solution to be unique, stable and accurate. Listed below are two boundary conditions described, that will be used in the numerics of the ComFLOW executable. Namely, the solid boundary and free surface condition.

Solid boundary

For the application of in-deck tanks, the boundaries are considered to be solid. Which conclude in the following condition

$$\mathbf{u} = 0 \tag{B.3}$$

The equation states that the solid boundary is impenetrable and the fluid does not slip along the boundary. This is often referred to as the Dirichlet or no-slip condition. Both normal and tangential components of the velocity vector become zero.

Free Surface

As described in section 2.4 at page 7, only the air and fluid are considered for the in-deck tank cases. The separation layer between the air and the fluid is called the free surface or interface layer. Since the air is modelled as a void, the term of free surface is more suitable for this occasion. At the free surface, the normal and tangential forces are balanced. When continuity of the normal and tangential stresses is applied, the following equations can be defined

$$\mu\left(\frac{\partial u_n}{\partial t} + \frac{\partial u_t}{\partial n}\right) = 0 \tag{B.4}$$

$$-p + 2\mu\frac{\partial u_n}{\partial n} = -p_0 + \sigma\kappa \tag{B.5}$$

Where u_n and u_t correspond to the normal and tangential component of the velocity, respectively, p_0 is the atmospheric pressure, σ is the surface tension, and κ denotes the total curvature of the free surface.

Furthermore, the evolution of the free surface in time with respect to the underlying velocity field must be modelled as well. This is established using the volume-of-fluid (VOF) method, which will be explained in the next section B.2

Calculation of Forces.

The fluid in a flow domain introduces a force on the objects inside its domain and on the boundaries. This force normally consist of two parts, namely the pressure force and the shear force. In ComFLOW the shear force is neglected in the calculation of the force. Typically the shear force is much smaller then the pressure force. Therefore, it is assumed that the shear force is so small it can be neglected from calculation. The pressure force is calculated as an integral of the pressure along the boundary Γ of the observed object. This results in the following formula

$$\mathbf{F}_p = \int_\Gamma p\mathbf{n}\, d\Gamma \tag{B.6}$$

B.2. Numerical Model

Before starting the numerical treatment of the terms in the governing equations, the computational framework of the spatial discretization employed in the numerical method is described. This includes the computational domain and grid, object and fluid configuration, and cell labeling. Thereafter, the spatial discetization of the governing equations will be treated.

Computational Domain and Grid

The computational domain Ω is rectangular and a Cartesian grid or grid refinement has been applied. The spatial step of the grid is defined as a 'numerical number' in order to identify the fine or coarseness of the grid. In the ideal situation one likes to indicate the cell size by number of cells per fluid flow feature. However, in the case of different sloshing scenarios, this is not a clear solution. Figure B.1 below provides a visualization of the two different grid types applied.

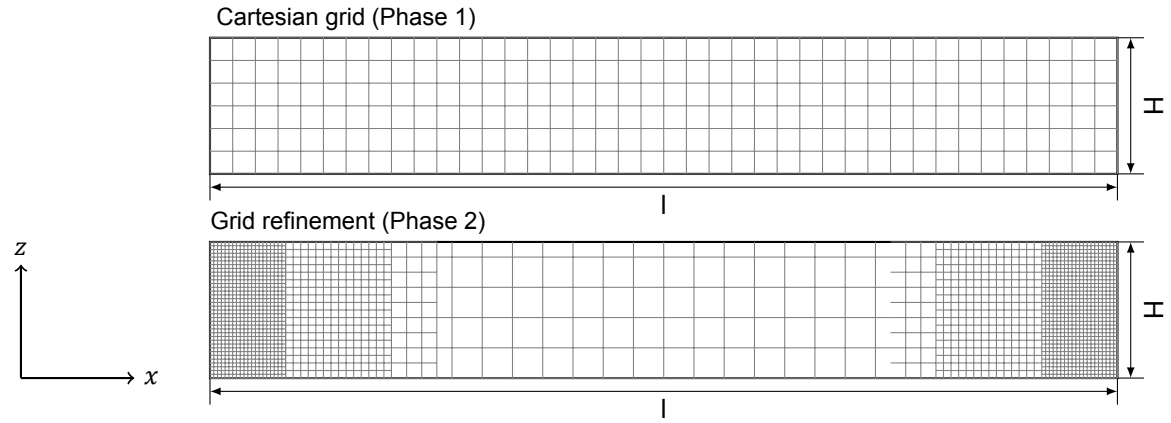

Figure B.1: Cartesian grid and grid refinement

The flow variables $\mathbf{u} = (u, v, w)$ and p, which are described in the conservation formulas, are positioned in a grid cell using the staggered grid arrangement. The velocity components are located at the face centers, while the pressure is located at the center of the grid cell. An illustration of the staggered grid arrangement is presented in Figure B.2 below.

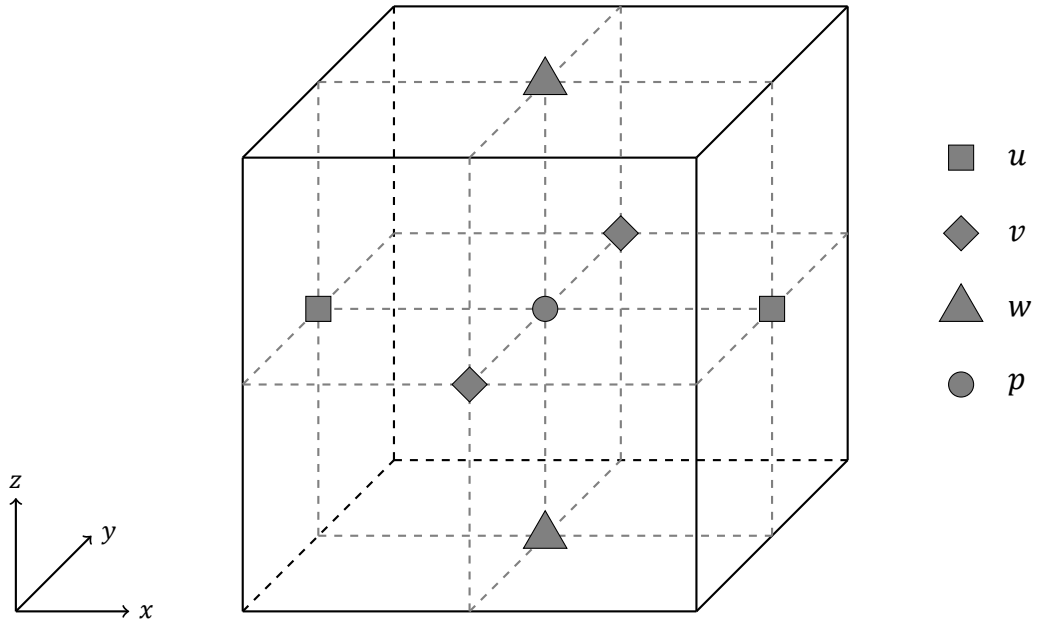

Figure B.2: Staggered grid arrangement in a grid cell - Positions of velocity and pressure components

Cell labeling
In order to distinguish the different type of cells and the character of the cell, labeling is done. This difference in character is incorporated in the numerical method by introducing edge and volume apertures. These apertures are used to measure for which part of the cell, the face or cell volume is open to flow. The following labels are used: a boundary (B), an empty cell (E), a surface cell (S) and a fluid cell (F). Where the free surface labeling is updated for each time step. No uncut cells are used for the in-deck tank configuration. An example of the labeling is given in Figure B.3 below.

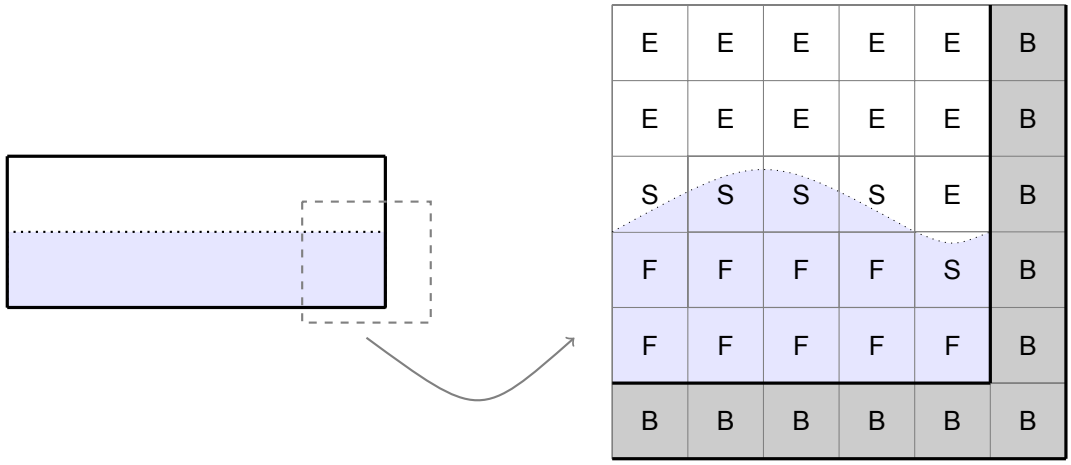

Figure B.3: Cell labeling example - In-deck tank 2D

Spatial discretization of the governing equations
In order to spatially discretize the governing equations inside the computational domain, the finite volume formulation is applied. Each term of the governing equations will be treated separately based on the numerical framework explained in the previous sections. The discretization will be carried out for the 2D application. For the sake of simplicity. The extension to 3D is considered to be straightforward.

When the matrix-vector notation is used, the equations of motion (Eq. (B.1) and (B.2)) can be rewritten as

$$\mathbf{D}\mathbf{u}_h = 0 \tag{B.7}$$

$$\Omega \frac{d\mathbf{u}_h}{dt} + \mathbf{C}(\mathbf{u}_h)\mathbf{u}_h + \mathbf{V}\mathbf{u}_h + \mathbf{G}\mathbf{p}_h = 0 \tag{B.8}$$

where $\mathbf{D}$ and $\mathbf{G}$ denote the discrete divergence and gradient operators. Ω is a diagonal matrix containing the sizes of the control volumes, where, $\mathbf{u}_h$ contains the discrete velocities, $\mathbf{p}_h$ contains the discrete pressures, and $\mathbf{C}(\mathbf{u}_h)$ and $\mathbf{V}$ include the convective and viscous diffusive coefficient operators, respectively.

At this moment the specific discretization technique, symmetry preserving discretization, comes into play. After the analysis related to the discrete energy of the discrete governing equations, Verstappen and Veldman [25] state that it decreases in time when the symmetry preserving discretization is employed. Resulting, consequently, in a stable system. This allows that a solution to the system motioned above can be determined on any arbitrary grid. More information can be found in Droge and Verstappen [9].

Discretization of Continuity equation

The continuity equation (B.1) is applied in the cell centers, and discretized using the staggered grid arrangement presented in Figure B.2. The velocity components are defined to be located at the face centers of the cell. Where the discretization (see Figure B.4) of the continuity equation in the cell yields

$$u_w \Delta z - u_e \Delta z + w_s \Delta x - w_n \Delta x = 0 \tag{B.9}$$

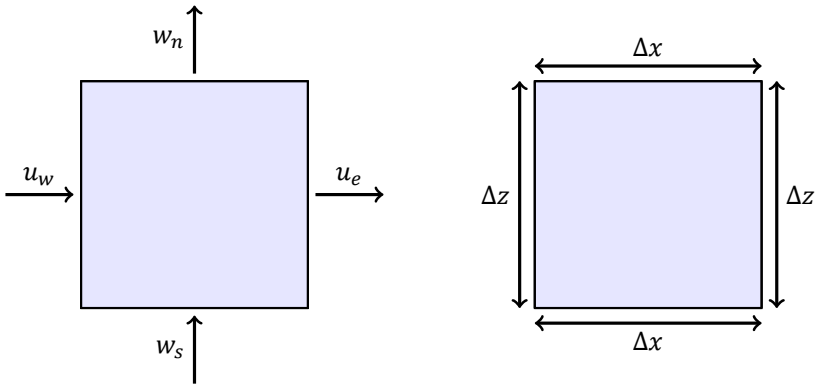

Figure B.4: A 2D cut-cell in which the continuity equation is applied

Discretization of Momentum equation

The spatial discretization of the momentum equation shall be explained for every term in 2D in the x-direction and can be applied for the other axes y and z as well. The momentum conservation equation, (B.2), is split in five parts. Rewritten for the x-direction follows

$$\underbrace{\int_{\Omega_f} \frac{\partial u}{\partial t}\, d\Omega_f}_{\text{Time Derivative}} + \underbrace{\int_{\partial\Omega_f} u\, \mathbf{u}\cdot\mathbf{n}_f\, d\partial\Omega_f}_{\text{Convection term}} = \underbrace{-\frac{1}{\rho}\int_{\partial\Omega_f} p n_x\, d\partial\Omega_f}_{\text{Pressure term}} + \underbrace{\int_{\partial\Omega_f} \nabla\mathbf{u}\cdot\mathbf{n}_f\, d\partial\Omega_f}_{\text{Diffusion term}} + \underbrace{\int_{\Omega_f} \mathbf{f}\, d\Omega_f}_{\text{Body Force term}} \tag{B.10}$$

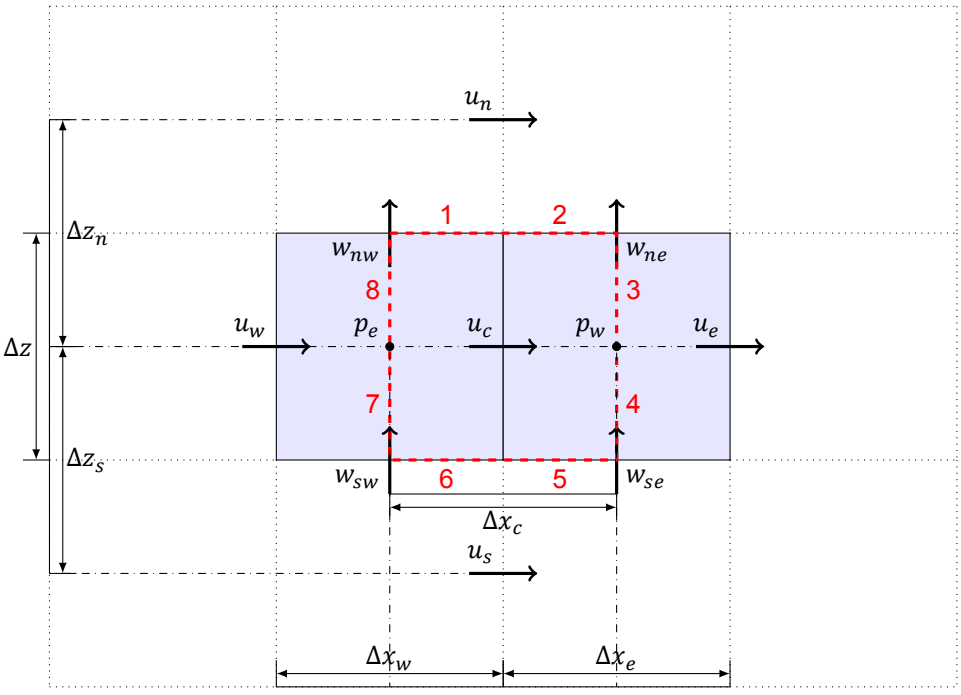

Figure B.5: A 2D cut-cell used in the discretization of the momentum equation, control volume is indicated by a red dashed line

Time Derivative

$$\int_{\Omega_f} \frac{\partial u}{\partial t}\, d\Omega_f$$

For the spatial discretization of the time derivative in Eq. B.10, the midpoint rule is applied. Which concludes in:

$$\int_{\Omega_f} \frac{\partial u}{\partial t}\, d\Omega_f = \frac{\partial u_c}{\partial t}\, \Omega_c \tag{B.11}$$

where Ω_c denotes the control volume enclosed by the red line that belongs to the horizontal velocity u_c, illustrated in Figure B.5. Taking F_c^b as the volume aperture of the control volume, Ω_c can be computed with the following expression

$$\Omega_c = F_c^b \cdot \Delta x_c \cdot \Delta z \tag{B.12}$$

Convection term

$$\int_{\partial\Omega_f} u\, \mathbf{u} \cdot \mathbf{n}_f\, d\partial\Omega_f$$

The convection term can be split into two scalars, where u denotes the velocity component in the x-direction and $\mathbf{u} \cdot \mathbf{n_f}\ d\partial\Omega_f$ denotes the mass flux through the entire boundary of the control volume. In order to simplify the discretization of the mass flux term, the control volume is divided into eight segments, see Figure B.5. This approach allows to evaluate the integral over each of the segments separately, concluding in

$$\int_{\partial\Omega_f} u\, \mathbf{u} \cdot \mathbf{n}_f\, d\partial\Omega_f = \sum u_i\, m_i \tag{B.13}$$

where u_i and m_i represent the velocity component in the x-direction at the ith segment and the mass flux through the ith segment, respectively. Concluding that the mass flux through each segment can be calculated as follows

$$m_1 = -\frac{1}{2}\, w_{nw}\, \Delta x_w$$

$$m_2 = -\frac{1}{2}\, w_{ne}\, \Delta x_e$$

$$m_{3,4} = -\,(u_e + u_c)\ \Delta z$$

$$m_5 = \frac{1}{2}\, w_{se}\, \Delta x_e$$

$$m_6 = \frac{1}{2}\, w_{sw}\, \Delta x_w$$

$$m_{7,8} = (u_w + u_c)\ \Delta z$$

Now, determining the u_i at the ith segment of the boundary is more critical. The simplest and most straightforward approach would be taking the average of the velocities on each side of the ith segment. For example, for the segment of $u_1 = (u_n + u_c)/2$. Or for segment u_3, it concludes in $u_3 = (u_e + u_c)/2$. Consequently, substituting u_i and m_i described above in Eq. B.13 completes the discretization for the convective term of the x-momentum equation.

Diffusion term

$$\int_{\partial\Omega_f} \nabla\mathbf{u}\cdot\mathbf{n}_f \, d\partial\Omega_f$$

Factor ν is omitted from this equation.

[10] describes the diffusion term as a volume integral,

$$\int_{\partial\Omega_f} \nabla\mathbf{u}\cdot\mathbf{n}_f \, d\partial\Omega_f = \int_{\Omega} \nabla\cdot\nabla u \, d\partial\Omega \tag{B.14}$$

The volume integral results in a second order derivative and is calculated using the midpoint rule, which was applied previously when discretizing the time derivative. The inner derivative is applied at the boundary faces of the control volume 1 - 8, where the outer derivative is applied at the center of the control volume, see Figure B.5 for the notation. Resulting in

$$\nabla\cdot\nabla u = \frac{\left(\frac{\partial u}{\partial x}\right)_3 + \left(\frac{\partial u}{\partial x}\right)_4 - \left(\frac{\partial u}{\partial x}\right)_7 - \left(\frac{\partial u}{\partial x}\right)_8}{\Delta x_c} + \frac{\left(\frac{\partial u}{\partial z}\right)_1 + \left(\frac{\partial u}{\partial z}\right)_2 - \left(\frac{\partial u}{\partial z}\right)_5 - \left(\frac{\partial u}{\partial z}\right)_6}{\Delta z_c} \tag{B.15}$$

where $\Delta x_c = (\Delta x_e + \Delta x_w)/2$, $\Delta z_c = (\Delta z_n + \Delta z_s)/2$, and the derivative at a face can be obtained by

$$\left(\frac{\partial u}{\partial x}\right)_{3,4} = \frac{u_e - u_c}{\Delta x_e} \qquad \text{or} \qquad \left(\frac{\partial u}{\partial z}\right)_{1,2} = \frac{u_n - u_c}{\Delta z_n} \tag{B.16}$$

The derivatives of the other faces can be computed in a similar fashion.

Pressure term

$$\int_{\partial\Omega_f} p n_x \, d\partial\Omega_f$$

Factor $-\,1/\rho$ is omitted from this equation. The pressure term is assumed to have a constant value representing the whole grid cell. Where n_x is the x-component of the outward pointing normal along the boundary of the control volume. Similarly to the treatment of the convection and diffusion terms, this term is also evaluated for each segment of the control volume boundary as follows

$$\int_{\partial\Omega_f} p n_x \, d\partial\Omega_f = \sum p_i \int_i n_{x_i} \, d\partial\Omega_f \tag{B.17}$$

From Figure B.5 one can conclude that $p = p_e$ holds for segments 1,6,7 and 8, and $p = p_w$ holds for segments 2,3,4 and 5. However, segments 1,2,5 and 6 do not contribute to the integral as $n_x = 0$ applies along them. This leaves segments 3,4,7 and 8 for which their contributions are calculated as

$$\int_{\partial\Omega_f} p n_x \, d\partial\Omega_f = \frac{1}{2} p_w \, \Delta z + \frac{1}{2} p_w \, \Delta z - \frac{1}{2} p_e \, \Delta z - \frac{1}{2} p_e \, \Delta z \tag{B.18}$$

$$\int_{\partial\Omega_f} p n_x \, d\partial\Omega_f = (p_w - p_e) \; \Delta z \tag{B.19}$$

Body Force term

$$\int_{\Omega_f} \mathbf{f} \, d\Omega_f$$

Gravity is the only external force present, thus $\mathbf{f} = \mathbf{g} = (g_x, g_y, g_z)^T$. The discretization have to match that of the pressure term. In absence of all other terms, the change in pressure must be related to this gravity term. This concludes in the discretization of the gravity term, $\mathbf{g} = (0, 0 - g)^T$, for the momentum

equation in the z-direction. With the help of Gauss' divergence theorem, the volume integral is written as a boundary integral. The following expression is obtained

$$\int_{\partial\Omega_f} -gzn_z \, d\partial\Omega_f. \tag{B.20}$$

When the boundary integral for the hydrostatic pressure potential is computed, it results in

$$\int_{\partial\Omega_f} -gzn_z \, d\partial\Omega_f = -\Delta x g(z_n - z_s) \tag{B.21}$$

in which z_n and z_s stands for the center locations along the z-direction of the northern and southern cells, respectively.

Temporal discretization and solution technique

The discetization of the equations of motion (B.1) and (B.2) in time will be explained briefly. This process is realized with the use of the first-order Euler forward method. For a simple time derivative term $d\varphi/dt = f(\varphi)$, the forward Euler takes the following form

$$\varphi^{n+1} = \varphi^n + \Delta t f(\varphi^n) \tag{B.22}$$

Now, for a better explanation of the solution technique that is used in the ComFLOW program, the equations of motion shall be rewritten in a more schematic formulation. The conservation of Mass and conservation of Momentum, respectively

$$\text{div } \mathbf{u}^{n+1} = 0 \tag{B.23}$$

$$\frac{\mathbf{u}^{n+1} - \mathbf{u}^n}{\Delta t} + \frac{1}{\rho} \text{ grad } p^{n+1} = \mathbf{R}^n \tag{B.24}$$

where n and $n+1$ represent the old and new time level, Δt is the time step, and $\mathbf{R}$ contain all the convective, diffusive and body forces

$$\mathbf{R}^n = -(\mathbf{u}^n \cdot \text{grad})\mathbf{u}^n + \nu \text{ div grad } \mathbf{u}^n + \mathbf{F}^n \tag{B.25}$$

where ν is the kinematic viscosity.

When discretizing the continuity equation (B.23) at the new time level, a divergence-free velocity field is ensured. If the terms of Eq. (B.24) are rearranged, it can be rewritten to

$$\mathbf{u}^{n+1} = \bar{\mathbf{u}}^n - \frac{\Delta t}{\rho} \text{ grad } p^{n+1} \tag{B.26}$$

where

$$\bar{\mathbf{u}}^n = \mathbf{u}^n + \Delta t \mathbf{R}^n \tag{B.27}$$

Whereby the term $\bar{\mathbf{u}}^n$ is referred to as an auxiliary velocity and calculated first in the solution process.

After the substitution of Eq. (B.26) into (B.23), the so called Poisson equation can be defined

$$\text{div grad } p^{n+1} = \frac{\rho}{\Delta t} \text{ div } \bar{\mathbf{u}}^n \tag{B.28}$$

The Poisson equation is solved by application of the SOR (Successive Over Relaxation) and BiCGSTAB pressure solvers. The interested reader can find more elaboration on the solvers at [1] and [23]. Once the new (p^{n+1}) pressure field is obtained, the velocity field for the new time level can be calculated with Eq. (B.26).

B.3. Main Input File

ComFLOW.in

The input file of the ComFLOW executable is separated into ten parts. In order to get a general understanding of the content of the input file, basic information is described for each part. As an example, Case 14 has been used. More information on this specific case can be found in section 7.1 at page 28.

B.3.1. Initial Definition

The initial definition includes title naming and general variables. The input file start off with the definition of which version of ComFLOW one would like to use. Where the most recent version is chosen. The title of the file gives space to generally define the simulation case.

```
@v312-------------------------------------------------------------
--Title----Sloshing pressures in in-deck tanks--------------------
#14, FPSO, 2D, OVERSIZED - II, 50%, MEG, M#2, Pitch
------------------------------------------------------------------
```

For the general variables the parameters that are set define whether there is a free surface present in the simulation, whether there is a moving object present and (in case of sloshing) if the gas phase is computed.

```
------------------------------------------------------------------
slosh mvbd twph nproc
1     0    0    2
------------------------------------------------------------------
```

slosh Integer describes if a free surface is present (**1**), valid for both 2D and 3D simulations.

mvbd Integer describes the presence of a moving body (**1**) or (**2**). However, this is not the case (**0**).

twph Integer defines the use of a one-phase (**0**) or two-phase simulation (**1**).

nproc Defines the number of processors to be used, which normally is (**1**). Only for SOR-iterations the process is parallel and two processors may be used (**2**). For the 2D and 3D cases, different Poisson solving methods have been applied, where either 1 or 2 processors are used.

B.3.2. Domain Definition

The size of the simulation domain is stated in the lines of the domain definition. The in-deck tanks are assumed to be rectangular, smooth and closed. Therefore, the domain definition includes the exact in-deck tank geometry. For the 2D simulations, the x and z-axis are mainly used. Where the y-axis depends on the cell size of the grid.

```
------------------------------------------------------------------
-- domain definition ---------------------------------------------
xmin   xmax   ymin    ymax   zmin   zmax
-10.0  10.0   - 0.03  0.03   - 0.9  0.9
------------------------------------------------------------------
```

B.3.3. Initial liquid configuration

The initial liquid configuration states the initial liquid distribution of the CFD model. For all in-deck tank cases, the initial fluid distribution is a steady state fill level. Therefore, the entries of the x and y-axis are similar to the domain definition. The fill level is included in the definition of the lqzmax entry.

```
------------------------------------------------------------------
--definition initial liquid configuration-------------------------
liqcnf lqxmin lqxmax lqymin lqymax lqzmin lqzmax
1      - 10   10     - 0.03 0.03   - 0.9  0
------------------------------------------------------------------
```

linqcnf Determines whether the initial fluid distribution is defined in the input comflow.in file (**1**).

B.3.4. Physical parameters

The physical parameters define the characteristics of the fluids considered. There are two entries for both one-phase and two-phase flows. Note that for a one phase flow only the first entry of the density and viscosity values $rho1$ and $mu1$ are used, in that case the $mu2$ and $rho2$ are dummy variables.

```
– – – – – – – – – – – – – – – – – – – – – – – – – – – – – – – – – – – – – – – – – – – – – – – – – – – – – –
– – physical parameters – – – – – – – – – – – – – – – – – – – – – – – – – – – – – – – – – – – – – – – – – –
rho1        rho2   mu1          mu2   sigma        theta   patm         gamma
1.13E + 03  1      2.10E − 02   1     4.84E − 02   90      1.00E + 05   1.4
– – – – – – – – – – – – – – – – – – – – – – – – – – – – – – – – – – – – – – – – – – – – – – – – – – – – – –
```

rho1 $\frac{kg}{m^3}$ density of the liquid phase.

rho2 $\frac{kg}{m^3}$ density of the second liquid phase considered.

mu1 $\frac{kg}{m \cdot s}$ dynamic viscosity coefficient of the dense phase.

mu2 $\frac{kg}{m \cdot s}$ dynamic viscosity coefficient of the second dense phase considered.

sigma $\frac{N}{m}$ kinematic surface tension of the fluid.

theta deg contact angle free surface and solid boundary in-deck tank.

patm Pa atmospheric reference pressure.

gamma - expansion coefficient in equation of state, for air $\gamma = 1.4$.

B.3.5. Grid Parameters

There are two options for the grid parameters to be defined. It can be specified directly in the comflow.in file by setting the griddef parameter to (**1**) or with the use of a separate grid.cfi file by setting the parameter to (**0**). The grid.cfi file allows to precisely customize the grid in any way and is ideal for conducting grid refinement.

```
– – – – – – – – – – – – – – – – – – – – – – – – – – – – – – – – – – – – – – – – – – – – – – – – – – – – – –
– – grid parameters – – – – – – – – – – – – – – – – – – – – – – – – – – – – – – – – – – – – – – – – – – – –
griddef
1
imax  jmax  kmax  xc  yc  zc  sx  sy  sz
666.7 1     60    0   0   0   1   1   1
– – – – – – – – – – – – – – – – – – – – – – – – – – – – – – – – – – – – – – – – – – – – – – – – – – – – – –
```

imax Number of cells in the reference grid for the x-axis

jmax Number of cells in the reference grid for the y-axis

kmax Number of cells in the reference grid for the z-axis

xc center point of x-axis cells for stretching. Not used, parameter (**0**).

yc center point of y-axis cells for stretching. Not used, parameter (**0**).

zc center point of z-axis cells for stretching. Not used, parameter (**0**).

sx stretching ratio of the cells for the x-axis. Not used, parameter (**1**).

sy stretching ratio of the cells for the y-axis. Not used, parameter (**1**).

sz stretching ratio of the cells for the z-axis. Not used, parameter (**1**).

B.3.6. Numerical Parameters

– – numerical parameters								
eps	*omega*	*itmax*	*alpha*	*feab0*	*feab1*	*feab2*	*nrintp*	*linext*
$1.00E-07$	1	10000	1	0	1	0	4	1

– – additional numerical parameters							
imilu	extrap	restol	imptol	upwind	imprel	irhoav	itscr
10	0	$1.00E-07$	$1.00E-03$	1	1	1	0

The line of Numerical Parameters and Additional Numerical Parameters contains the following input entries.

eps This parameter specifies the convergence tolerance for the inner iteration loop of the Poisson solver. It determines the stopping criterion of the Poisson solver. Set to be $1.0E-5$.

omega Integer which includes the initial relaxation factor for the pressure solver. Set standard as (**1**).

itmax Integer that set the maximum number of iterations used for the Poisson solver per time step.

alpha This integer sets the upwind scheme of '1st-order upwind' that is used, parameter input (**1**).

feab Time integration variable integer. For the chosen forward Euler time integration method the parameter input is set to (**0**), (**1**) and (**0**).

nrintp Integer indicates the number of integration points in one grid cell. Default value of (**4**) has been used.

fslinext This parameter controls the velocity extrapolation near the free surface. The forward Euler method is used, input number (**1**).

imilu Integer determines the pressure solver used. Two types of solvers are used. Namely, SOR solver (**10**) and CGSTAB solver (**5**).

extrap Dummy variable, set to (**0**).

restol Integer describes the convergence tolerance for the pressure solvers. Smaller values result in accuracy improvements of the pressure solution. Generally good value of **1.00E-07** is used.

imptol Dummy variable, set to **1.00E-03**.

upwind Integer specifies spatial stencil for upwind discretization. First-order upwind integer is used, parameter set to (**1**).

imprel Dummy variable, set to (**1**).

irhoav Parameter describes the density averaging method for density values at cell edges. A gravity-consistent density averaging method is used, value (**1**).

itscr Integer determined the amount of pressure solver output that is written to the screen. A minimal output value of (**0**) is used.

B.3.7. Time Parameters

```
------------------------------------------------------------------
--time parameters/cfl number--------------------------------------
dt        tmax  dtmax  cfl  cflmin  clfmax  divl
1.00E-02  30    1      1    0.2     0.5     0
------------------------------------------------------------------
```

The line of time parameters contains the following input entries.

dt Includes the initial time step of the simulation. During the simulation the time step will be adapted according to the CFL-number. Set to be **1.00E-02**.

tmax Simulation time.

dtmax The maximum time step used in the simulation, normally a high number pick shall not be reached. Set to (**1**).

cfl Integer to use the CFL time step method, value (**1**).

cflmin Minimum CFL number, suggested to be **0.2**.

cflmax Maximum CFL number, suggested to be **0.5**.

divl Dummy variable, will be set in the free surface methods. Set to (**0**).

B.3.8. Free surface methods

```
------------------------------------------------------------------
-- free surface methods -------------------------------------------
vofmth  vofcor  divl
1       2       0
------------------------------------------------------------------
```

The line of free surface methods contains the following input entries.

vofmth Determined the VOF method, set to be (**1**) for the method of Hirt and Nichols.

vofcor Determines the VOF correction after the flux transport has been carried out. A symmetrical version of the local height-function correction is used, set to be (**2**).

divl Integer for description of small holes in the fluid. These holes will not be filled, set to (**0**).

B.3.9. Gravitation

```
------------------------------------------------------------------
--gravitation-----------------------------------------------------
gravx  gravy  gravz  ginrt  finrt
0      0      -9.81  1      1
------------------------------------------------------------------
```

The line of gravitation contains the input entries of gravitation and inertial forces.

gravx Denote gravitation in x-direction, concludes in **0.0**.

gravy Denote gravitation in y-direction, concludes in **0.0**.

gravz Denote gravitation in z-direction, concludes in **-9.81**.

ginrt Integer controls the gravitational forces. Use of moving coordinate frame, set to (**1**).

finrt Integer controls the external forces. Use of moving coordinate frame, set to (**1**).

B.3.10. Post-processing Snapshots and Monitor points

```
– – – – – – – – – – – – – – – – – – – – – – – – – – – – – – – – – – – – – – – – – – – – – – – – – – – – –
– – post-processing: snapshots/screen print/center of mass – – – – – – – – – – – – – – – – – – – – – – – –
npm2d    npm3d    compr    nprnt    ntcom
0          150        0        3000     0
– – – – – – – – – – – – – – – – – – – – – – – – – – – – – – – – – – – – – – – – – – – – – – – – – – – – –
```

The line of post-processing contains the input entries for the set-up of snapshot data, screen output and time series of the centre of mass.

npm2d Total number of snapshot files for 2D post-processing GUI in Matlab.

npm3d Total number of snapshot files for 3D post-processing GUI in Matlab.

compr Integer gives option to compress files to zipped format. Not used, set to (**0**).

nprint Integer sets the number of outputs to the screen during simulation. Set for each time step.

ntcom Integer to set the number of times the centre of mass of the liquid is written to a data file. Not used, set to (**0**).

Besides the snapshots; monitor points, monitor lines and fill boxes can be defined. More information on the post-processing set up is defined for Phase 1 at D.2 at page 98 and Phase 2 at E.2 at page 104.

B.4. Motion Input Files

dis.geo.in, vel.geo.in, acc.geo.in

In order to establish the time traces necessary for the input files des.geo.in, vel.geo.in and acc.geo.in, a superposition of 6 DOF is used. It is assumed in section 2.4 that CoG of the in-deck tank is straight above the CoG of the offshore structure. Therefore, a superposition analysis can be defined for the 2D simulation motions. A visualisation have been created in Figure B.6 below.

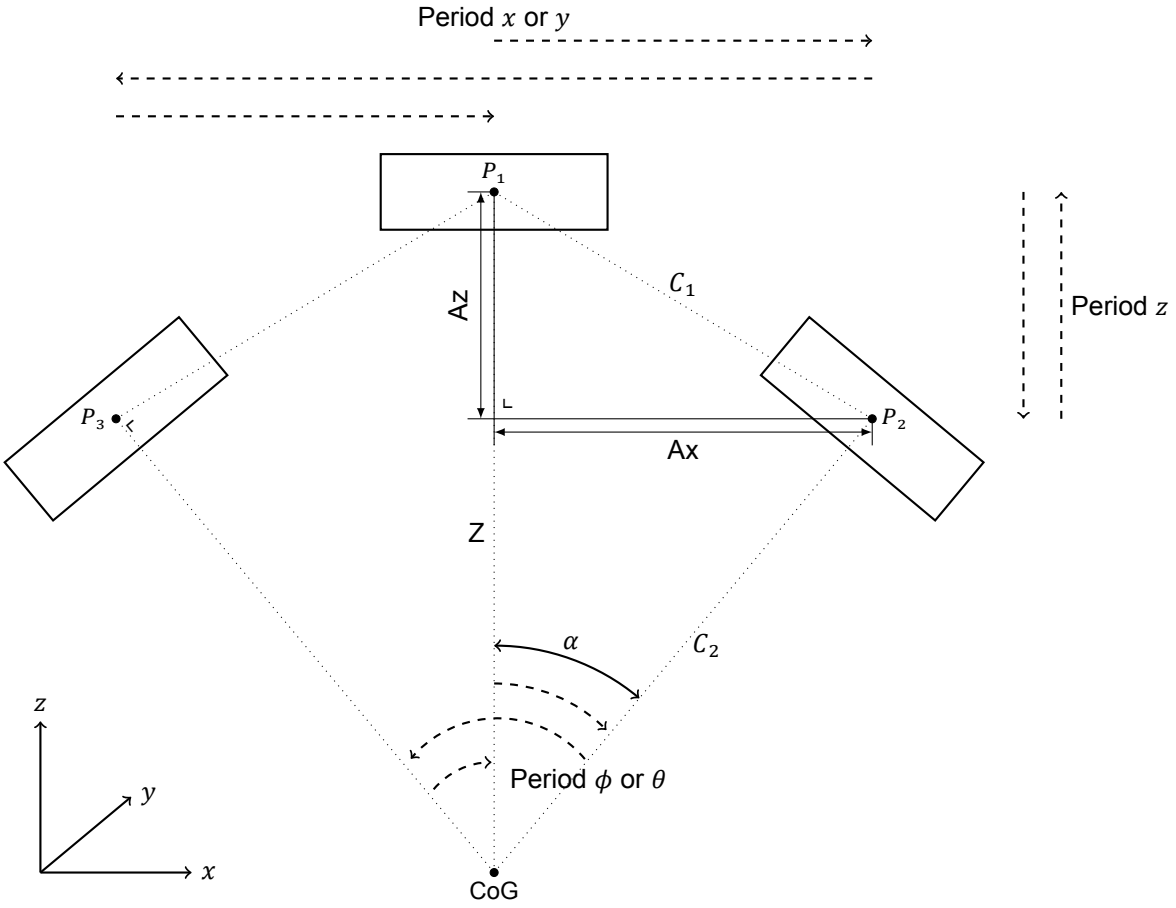

Figure B.6: Superposition sketch of Horizontal (x or y), Vertical and Rotational (ϕ or θ) motion.

The amplitudes A_x and A_z can be determined with the input parameters Z and α, witch are the relative distance between the in-deck Tank and CoG of the structure and the maximum heeling angle. When applying geometric rules, the following formulas can be defined:

Geometry relations

$$C_1 = Z \cdot sin(\alpha) \tag{B.29a}$$

$$A_x^2 + A_z^2 = C_1^2 \tag{B.29b}$$

$$C_1^2 + C_2^2 = Z^2 \rightarrow C_2 = \sqrt{Z^2 - C_1^2} \tag{B.29c}$$

$$A_x = C_2 \cdot sin(\alpha) \tag{B.29d}$$

$$A_z = \sqrt{C_1^2 - A_x^2} \tag{B.29e}$$

Substitution and rearrangement of equations B.29a, B.29b and B.29c into B.29d yields:

$$A_x = \sqrt{Z^2 - (Z \cdot (sin(\alpha))^2} \cdot sin(\alpha) \tag{B.30}$$

Furthermore, substitution of equation B.29a into B.29e yields:

$$A_z = \sqrt{(Z \cdot sin(\alpha))^2 - A_x^2} \tag{B.31}$$

Surge x

$$P_x = A_x \cdot sin(\omega_x \cdot t) \tag{B.32a}$$
$$\dot{P}_x = A_x \cdot \omega_x \cdot sin(\omega_x \cdot t) \tag{B.32b}$$
$$\ddot{P}_x = -A_x \cdot \omega_x^2 \cdot cos(\omega_x \cdot t) \tag{B.32c}$$
$$A_x = \sqrt{z^2 - (z \cdot sin(\alpha_x))^2} \cdot sin(\alpha_x) \tag{B.32d}$$
$$\omega_x = \frac{2 * \pi}{T_x} \tag{B.32e}$$

Sway y

$$P_y = A_y \cdot sin(\omega_y \cdot t) \tag{B.33a}$$
$$\dot{P}_y = A_y \cdot \omega_y \cdot cos(\omega_y \cdot t) \tag{B.33b}$$
$$\ddot{P}_y = -A_y \cdot \omega_y^2 \cdot sin(\omega_y \cdot t) \tag{B.33c}$$
$$A_y = \sqrt{z^2 - (z \cdot sin(\alpha_y))^2} \cdot sin(\alpha_y) \tag{B.33d}$$
$$\omega_y = \frac{2 * \pi}{T_y} \tag{B.33e}$$

Heave z [1]

$$P_z = \frac{1}{2} \cdot A_z \cdot cos(2\omega_z \cdot t) \tag{B.34a}$$
$$\dot{P}_x = -A_z \cdot \omega_z \cdot sin(2\omega_z \cdot t) \tag{B.34b}$$
$$\ddot{P}_x = -2 \cdot A_z \cdot \omega_z^2 \cdot cos(2\omega_z \cdot t) \tag{B.34c}$$
$$A_{zx} = \sqrt{z(z \cdot sin(\alpha_x))^2 - A_x^2} \tag{B.34d}$$
$$A_{zy} = \sqrt{z(z \cdot sin(\alpha_y))^2 - A_y^2} \tag{B.34e}$$
$$\omega_{zx} = \frac{2 * \pi}{T_x} \tag{B.34f}$$
$$\omega_{zy} = \frac{2 * \pi}{T_y} \tag{B.34g}$$

Roll ϕ

$$P_\phi = A_\phi \cdot sin(\omega_\phi \cdot t) \tag{B.35a}$$
$$\dot{P}_\phi = A_\phi \cdot \omega_\phi \cdot cos(\omega_\phi \cdot t) \tag{B.35b}$$
$$\ddot{P}_x = -A_\phi \cdot \omega_\phi^2 \cdot cos(\omega_\phi \cdot t) \tag{B.35c}$$
$$A_\phi = \alpha_x \cdot \frac{\pi}{180} \tag{B.35d}$$
$$\omega_\phi = \frac{2 * \pi}{T_x} \tag{B.35e}$$

[1] Amplitude A_z and frequency ω_z depend on the 2D motion considered, Roll or Pitch motion

Pitch θ

$$P_\theta = A_\theta \cdot sin(\omega_\theta \cdot t) \tag{B.36a}$$

$$\dot{P}_\theta = A_\theta \cdot \omega_\theta \cdot cos(\omega_\theta \cdot t) \tag{B.36b}$$

$$\ddot{P}_x = -A_\theta \cdot \omega_\theta^2 \cdot cos(\omega_\theta \cdot t) \tag{B.36c}$$

$$A_\theta = \alpha_y \cdot \frac{\pi}{180} \tag{B.36d}$$

$$\omega_\theta = \frac{2 * \pi}{T_y} \tag{B.36e}$$

Yaw ψ

For the 2D analysis, the yaw motion of the in-deck tank will be excluded.

C

CB&I Case Study

This appendix include the study of four influential parameters for sloshing, namely; fluid type and properties, fill level, tank geometry and floating structure motions. Each section elaborates the parameters values that will be used in this study and implemented in the set-up for the cases of Phase 1.

In order to establish research scenarios for the in-deck tanks, the Aasta Hansteen SPAR reference project has been used. So far, only this project include the application of in-deck tanks. An assessment of the Aasta Hansteen SPAR project have resulted in a basic insight on the materials, fill levels and tank geometry. Other projects which include FPSO and FLNG vessels have been studied in contribution to the establishment of possible geometric applications of in-deck tanks. The results of this study are described in sections C.1, C.2 and C.3.

The analysis of the motion behaviour have been carried out differently. Globally, different Nautical Zones are included in this research. The motions of offshore structures and therefore the in-deck tanks, varies for each different Nautical Zone in the world. In collaboration with colleagues of CB&I, a separate study has been performed in establishing the different motion cases. More elaboration can be found in section C.4.

C.1. Fluid Type

For the Aasta Hansteen In-deck tanks, three different fluids have been used. MEG, Water and Diesel fuel. Noted, same tanks also consist of used or dirty MEG and water. However, these will be excluded in this scenario assessment. It is assumed the fluid properties of used or dirty MEG and Water are almost the same. Therefore, the differences are negligible.

In agreement with CB&I, it is chosen to assess two fluids for the CFD analysis, namely water and MEG. These are considered to give sufficient insight on the standard case of water and some difference in fluid properties by the MEG. The input characteristics of the fluids are listed in table C.1 below.

Fluid Type	ρ [kg/m³]	μ [kg/(m*s)]	σ [N/m]
Water	1000	$1.0 * 10^{-}3$	$7.28 * 10^{-}2$
MEG	1133	$21.0 * 10^{-}3$	$4.84 * 10^{-}2$

Table C.1: Characteristics of fluid type

Where ρ is the density of the liquid phase, μ is the dynamic viscosity coefficient of the dense phase and σ is the kinematic surface tension of the fluid compared to air.

Note, for these fluid properties it is assumed that the operating conditions are about 20-25 degrees Celsius. For the CFD simulations, these input parameters will not change in the process and are considered to be constant.

C.2. Fill

Another important parameter related to sloshing is the fill level. In order to determine the fill levels in the in-deck tanks, assumptions have been made. One of the practical issues encountered is a fluctuating fill level in the tank. Fluctuations between the highest and lowest fill levels during operating conditions are present. In order to account for the fluctuations of the fill level, the lowest and highest fill levels have been cut into five pieces. Namely, a Low, Low-Mid, Mid, Mid-High and High case.

Fluid type	Tank Height [m]	Fill level									
		Low		Low-Mid		Mid		Mid-High		High	
		h [m]	%	h [m]	%	h [m]	%	h [m]	%	h [m]	%
Water	1.8	0.20	11	0.55	30	0.90	50	1.08	60	1.26	70
MEG	1.8	0.55	31	0.83	45	1.10	61	1.26	70	1.44	80

Table C.2: Fill levels related to fluid type

The aim of the 2D simulations is to get a grasp on the maximum sloshing pressure peaks that may occur for different fill levels. Therefore, the lowest fill level shall be excluded from the 2D CFD simulations.

C.3. Tank Geometry

To get an indication on the order of magnitude for the tank dimensions. Again, some basic insight will be provided by the Aasta Hansteen SPAR project. However, also other projects related to FPSO and FLNG vessels have been studied. In order to determine the effective length and breadth, assumptions have been made. As described in chapter 2, the in-deck tanks are considered to be smooth and rectangular. Resulting in the exclusion of all the small implications of the structure. However, sometimes bigger beams may cross through the in-deck tank. These so called 'disturbances' are not a part of this research. In the future event that considerable sized beams are present in the tank, a special assessment for these beams have to be made. To take a considerable amount of different geometrical in-deck tank cases into account, several geometry types have been defined. Important to note is that the height of the in-deck tanks are chosen to be fixed to 1.8 meters. The remaining geometry for the in-deck tank type can be defined as; 7 m, 12 m, 15 m and 20 m. More elaboration on each of these cases is described in the following subsections.

C.3.1. Tank length - 7 m

When the geometry type is labelled as ' 7 m', it refers to a square shaped tank with an aspect ratio of 1.5. This type of tank has the smallest dimensions which will be considered in the CFD analysis. This type of tank has a length of 7.0 meters and a width of 5.0 meters, with a fixed height of 1.8 meters. A sketch is presented in Figure C.1 below.

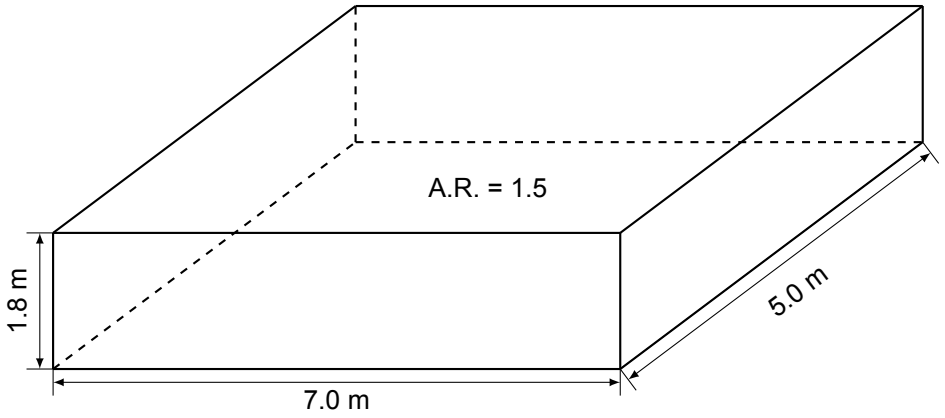

Figure C.1: In-deck tank geometry - 7 m

C.3.2. Tank length - 12 m

When the geometry type is labelled as ’12 m’, it refers to a more rectangular shaped tank with an aspect ratio of 3.2. This type of tank is considered to have normal in-deck tank dimensions. This type of tank has a length of 12.0 meters and a width of 3.8 meters, with a fixed height of 1.8 meters. A sketch is presented in Figure C.2 below.

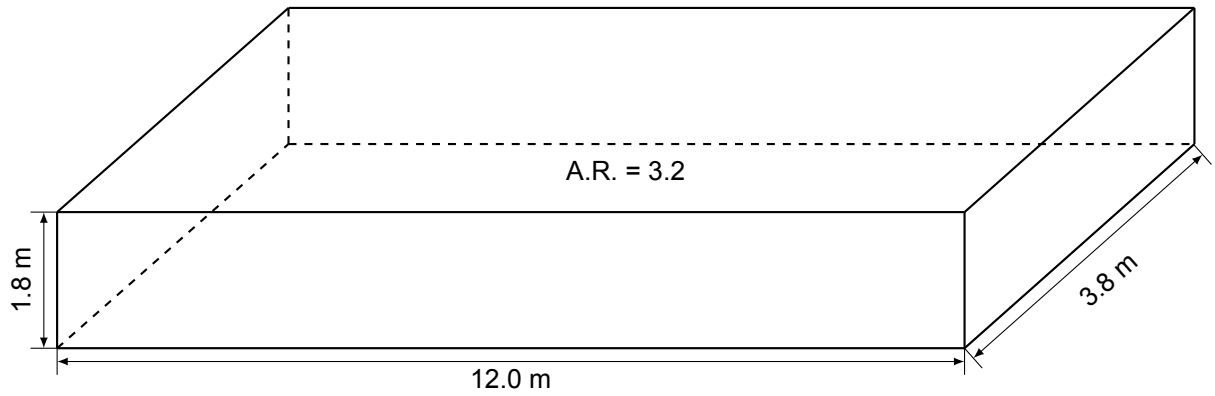

Figure C.2: In-deck tank geometry - 12 m

C.3.3. Tank length - 15 & 20 m

The geometry type of tanks that are not applied yet, can be split up into two parts, ’15 m’ and ’20 m’. These types refer to over sized rectangular shaped tanks and are considered to be possible applicable in future projects.

When the geometry type is labelled ’15 m’, it refers to an over sized rectangular shaped tank with an aspect ratio of 3.9. These effective sloshing lengths have not yet occurred in recent projects, but maybe possible in the future. This type of tank has a length of 15.0 meters and a width fixed to the ’12 m’ case, 3.8 meters. The height is fixed at 1.8 meters, just like all other geometry types. A sketch is presented in Figure C.3.

When the geometry type is labelled ’20 m’, it refers to an over sized rectangular shaped tank with an aspect ratio of 5.3. These effective sloshing lengths have not yet occurred in recent projects, but maybe possible in the future. This type of tank has a length of 20.0 meters and a width fixed to the ’12 m’ case, 3.8 meters. The height is fixed at 1.8 meters, just like all other geometry types. A sketch is presented in Figure C.4.

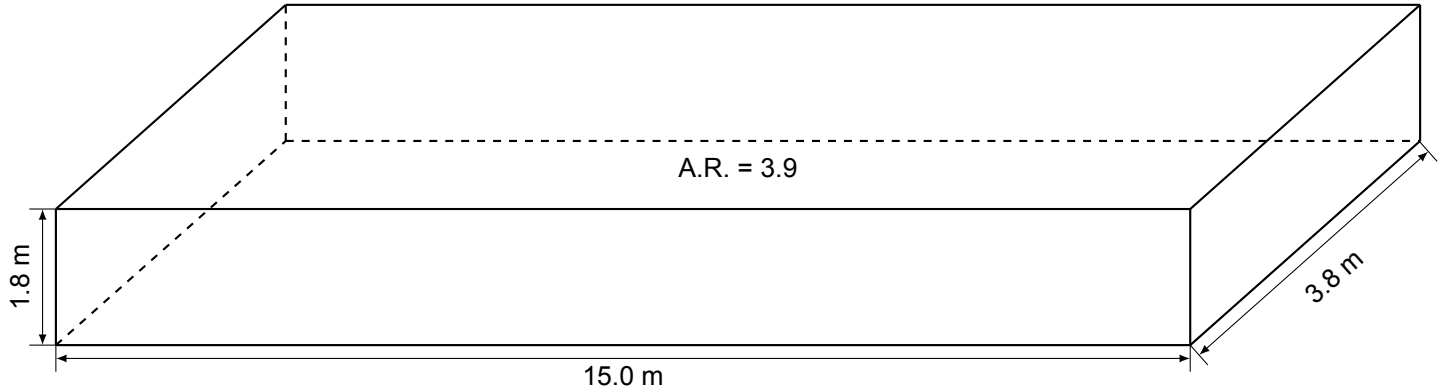

Figure C.3: In-deck tank geometry - 15 m

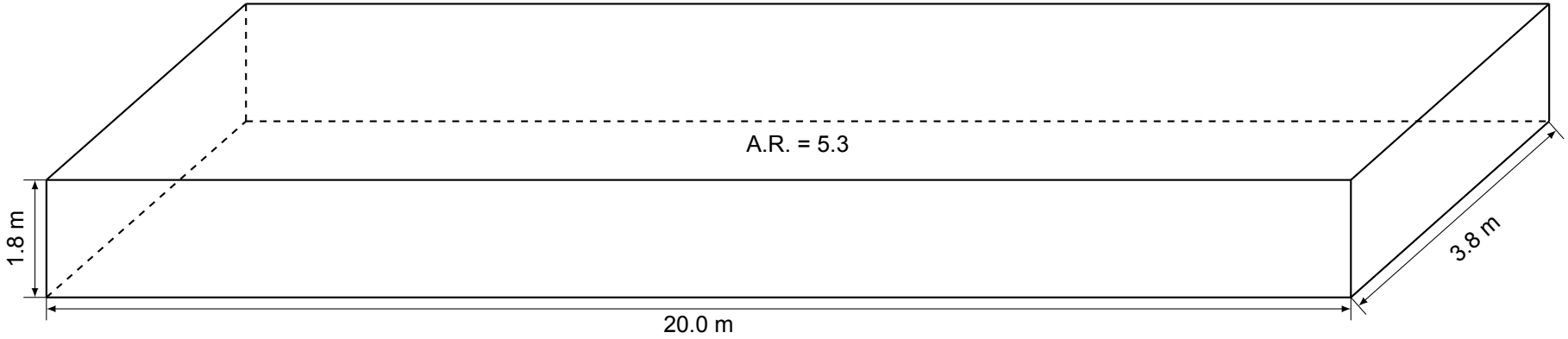

Figure C.4: In-deck tank geometry - 20 m

C.4. Motions

One of the most important sloshing input parameters are the motions of the in-deck tanks. The motions have a big share in the occurrence of sloshing. However, the eventual motions of the in-deck tank is closely related to parameters as; the Nautical Zone of the structure, the behaviour of the offshore structure and the place of the in-deck tanks relative to the vessel. A combination of these parameters conclude in a so called 'Motion Case'. The type and size of the offshore structure together with the Nautical Zone result in a specific case.

For the 2D analysis it is assumed that the location of the in-deck tank is directly above the CoG of the structure. There is an alignment of the tank and structure CoG in the vertical axis. This assumption is made in relation to the broad and general approach of this research.

First, Nautical Zones will be described in the subsection below, followed by the motion case Table C.3 that is defined. Thereafter, each motion case is discussed briefly in subsection C.4.3 till C.4.9. The motion cases are established in collaboration with with Naval Architects of CB&I.

C.4.1. Nautical Zones

Offshore structures operate worldwide and in many different areas. These different areas are mapped and numbered by the DNV in so called 'Nautical Zones', see Figure C.5. Different nautical zones are implemented in this research in order to get a global and broad understanding on the offshore structure motions. The combination of the Nautical Zone and type of offshore structure result in a 'Motion Case'. The first motions case is related to the Aasta Hansteen SPAR behaviour, while the rest of the motion cases will be build up for FPSO vessels.

Six nautical zones have been picked for the motions assessment of the FPSO. A base case for the FPSO is defined, namely the Skarv FPSO. This is a 300 meter long Floating Production Storage and Offloading vessel, designed for BP and situated at the west coast of Norway. The behaviour of this ship has been used to get a general understanding of FPSO vessel motions. It is determined to include the significant wave height H_s related to a 100 year return period. The selection of this specific ship is due to its extreme vessel behaviour. The Skarv is situated in one of the worst areas in the world where FPSO's are applied, with regard to sea state.

As shown in Table C.3 below, the natural periods for the FPSO does not change for the different Nautical Zones. Also the Centre of Gravity for each FPSO motion case is set for the same 14.0 meters. This height has been established by a general vessel geometry study and can be considered a rough number. However, the maximum heeling angle does change. The change of the heeling angles for both roll and pitch are due the difference of significant wave height H_s related to the 'base case' of west coast Norway. The significant wave height H_s for a 100 year return period is defined for the six Nautical Zones that are assessed.

Motion Case	Offshore Structure	Nautical Zone	Global Area	Motion				CoG [m]
				max. angle [deg]		nat. period [s]		
				Roll	Pitch	Roll	Pitch	
1	SPAR	4	West Coast Norway	10.12	10.12	58.1	57.5	85.6
2	FPSO	4	West Coast Norway	16.00	8.00	20.8	9.7	14.0
3	FPSO	58	West Coast Africa	4.71	2.36	20.8	9.7	14.0
4	FPSO	78	North-West Australia	13.55	6.77	20.8	9.7	14.0
5	FPSO	1	North Cape	12.47	6.23	20.8	9.7	14.0
6	FPSO	15	East Canada	18.16	9.08	20.8	9.7	14.0
7	FPSO	32	Gulf of Mexico	15.41	7.71	20.8	9.7	14.0

Table C.3: Definition of Motion Cases

The next page will show a Figure (C.5) of the Nautical Zones defined by the DNV. The six regions that will be assessed are highlighted.

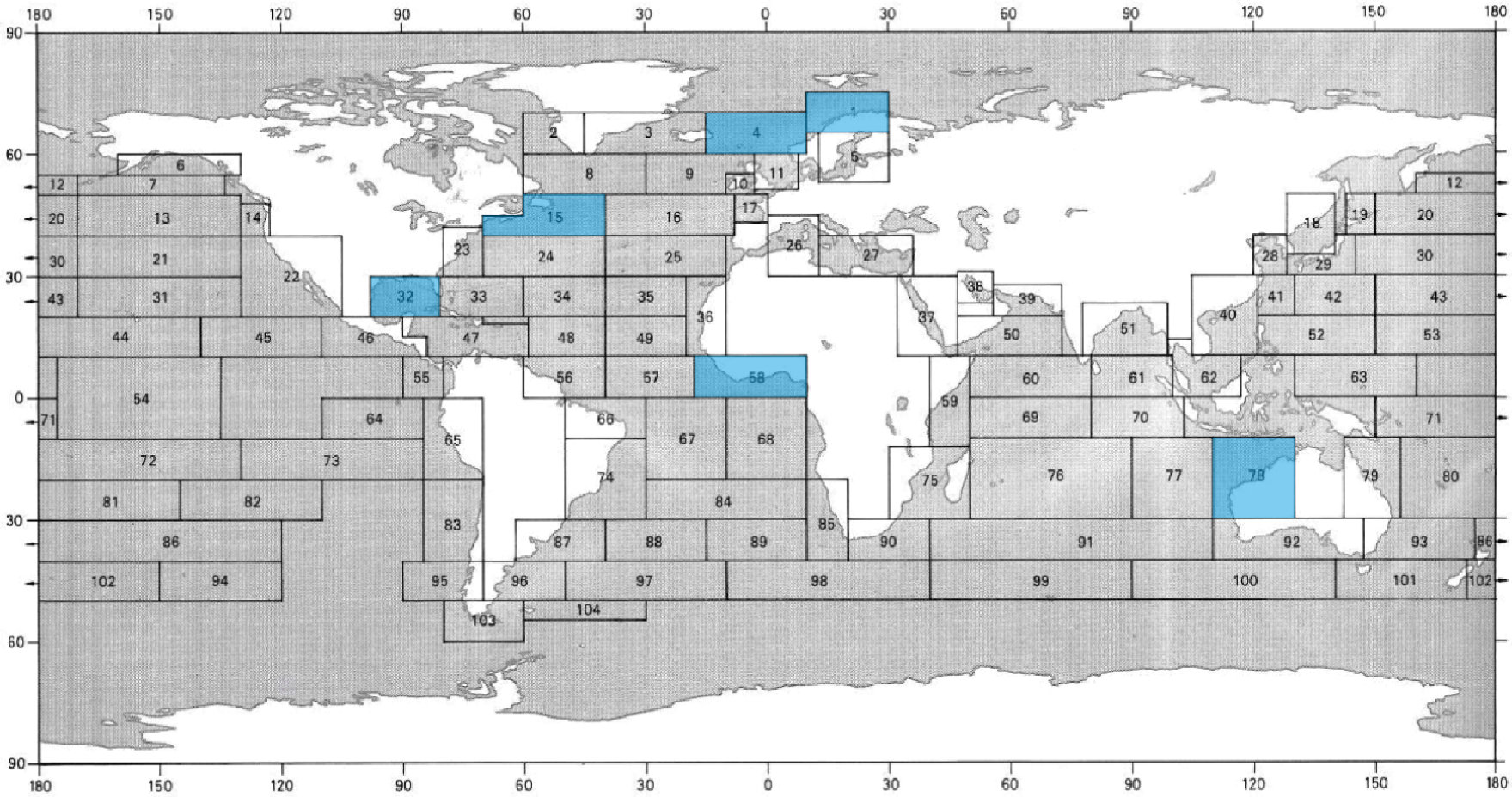

Figure C.5: Nautical Zones defined by the DNV

C.4.2. Motion Case Initial Set-up

In order to determine the motions related to different areas in the world, as mentioned, an initial base case has been set up. The base case closely coincide to the behaviour of Skarv FPSO vessel, which is operating in the west coast of Norway. It has been chosen to relate the different vessel motions to the significant wave height H_S. Noted, this is a rough estimation of the vessel behaviour. However, considered to be sufficient as input for this research. The difference in significant wave height H_S relates proportionally to the heeling angles for roll and pitch. The H_S for each Nautical Zone is defined for a 100 year return period. A selection of Nautical Zones is done with a short study of areas where FPSO's operate. This resulted in six possible areas.

Information of the Skarv FPSO is stated in table C.4 below.

Length [m]	Width [m]	Depth [m]	Draft [m]	Block Coefficient [-]	Displacement [m³]	GMt [m]	Roll Radius [m]	CoG In-deck Tank [m]
292	50.6	29	17.2	0.67	171,540	4.20	18.0	14.0

Table C.4: General Information Base Case

C.4.3. Motion Case 1

The first motions case is related to the Aasta Hansteen reference project. It is located in the West Coast of Norway. Logically, the SPAR motions are well defined in the reference project. Defined by Table C.5 and Figure C.6 below.

Location: West coast Norway	**DNV nr. 4**	H_S **16.3 m**	Max. Angle [deg]	Nat. Period [s]
		Roll	10.12	58.1
		Pitch	10.12	57.5

Table C.5: Motion Case 1

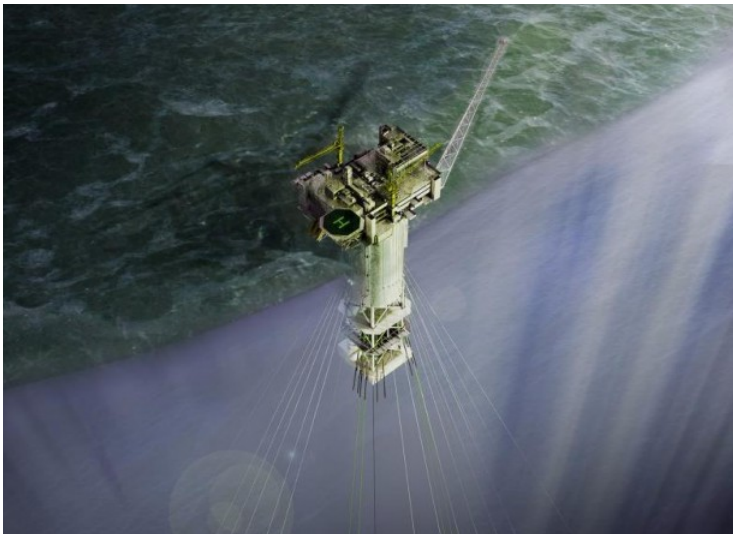

Figure C.6: Example Floater - Aasta Hansteen SPAR

C.4.4. Motion Case 2

The second motion case is related to the Skarv FPSO, the base case vessel of the motion set-up. It is also located at West coast Norway and involves the FPSO vessel motions in that area. Defined by Table C.6 and Figure C.7 below.

Location: West coast Norway	**DNV nr. 4**	H_s **16.3 m**	Max. Angle [deg]	Nat. Period [s]
		Roll	16.00	20.8
		Pitch	8.00	9.7

Table C.6: Motion Case 2

Figure C.7: Example Floater - Skarv FPSO

C.4.5. Motion Case 3

The third motion case is related to the location of West coast Africa. An FPSO example for this area is the Garissol. Defined by Table C.7 and Figure C.8 below.

Location: West coast Africa	**DNV nr. 58**	H_s **4.8 m**	Max. Angle [deg]	Nat. Period [s]
		Roll	4.71	20.8
		Pitch	2.36	9.7

Table C.7: Motion Case 3

Figure C.8: Example Floater - Girassol FPSO

C.4.6. Motion Case 4

The fourth motion case is related to the location of North West Australia. An FPSO example for this area is the Laminaria. Defined by Table C.8 and Figure C.9 below.

Location: North West Australia	**DNV nr. 78**	H_s **13.8 m**	Max. Angle [deg]	Nat. Period [s]
		Roll	13.55	20.8
		Pitch	6.77	9.7

Table C.8: Motion Case 4

Figure C.9: Example Floater - Laminaria FPSO

C.4.7. Motion Case 5

The fifth motion case is related to the Arctic area. At the moment a lot of ongoing research is carried out for offshore possibilities in the north pole area. However, no particular FPSO vessel for this area have been build yet. The following Table C.9 of the motions is defined below.

Location: North Cape	**DNV nr. 1**	H_s **12.7 m**	Max. Angle [deg]	Nat. Period [s]
		Roll	12.47	20.8
		Pitch	6.23	9.7

Table C.9: Motion Case 5

C.4.8. Motion Case 6

The sixt motion case is related to the location of East Canada. An FPSO example for this area is the White Rose. Defined by Table C.10 and Figure C.10 below.

Location: East Canade	**DNV nr. 15**	H_s **18.5 m**	Max. Angle [deg]	Nat. Period [s]
		Roll	18.16	20.8
		Pitch	9.08	9.7

Table C.10: Motion Case 6

Figure C.10: Example Floater - White Rose FPSO

C.4.9. Motion Case 7

The seventh (and last) motion case is related to the location of the Gurlf of Mexico. An FPSO example for this area is the Turritella. Defined by Table C.11 and Figure C.11 below.

Location: Gulf of Mexico	**DNV nr. 32**	H_s **15.7 m**	Max. Angle [deg]	Nat. Period [s]
		Roll	15.41	20.8
		Pitch	7.71	9.7

Table C.11: Motion Case 7

Figure C.11: Example Floater - Turritella FPSO

D

Phase 1 - CFD

This appendix will describe the Pre- and Post processing of phase 1, together with tables of the simulated results.

D.1. Pre-Processing

In order to run a CFD simulation at all, pre-processing has to be done. In the stage of pre-processing, all the input parameters have to be defined. An elaborate example of the input file used for the ComFLOW executable is described in appendix **??**. The input file has to agree a specific format in order for the CFD executable to read and understand it.

All the input information is implemented in four file types. One is the general input file where the material type, tank geometry and fill level is included, which is called the ”comflow.in” file. This file also contains the numerical and post processing preferences. The other three input files contain the motions of the tank and are defined as; dis.geo.in, vel.geo.in and acc.geo.in. The motion input is described as a time trace which include the position, velocity and acceleration of the tank for each second.

The CFD executable is split into two parts. First the domain and liquid configuration are defined in the ”GEODEF” part. The input is delivered by a section of the ”comflow.in” file and results in a initial model of the in-deck tank and fluid. The ”GEODEF” executable generates a separate ”apertures.in” file. The next step is to run the ”ComFLOW” executable. This program is actually doing the simulation, where it simulates the fluid behaviour for each time step. Altogether, the executable make use of five input files, namely; apertures.in, comflow.in, dis.geo.in, vel.geo.in, acc.geo.in. A clear overview of the input file and calling sequence is presented in Figure D.1 below.

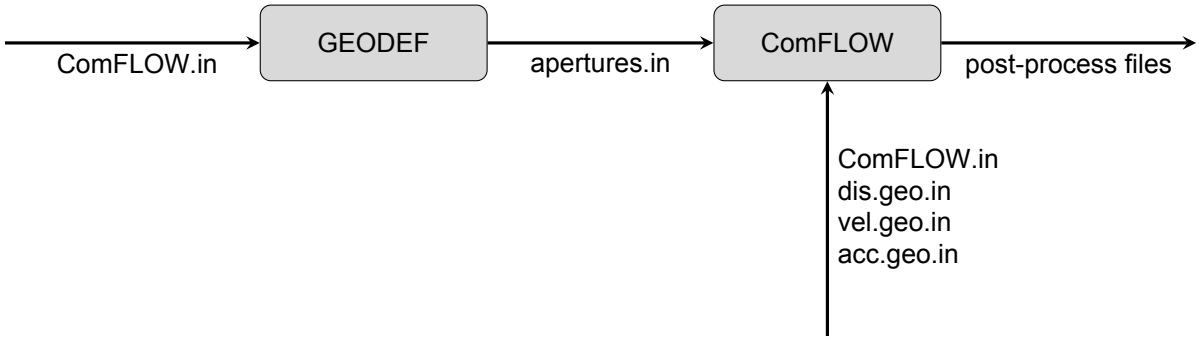

Figure D.1: Flow diagram of the pre-processing calling sequence for the ComFLOW executable

D.2. Post-Processing

As mentioned, the aim of the first phase is focused on a general idea of the occurrence of sloshing. Therefore, it is chosen to generate snapshots and log the pressures for defined points in the tank. An illustration of these so called ’monitor points’ is presented in Figure D.2 below.

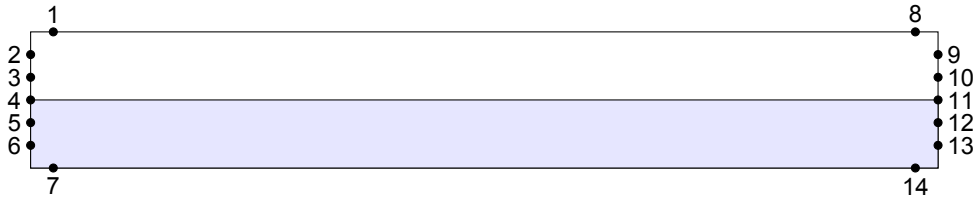

Figure D.2: Phase 1 - CFD - Monitor Points

D.3. Results - Pressure Tables

Input Parameters							Output Monitor points - Highest Pressure Simulated [kPa]													Sloshing
Case	Struc.	In-deck Tank	Fill	Liquid	N.A [cm]	Motion Case	Left							Right						
							1	2	3	4	5	6	7	8	9	10	11	12	13	14	
1	SPAR	12 m	50%	Water	3	1-Pitch	3	7	9	12	15	18	20	3	7	10	12	15	18	21	No
2	SPAR	12 m	60%	Water	3	1-Pitch	5	8	11	14	17	19	22	5	9	11	14	17	20	22	No
3	SPAR	12 m	70%	Water	3	1-Pitch	8	11	14	17	20	23	25	8	11	14	17	20	23	25	No
4	SPAR	12 m	61%	MEG	3	1-Pitch	6	11	13	16	19	23	25	6	10	13	17	20	23	26	No
5	SPAR	12 m	70%	MEG	3	1-Pitch	8	12	15	18	21	25	27	9	12	16	19	22	26	28	No
6	SPAR	12 m	80%	MEG	3	1-Pitch	11	16	18	21	25	28	30	12	16	19	23	25	29	32	No
7	FPSO	7 m	50%	Water	3	2-Pitch	0	3	6	9	12	15	17	0	4	7	10	13	15	18	No
8	FPSO	12 m	50%	Water	3	2-Pitch	26	29	31	33	36	39	41	25	29	33	35	37	39	42	Semi
9	FPSO	15 m	50%	Water	3	2-Pitch	36	39	42	45	47	51	54	22	25	28	29	33	38	40	Semi
10	FPSO	20	50%	Water	3	2-Pitch	72	75	77	80	83	87	89	44	47	48	49	50	54	56	Yes
11	FPSO	7 m	50%	MEG	3	2-Pitch	0	4	7	10	13	17	19	0	5	8	11	14	17	20	No
12	FPSO	12 m	50%	MEG	3	2-Pitch	24	27	29	31	34	37	40	27	30	30	34	37	40	42	Semi
13	FPSO	15 m	50%	MEG	3	2-Pitch	35	38	39	39	38	42	44	33	37	40	43	47	51	54	Semi
14	FPSO	20 m	50%	MEG	3	2-Pitch	74	77	81	85	89	92	94	55	59	60	62	65	69	72	Yes
15	FPSO	12 m	30%	Water	3	2-Pitch	13	16	19	22	25	28	30	10	13	16	19	21	23	26	Semi
16	FPSO	15 m	30%	Water	3	2-Pitch	21	22	23	24	26	36	39	8	13	16	21	26	32	35	Semi
17	FPSO	20 m	30%	Water	3	2-Pitch	47	46	29	29	31	45	44	69	27	27	39	28	27	27	Semi
18	FPSO	12 m	60%	Water	3	2-Pitch	20	23	26	29	32	43	38	18	21	24	27	30	33	36	Semi
19	FPSO	15 m	60%	Water	3	2-Pitch	28	31	34	37	40	43	46	21	24	27	30	33	36	39	Semi
20	FPSO	20 m	60%	Water	3	2-Pitch	24	30	32	34	37	40	43	35	38	41	44	47	50	53	Semi
21	FPSO	12 m	70%	Water	3	2-Pitch	18	21	24	27	30	33	36	18	21	24	27	30	33	36	Semi
22	FPSO	15 m	70%	Water	3	2-Pitch	51	54	57	60	63	66	69	87	90	93	96	99	102	105	Yes
23	FPSO	20 m	70%	Water	3	2-Pitch	30	32	34	36	38	40	41	70	73	76	74	77	80	83	Yes

Table D.1: Phase 1 - CFD - Results - Part 1

Input Parameters							Output Monitor points - Highest Pressure Simulated [kPa]													Sloshing
Case	Struc.	In-deck Tank	Fill	Liquid	N.A [cm]	Motion Case	Left							Right						
							1	2	3	4	5	6	7	8	9	10	11	12	13	14	
24	FPSO	12 m	45%	MEG	3	2-Pitch	33	33	34	34	35	37	39	29	30	31	32	32	35	38	Semi
25	FPSO	15 m	45%	MEG	3	2-Pitch	32	34	37	38	40	44	47	53	56	59	62	65	68	71	Yes
26	FPSO	20 m	45%	MEG	3	2-Pitch	54	55	56	57	58	59	60	41	44	48	51	57	60	63	Semi
27	FPSO	12 m	70%	MEG	3	2-Pitch	19	22	26	30	33	37	40	20	23	26	29	32	36	39	Semi
28	FPSO	15 m	70%	MEG	3	2-Pitch	25	31	33	36	38	42	45	28	31	34	38	42	45	48	Semi
29	FPSO	20 m	70%	MEG	3	2-Pitch	20	23	27	31	34	37	40	85	87	89	92	95	98	100	Yes
30	FPSO	12 m	80%	MEG	3	2-Pitch	40	43	46	49	52	55	58	23	26	31	34	37	41	44	Semi
31	FPSO	15 m	80%	MEG	3	2-Pitch	35	36	39	41	44	47	50	34	38	42	45	48	52	55	Semi
32	FPSO	20 m	80%	MEG	3	2-Pitch	36	40	42	44	48	51	54	55	58	61	64	67	71	75	Semi
33	FPSO	12 m	50%	Water	3	3-Pitch	4	5	7	9	12	26	17	4	6	8	10	11	17	17	No
34	FPSO	15 m	50%	Water	3	3-Pitch	18	19	20	21	22	24	25	4	7	10	13	16	19	23	Semi
35	FPSO	20 m	50%	Water	3	3-Pitch	26	17	19	21	23	26	28	6	7	7	8	13	16	18	Semi
36	FPSO	12 m	50%	Water	3	4-Pitch	27	29	30	31	32	35	37	18	21	23	26	29	34	36	Semi
37	FPSO	15 m	50%	Water	3	4-Pitch	30	33	35	36	38	42	45	30	33	36	39	41	46	48	Semi
38	FPSO	20 m	50%	Water	3	4-Pitch	29	31	33	35	37	39	41	30	32	34	36	38	41	44	Semi
39	FPSO	12 m	50%	Water	3	5-Pitch	27	29	31	33	34	35	36	16	19	22	25	28	35	34	Semi
40	FPSO	15 m	50%	Water	3	5-Pitch	20	23	26	29	32	35	37	14	17	20	23	26	29	32	Semi
41	FPSO	20 m	50%	Water	3	5-Pitch	24	25	26	27	30	34	37	17	19	22	25	28	31	33	Semi
42	FPSO	12 m	50%	Water	3	6-Pitch	27	30	31	33	35	38	41	36	37	38	39	40	41	42	Semi
43	FPSO	15 m	50%	Water	3	6-Pitch	41	49	56	58	60	63	65	31	32	33	34	35	37	42	Yes
44	FPSO	20 m	50%	Water	3	6-Pitch	78	55	33	35	37	39	41	51	53	55	57	59	61	63	Yes
45	FPSO	12 m	50%	Water	3	7-Pitch	17	20	23	25	27	31	34	16	19	22	25	28	31	34	Semi
46	FPSO	15 m	50%	Water	3	7-Pitch	20	23	26	29	32	35	38	25	28	30	33	37	41	43	Semi
47	FPSO	20 m	50%	Water	3	7-Pitch	84	87	90	93	96	99	102	30	33	36	39	42	45	48	Yes
48	FPSO	7 m	50%	Water	3	6-Roll	4	7	10	13	16	19	20	3	7	10	13	15	19	20	No
49	FPSO	12 m	50%	Water	3	6-Roll	17	20	21	22	25	34	38	18	21	24	26	29	33	35	Semi
50	FPSO	15 m	50%	Water	3	6-Roll	36	39	42	45	48	51	54	21	24	27	30	33	36	39	Semi
51	FPSO	20 m	50%	Water	3	6-Roll	57	60	63	66	69	71	73	69	72	75	78	81	85	88	Semi

Table D.2: Phase 1 - CFD - Results - Part 2

Input Parameters							Output Monitor points - Highest Pressure Simulated [kPa]													Sloshing
Case	Struc.	In-deck Tank	Fill	Liquid	N.A [cm]	Motion Case	Left							Right						
							1	2	3	4	5	6	7	8	9	10	11	12	13	14
52	FPSO	20 m	50%	MEG	3	2-Pitch	74	77	81	85	89	92	94	55	59	60	62	65	69	72	Yes
53	FPSO	15 m	50%	Water	3	6-Pitch	41	49	56	58	60	63	65	31	32	33	34	35	37	42	Yes
54	FPSO	15 m	70%	Water	3	2-Pitch	51	54	57	60	63	66	69	87	90	93	96	99	102	105	Yes
55	FPSO	20 m	50%	Water	3	7-Pitch	17	20	23	25	27	31	34	300	263	227	195	175	170	160	Yes
56	FPSO	20 m	50%	MEG	10	2-Pitch	36	39	42	44	46	48	51	29	32	35	39	42	46	48	Semi
57	FPSO	20 m	50%	MEG	5	2-Pitch	33	35	37	38	40	44	47	54	56	57	58	59	61	63	Yes
58	FPSO	20 m	50%	MEG	2	2-Pitch	37	38	42	46	50	68	58	51	52	53	51	51	54	55	Semi
59	FPSO	20 m	50%	MEG	1	2-Pitch	40	33	39	41	45	50	53	102	105	106	107	111	120	122	Yes
60	SPAR	20 m	70%	Water	3	1-Pitch	18	21	24	27	30	33	36	18	21	24	27	30	33	36	No
61	FPSO	7 m	50%	Water	10	2-Pitch	0	3	6	9	12	15	17	0	4	7	10	13	15	18	No
62	FPSO	7 m	50%	Water	5	2-Pitch	0	3	6	9	12	15	17	0	4	7	10	13	15	18	No
63	FPSO	7 m	50%	Water	2	2-Pitch	0	3	6	9	12	15	17	0	4	7	10	13	15	18	No
64	FPSO	12 m	50%	Water	10	7-Pitch	16	19	22	25	26	28	30	10	13	16	19	22	24	26	Semi
65	FPSO	12 m	50%	Water	5	7-Pitch	20	23	26	29	32	35	37	24	27	30	33	36	36	41	Semi
66	FPSO	12 m	50%	Water	2	7-Pitch	18	20	22	24	27	30	33	40	43	46	49	52	54	56	Semi

Table D.3: Phase 1 - CFD - Results - Part 3

E

Phase 2 - CFD

This appendix will describe the Pre- and Post processing of phase 2, together with an elaborate presentation of the results and sensitivity tornado's.

E.1. Pre-Processing

The pre-processing in Phase 2 is somewhat extended. Force boxes are defined for post-processing and grid refinement has been applied. Therefore, two extra files are included in the calling sequence describes in section D.1. The "grid.cfi" and "geometry.in" are added. A clear overview of the input file and calling sequence is presented in Figure E.1 below.

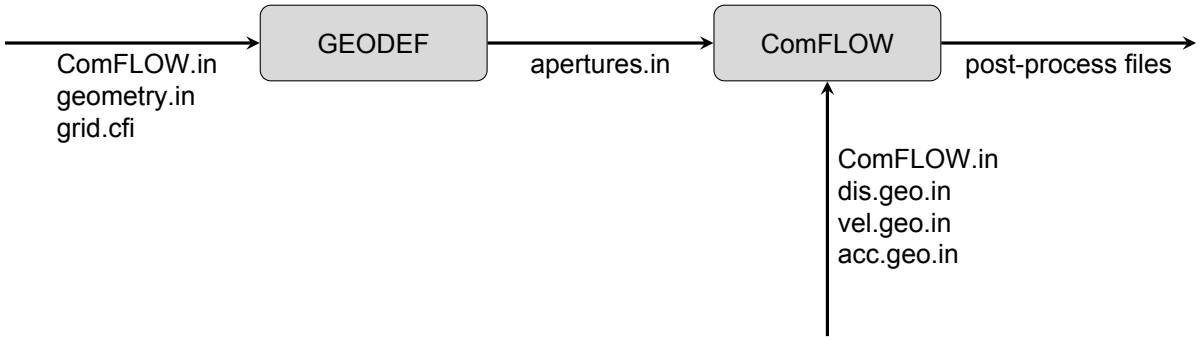

Figure E.1: Flow diagram of the pre-processing calling sequence for the ComFLOW executable

E.2. Post-Processing

The second phase includes a detailed analysis of the sloshing cases resulting from Phase 1. In addition to Phase 1, force boxes related to the impact area have been defined, see Figure 7.3. A combination of force boxes (gray) and monitor points (black) is used as input for the statistical analysis. A detailed presentation of the results is listed in Appendix **??**.

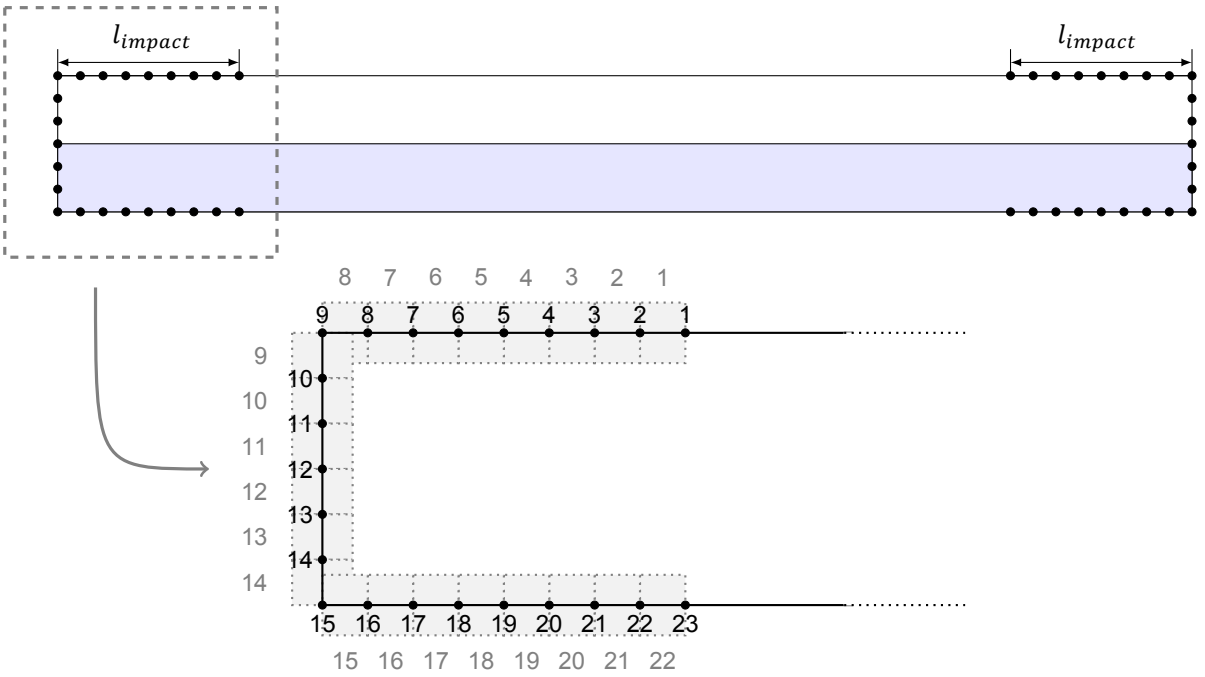

Figure E.2: Monitor Points & Force Boxes In-deck tank

E.3. Results - Statistical Analysis

The presentation of the results consist of the statistical procedure described in section 8.2 at page 39. Where for each case the following Figures are presented:

1. Peak-over-Threshold method, consisting of the 'raw' simulated data coloured by impact area and indicated threshold.
2. Binned Histogram for each combined box, related to numbering of Figure 8.3 at page 8.3. For convenience, a part of this figure is presented below.

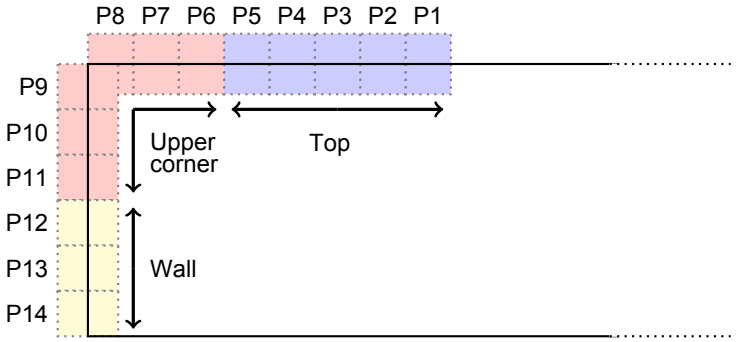

3. Combined histogram of all boxes, again coloured by impact area. Concluding in a clear overview on the areas where higher impact pressures occur.
4. Statistical probability procedure concluding in 4 Figures that indicate each step in this procedure. First the total data from the combined histogram is taken into account. Followed by the Probability Density Function (PDF) and fitting curves. The next step includes the Cumulative Density Function (CDF) and takes care of the Kolmogorov-Smirnov test, described in section s:phase2-statistical-analysis The results of this test are presented in Table E.1 below. If value is present in the table, the fitting is accepted by maximum reduction of the stated Alpha. When no Value Present (-), the fitting is rejected. Underlining that Alpha stands for an extra safety margin. Finally, the Exceeding Probability Function (EPF) can be drawn as an end result.

Fitting	Alpha	Case 67	68	69	70	71	72	73	74
Kernel smooth.	Value	0.0023	0.0019	0.0330	0.0010	-	0.0009	0.0086	0.1834
	Percentage	99.77 %	99.81%	96.70%	99.90%	-	99.91%	99.14%	81.66%
Gen. Pareto	Value	0.0001	-	0.0183	0.0003	-	-	-	0.0013
	Percentage	99.99 %	-	98.17%	99.97%	-	-	-	99.87%

Table E.1: Kolmogorov-Smirnov test results

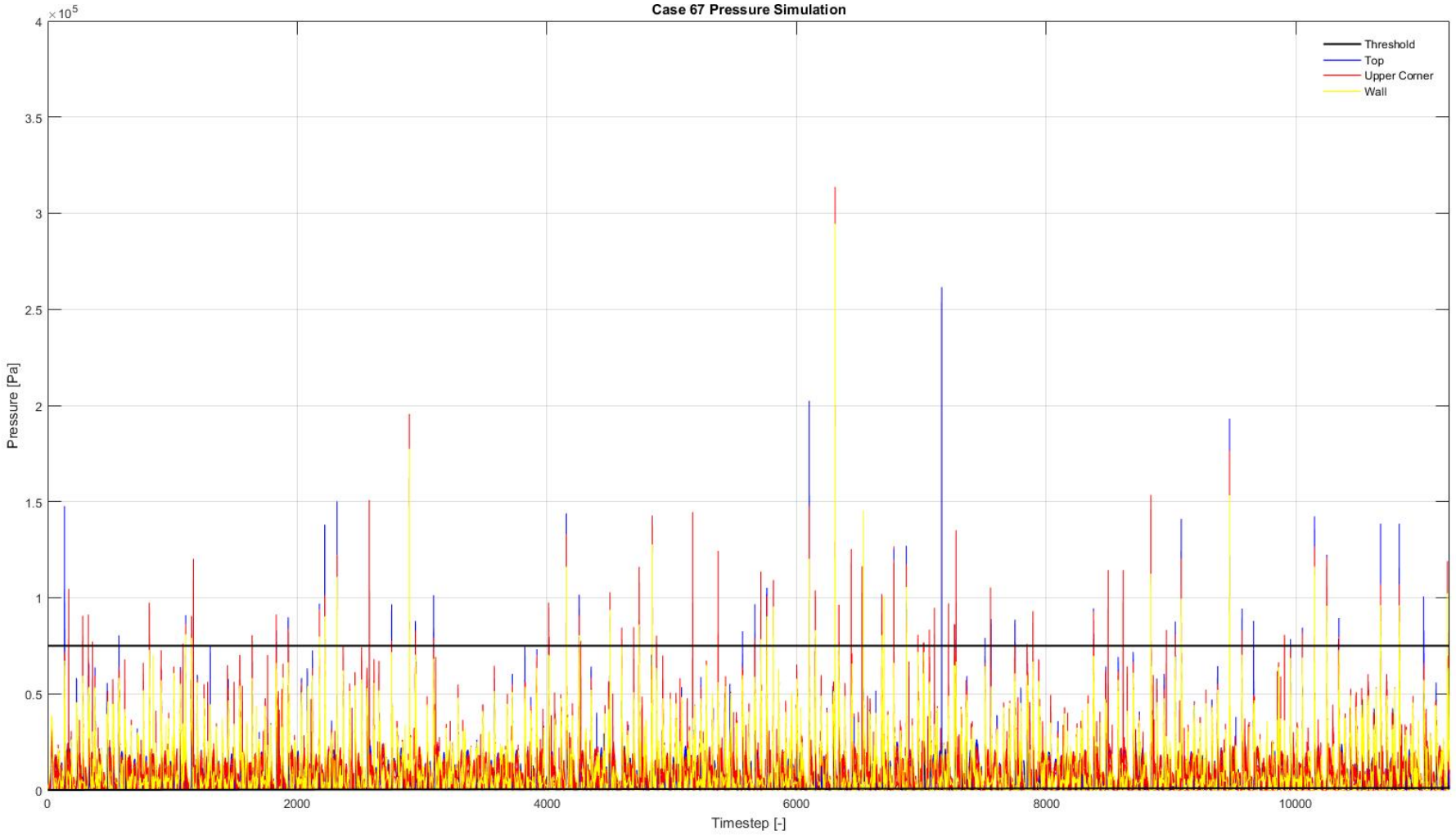

Figure E.3: Case 67 - Peak-over-Threshold

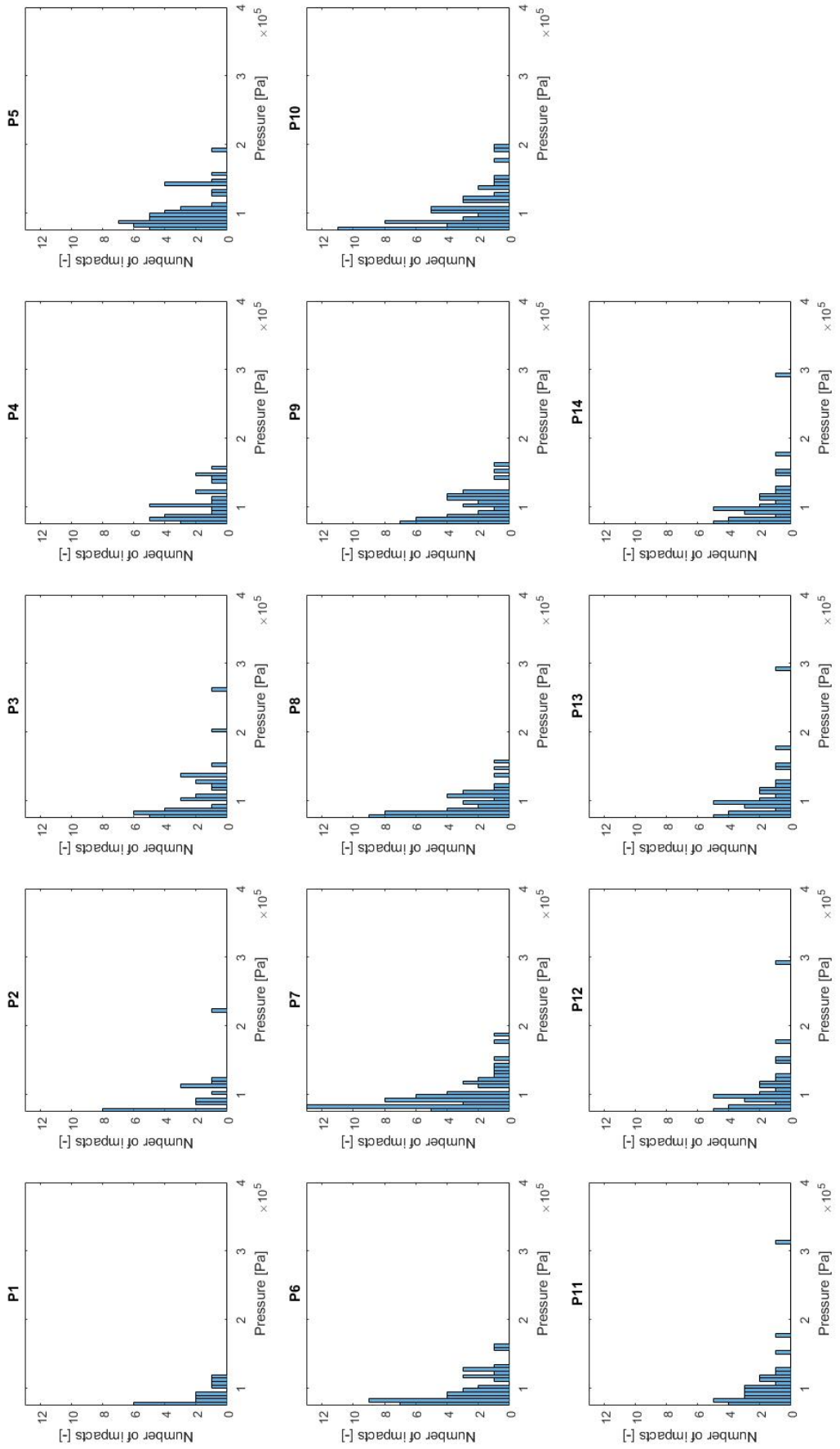

Figure E.4: Case 67 - Binned impact pressures of boxes

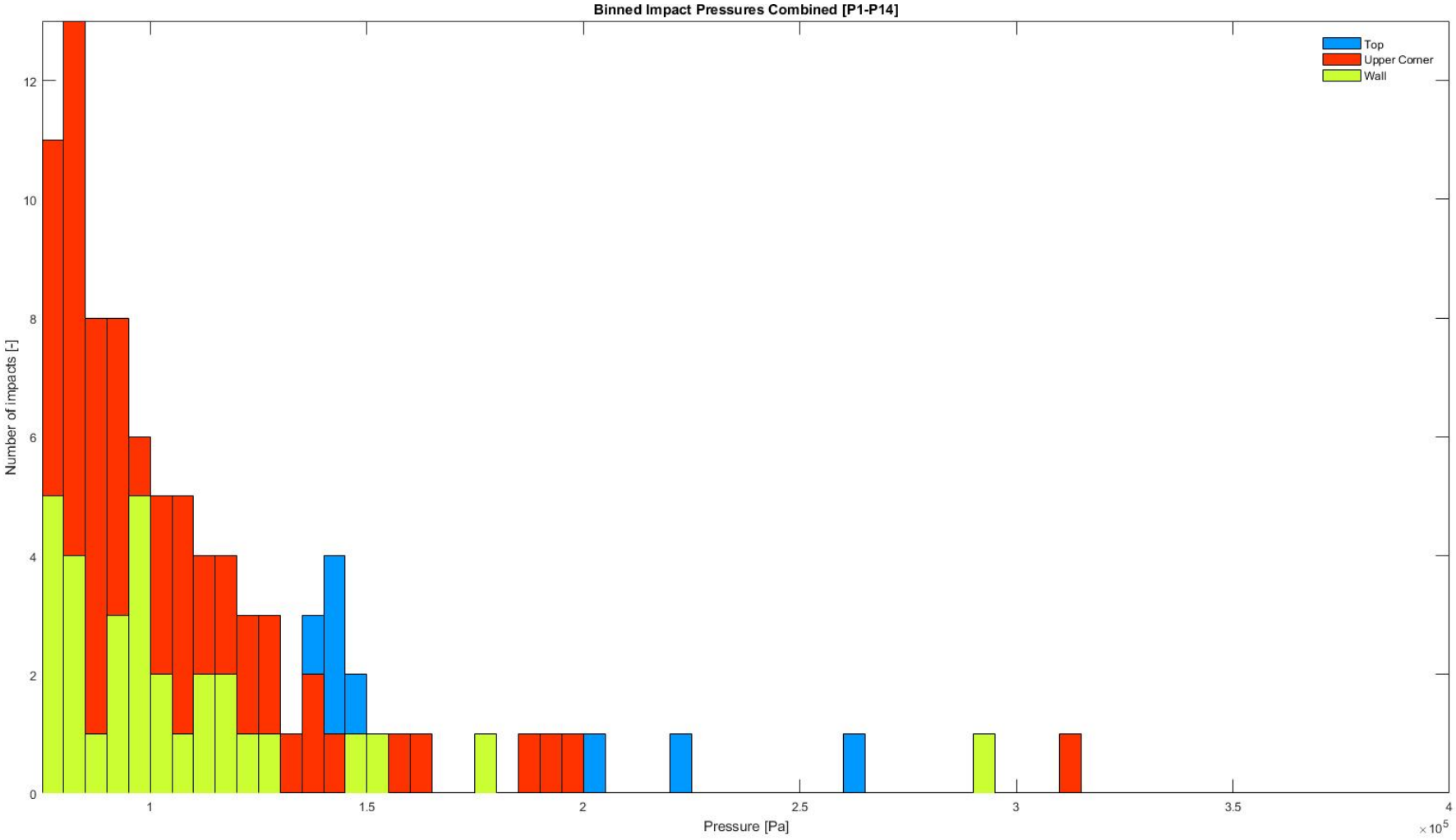

Figure E.5: Case 67 - Combined binned impact pressures

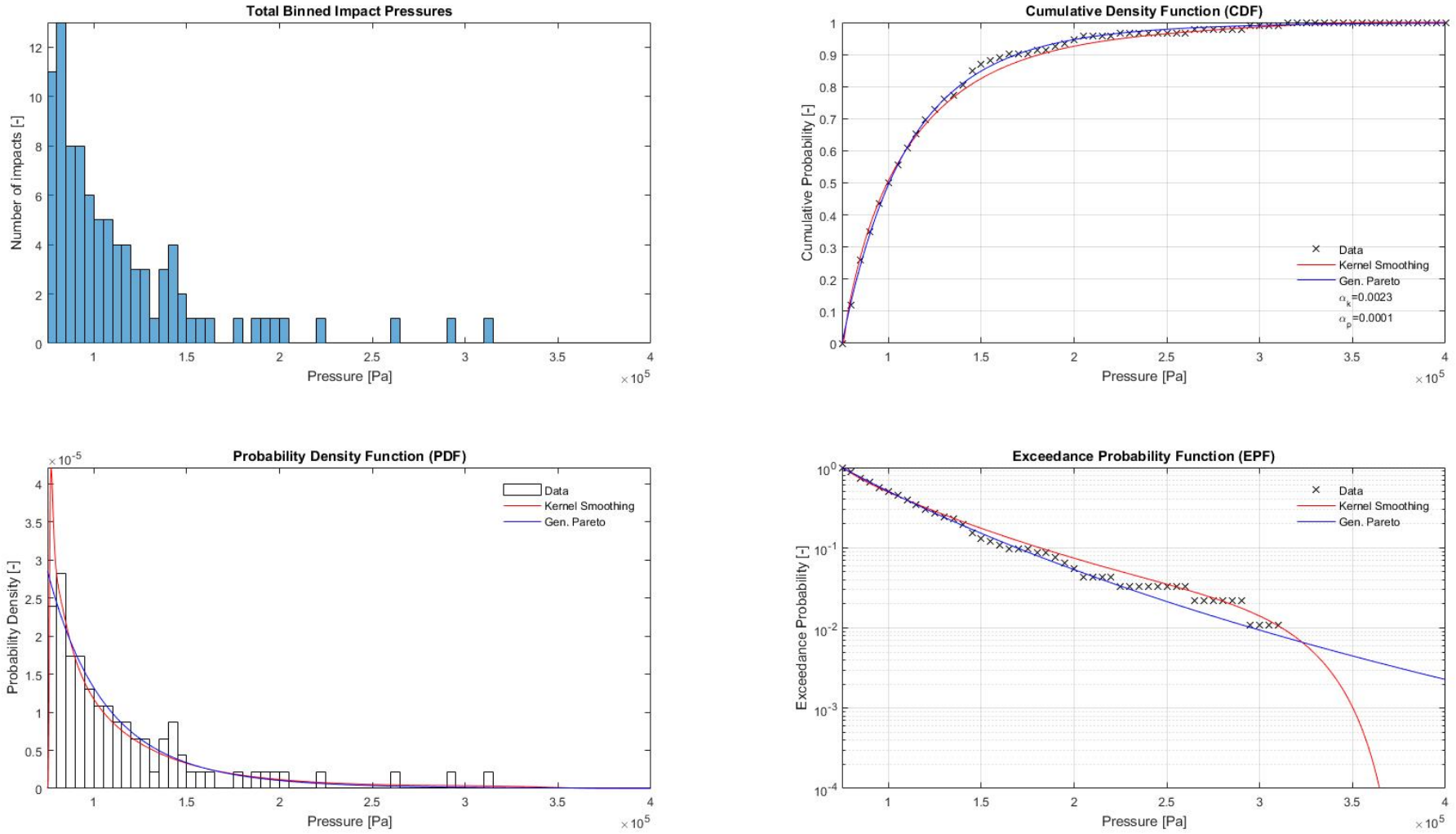

Figure E.6: Case 67 - Statistical fitting PDF, CDF and EPF

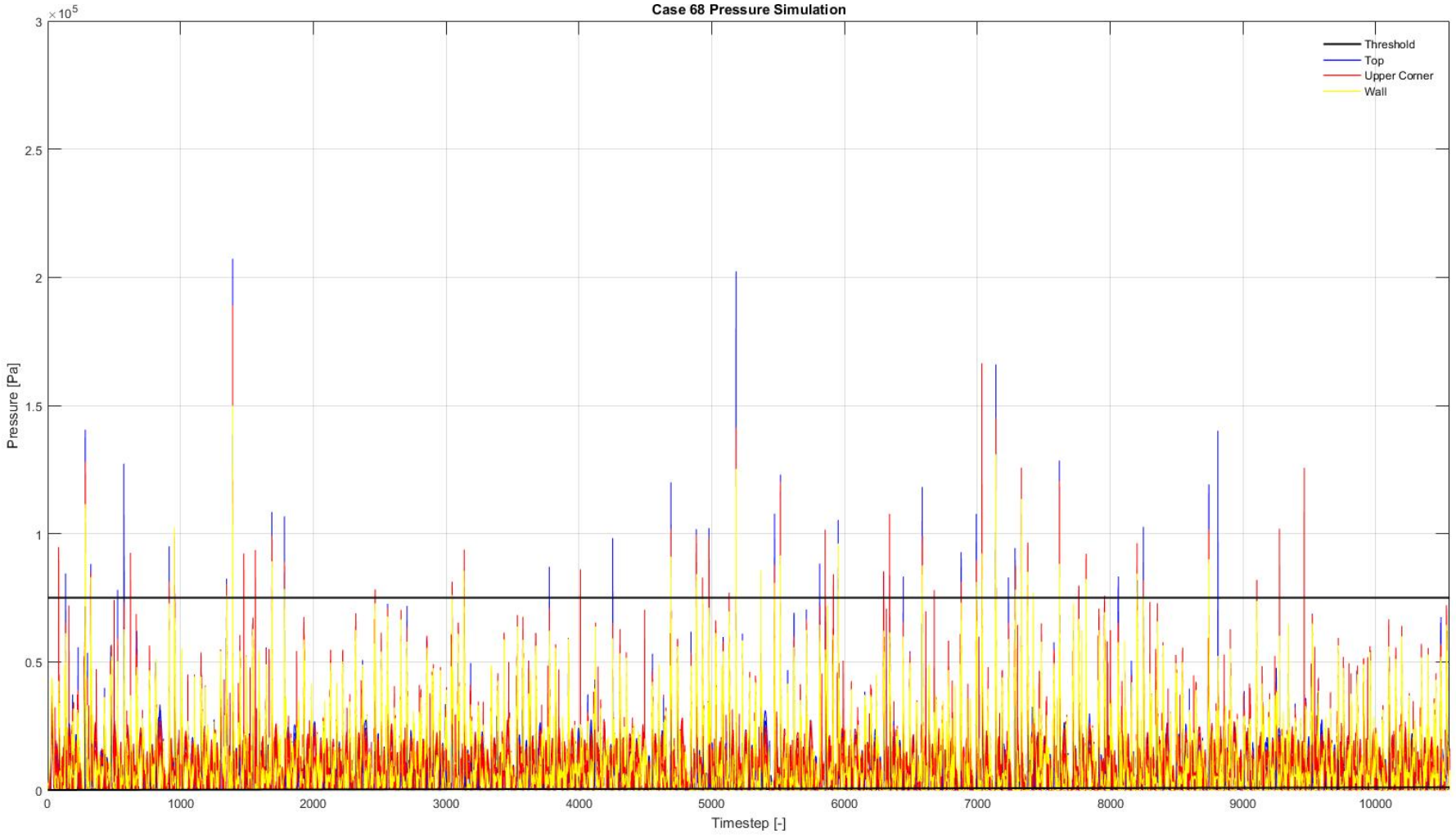

Figure E.7: Case 68 - Peak-over-Threshold

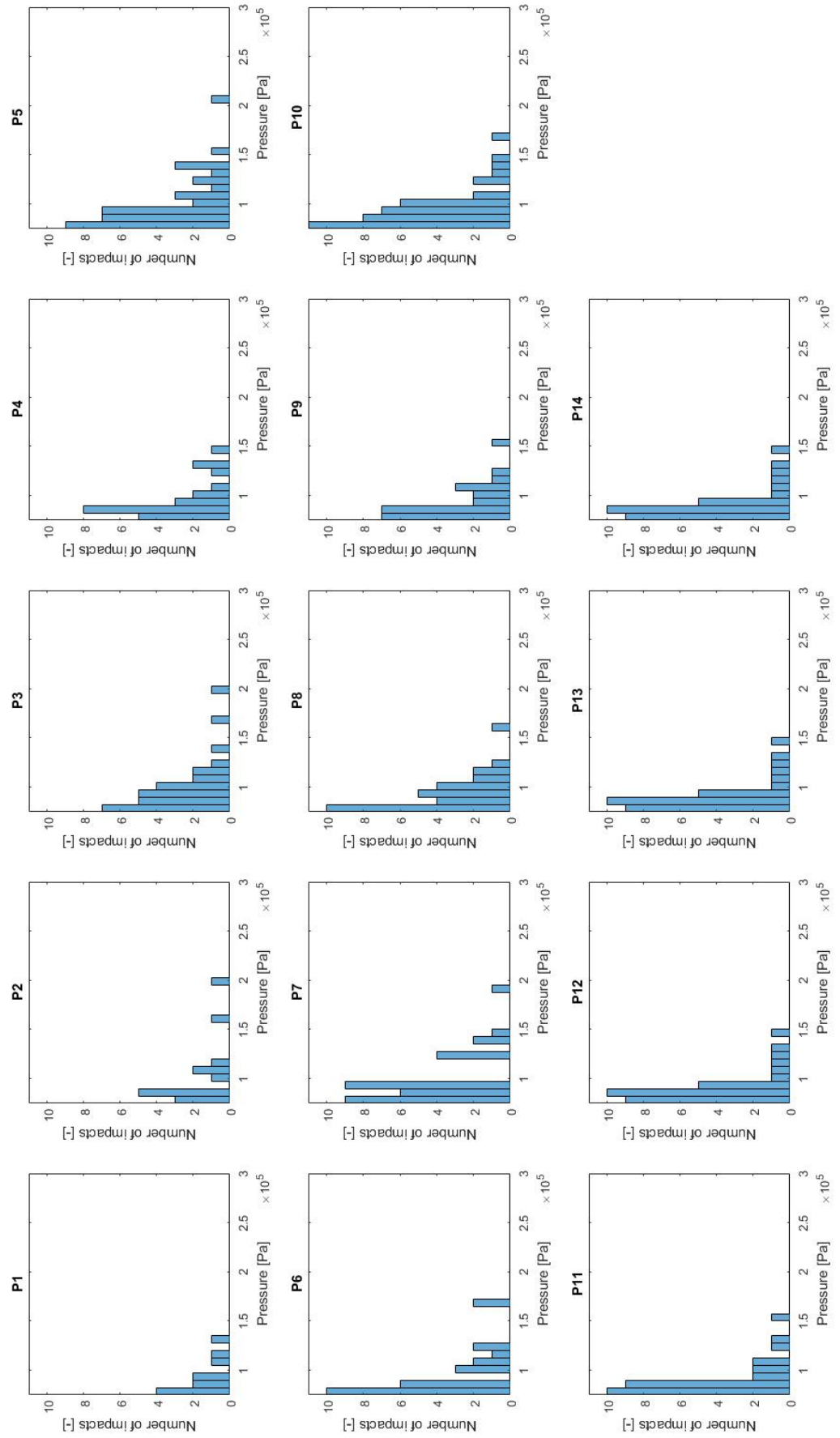

Figure E.8: Case 68 - Binned impact pressures of boxes

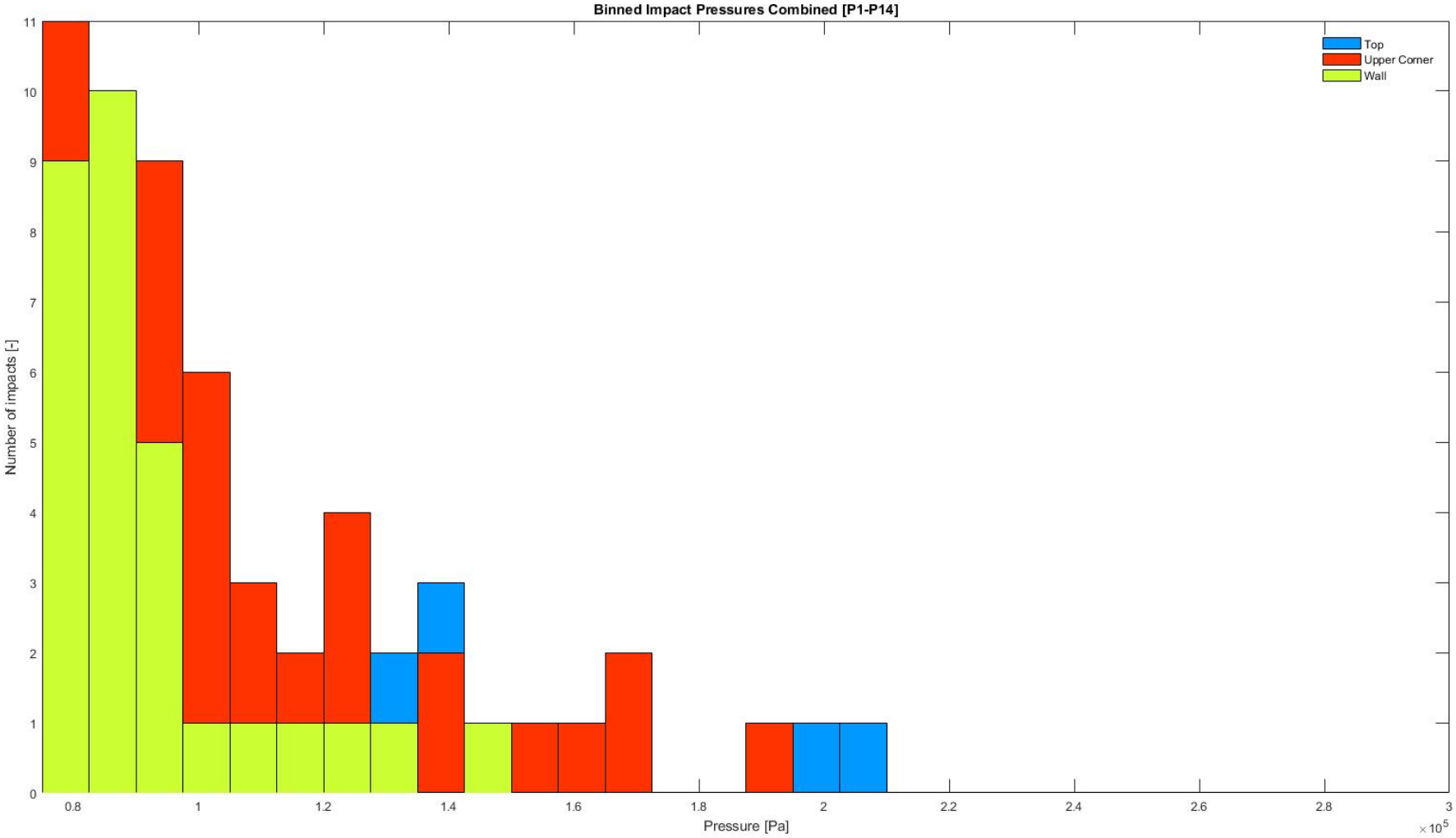

Figure E.9: Case 68 - Combined binned impact pressures

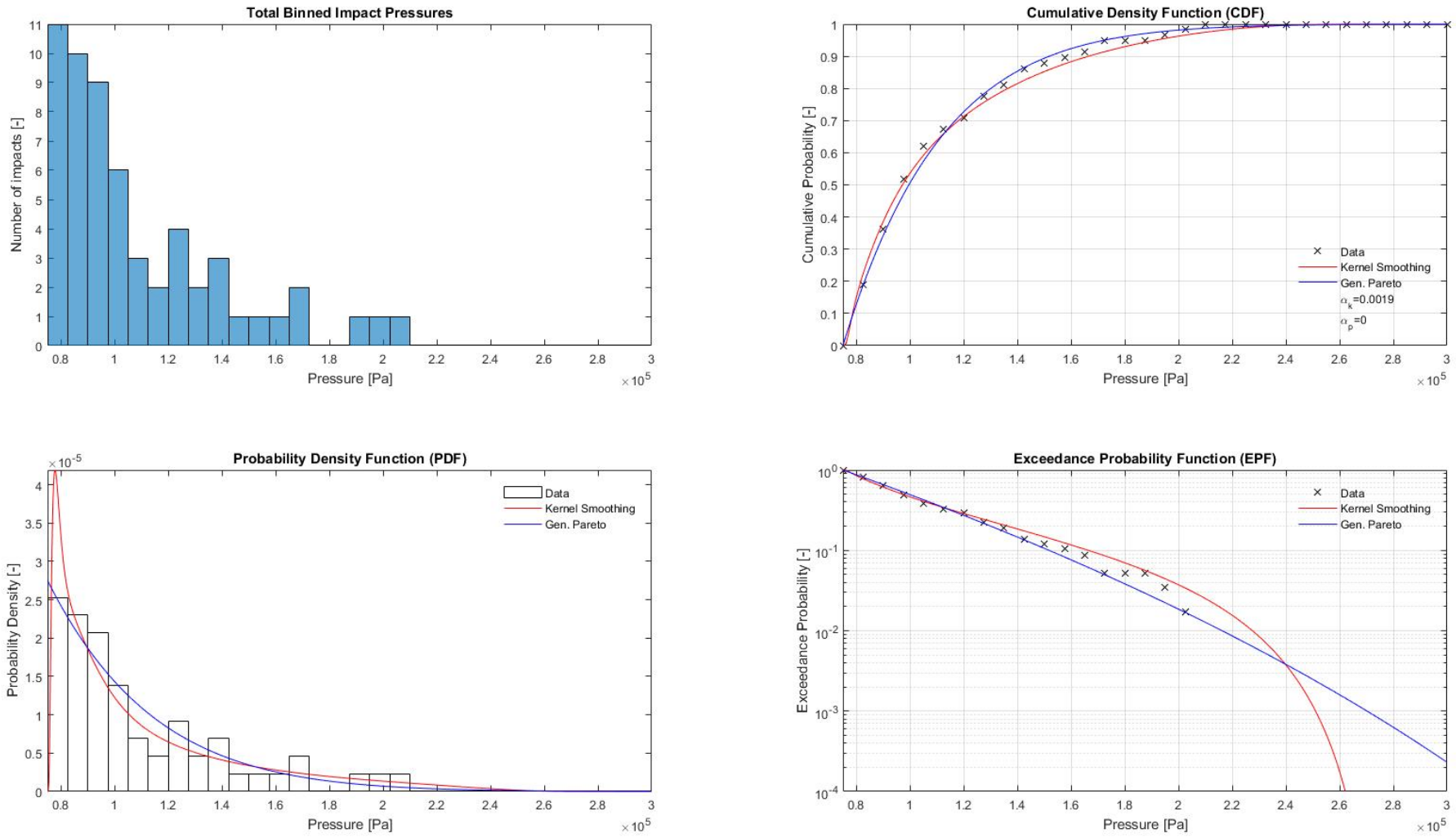

Figure E.10: Case 68 - Statistical fitting PDF, CDF and EPF

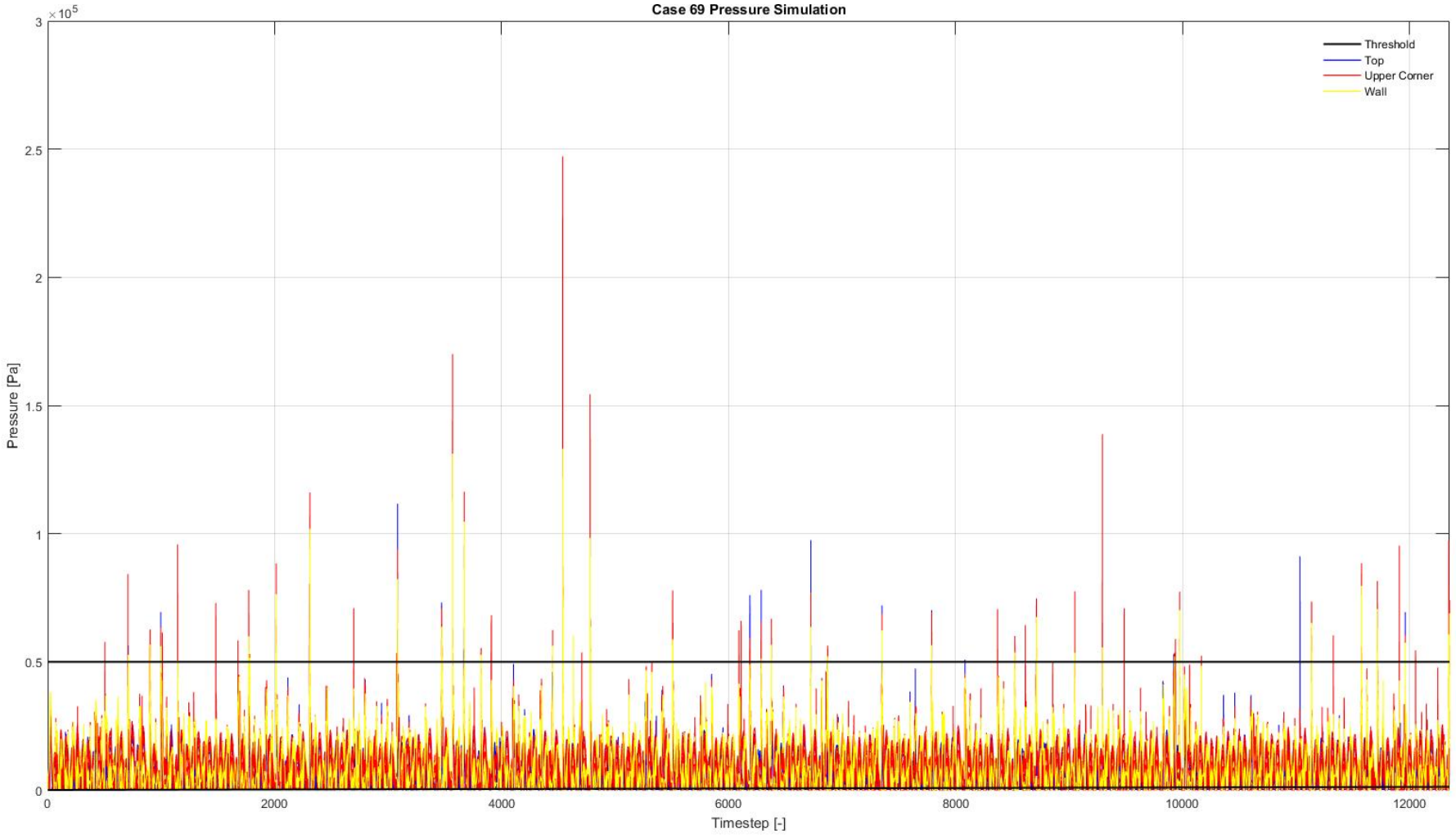

Figure E.11: Case 69 - Peak-over-Threshold

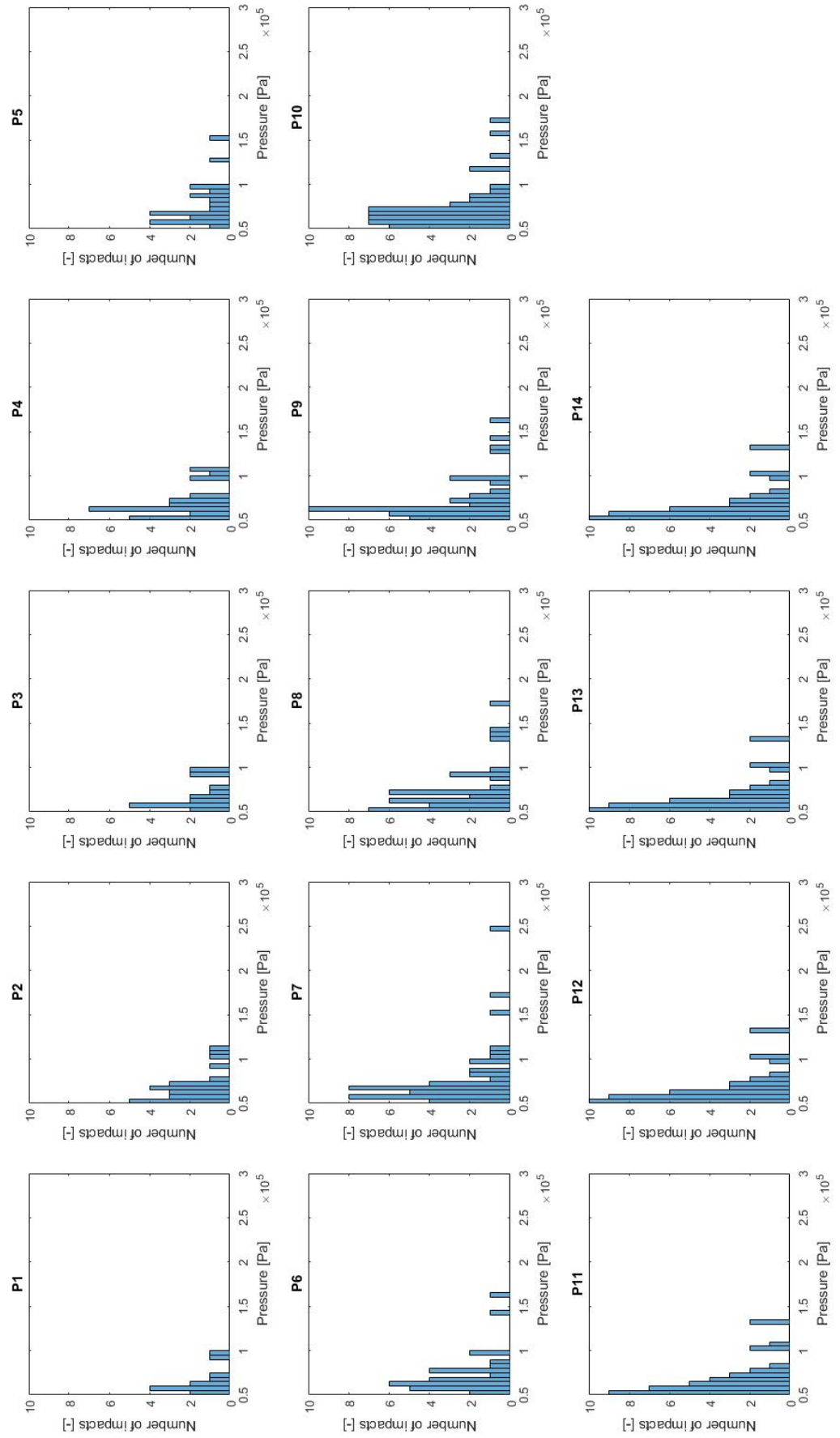

Figure E.12: Case 69 - Binned impact pressures of boxes

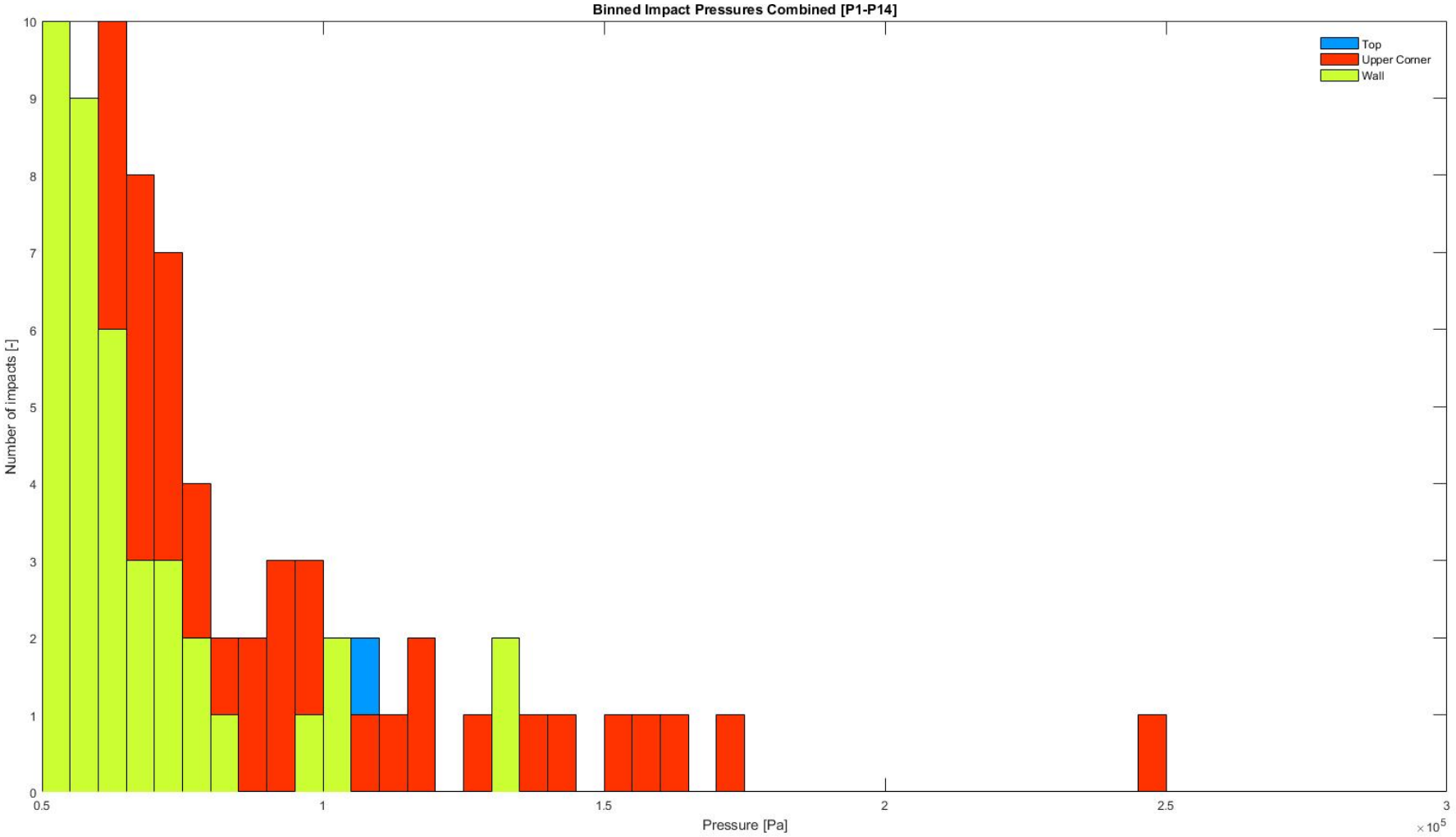

Figure E.13: Case 69 - Combined binned impact pressures

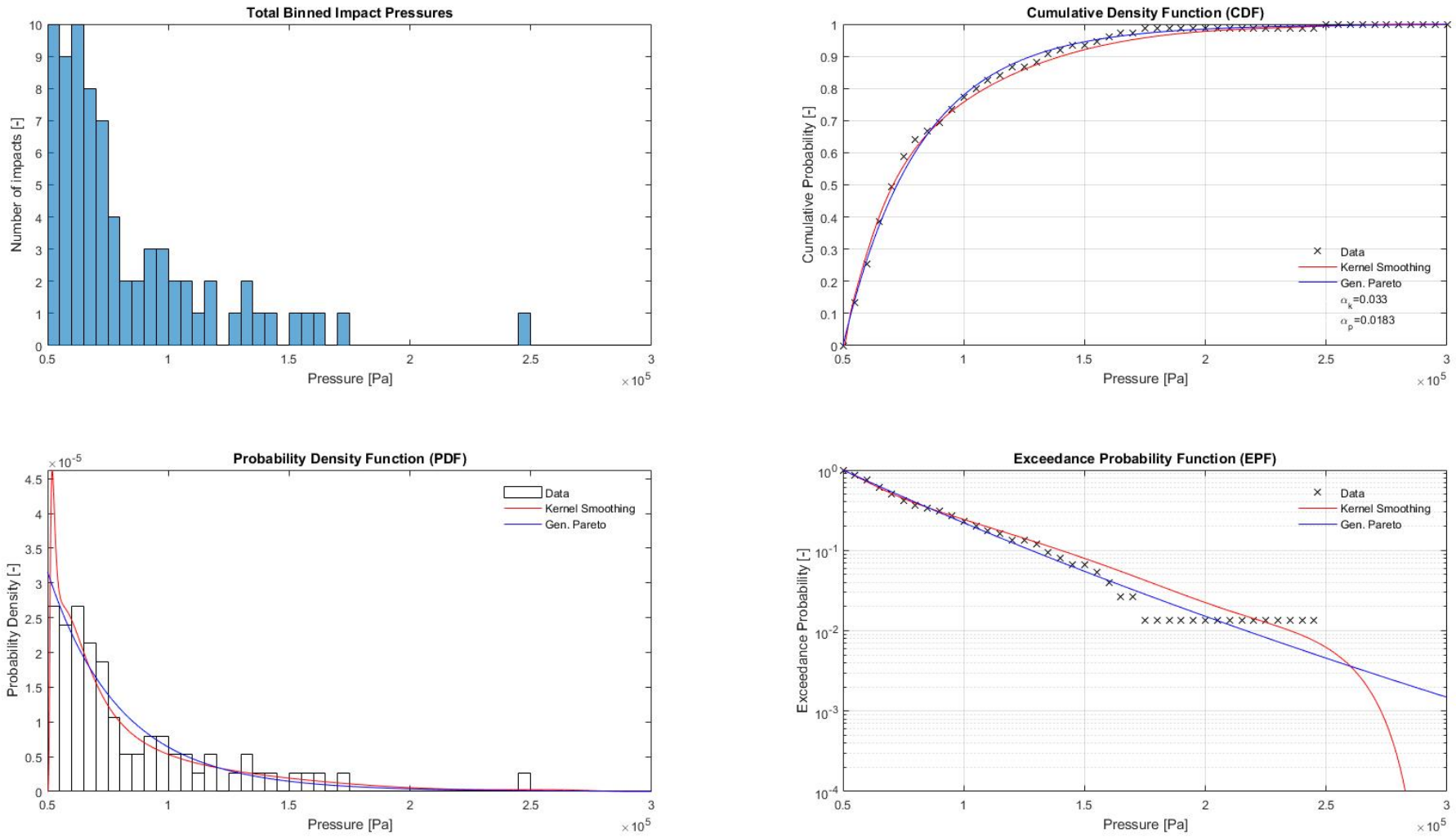

Figure E.14: Case 69 - Statistical fitting PDF, CDF and EPF

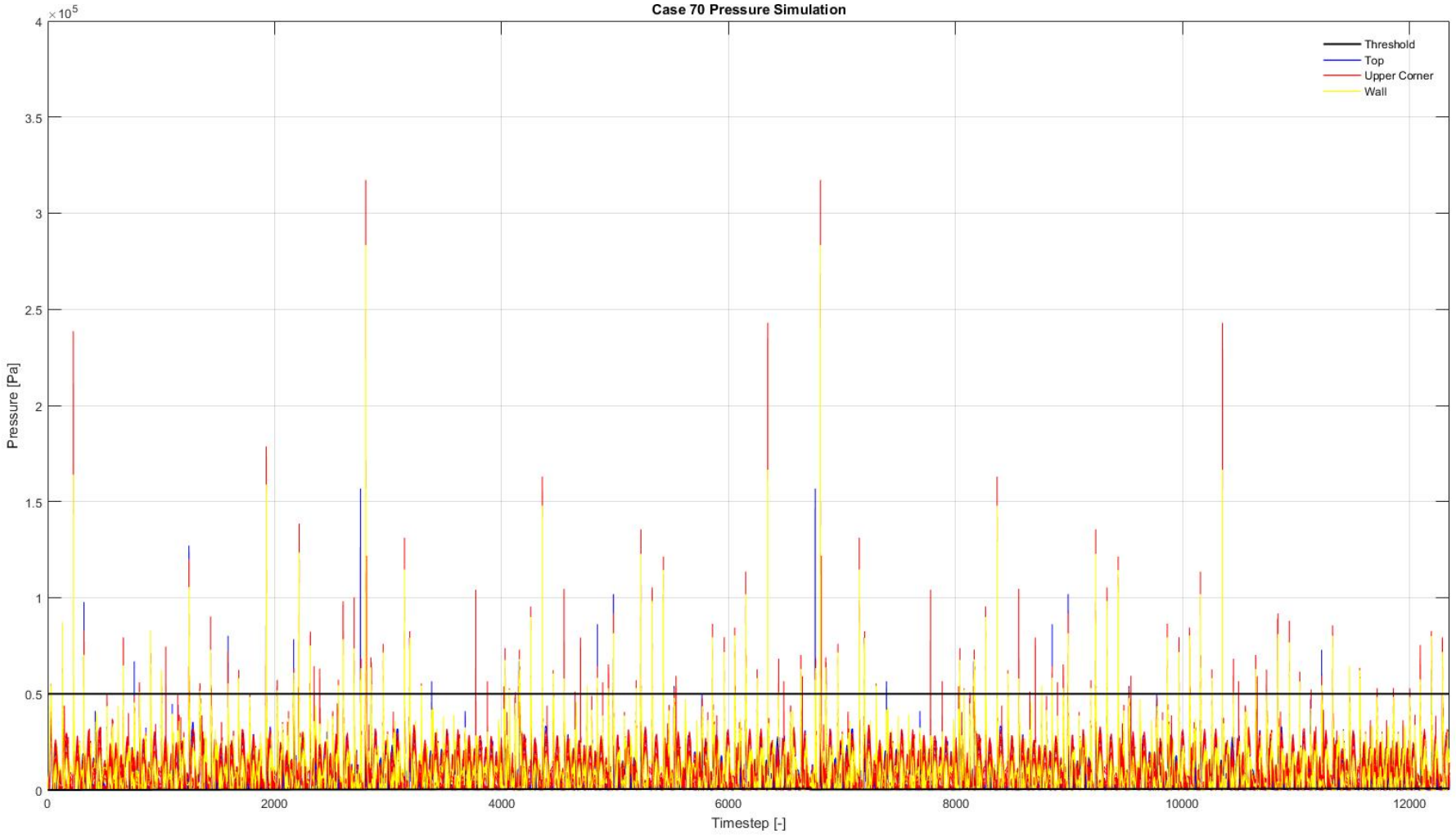

Figure E.15: Case 70 - Peak-over-Threshold

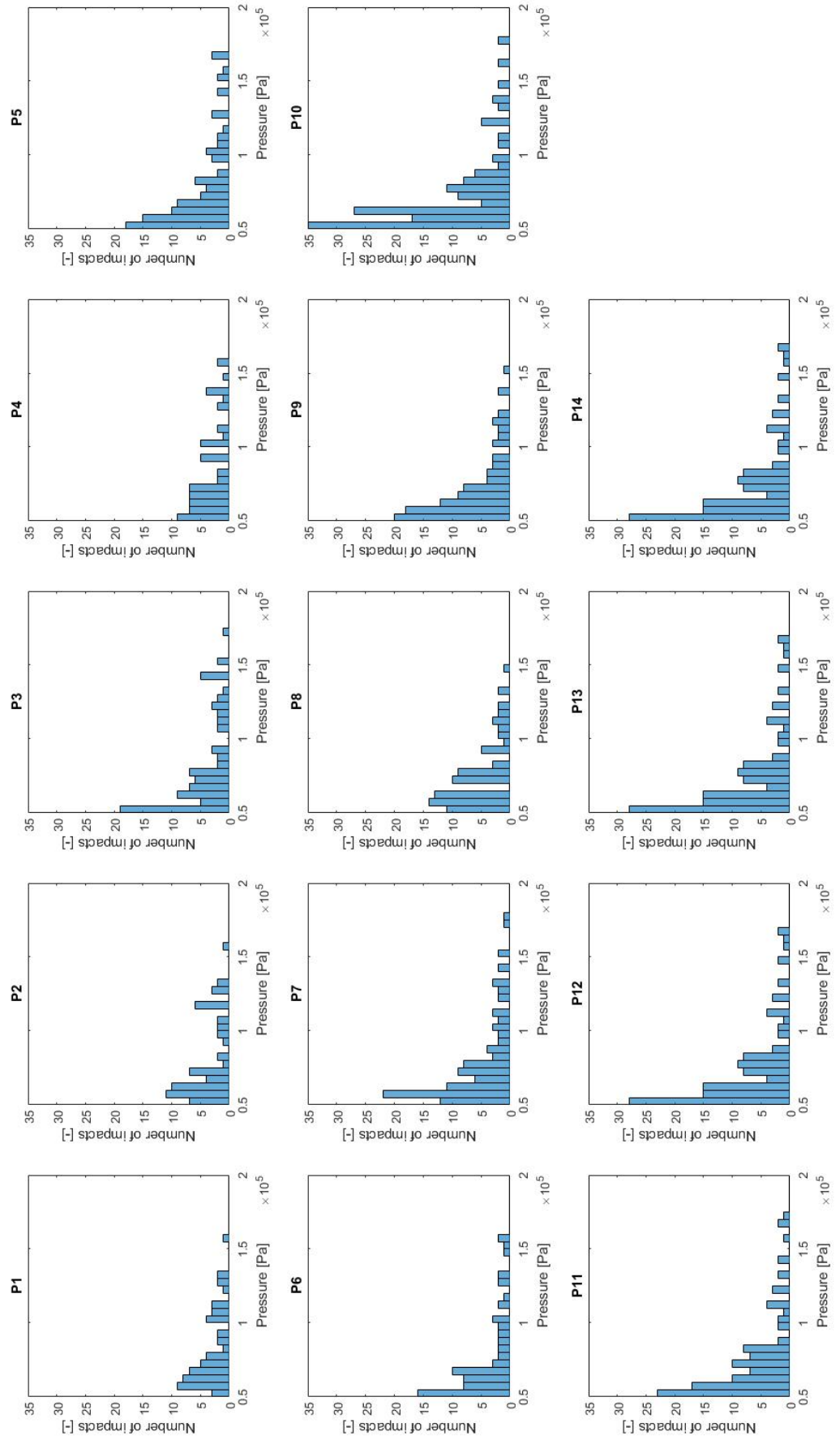

Figure E.16: Case 70 - Binned impact pressures of boxes

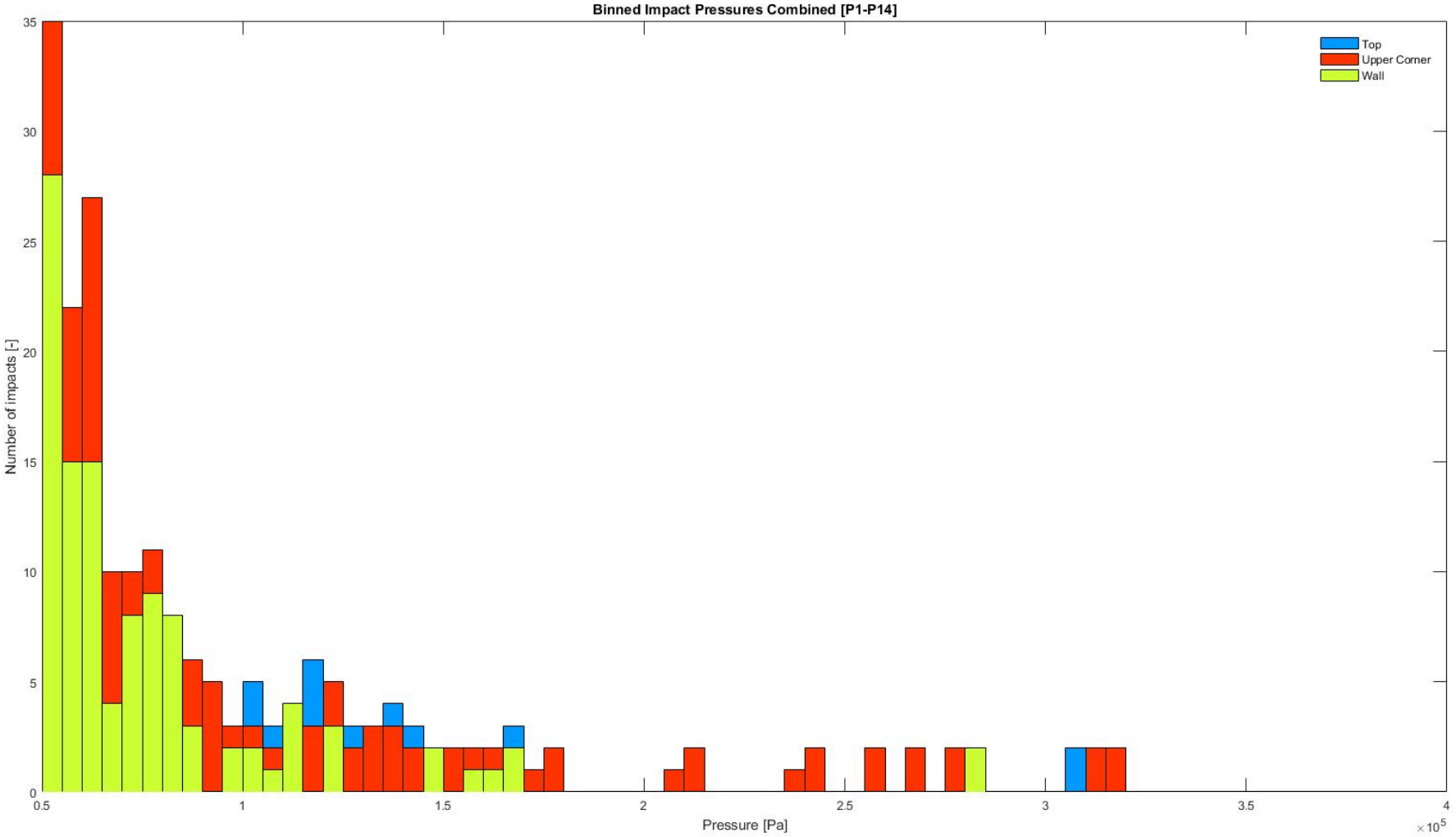

Figure E.17: Case 70 - Combined binned impact pressures

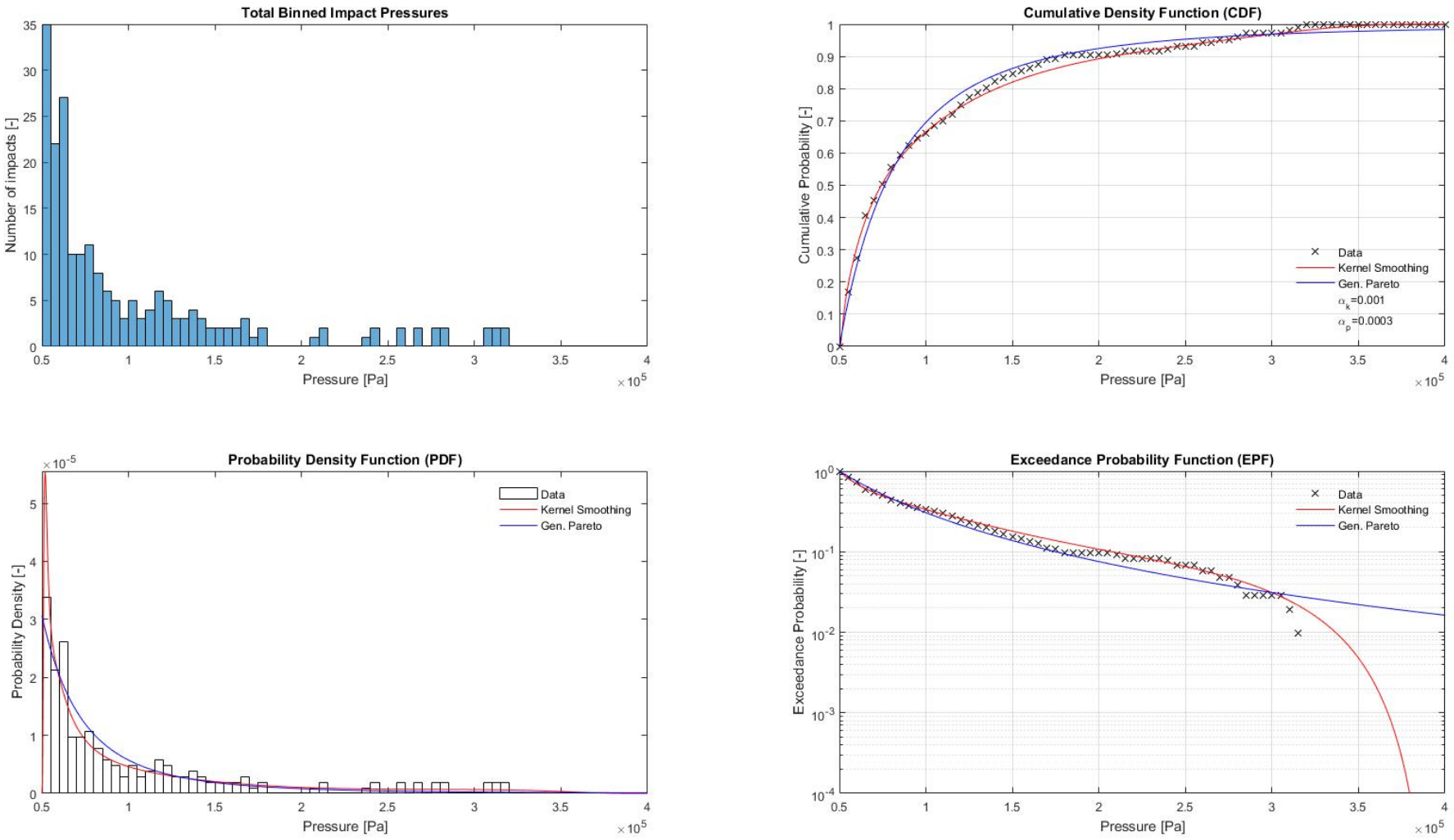

Figure E.18: Case 70 - Statistical fitting PDF, CDF and EPF

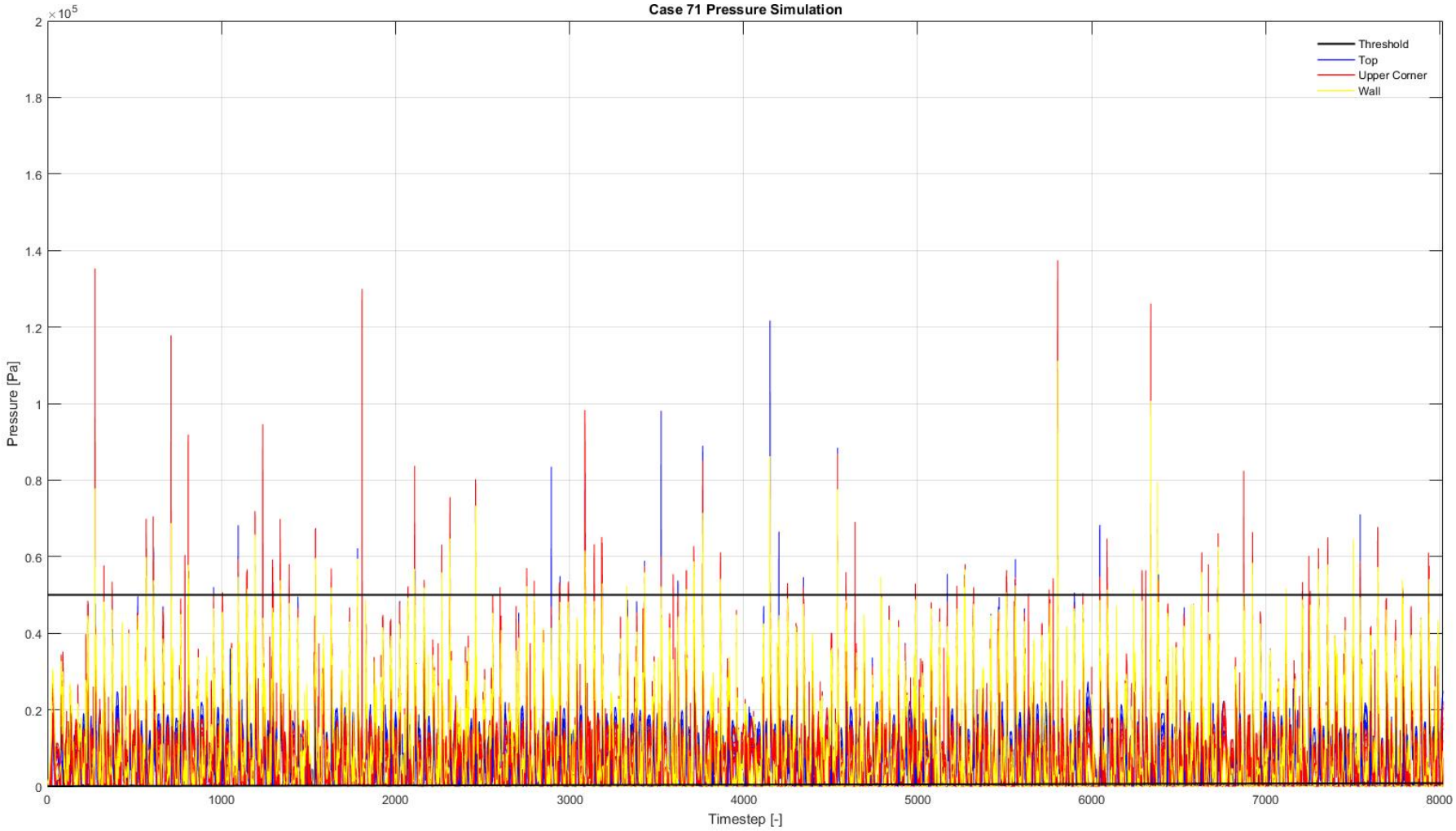

Figure E.19: Case 71 - Peak-over-Threshold

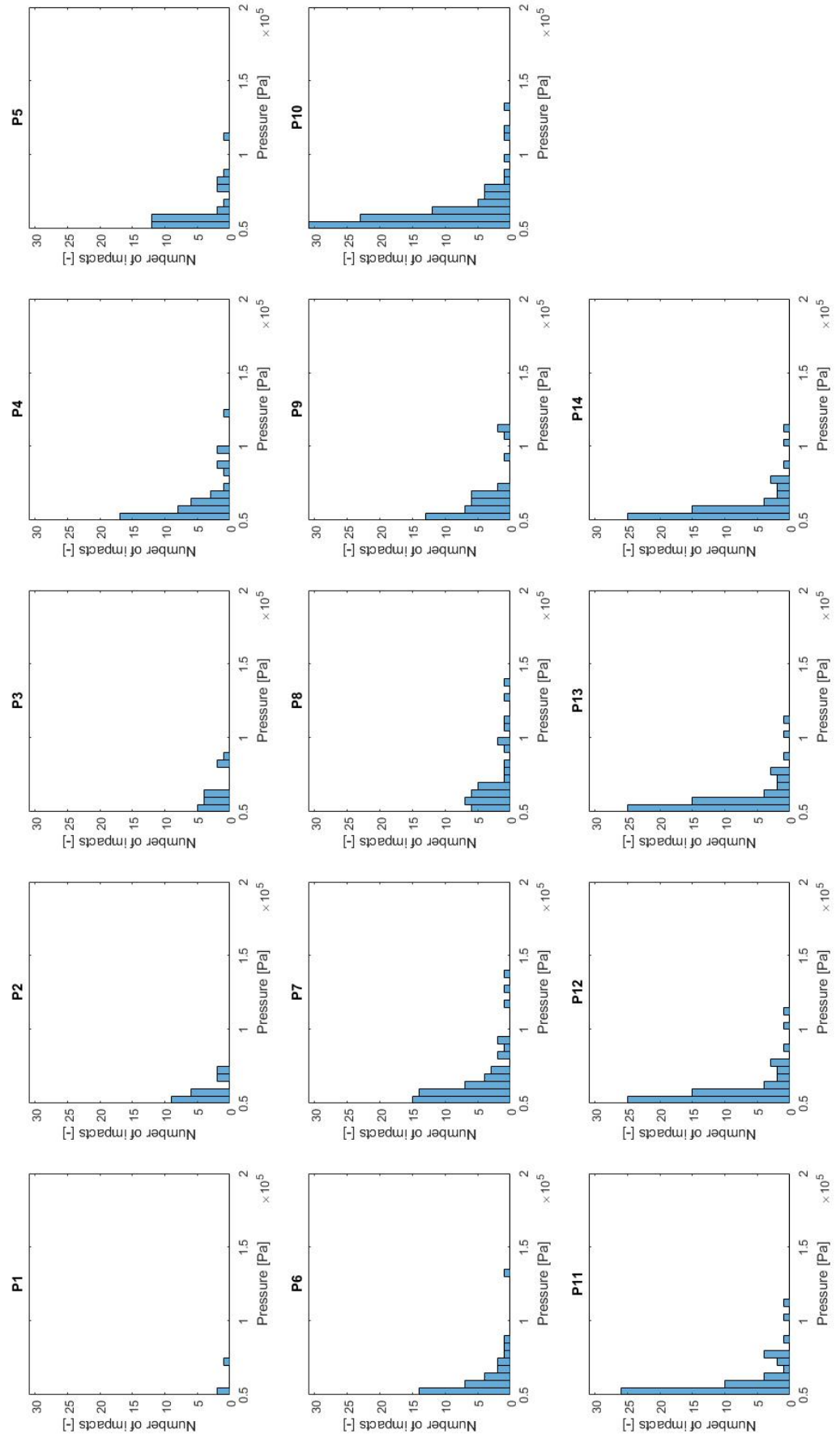

Figure E.20: Case 71 - Binned impact pressures of boxes

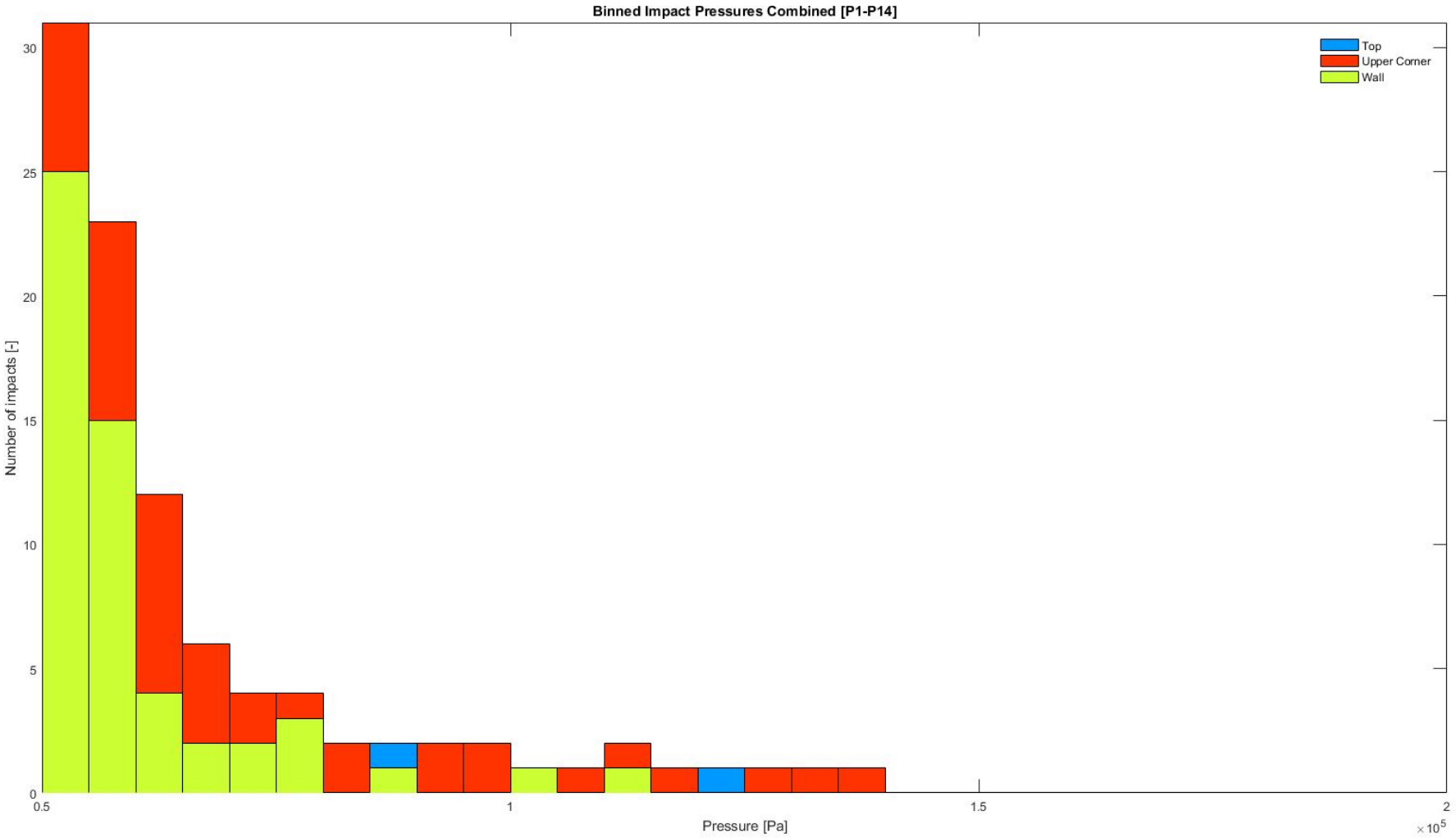

Figure E.21: Case 71 - Combined binned impact pressures

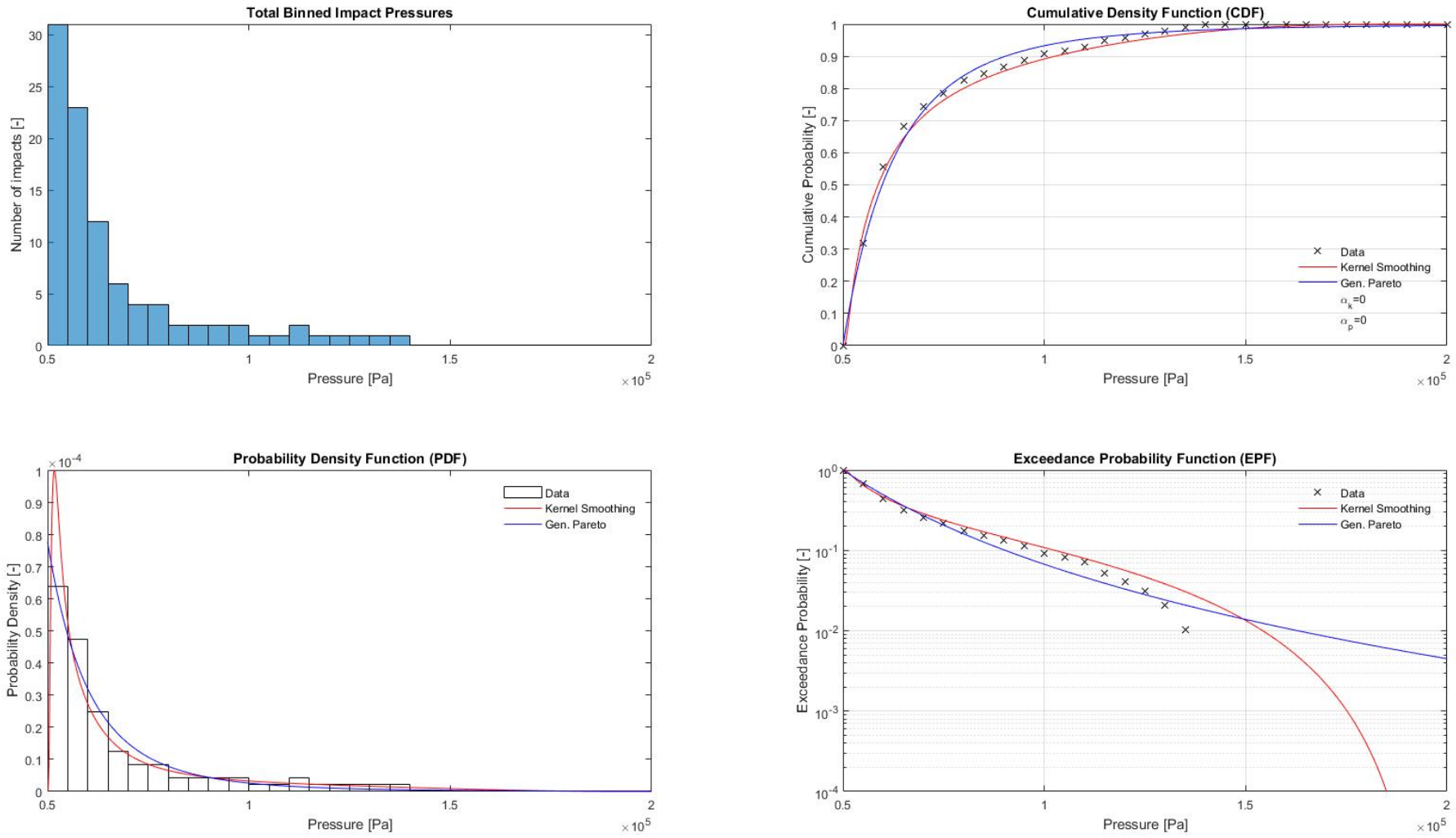

Figure E.22: Case 71 - Statistical fitting PDF, CDF and EPF

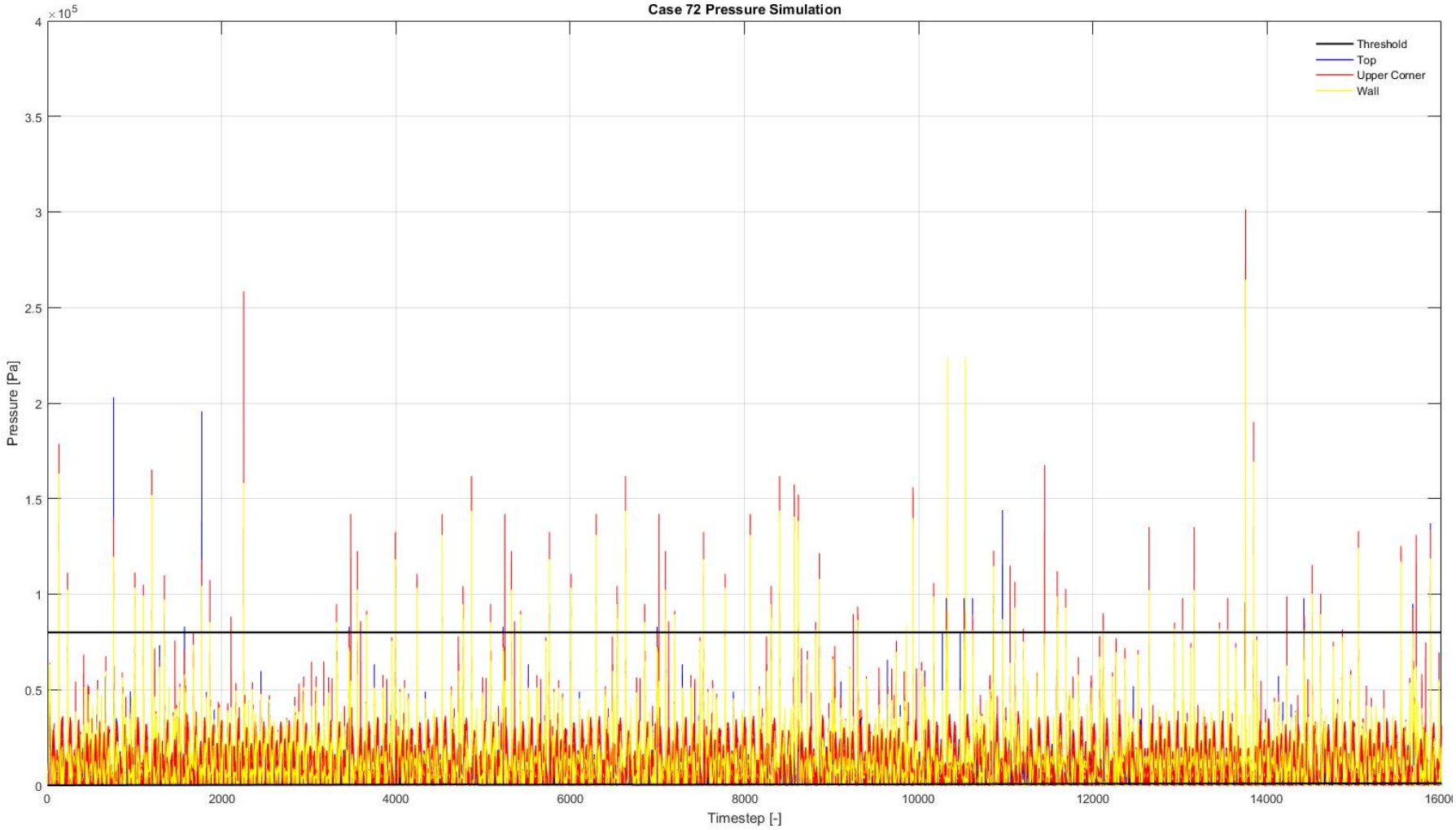

Figure E.23: Case 72 - Peak-over-Threshold

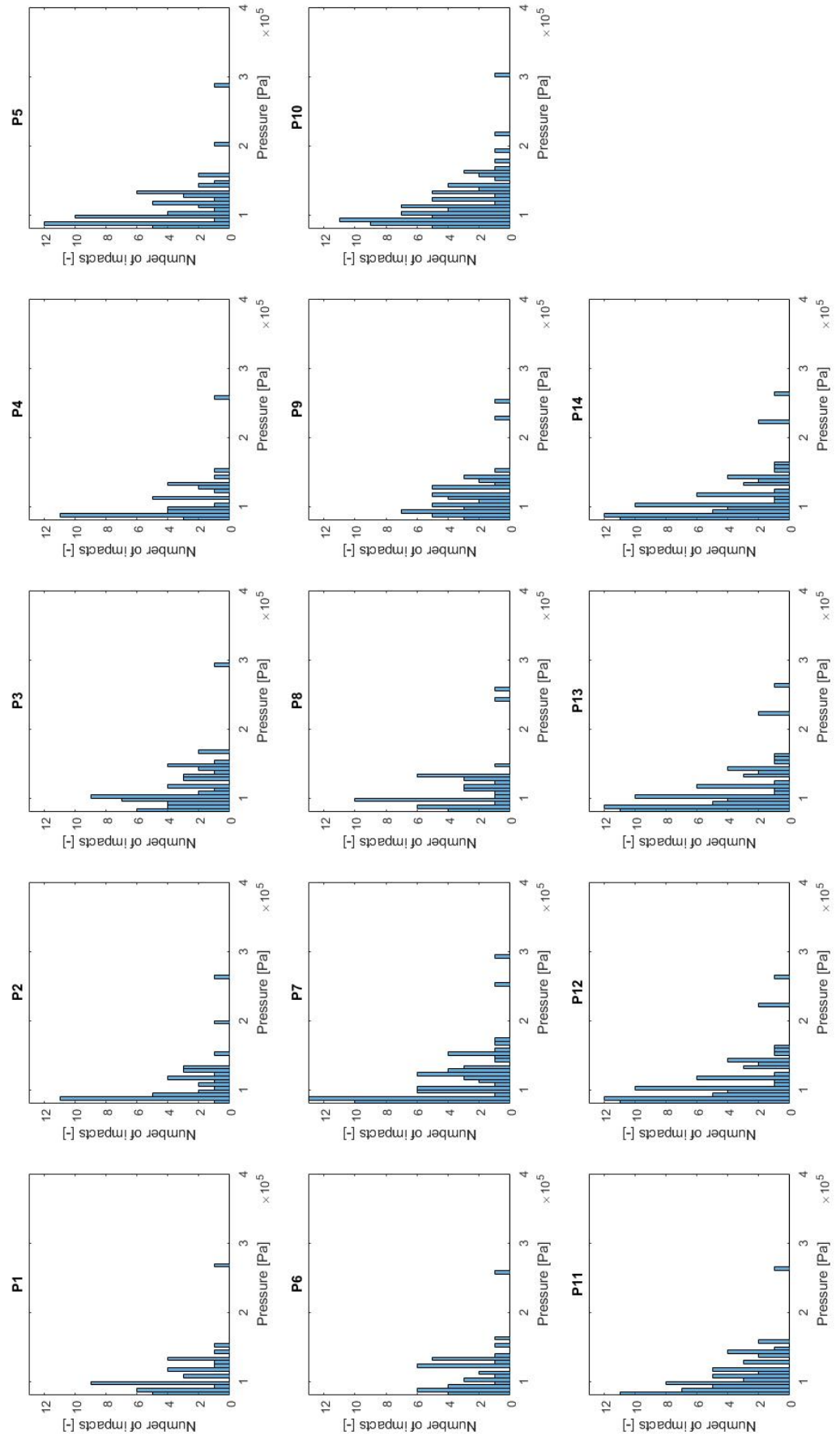

Figure E.24: Case 72 - Binned impact pressures of boxes

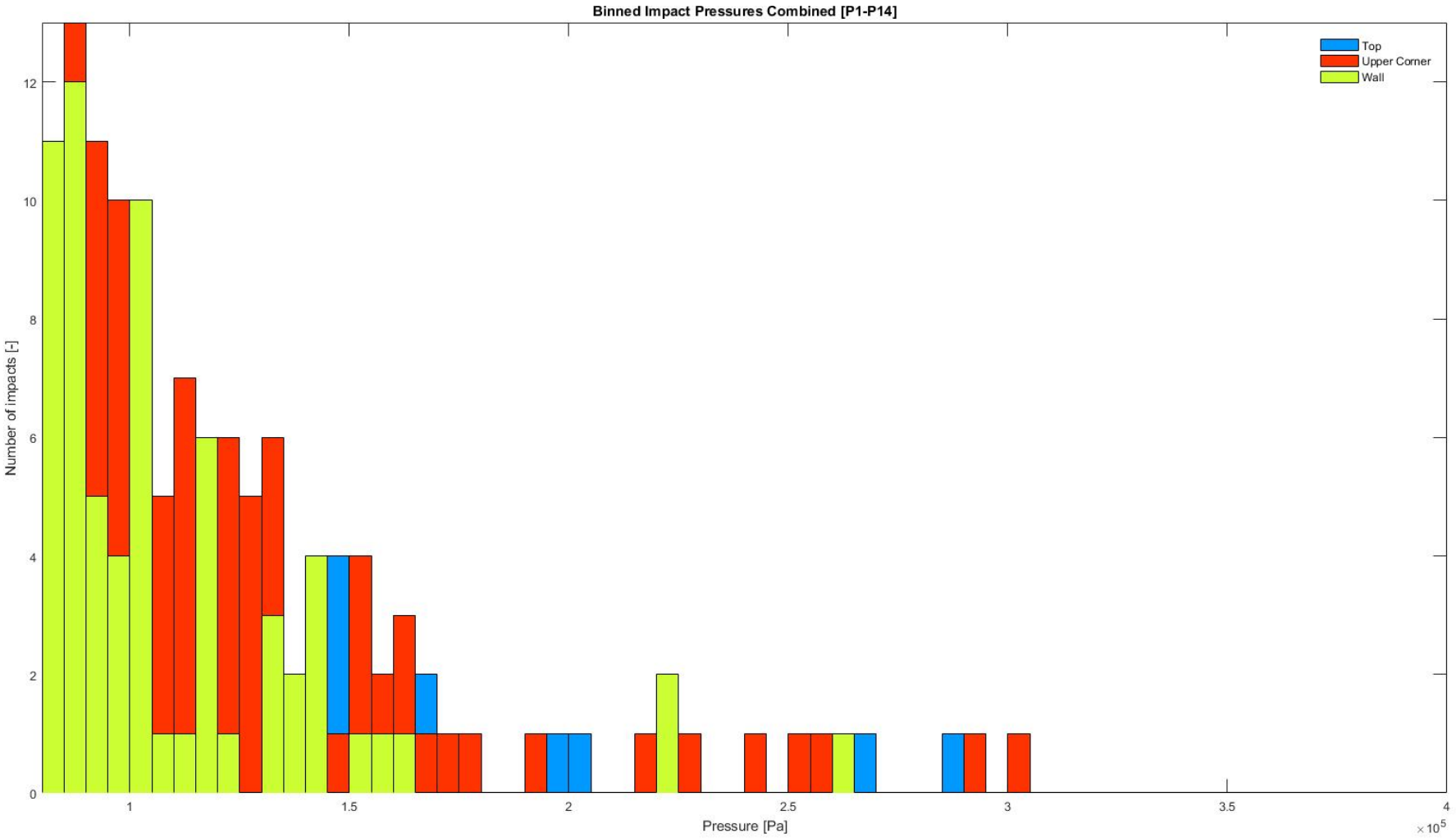

Figure E.25: Case 72 - Combined binned impact pressures

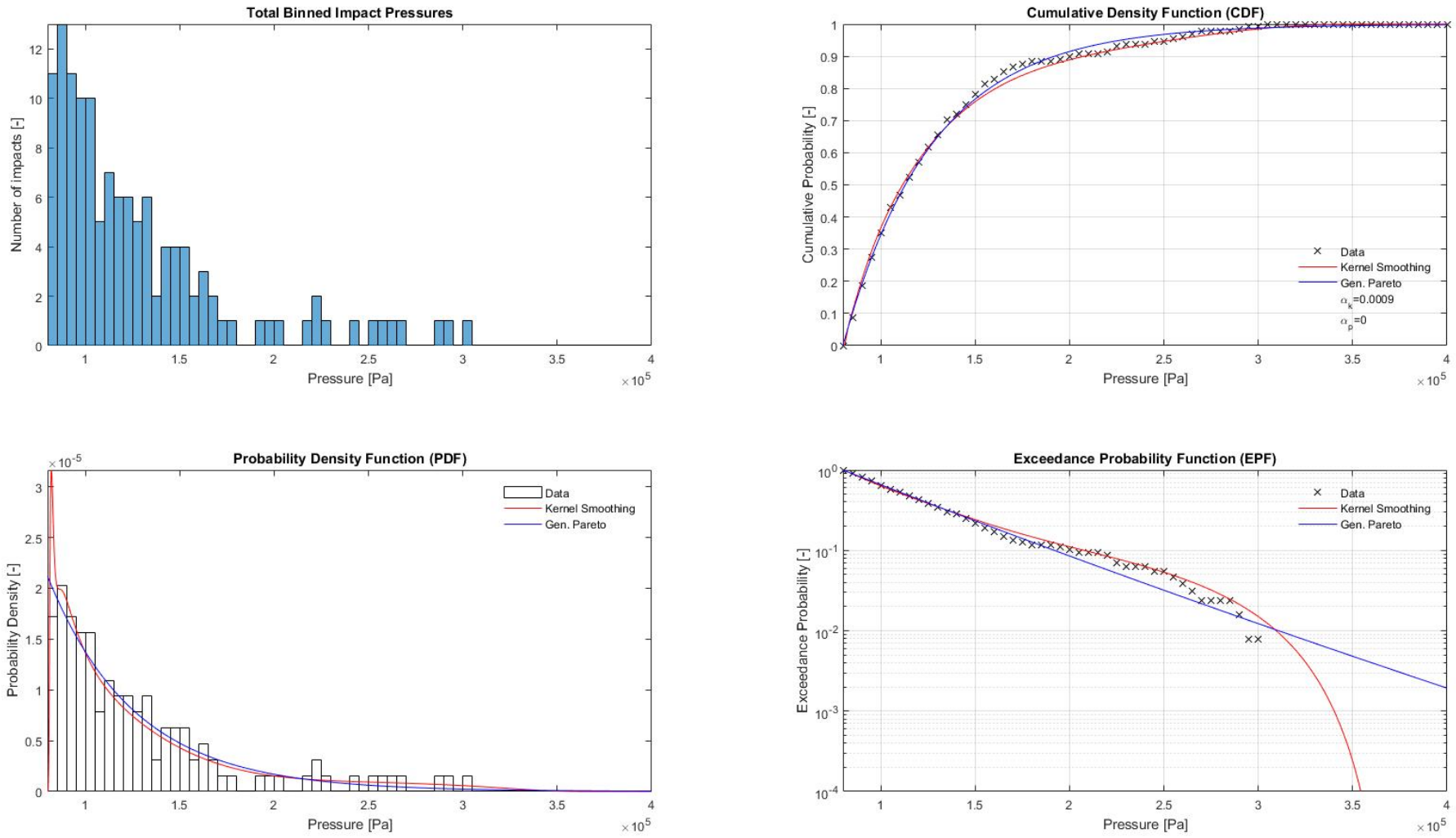

Figure E.26: Case 72 - Statistical fitting PDF, CDF and EPF

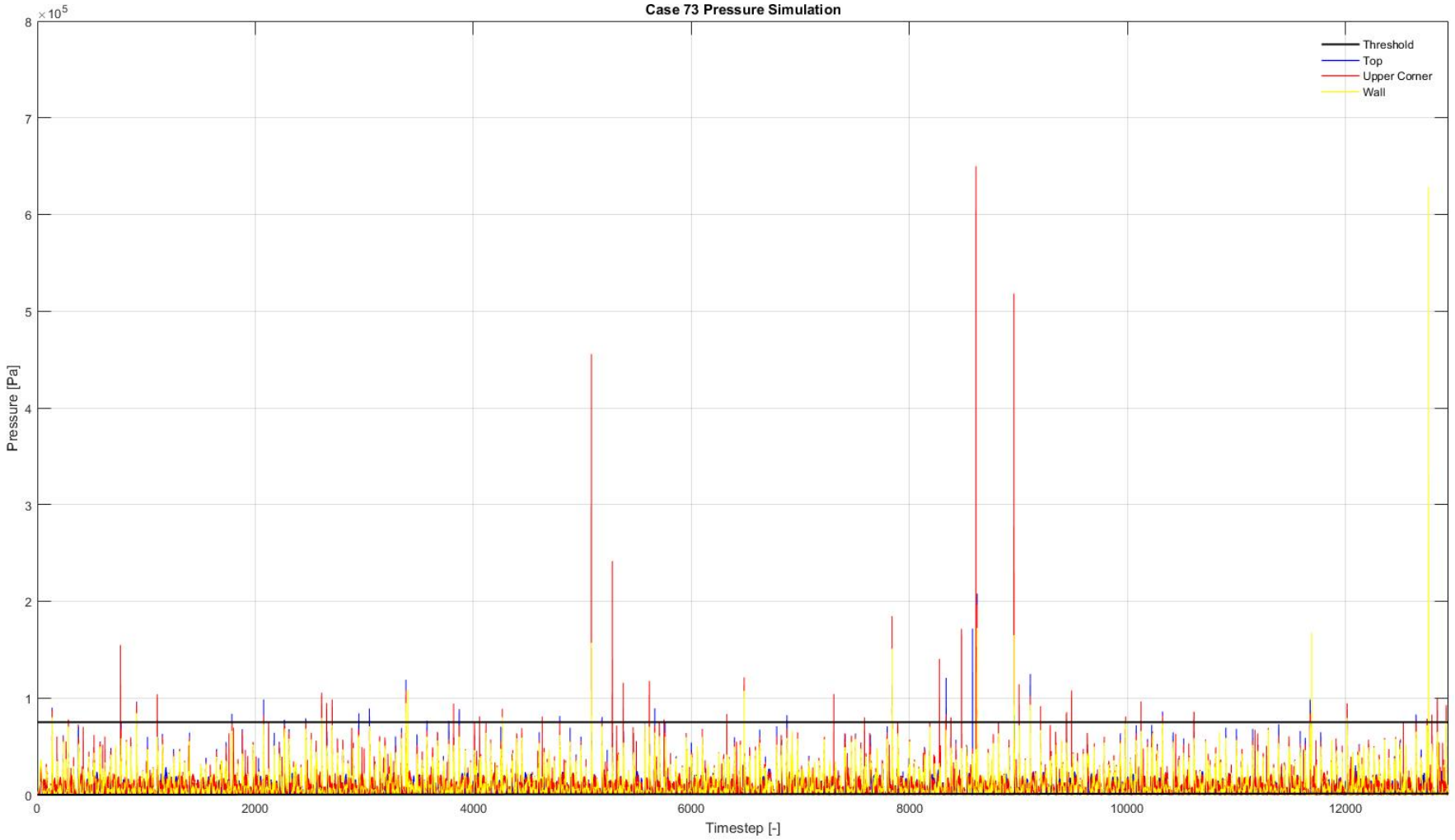

Figure E.27: Case 73 - Peak-over-Threshold

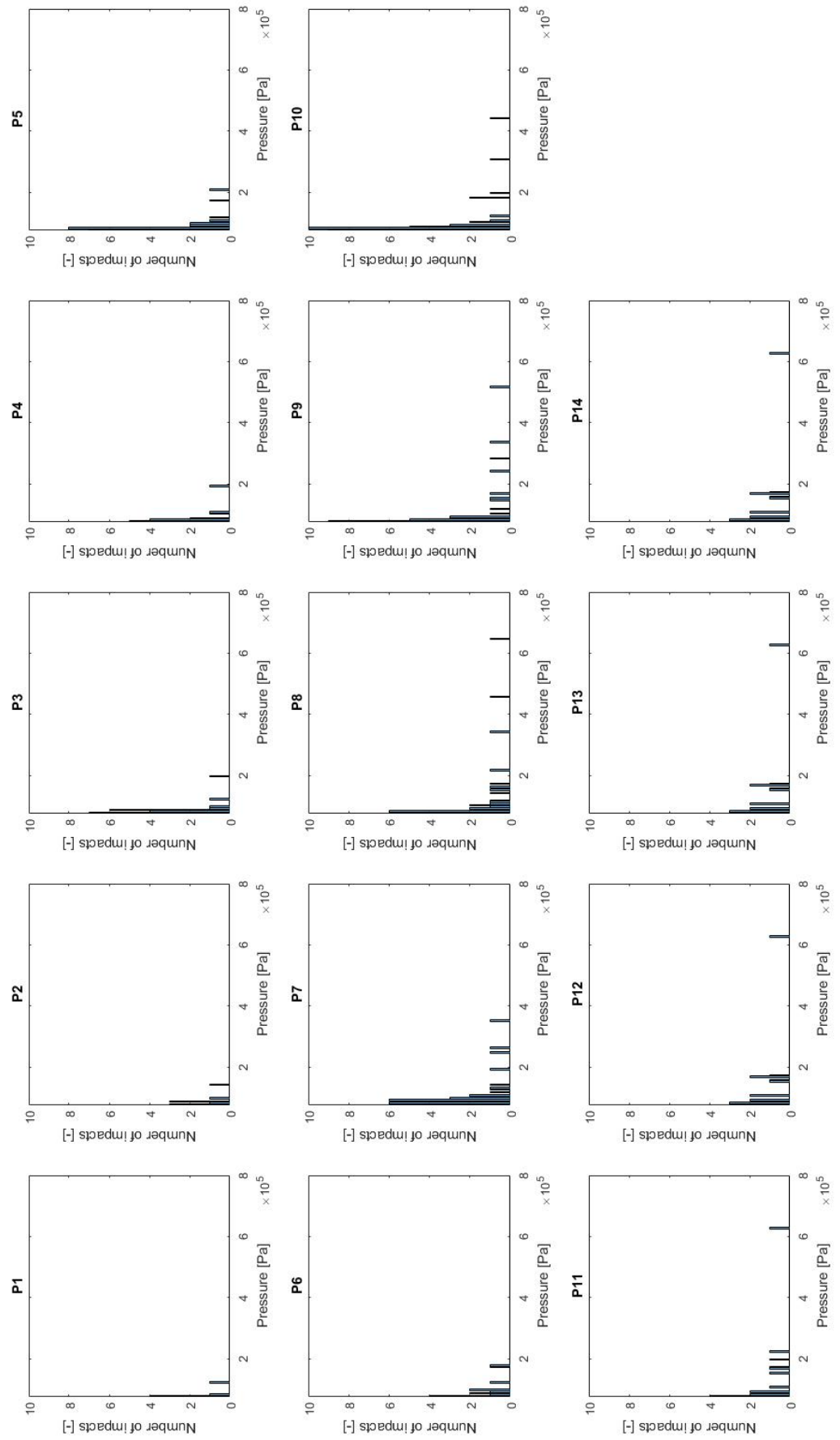

Figure E.28: Case 73 - Binned impact pressures of boxes

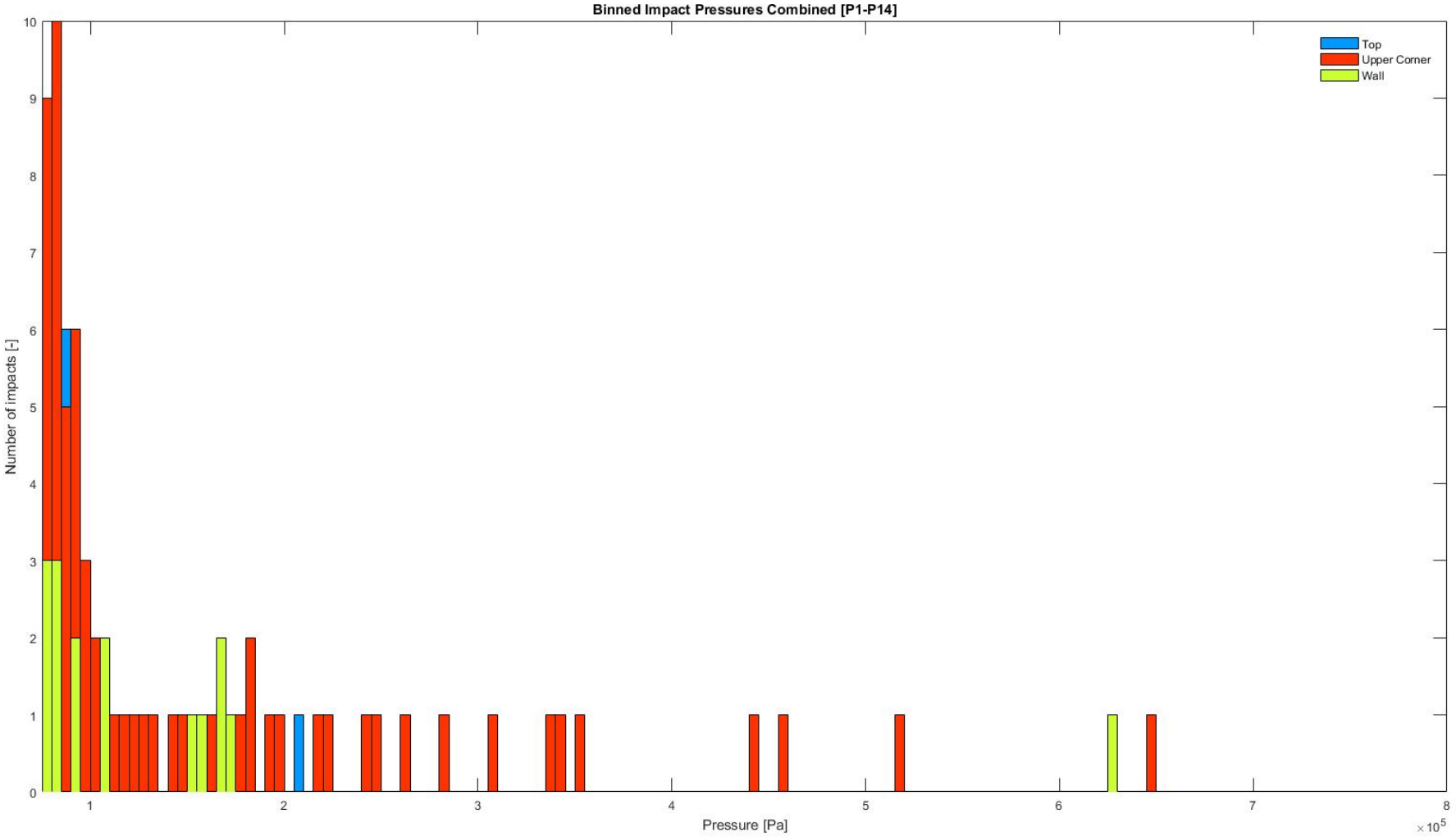

Figure E.29: Case 73 - Combined binned impact pressures

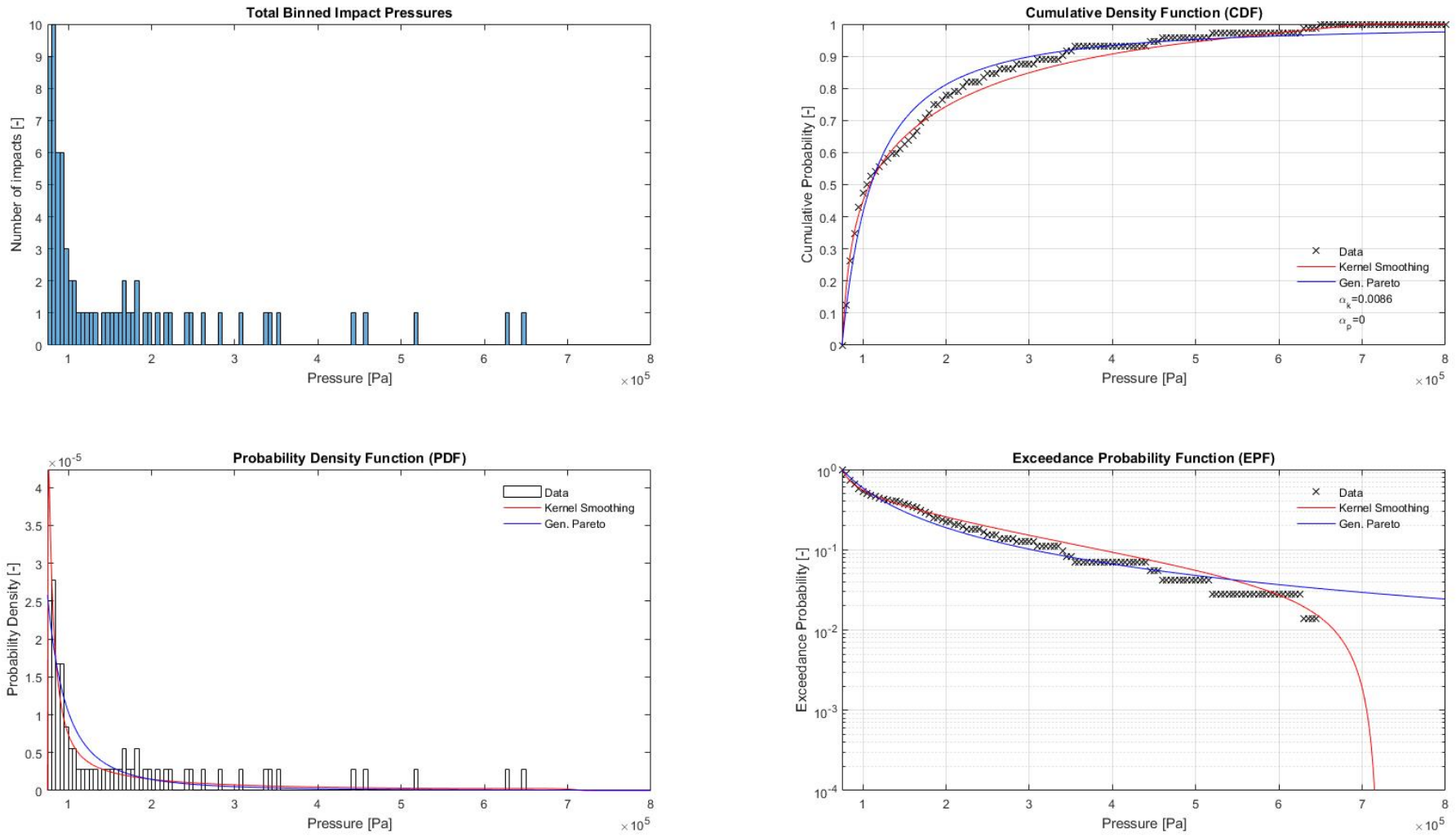

Figure E.30: Case 73 - Statistical fitting PDF, CDF and EPF

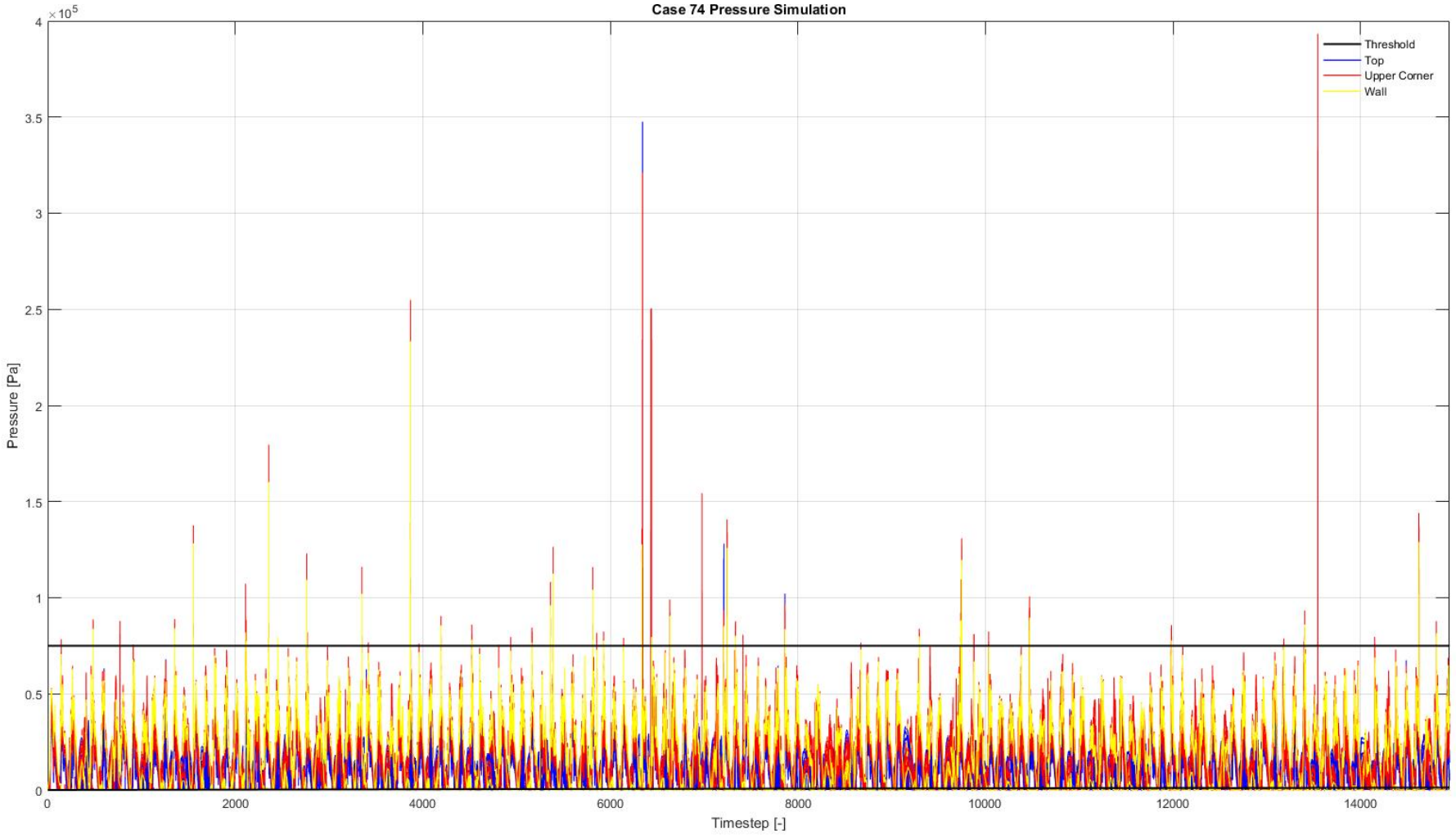

Figure E.31: Case 74 - Peak-over-Threshold

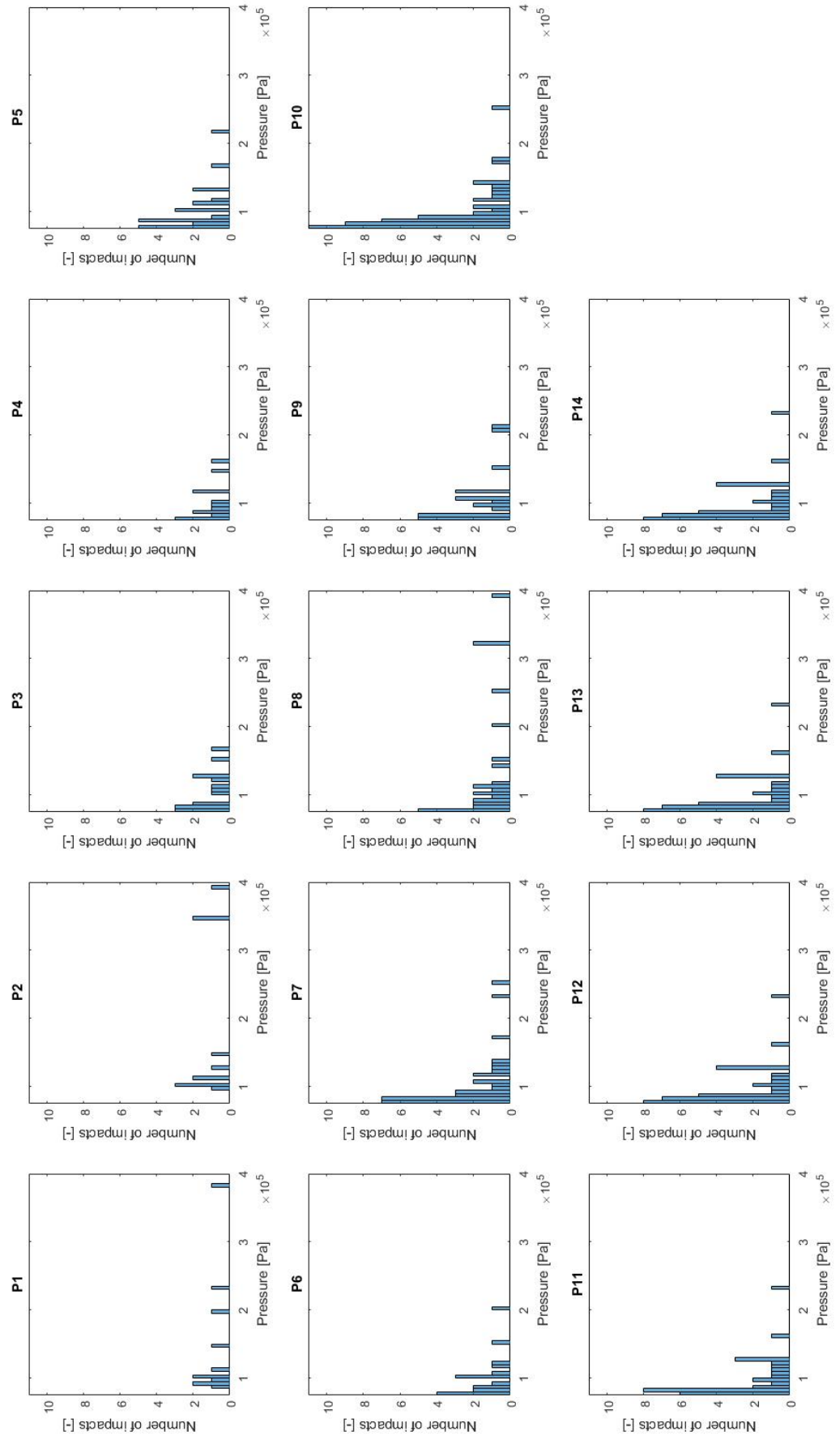

Figure E.32: Case 74 - Binned impact pressures of boxes

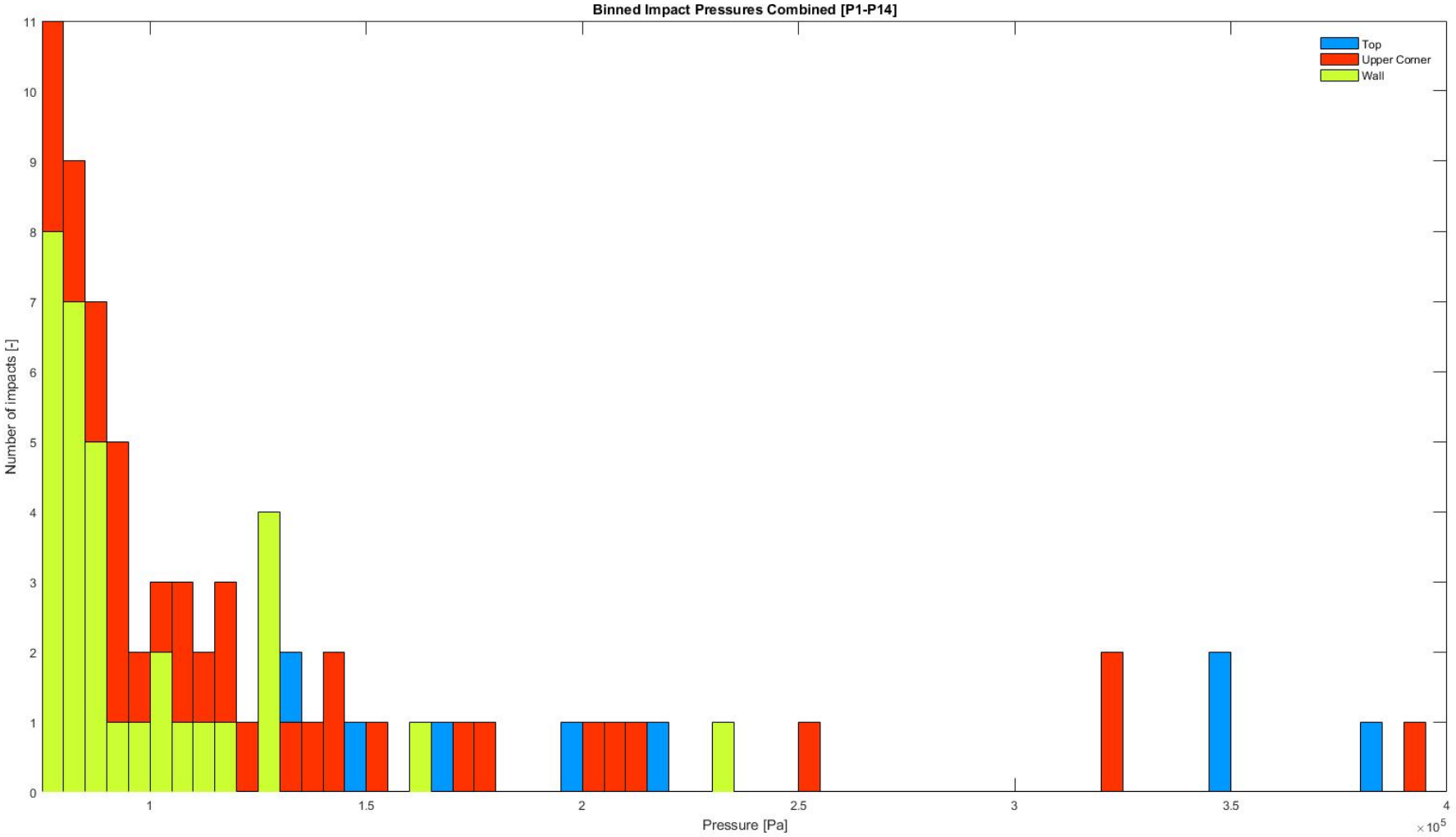

Figure E.33: Case 74 - Combined binned impact pressures

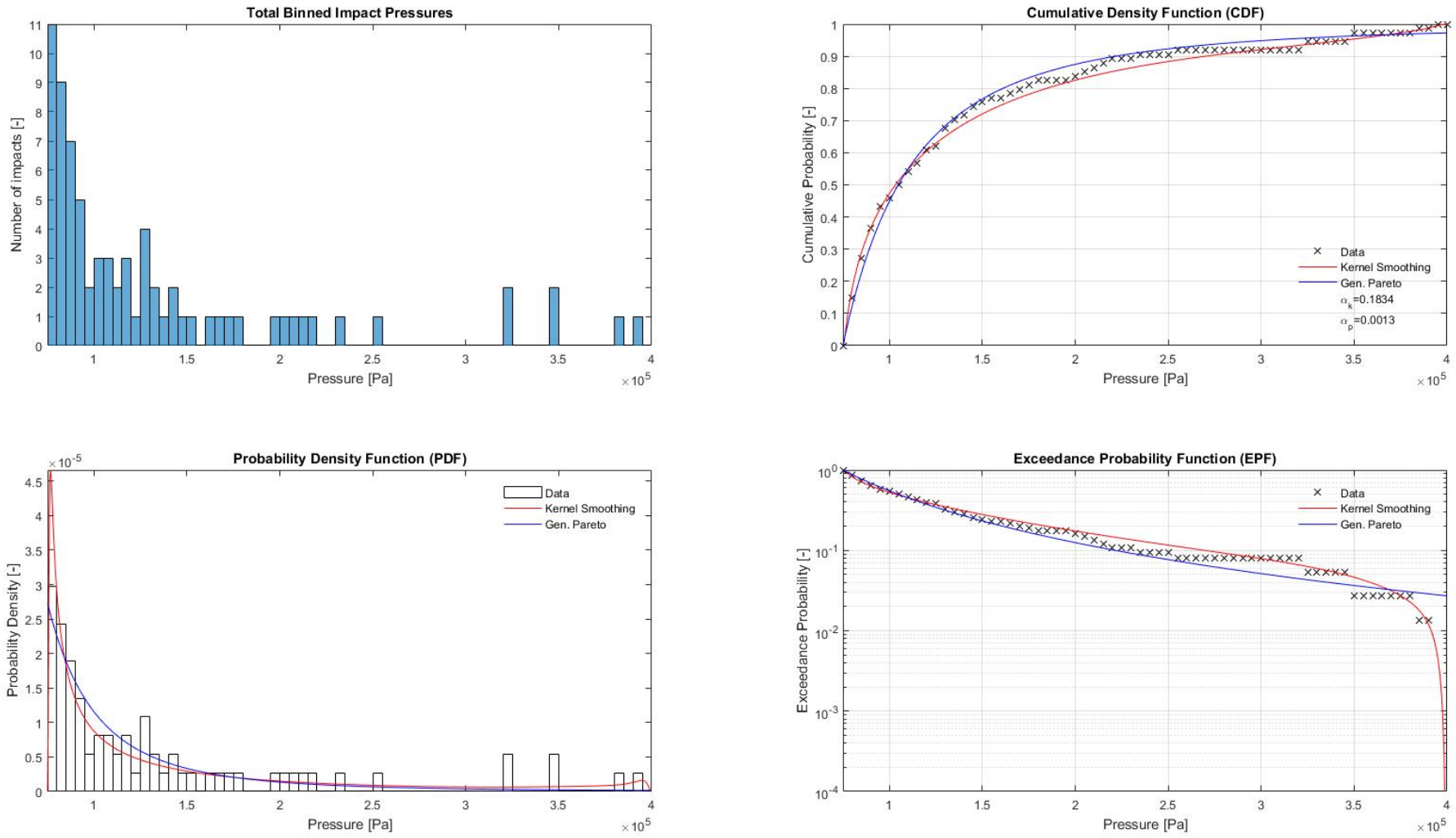

Figure E.34: Case 74 - Statistical fitting PDF, CDF and EPF

E.4. Results - Sensitivity Tornado's

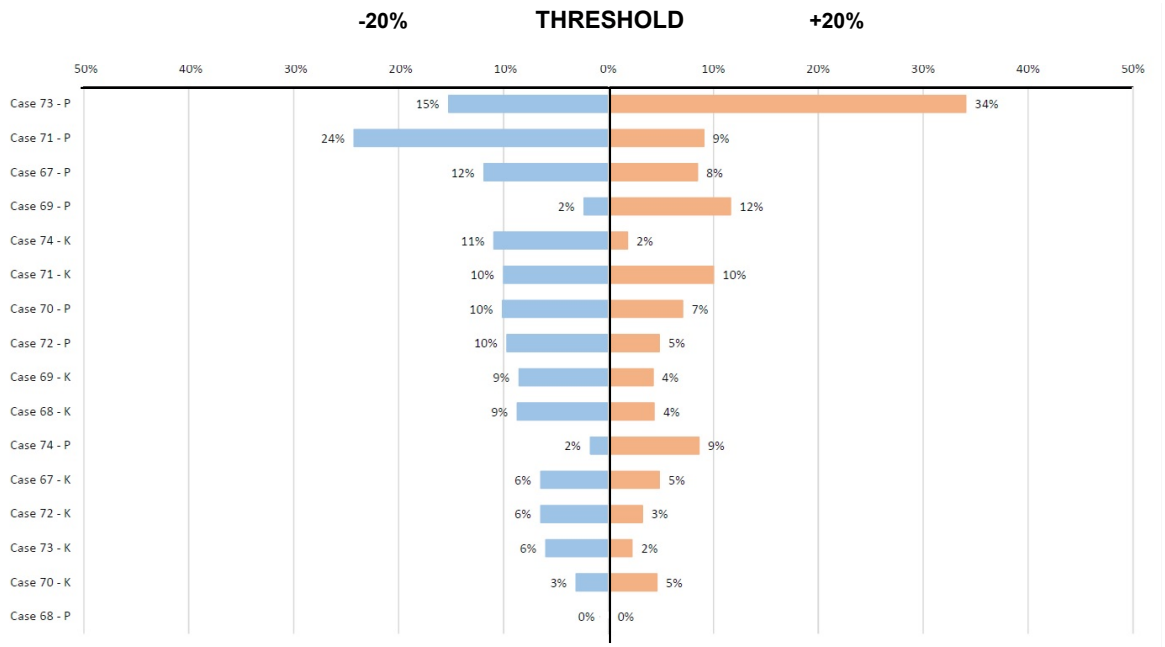

Figure E.35: Sensitivity Tornado - Threshold

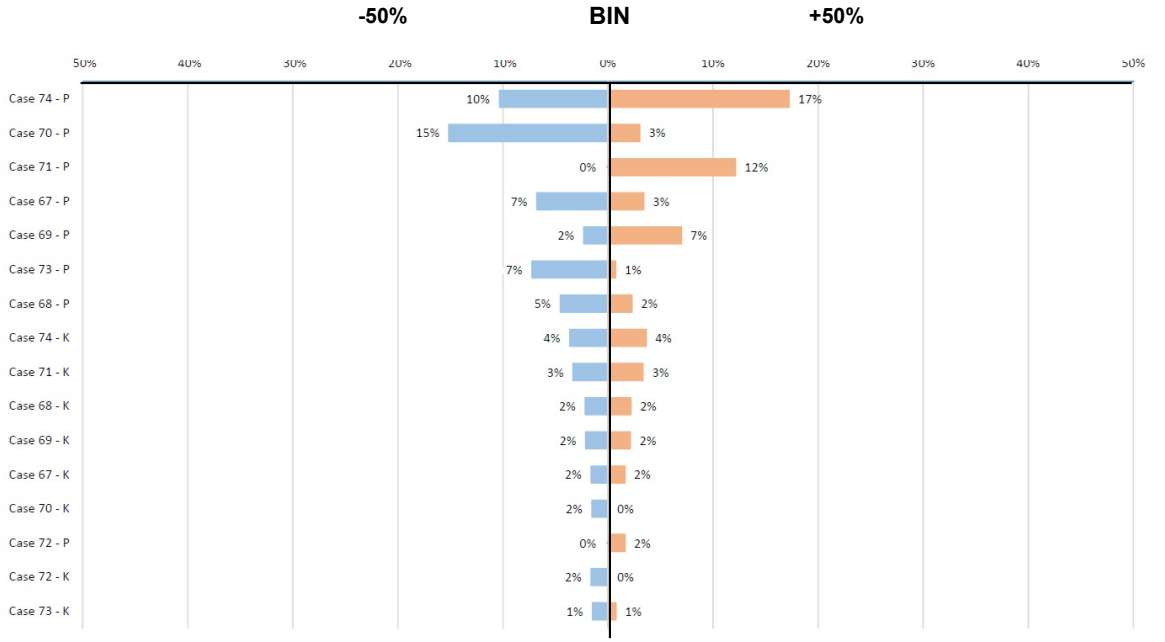

Figure E.36: Sensitivity Tornado - Bin

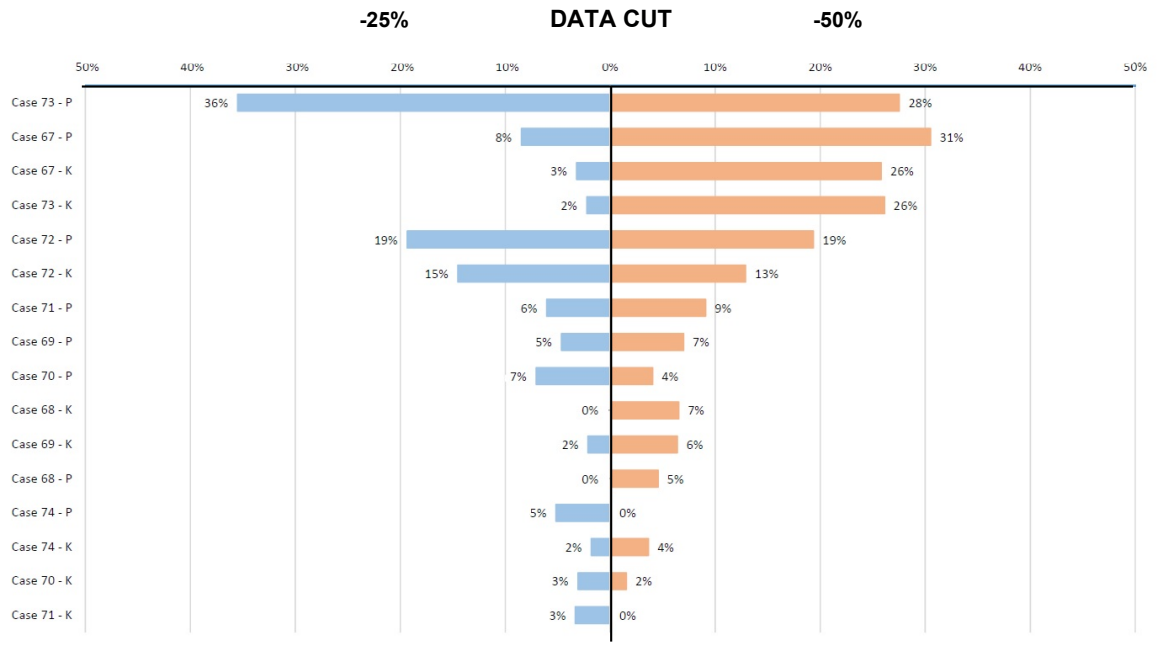

Figure E.37: Sensitivity Tornado - Data (Cut)

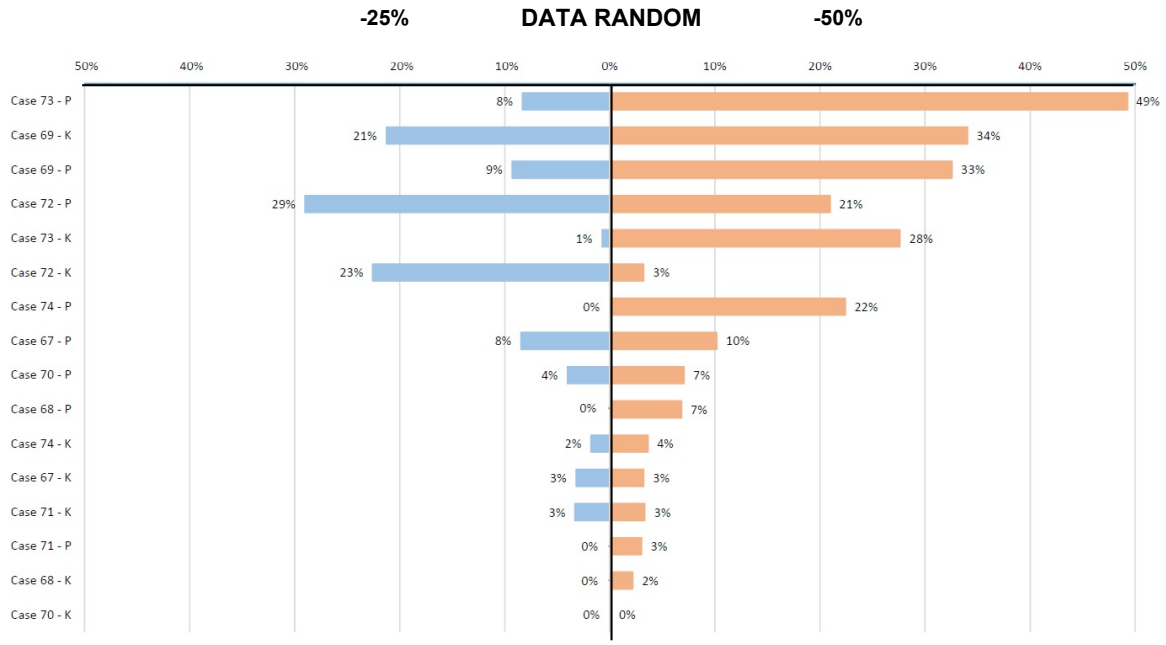

Figure E.38: Sensitivity Tornado - Data (Random)

F

Verification ComFLOW

The verification of the ComFLOW executable is done by a so called 'grid independence study'. Verification includes the main question of: **do we solve the equations right?**

The grid independence study gives more insight on the chosen cell size. For a finer mesh, the difference in results for the same point and time instant should converge. In the case of convergence, one may conclude that grid independence is present and the grid size is sufficient enough. In the event of no convergence, the cell size is not fine enough and located in the so called 'scatter zone'. The zone of convergence depends heavily on the non-linear behaviour of the fluid.

This appendix includes a grid independence analysis for the simulated cases in Phase 1 and Phase 2 of the research. For Phase 1, thee types of fluid behaviour are assessed. Namely, 'no sloshing', 'semi sloshing' and 'sloshing'. Where Phase 2 includes the analysis of sloshing cases only.

For clarity purposes, an example sketch is presented in Figure F.1 below. Where the horizontal axis indicate the size and fineness of the mesh $\left(\frac{1}{h}\right)$, and the vertical axis indicate the difference in result for a specific point and time indication (E).

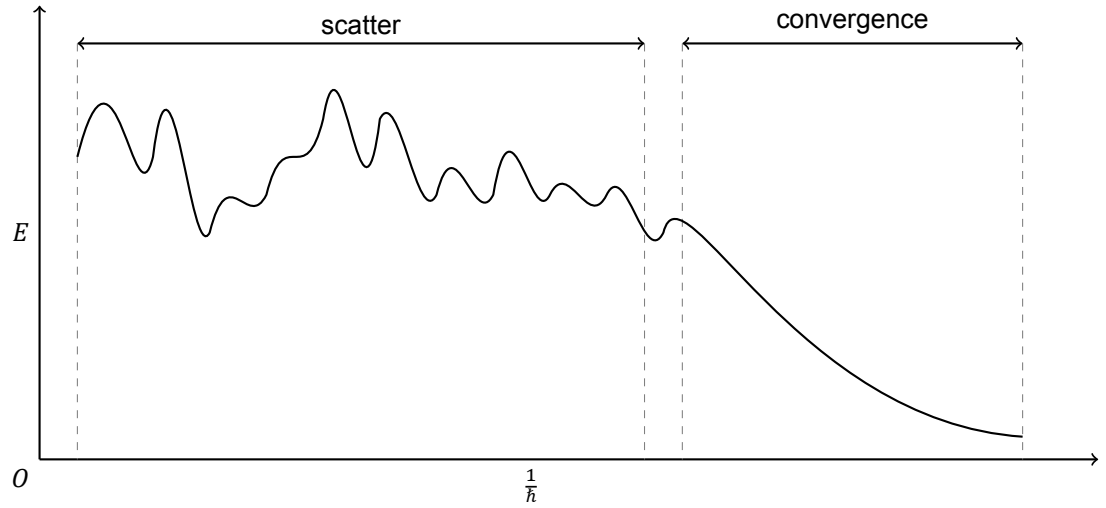

Figure F.1: Sketch - Grid independence related to a specific point and time indication

F.1. Phase 1

As mentioned, the verification of Phase 1 is divided into three parts. Namely; no sloshing, semi sloshing and sloshing. For each type fluid behaviour a separate grid size assessment has been carried out. Test simulation runs resulted in different cell sizes of 10, 5, 3 and 2 cm, defined in Table 7.1 at page 27. Additionally a simulation for 1 cm is made for the sloshing case. The calculation time for the 1 cm was to expensive, therefore it is left out for the verification of the no sloshing and semi-sloshing cases. Furthermore, three monitor points are chosen to compare the results. For a general approach the top (1), wall (4) and bottom (7) monitor points on the left size of the tank are selected. Indicated in Figure F.2 below.

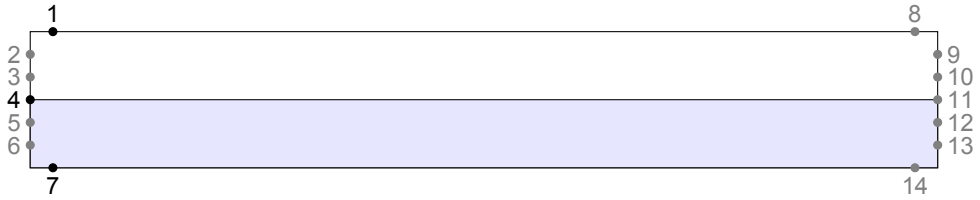

Figure F.2: Verification - Monitor Points In-deck tank

F.1.1. No sloshing

Case 7 is the selected no sloshing case, more information on the case can be found at section 7.1. When there is no sloshing, mild oscillations are present. The comparison for the three monitor points are presented in Figure F.3, F.4 and F.5.

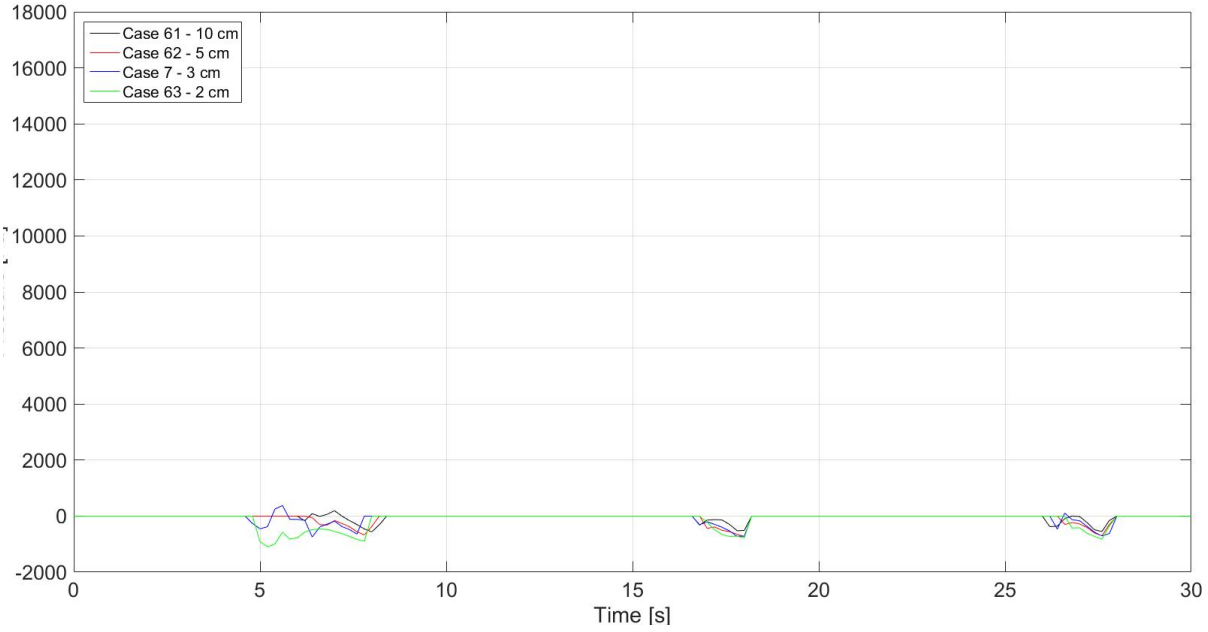

Figure F.3: Phase 1 - Verification - No sloshing - Monitor point 1

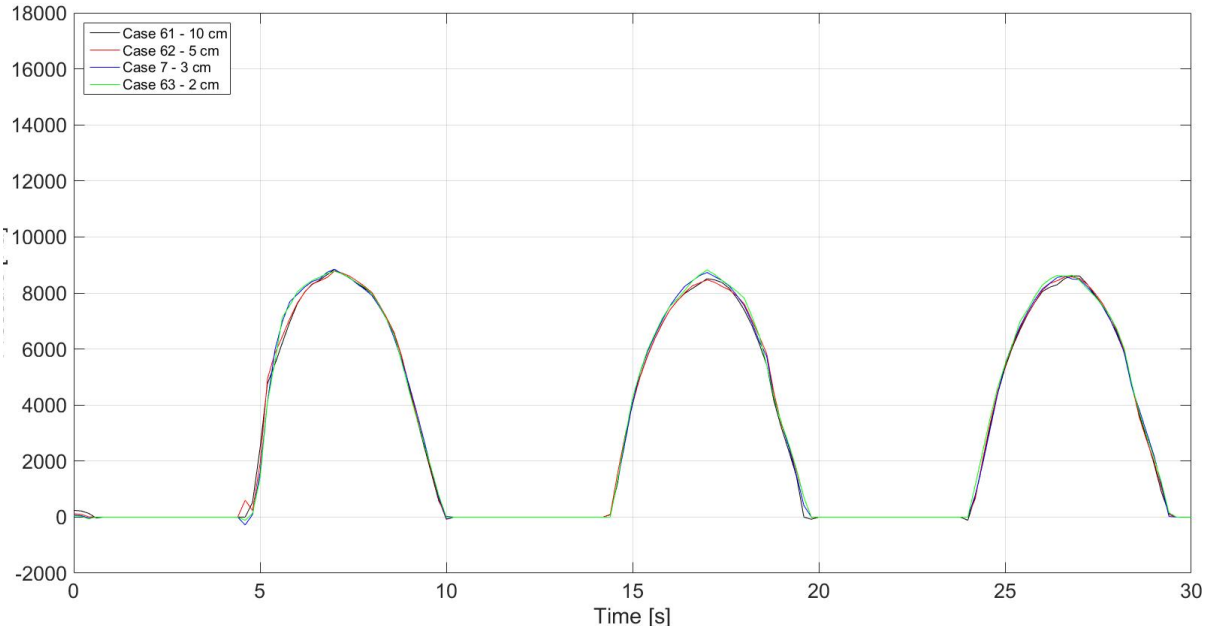

Figure F.4: Phase 1 - Verification - No sloshing - Monitor point 4

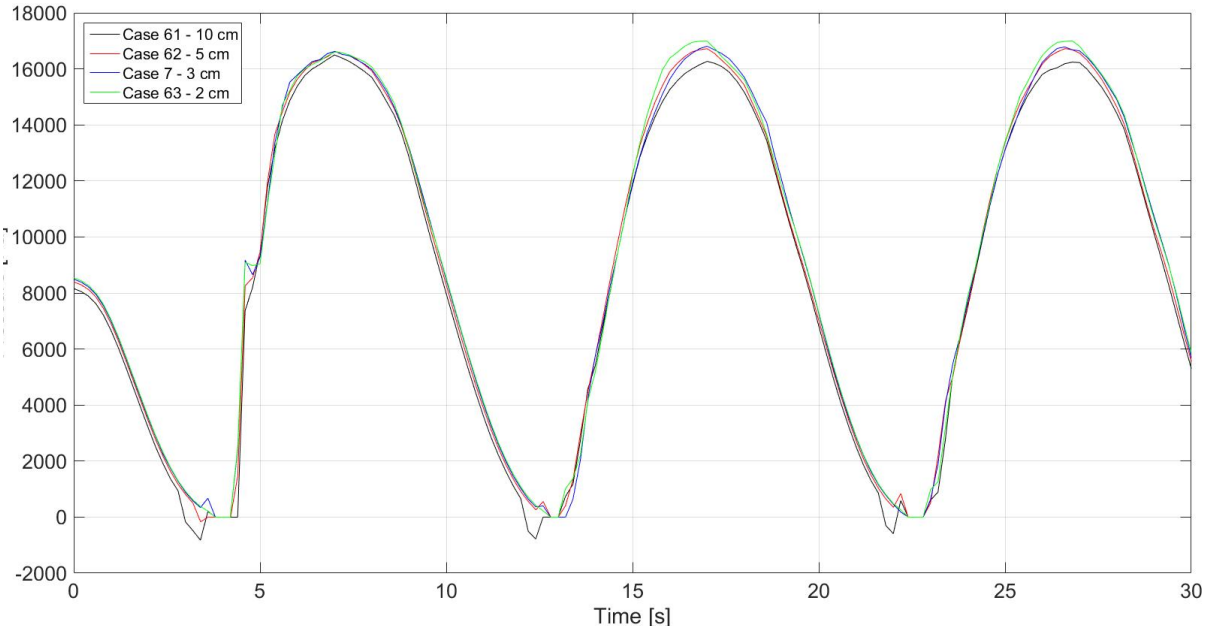

Figure F.5: Phase 1 - Verification - No sloshing - Monitor point 7

Conclusion

Especially Figures F.4 and F.5 show a strong convergence of the results when approaching a finer mesh. Where Figure F.3 has more issues to converge. This is mainly due to droplets and minor non-linear behaviour at the tank upper corner. However, the Figures altogether show a firm convergence for the finer mesh. Concluding that the results of the cases for no sloshing can be interpret as grid independent, part of the convergence regime of Figure F.1.

F.1.2. Semi sloshing

Case 45 is the selected semi sloshing case, more information on the case can be found at section 7.1. Semi sloshing include the transition period between oscillation and sloshing fluid behaviour. Non linearity's are present, but no extreme sloshing pressure impact spikes occur. The comparison for the three monitor points are presented in Figure F.6, F.7 and F.8.

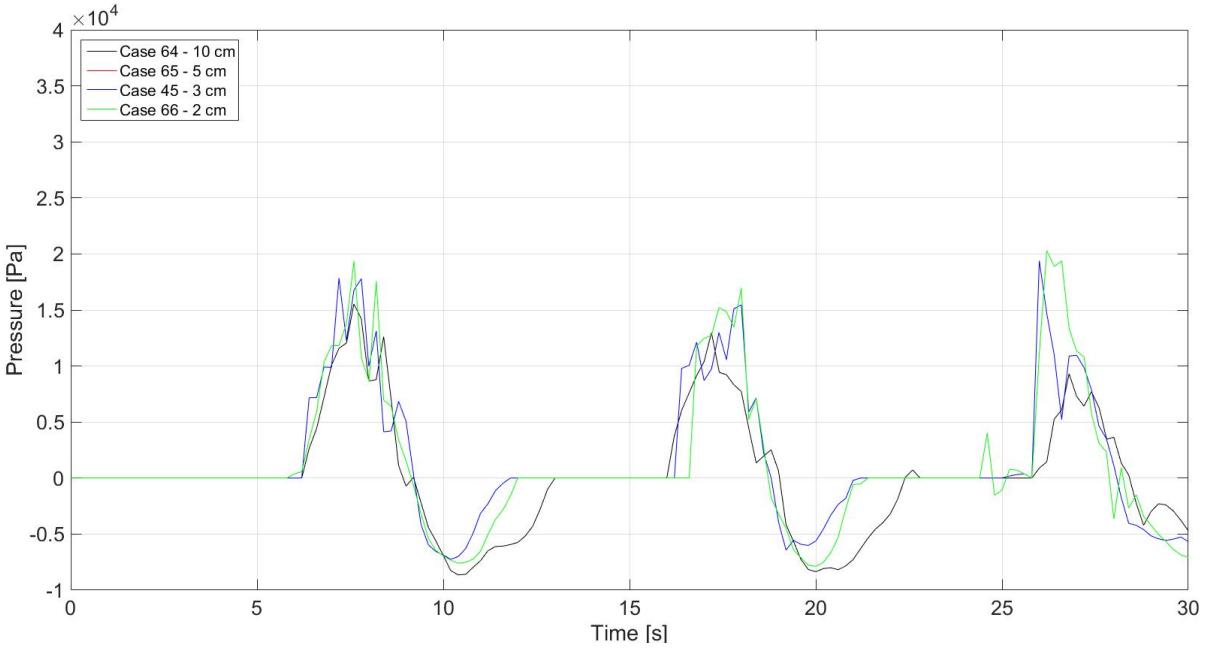

Figure F.6: Phase 1 - Verification - Semi sloshing - Monitor point 1

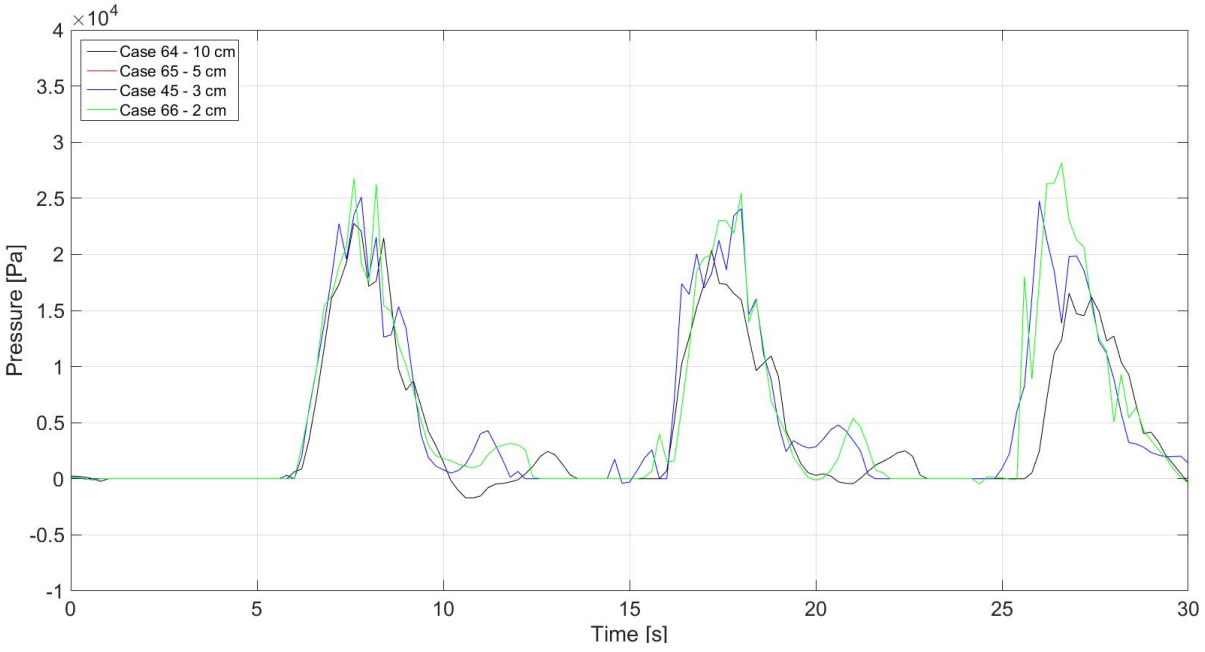

Figure F.7: Phase 1 - Verification - Semi sloshing - Monitor point 4

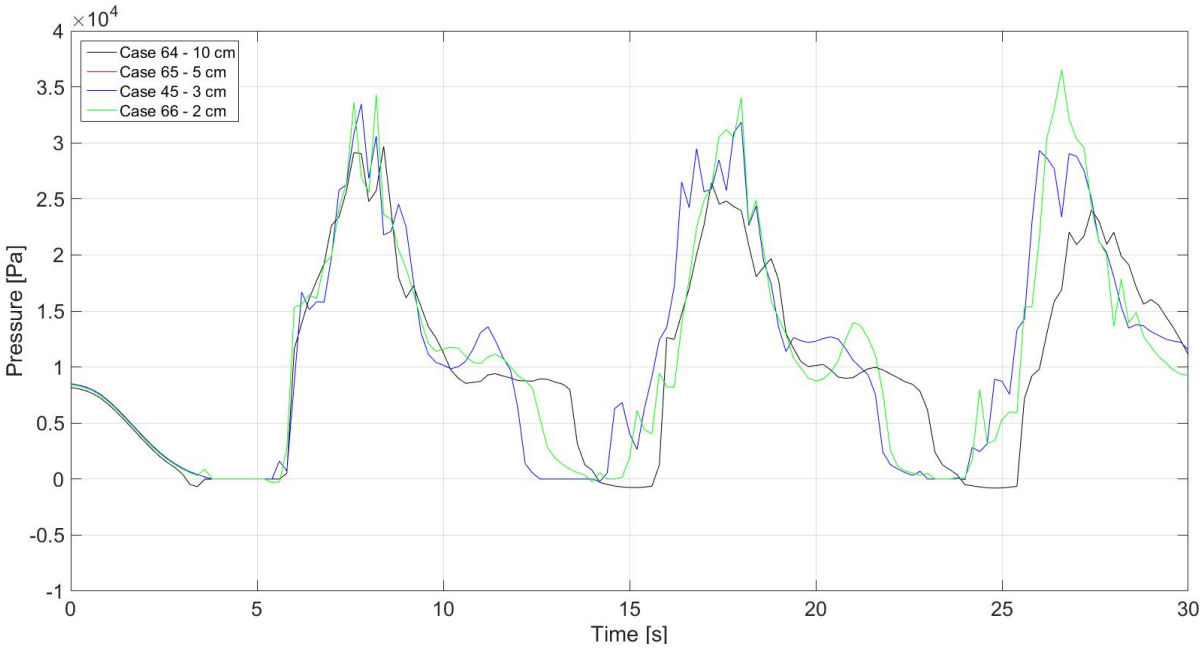

Figure F.8: Phase 1 - Verification - Semi sloshing - Monitor point 7

Conclusion

All three of the semi sloshing figures show scatter and do not converge for finer grids. The finest grid size, green line, contain small pressure peaks, which is an indication of scatter as well. The last notion that can be made is the occurrence of non linear behaviour. Where the results for the 1st, 2nd and 3rd periodic pressure peak increase in difference. Concluding that the results of the cases for semi sloshing can be interpret as grid dependent, part of the scatter regime of Figure F.1.

F.1.3. Sloshing

Case 14 is the selected sloshing case, more information on the case can be found at section 7.1. Sloshing includes major non linear behaviour of the fluid flow. Clear notion of sloshing in pressure graphs is the presence of spikes. The comparison for the three monitor points are presented in Figure F.9, F.10 and F.11. Note, the finest cell size of 1 cm is stopped at around 21 seconds due to computational and time limitations.

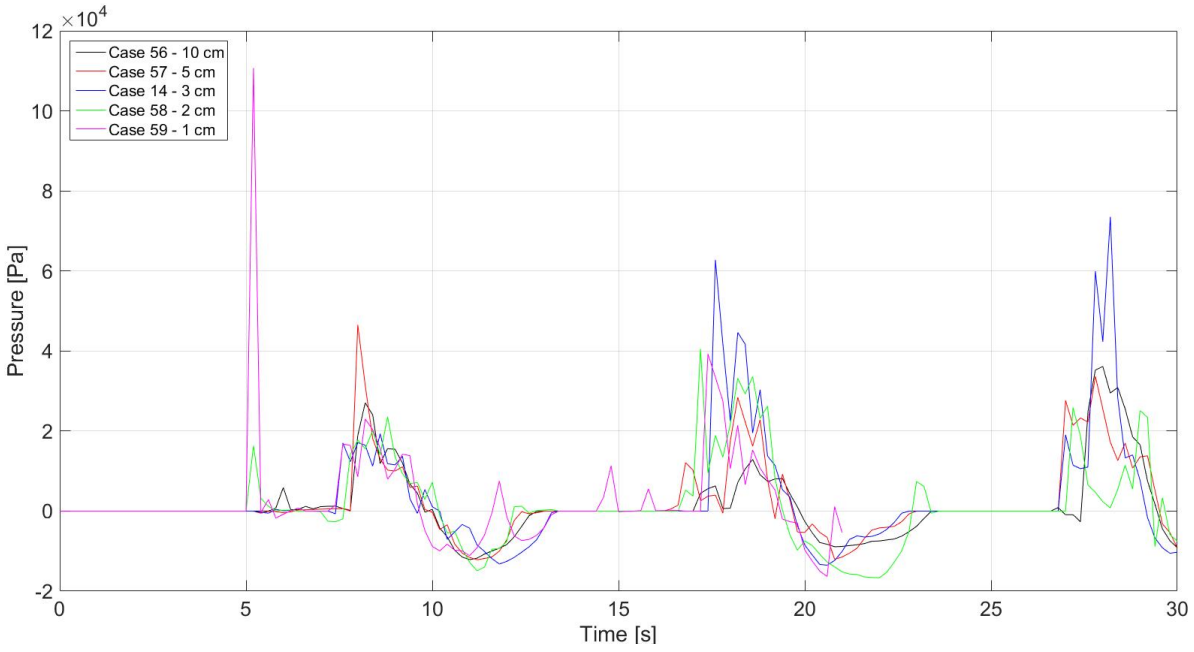

Figure F.9: Phase 1 - Verification - Sloshing - Monitor point 1

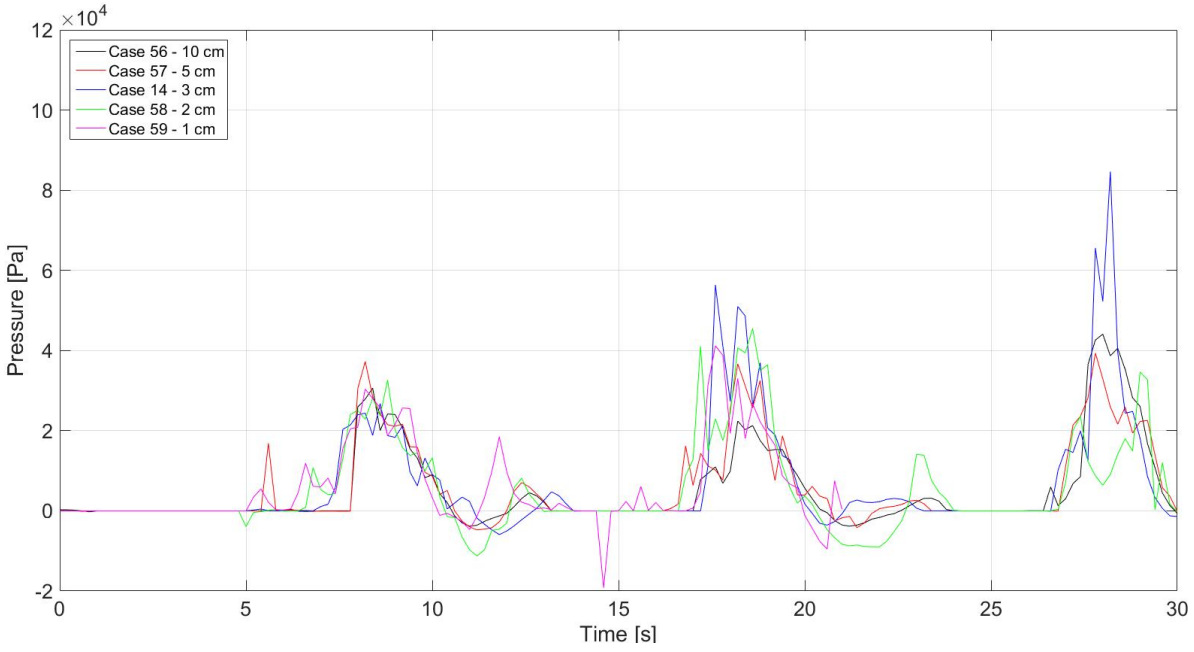

Figure F.10: Phase 1 - Verification - Sloshing - Monitor point 4

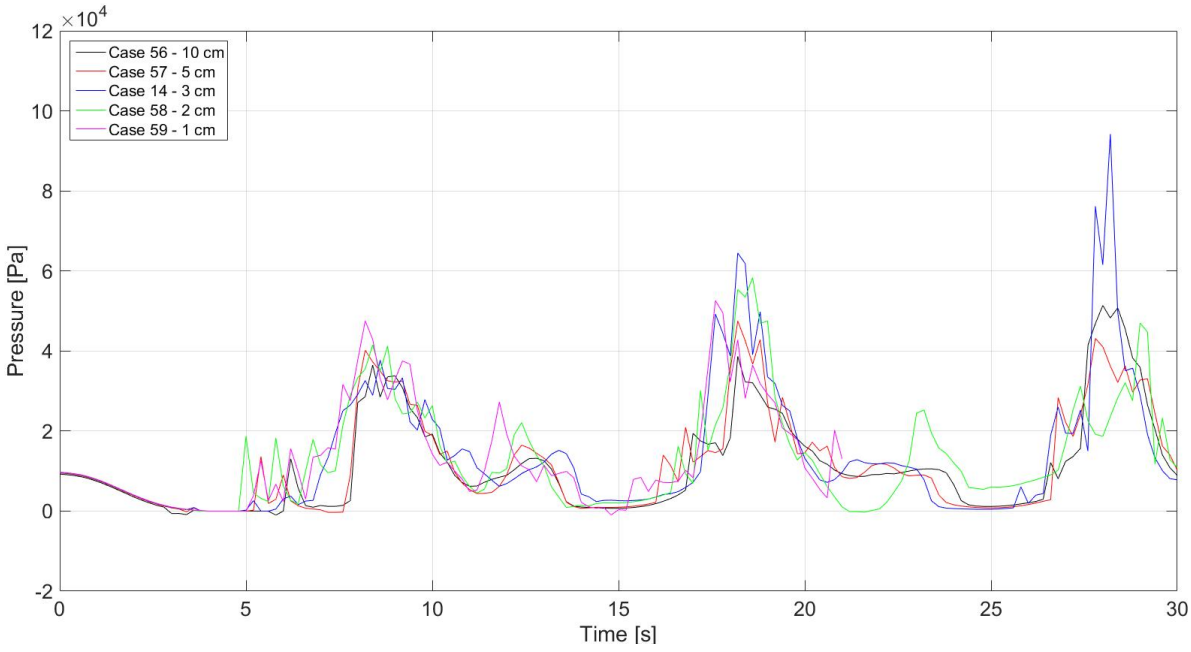

Figure F.11: Phase 1 - Verification - Sloshing - Monitor point 7

Conclusion

The scatter that is present for the sloshing case is more severe compared to the semi sloshing case. Which is influenced by the increased non linear behaviour of the fluid. Also, the difference in results for the 1st, 2nd and 3rd periodic pressure peak is bigger compared to semi sloshing. Concluding that the results of the cases for sloshing can be interpret as grid dependent, part of the scatter regime of Figure F.1. In the second Phase, more intensive refinement of the grid is necessary in order to achieve grind independence.

F.2. Phase 2

The verification of Phase 2 is specifically focused on sloshing cases only. With the application of grid refinement, illustrated in Figure 8.1 at page 38, a more extensive grind independence study could be carried out. The grid is refined three times, which means that for a 8 cm cell size start, the corner of the tank shall include 1 cm cell size. The grid sizes applied are illustrated in Table F.1 and Figure F.12 below. Which are defined with the help of test simulations, described in Table 8.1 at page 37.

Case	Area, N.A. [cm]			
	I	II	III	IV
68	8	4	2	1
75	4	2	1	0.5
76	2	1	0.5	0.25

Table F.1: Verification Phase 2 - Grid size

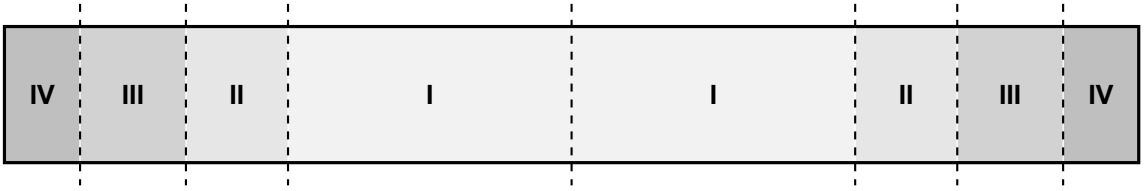

Figure F.12: Verification Phase 2 - Grid size Areas

F.2.1. Sloshing

In continuation of Phase 1, the pressure graphs for the top, wall and bottom of the tank are created. Figures F.13 (top), F.14 (wall) and F.15 (bottom) present the pressure graphs where cases 68, 75 and 76 are included. The monitor points of the simulations for Phase 1 and Phase 2 are exactly on the same location. Therefore, even with the application of grid refinement, the results can be compared to one another. Note, the finest cell size of 2 - 0.25 cm is stopped at around 16 seconds due to computational and time limitations.

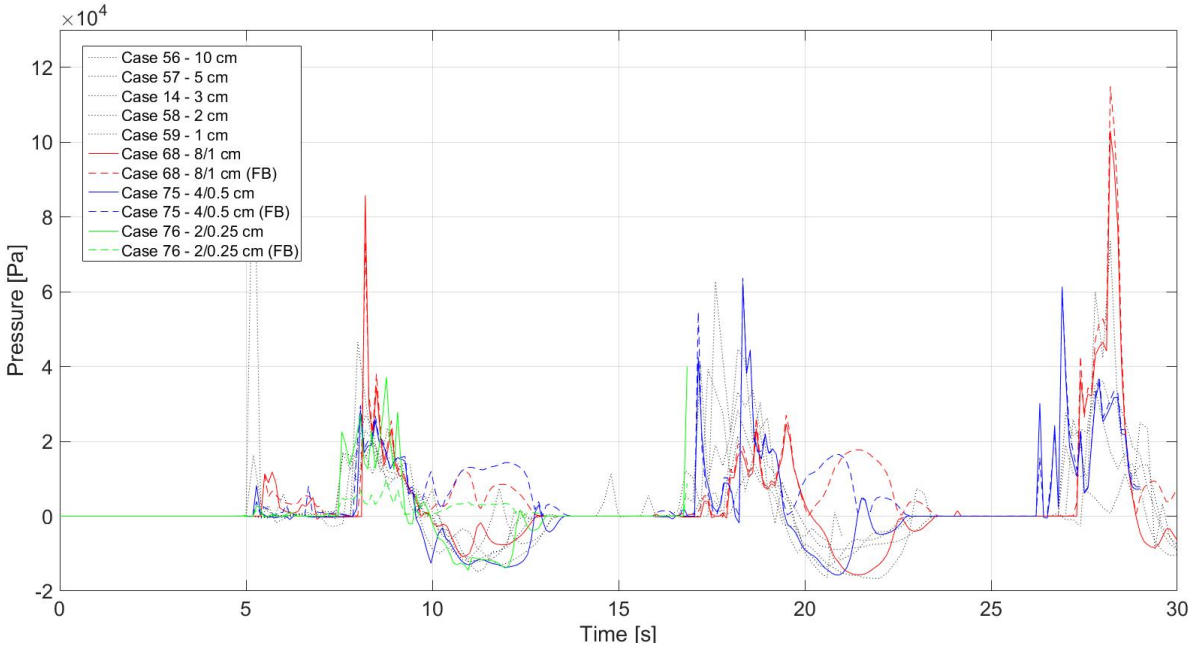

Figure F.13: Phase 2 - Verification - Sloshing - Monitor point 1

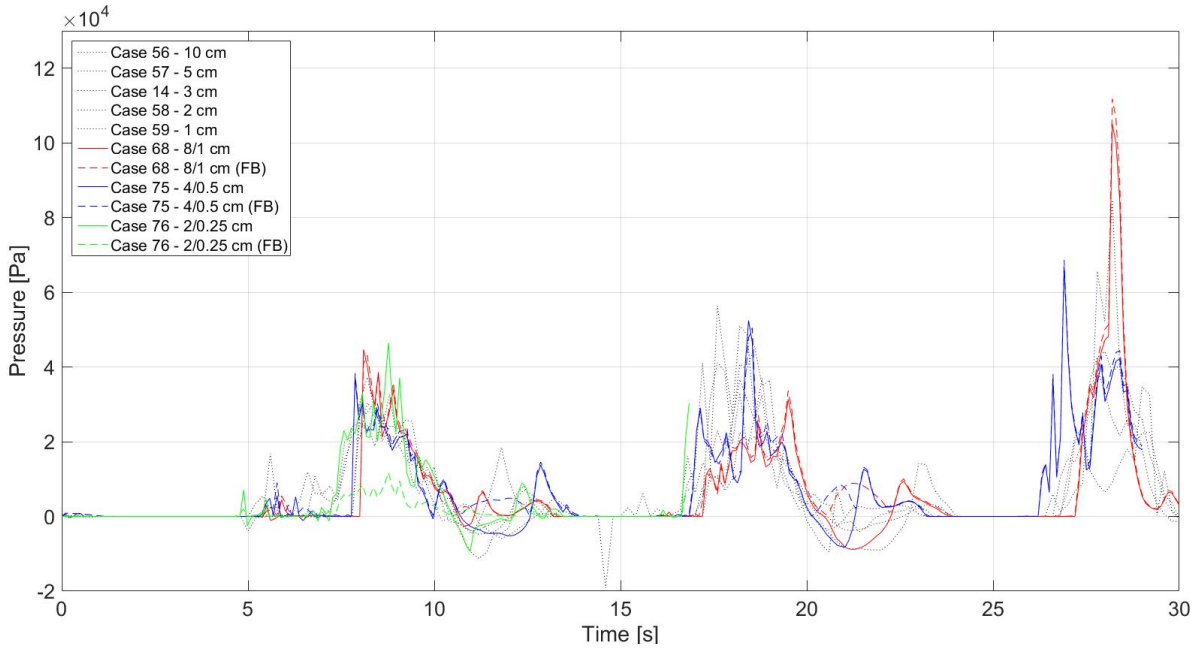

Figure F.14: Phase 2 - Verification - Sloshing - Monitor point 4

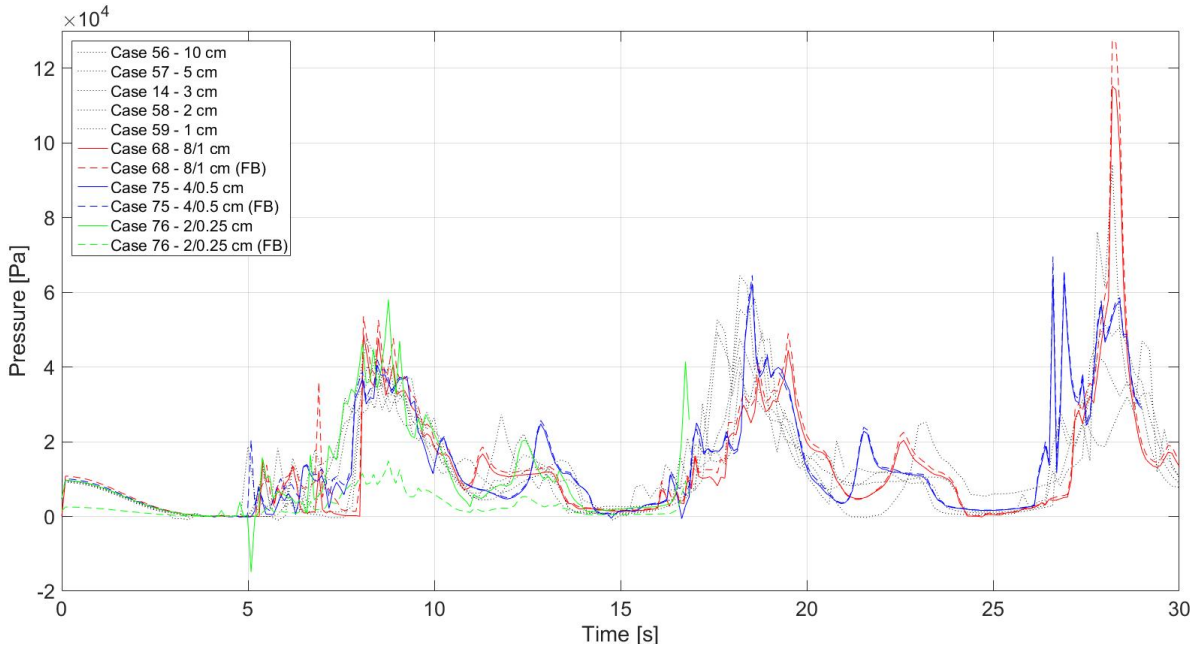

Figure F.15: Phase 2 - Verification - Sloshing - Monitor point 7

Conclusion

Unfortunately, the refinement does not show a clear sign of convergence and therefore it can be concluded that the grid size is still in the scatter regime. However, the presence of a trend is undeniable. The next step includes averaging the pressure distribution to its period and see weather the mean value show any sign of convergence.

F.2.2. Sloshing - Mean Pressure Distribution

Figures F.13 - F.15 show no indication of convergence in the pressure distribution. The next step in finding convergence is taking the average of the peaks in the pressure distribution. This is done by overlapping the three periods of the tank motion (0 s - 9.7 s, 9.7 s - 19,4 s, 19,4 s - 29,1 s) and taking the mean value of the three distributions. The tank left side includes a pressure peak in the zone of 7.5 - 9.5 seconds. The result of this procedure is found in Figure F.16 on the next page.

The results show no clear convergence. However, there is no mean pressure distribution possible for the finest case (76). Due to the limitation of 16 seconds. Case 68 (8-1 cm) and 75 (4-0.5) show an indication of convergence but can't be confirmed by case 76. Again, it has to be mentioned that the pressure trend coincides for all cases.

The last step into assessing the data to convergence is the application of the Root-Mean-Squared (RMS) and the Peak-to-RMS ratio. The RMS level is calculated for the mean pressures by Eq. F.1 stated below, where the Peak-to-RMS ratio is calculated by Eq. F.2.

$$X_{RMS} = \sqrt{\frac{1}{N}\sum_{n=1}^{N} |X_n|^2} \tag{F.1}$$

$$X_{RMS} = \frac{\| X \|_\infty}{\sqrt{\frac{1}{N}\sum_{n=1}^{N} |X_n|^2}} \tag{F.2}$$

The results of the RMS and ratio calculations are presented in Figure F.17 and complemented by Table F.2, at page 153. Both the RMS and ratio behave quite drastically between the 10 cm and 1 cm cell size. However, for the finer size of 1 cm - 0.25 cm the RMS and ratio tend to stabilize. This could be an indication of the transition between the scatter and convergence zone. That implies that the mesh size of 0.25 cm enters the convergence zone.

Conclusion

Even though no clear grid independence can be shown, the results look trustworthy and reasonable. The mean pressure distribution shows a clear trend and phase of the sloshing impact. Both the RMS level and ratio show scatter behaviour up to a cell size of 1 cm. Finer mesh cases present a stable convergence that could imply entering the convergence zone of the grid independence.

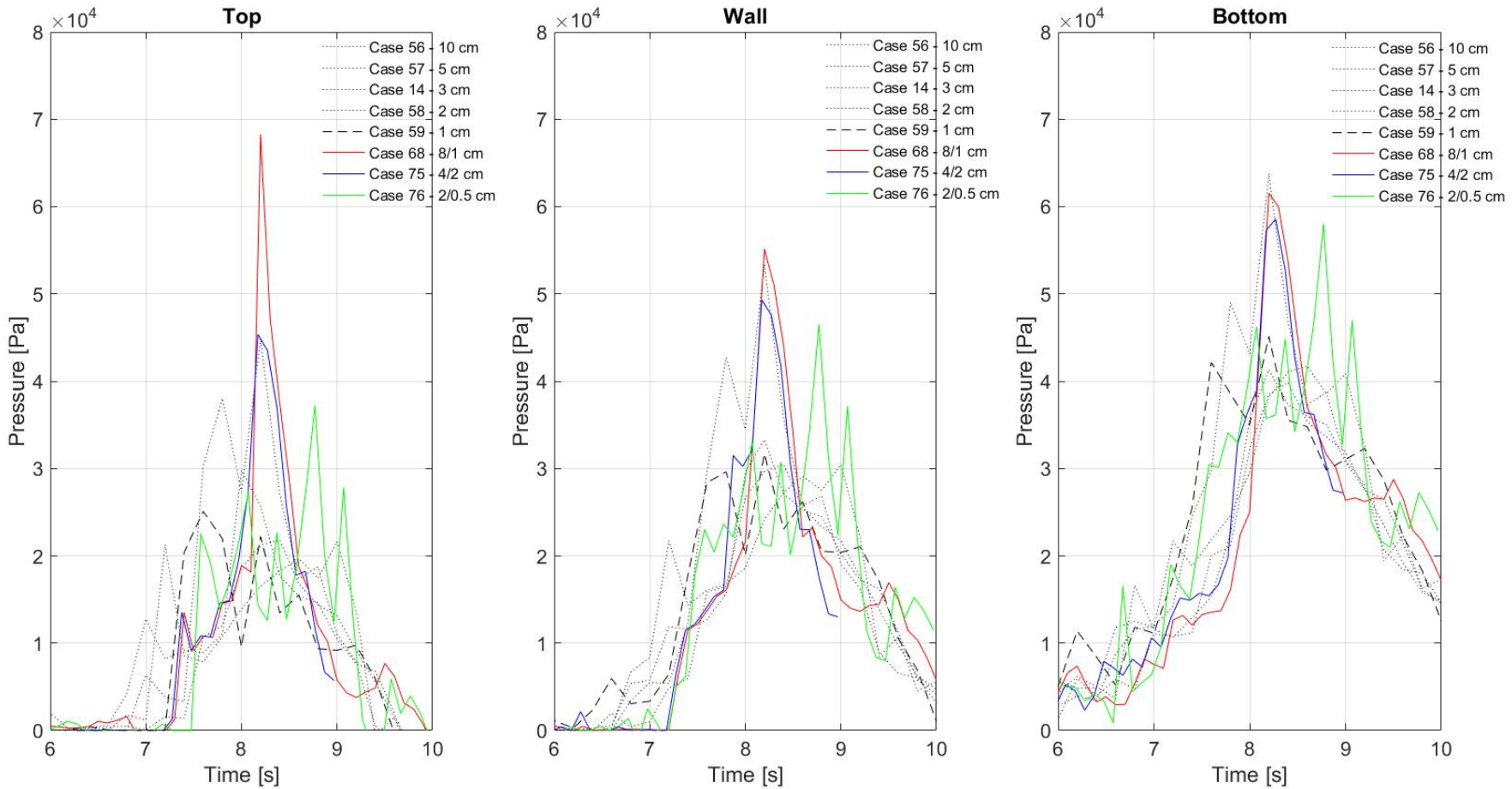

Figure F.16: Phase 2 - Verification - Sloshing - Mean pressure distribution

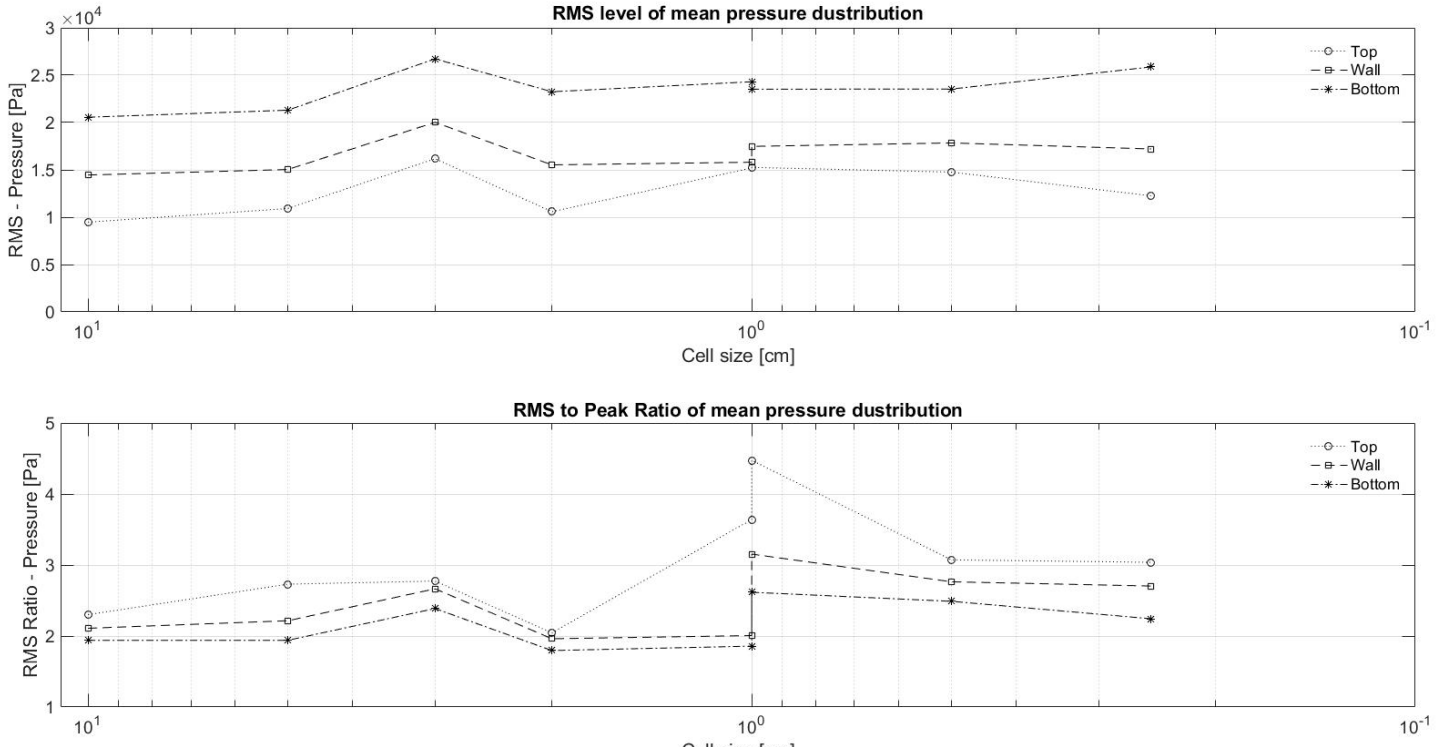

Figure F.17: Phase 2 - Verification - Sloshing - RMS level and Peak to RMS Ratio

	Case															
	56		57		14		58		59		68		75		76	
	RMS [Pa]	Ratio [-]	RMS [Pa]	Ratio [-]	RMS [Pa]	Ratio [-]	RMS [Pa]	Ratio [-]	RMS [Pa]	Ratio [-]	RMS [Pa]	Ratio [-]	RMS [Pa]	Ratio [-]	RMS [Pa]	Ratio [-]
Top	9,480	2.30	10,917	2.73	16,180	2.77	10,582	2.05	15,197	3.64	15,263	4.47	14,763	3.07	12,253	3.04
Wall	14,455	2.11	15,039	2.22	20,019	2.66	15,526	1.96	15,808	2.01	17,479	3.15	17,843	2.76	17,207	2.70
Bottom	20,556	1.94	21,304	1.94	26,720	2.39	23,251	1.80	24,306	1.86	23,522	2.62	23,536	2.49	25,872	2.24

Table F.2: Phase 2 - Verification - Sloshing - RMS level and Peak to RMS Ratio

G

Validation ComFLOW

G.1. Phase 2

The validation of the ComFLOW executable is one of the key factors related to the reliability of the results. Normally, this is done by conducting experiments and is an important indicator when CFD is used. Validation includes the main question of: **do we solve the right equations?** The validation will only include global liquid impacts and behaviour. Local and detailed liquid behaviour does not lie in the scope of this research and is excluded.

There are different possibilities in order to validate a CFD model. Experiments are preferred, but not always applicable due to time or financial restrictions. ComFLOW has already been validated in a broad sense, as described in the ComFLOW manual [24]. However, it is essential to validate specific situations as well. The second best validation possibility would be the use of experimental or numerical data that are published. Unfortunately, there is no data available which include 3 DOF motions that occur for the in-deck tanks. The next best possibility is applied and generally include 1 DOF single impact wave experiments for surge and roll motions.

Two benchmark tests on Sloshing Model Test (SMT) installations have been conducted and involved nine participants. The context of these benchmarks is the comparison of fluid behaviour, especially impact pressures, from sloshing model test performed by different laboratories involving the same input conditions. The benchmark include a 2D rectangular tank filled with water and air. A wide variety of motions are specified, where two are selected for validation of the ComFLOW executable in this research. These two cases are selected because the results were repeatable, even in terms of pressure measurement. Loysel et al. [11] describes the results of the 1^{st} benchmark test, where Loysel et al. [12] and Neugebauer et al. [13] present the results of the 2^{nd} benchmark test. Note, these cases are not sufficient to fully validate ComFLOW for liquid impacts, but it's considered to be a good start.

In repetition of the cases described in Chapter 8.1, Table G.1 below describes the two validation cases. Followed by a comparison of the results between the benchmark experiments and the ComFLOW simulation.

Case	Offshore Structure	Tank		Fill	Fluid	Motion		Numerical Accuracy [cm]	Cycles
		length [m]	height [m]			case	type		
77	HexaPOD	0.95	0.675	85%	water	8	Surge	0.2	2
78	HexaPOD	0.95	0.675	85%	water	9	Roll	0.2	2

Table G.1: Research Cases - Validation

The set-up of the numerical simulation includes the tank geometry, fluid type, fill level and tank motions.

G.1.1. Set-up

The test tank can be defined as a parallelepiped-shape where one dimension is much smaller than the two others, therefore considered to be 2D. The internal dimensions are 964 mm x 670 mm x 118 mm, a top and longitudinal view are shown in Figure G.1 below. Furthermore, the tank consists of a nominal 85% water fill for both motion cases.

A critical note has to be made in relation to the tank geometry. ComFLOW has a hard time mimicking the experimental fluid behaviour with the geometry used in the experiments. This is caused by a specific moment where the free surface nearly touches the top of the tank, $t = 1.1s$ and $t = 1.2s$ respectively. In order to simulate the exact same fluid behaviour with the given tank dimensions, the grid has to be extremely fine. Therefore, it is chosen to increase the height of the tank slightly with 5 mm. Concluding in an increase of the tank height from 0.670 m to 0.675 m (0.75%).

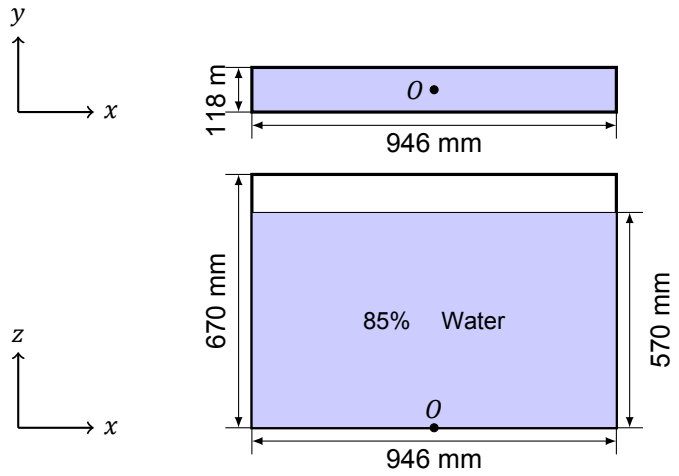

Figure G.1: Tank geometry, fluid type and fill of benchmark test

G.1.2. Tank motions

The tank motions $x(t)$ are defined as a regular sine motion with amplitude $\hat{A}$ and period T, together with a hyperbolic tangent which introduces ramps according to Eqs. G.1. This type of motion generates a perfect sine from 0.5π - 1.2π. The motions take place in 1 DOF for single impact wave conditions.

$$\begin{aligned} x(t) = &\quad \hat{A} \cdot \sin\left(\frac{2\pi t}{T}\right) \cdot \tanh\left(\frac{\pi t^2}{T}\right), && \text{for} \quad 0 \leq t \leq T \\ x(t) = &\quad \hat{A} \cdot \sin\left(\frac{2\pi t}{T}\right) \cdot \tanh\left(\frac{\pi (2T - t)^2}{T}\right), && \text{for} \quad T < t \leq 2T \end{aligned} \tag{G.1}$$

Case 78

This case holds a translation along the x-axis (surge) with an amplitude of 33 mm and a period of 0.975 s. It has been designed to create a large air pocket, where this kind of impact generates oscillating low frequency loads with a uniform moderate pressures inside the pocket. It is expected that the behaviour is easily captured and can be repeated accurately.

Case 79

This case holds a rotation along the y-axis (pitch) with an amplitude of 4.5 ºand a period of 1.207 s. It has been designed to generate a travelling pulse. The free surface hits the ceiling with a certain angle large enough for the gas to escape easy, so no air pockets are created.

Derivation of motion Eqs. G.1 are made in order to establish the time traces. Eqs. G.2 - G.5 describe the velocity and acceleration components of the first ($0 \leq t \leq T$) and second ($T < t \leq 2T$) period.

For $0 \leq t \leq T$

$$\dot{x}(t) = \hat{A} \cdot \frac{2\pi}{T} \cdot \cos\left(\frac{2\pi t}{T}\right) \cdot \tanh\left(\frac{\pi t^2}{T}\right) + \frac{2\pi t}{T} \cdot \sin\left(\frac{2\pi t}{T}\right) - \frac{2\pi t}{T} \cdot \sin\left(\frac{2\pi t}{T}\right) \cdot \tanh^2\left(\frac{\pi t^2}{T}\right) \tag{G.2}$$

$$\begin{aligned}\ddot{x}(t) = \hat{A} \cdot & -\frac{4\pi^2}{T^2} \cdot \sin\left(\frac{2\pi t}{T}\right) \cdot \tanh\left(\frac{\pi t^2}{T}\right) + \frac{4\pi^2 t}{T^2} \cdot \cos\left(\frac{2\pi t}{T}\right) \cdot \left[1 - \tanh^2\left(\frac{\pi t^2}{T}\right)\right] \\ & + \frac{2\pi}{T} \cdot \sin\left(\frac{2\pi t}{T}\right) + \frac{4\pi^2 t}{T^2} \cdot \cos\left(\frac{2\pi t}{T}\right) - \frac{2\pi}{T} \cdot \sin\left(\frac{2\pi t}{T}\right) \cdot \tanh\left(\frac{\pi t^2}{T}\right) \cdot \tanh\left(\frac{\pi t^2}{T}\right) \\ & - \frac{4\pi^2 t}{T^2} \cdot \cos\left(\frac{2\pi t}{T}\right) \cdot \tanh\left(\frac{\pi t^2}{T}\right) \cdot \tanh\left(\frac{\pi t^2}{T}\right) - \frac{8\pi^2 t^2}{T^2} \cdot \sin\left(\frac{2\pi t}{T}\right) \cdot \tanh\left(\frac{\pi t^2}{T}\right) \\ & \cdot \left[1 - \tanh^2\left(\frac{\pi t^2}{T}\right)\right]\end{aligned} \tag{G.3}$$

For $T < t \leq 2T$

$$\begin{aligned}\dot{x}(t) = \hat{A} \cdot & \frac{2\pi}{T} \cdot \cos\left(\frac{2\pi t}{T}\right) \cdot \tanh\left(\frac{\pi(2T-t)^2}{T}\right) + \left(\frac{2\pi t - 4\pi T}{T}\right) \cdot \sin\left(\frac{2\pi t}{T}\right) \\ & - \left(\frac{2\pi t - 4\pi T}{T}\right) \cdot \sin\left(\frac{2\pi t}{T}\right) \cdot \tanh^2\left(\frac{\pi(2T-t)^2}{T}\right)\end{aligned} \tag{G.4}$$

$$\begin{aligned}\ddot{x}(t) = \hat{A} \cdot & -\frac{4\pi^2}{T^2} \cdot \sin\left(\frac{2\pi t}{T}\right) \cdot \tanh\left(\frac{\pi(2T-t)^2}{T}\right) + \left(\frac{4\pi^2 t - 8\pi^2 T}{T^2}\right) \cdot \cos\left(\frac{2\pi t}{T}\right) \\ & \cdot \left[1 - \tanh^2\left(\frac{\pi(2T-t)^2}{T}\right)\right] + \frac{2\pi}{T} \cdot \sin\left(\frac{2\pi t}{T}\right) + \left(\frac{4\pi^2 t - 8\pi^2 T}{T^2}\right) \cdot \cos\left(\frac{2\pi t}{T}\right) \\ & - \frac{2\pi}{T} \cdot \sin\left(\frac{2\pi t}{T}\right) \cdot \tanh^2\left(\frac{\pi(2T-t)^2}{T}\right) - \left(\frac{4\pi^2 t - 8\pi^2 T}{T^2}\right) \cdot \cos\left(\frac{2\pi t}{T}\right) \\ & \cdot \tanh^2\left(\frac{\pi(2T-t)^2}{T}\right) - 2 \cdot \left(\frac{4\pi^2 t^2 - 16\pi^2 T t + 16\pi^2 T^2}{T^2}\right) \cdot \sin\left(\frac{2\pi t}{T}\right) \cdot \tanh\left(\frac{\pi(2T-t)^2}{T}\right) \\ & \cdot \left[1 - \tanh^2\left(\frac{\pi(2T-t)^2}{T}\right)\right]\end{aligned} \tag{G.5}$$